F.O.P. - 1990

Winter Fieldtrip

Western Salton Trough - Soils and Neotectonics

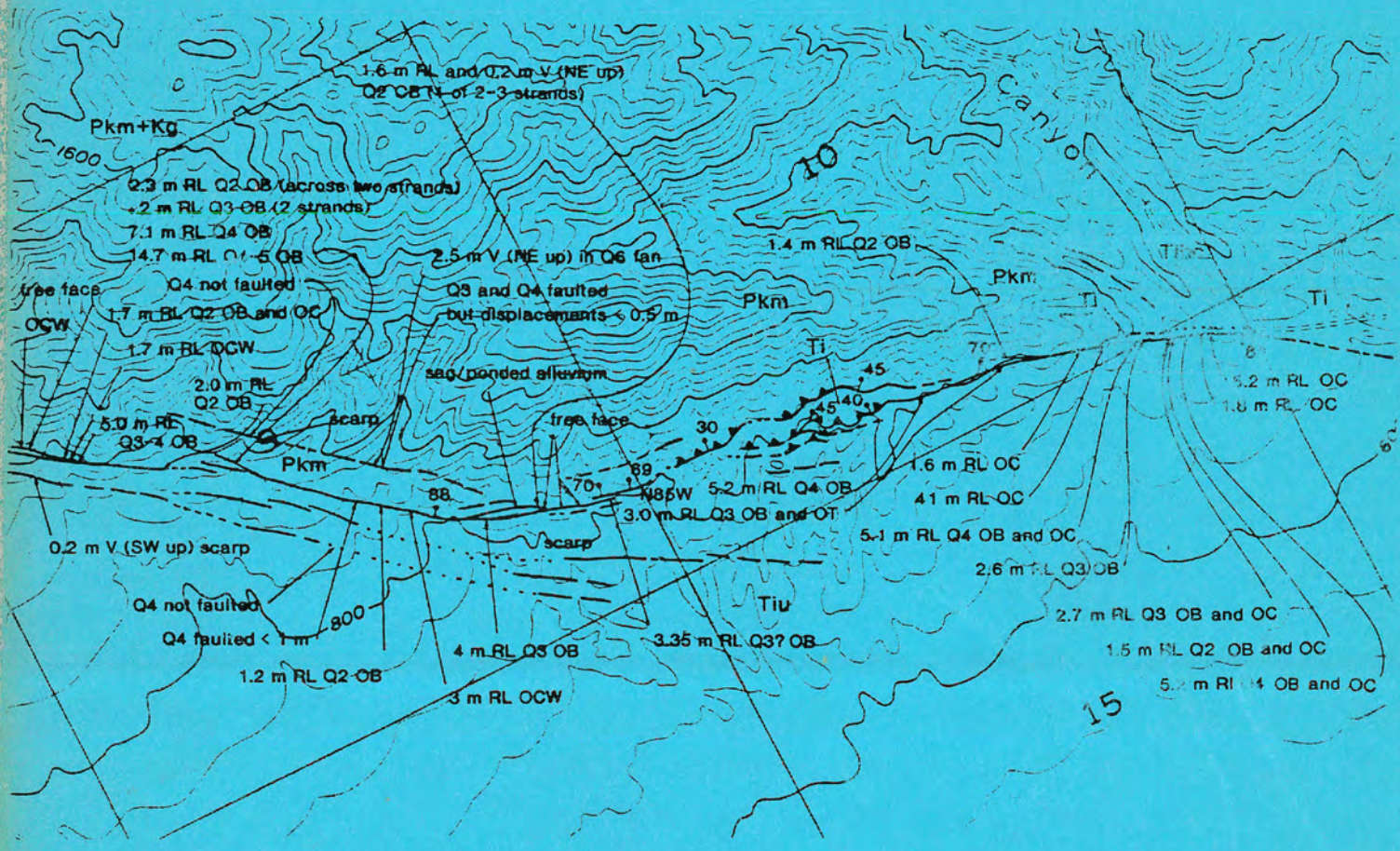

FRIENDS OF THE PLEISTOCENE

WINTER FIELDTRIP - 1990

WESTERN SALTON TROUGH SOILS AND NEOTECTONICS

Organized by Tom Rockwell
Department of Geological Sciences
San Diego State University
San Diego, CA 92182

LED BY A CAST OF THOUSANDS

Including: Robert Crisman, Jonathan Goodmacher, Ralph Klinger, Scott Lindvall, Andy Thomas and scores of other important and famous people.

FRIENDS OF THE PLEISTOCENE FIELDTRIP 1990

PREFACE

This guidebook is essentially a collection of papers that are either in print, in review, or are being prepared for submission for publication. Some are further along than others and your comments are welcome. Enjoy the trip.

TABLE OF CONTENTS

LATE QUATERNARY STRUCTURAL EVOLUTION OF THE WESTERN MARGIN OF THE SIERRA DE LOS CUCAPAS, BAJA CALIFORNIA NORTE

by

Karl J. Mueller*

and

Thomas K. Rockwell
Department of Geological Sciences
San Diego State University
San Diego, California 92182

*Present Address: Department of Geology and Geophyics
University of Wyoming
Laramie, Wyoming 82071

Abstract

The western margin of the Sierra de los Cucapas is defined by the Laguna Salada fault, a complex zone of active oblique-dextral slip faults. The northwestern section of the fault zone consists of a single fault strand which has had an oblique-dextral sense of slip throughout the late Pleistocene and Holocene. The south-eastward continuation of this single fault strand has been comparatively inactive during the Holocene. Slip during the late Quaternary has instead been stepped several hundred meters to the southwest onto two distinct oblique dextral fault strands. The more easterly of these strands extends southeastward until it intersects the Canon Rojo fault, a northwest dipping normal fault, active throughout much of the late Quaternary.

This zone of normal slip and other northwest dipping, normal faults have transferred dextral slip from the Laguna Salada fault zone during the late Quaternary to several other oblique-dextral zones lying successively farther to the southwest. This connected series of northwest striking oblique-dextral and northwest dipping normal fault zones collectively form a series of dilational right steps and are

responsible for basin subsidence and pull-apart within Laguna Salada. Geomorphic evidence suggests that pull-apart was not continuous during this period and ceased at least once within the northern portion of the Laguna Salada basin.

Introduction

The Sierra de los Cucapas lie astride the great structural depression of the Gulf of California tectonic province in the southwestern Salton Trough (Figure 1). This range contains many of the structural elements which have governed deformation in the trough since early in its history.

The well-exposed oblique-dextral and normal fault zones which bound the western margin of the Sierra de los Cucapas are directly responsible for the late-Quaternary uplift of the range and the development of a deep elongate stepped basin in Laguna Salada (Biehler et. al., 1964; Barnard, 1968; Gastil, 1968; Kelm, 1971; Strand, 1980). The vertical relief of the basin and the rugged topography of the range are themselves products of even greater horizontal displacements along these faults.

The purpose of this paper is to describe and discuss the sense and relative activity of faults exposed along the western margin of the Sierra de los Cucapas and their role in the development of the Laguna Salada basin. Field studies were concentrated on the western margin of the Sierra de los Cucapas along the central portion of the Laguna Salada fault zone (Figure 2). Study was concentrated in this region because of the presence of many tectonic and geomorphic indicators of recent and historical fault movement such as fault scarps and instrumentally recorded earthquake epicenters (Barnard, 1968; Hileman et.

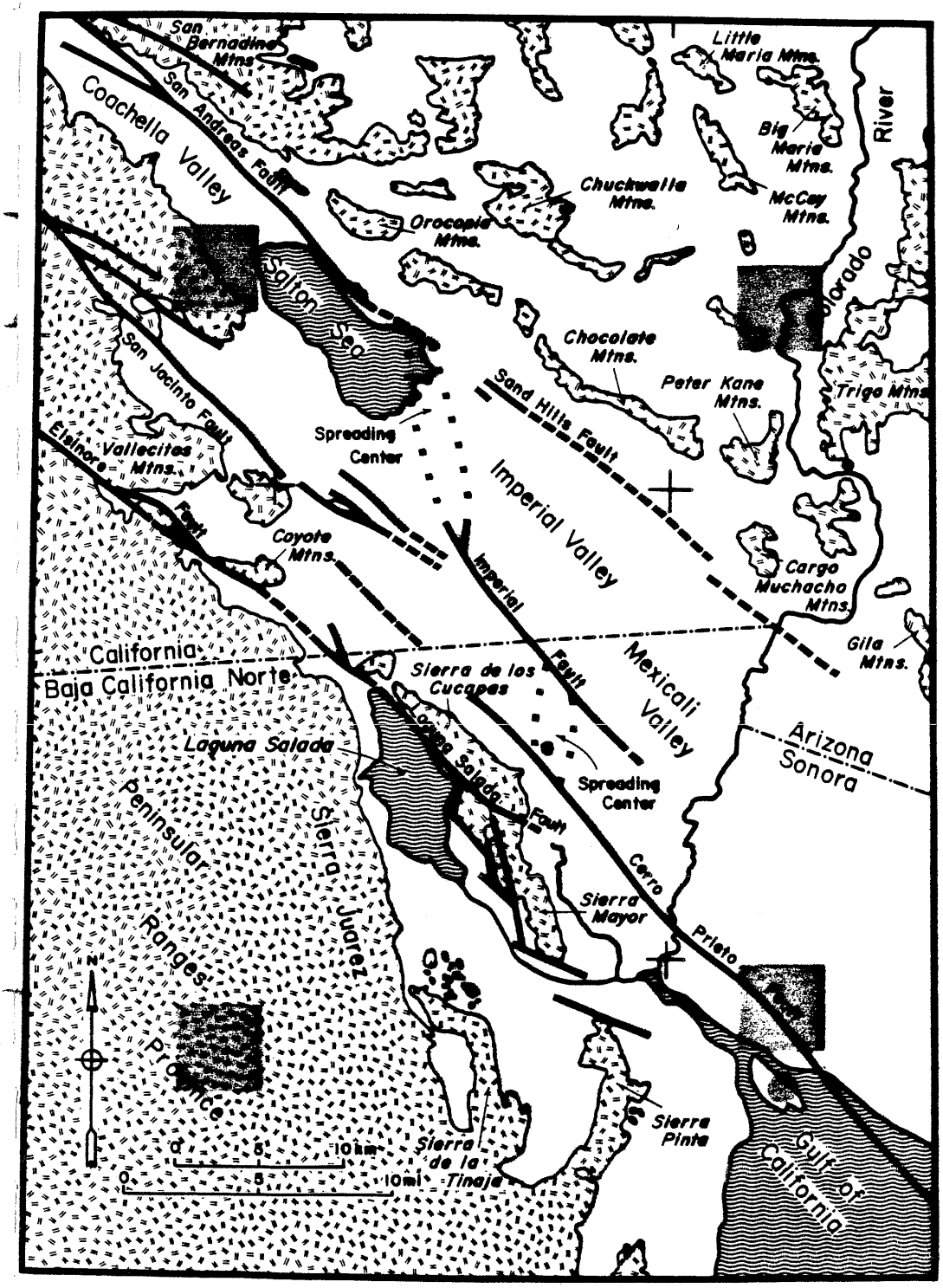

Figure 1. Map showing major structural and physiographic elements of the Salton Trough. Note location of the Laguna Salada basin and the Sierra de los Cucapas along its southwestern margin.

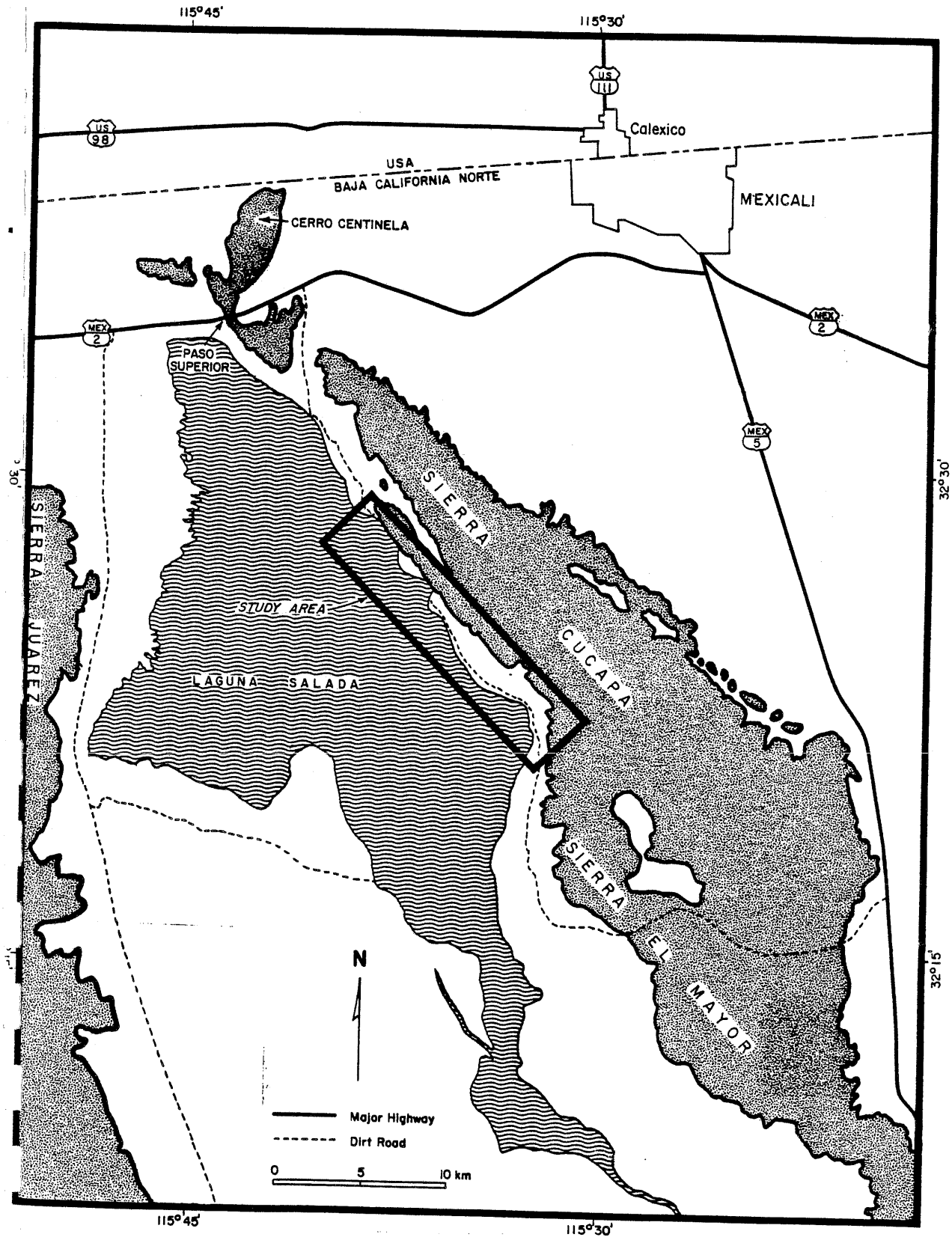

Figure 2. Diagram showing location of the detailed study area (Figure 4) along the southwestern margin of the Sierra de los Cucapas.

al., 1973; Strand, 1980). Large-scale mapping of displaced geologic and geomorphic surfaces was completed to evaluate the activity of individual fault strands contained within a northwest trending 1 km wide zone of deformation. The relative ages of faulted geomorphic surfaces was assessed by the degree of soil development present within them (Mueller, 1984). Rates of soil development, and therefore approximate absolute ages of the soils in the chronosequence, were estimated by comparison with other well-dated soil chronosequences formed in climatic environments similar to the southwestern Salton Trough (Gile et. al., 1960; Gile and Grossman, 1968; Gile, 1975; Bischoff et. al., 1976; Schlemon, 1976; Schlemon and Purcell, 1976; Alexander and Nettleton, 1977). Also, the timing of a dated climatic change at the end of the Pleistocene (7,800 - 12,000 ybp) was used to estimate the maximum age of the Holocene soils (Wells, 1976; Van Devender, 1977; Burrows, 1979; Galloway 1983). The Holocene soils were differentiated from the Pleistocene ones by their varying pedogenic characteristics, related to a change in the depth of soil wetting.

Previous Work

Early workers in the Laguna Salada basin and the Sierra de los Cucapas quickly recognized the presence and/or recency of faulting exposed there (Lindgren, 1888; Beal, 1948; Gastil, 1968; Gastil et. al., 1971). Later geophysical surveys by Kovach et. al., (1962) and Biehler et. al. (1964) contributed to an understanding of the region by using gravity surveys to develop models of the configuration of basin fill and underlying crustal characteristics. A more comprehensive gravity and magnetic study by Kelm (1971) further defined the shape and structure of the northern two-thirds of the basin. Sedimentological and stratigraphic

studies (Dibblee, 1954; Walker, 1967; Walker, et. al., 1967) defined gross stratigraphic sequences along the margins of the basin and studied diagenetic alteration within them.

Work in the Sierra de los Cucapas (Barnard, 1968) included reconnaissance mapping of fault zones and intervening rock types, which outlined a structural and geologic history of the range. Studies of historic seismicity (Hileman, et. al., 1973; Fuis, et. al, 1977) (Mike Reichle, personal communication, 1984) estimated epicentral locations of instrumentally recorded earthquakes in the area. Research into earlier historical earthquake accounts concluded that a major and possibly great earthquake occurred along the Laguna Salada fault zone on February 23, 1892 (Strand, 1980).

Geologic and Tectonic Setting

Deformation within the Salton Trough during the late-Tertiary and Quaternary has been in response to transcurrent and divergent motion between the Pacific and North American plates (Elders and Biehler, 1975; Crowell and Sylvester, 1979; Sharp, 1982). Divergence, or rifting has caused crustal attenuation, normal faulting, volcanism and increased heat flow along the northwest trending axis of the trough (Gastil, 1968; Muffler and White, 1969; Elders, et. al., 1972; Elders and Biehler, 1975; Robinson, et. al., 1976; Brown, 1978; Gastil, et. al., 1979). Transcurrent plate motion has led to major lateral displacements along northwest striking dextral fault zones (Crowell, 1952; 1960; 1962; 1975; Allen, 1957; Sharp, 1967; 1981; Clark, 1972; Clark, et. al., 1972).

The Sierra de los Cucapas consists of a series of tectonic slices of igneous, metamorphic and sedimentary rocks, which are separated by major oblique-dextral and normal fault zones (Barnard, 1968; Gastil, et. al., 1971). The oldest units in the study area are Paleozoic(?) prebatholithic metamorphic rocks comprised largely of well-banded, coarse-grained quartzofeldspathic gneiss and marble. Lesser amounts of biotite rich schist, amphibolite and quartzite are also present (Barnard, 1968). All these units were intruded during the Mesozoic by plutonic rocks of the Peninsular Ranges Province (Barnard, 1968; Gastil, et. al., 1971). The plutonic rocks are composed of coarse-grained biotite tonalite and leucocratic granodiorite.

These pre-Cenozoic igneous and metamorphic rocks have in-turn been partially overlain and/or intruded by Miocene volcanic units consisting of autobreccia flows and dikes. Pliocene and younger sedimentary units are exposed within and along the margins of the Sierra de los Cucapas and make up the bulk of basin fill within Laguna Salada (Dibblee, 1954; Curtis, 1963; Walker, 1967; Walker et. al., 1967; Barnard, 1968).

Deposition of these sediments into Laguna Salada has been dependent on: (1) Pliocene shallow marine incursions from the Gulf of California; (2) the position of the Pleistocene Colorado River Delta; and (3) continual, localized and variable uplift of the ranges which define the edges of the basin (Dibblee, 1954; Walker, 1967; Barnard, 1968). More importantly, deposition in Laguna Salada is controlled by subsidence of the basin itself.

Downwarping and attenuation of the crust underlying Laguna Salada has been generated by pull apart between en echelon, northwest striking, oblique-dextral fault zones. Ongoing extension or pull-apart between the

right-stepping faults has resulted in northeast striking normal faults which connect the northwest striking dextral faults, collectively forming a series of dilational right steps. These have created four northwest-southeast oriented, en echelon sub-basins which define the deep sedimentary fill in Laguna Salada (Figure 3).

Basins or uplifted areas therefore depend on the geometry and interactions of major lateral faults and are usually localized along steps or bends in fault trends (Crowell, 1974a; 1974b; Crowell and Baca, 1979; Dibblee 1977; Fuis, et. al., 1982; 1984). Uplift of the Sierra de los Cucapas has resulted from the complex interactions of a number of major oblique dextral fault zones. South of Mexican Highway 2, these include strands of the Cerro Prieto, Cucapa, Pescadores, Cascabel, Borrego and Laguna Salada faults (Figure 3); (Barnard, 1968; Gastil, 1968).

Although the geomorphic expression of these faults indicates that the level of activity on them has varied during the Quaternary (Barnard, 1968; Mueller, 1984), long-term interactions in a transpressive environment (Sylvester and Smith, 1975) have created crowding and subsequent uplift of intervening crustal slices. Uplift of fault slices is greatest where two bounding zones of oblique-dextral slip converge towards the southeast (Crowell, 1974a; Dibblee 1977,) as is particularly the case between the Pescadores, Borrego and Laguna Salada faults (Figure 3). Although southeasterly divergence is noted between the Cucapa and Pescadores faults, uplift of the area between them may instead be created by interactions between the southeasterly converging Pescadores and Cerro Prieto faults. Also, the Cucapa fault does not appear to have been very active during the late Quaternary based upon the relative lack of

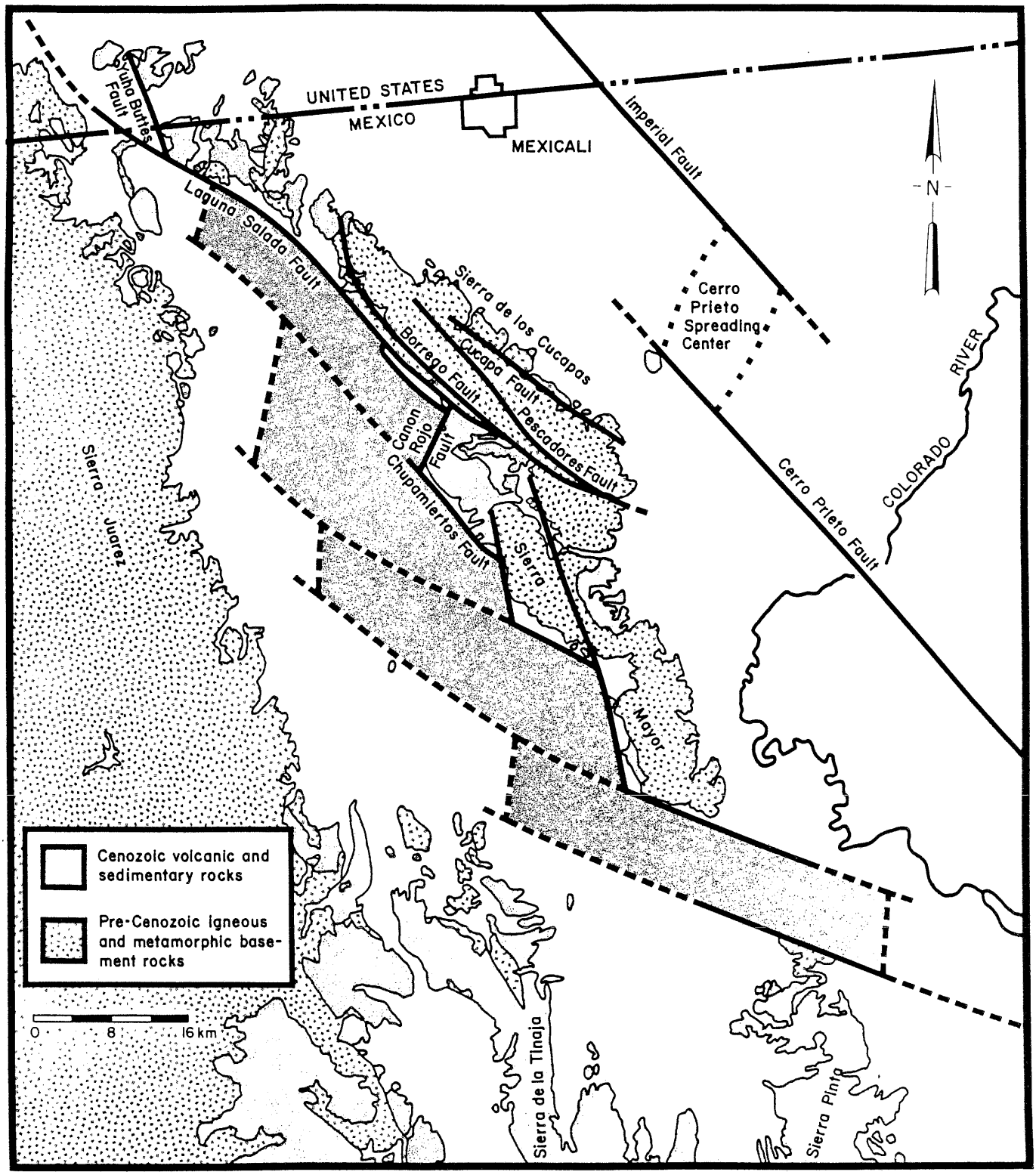

modified from Lomnitz et al., (1970); Gastil et al., (1971); Kelm (1971).

Figure 3. Diagram showing simplified area of basin fill (stippled region) in the Laguna Salada basin which is related to pull-apart between oblique-dextral faults presently visible along the western margins of the Sierra de los Cucapas and Sierra Mayor. Modified from Lomnitz et al. 1970; Gastil et al., 1971; Kelm 1971.

geomorphic indicators of active faulting; therefore, it's effect on the recent uplift of the range is assumed to be negligable.

The strong northwesterly trend of oblique-dextral fault zones in the Sierra de los Cucapas turns in the northern third of the range near Cerro Centinela to more northerly and northeasterly directions (Figure 3) (Barnard, 1968; Gastil, 1968). It is difficult at present to explain this divergence from regional strike, although it appears evident from sedimentological evidence (Barnard, 1968) that the northwestern quarter of the range has been intermittently uplifted throughout the Quaternary, possibly in a transpressive environment. The sense of slip on the fault zones bounding rapidly uplifted blocks in this area is presently unknown. Based on their present orientation, however, they may be oblique-sinistral and conjugate to the dominant, northwest-trending dextral faults developed in the area. Alternatively, these presently northeast-trending faults may have initially existed as northwest trending dextral or north-trending normal faults contained within a block rotated clockwise via simple shear between two bounding dextral-slip faults. These bounding dextral fault zones may have been the northern Laguna Salada fault and another less well defined fault zone adjacent to the northeastern margin of the Sierra de los Cucapas.

Laguna Salada Fault Zone

The central, southwestern margin of the Sierra de los Cucapas provides an excellent opportunity to evaluate the geometry and near surface interactions of deformation within a major oblique-dextral fault zone. This area is doubly important because the zone of deformation

bounds a deep, narrow, elongate stepped basin whose development appears to be directly linked to movement on the Laguna Salada and related faults (Figure 3). Detailed mapping of these faults, and the geomorphic surfaces they have offset, as well as the development of a soil chronosequence, has led to a better understanding of the spacial and temporal constraints of slip along individual fault strands in the area. Several important factors concern this diastrophism and need to be addressed. These include: (1) a description of exposed fault geometries; (2) their possible relationship to deeper crustal fault zones; and (3) the period of time over which they were active. For descriptive purposes, the mouth of each large antecedent stream canyon which cuts the horst formed between the Laguna Salada and Borrego faults is labeled LAS 1 through 7, beginning at the northwestern end of the field area (Figure 4) (plate)

The northern third of the Laguna Salada fault in the study area is directly exposed at the base of the crystalline rangefront and is covered, in part, by lake waters north and south of the large, solitary, alluvial fan formed by streams 1 and 2. This section of the fault zone is marked by a single, straight fault trace with a consistent southwesterly dip of 55 to 60 degrees (Figure 4) (see plate)

The remarkable linearity of this single fault strand is broken slightly where a gentle left step occurs several hundred meters north of stream 1 (Figure 4). This single fault strand has been highly active throughout the late Quaternary and appears to have defined the steep eastern wall of the Laguna Salada basin throughout this time interval.

The simple, straightforward geometry of the range bounding strand begins to change at stream 3 (Figure 4). Here the surficial geometry of

the fault plane steepens to a near vertical orientation. As the fault strand extends to the southeast, its surficial dip direction changes twice from SW to NE and back, suggesting that the fault probably aligns into an approximately vertical zone with depth. Also, southeast of stream 3, this northeastern strand is contained within crystalline rocks of the Sierra de los Cucapas and has only minor structural relief across it. Based on its geometry, the lack of structural relief across it, and laterally deflected streams, this strand has probably had a predominantly lateral sense of slip during the latest Tertiary and Quaternary. Little Holocene offset seems to have occurred on this strand southeast of stream 3 except for very minor (1 meter) down to the northeast slip (Figure 4).

Several hundred meters northwest of stream 3, two large alluvial fault scarps splay off the rangebounding fault strand at a sharp obtuse angle (Figure 4). Southeast of this juncture, latest Pleistocene and Holocene activity along the Laguna Salada fault zone steps to the southwest and is localized along an intermittently preserved line of fault scarps offsetting Holocene alluvial fans. The alluvial scarps strike northeast where they join the range bounding fault zone and begin to strike northerly and northwesterly as they extend southeastward down the rangefront. The more northeasterly of the two alluvial scarps extends down the length of the rangefront until it intersects the Canon Rojo fault zone; the other scarp extends only about 2.5 kilometers southeast of its intersection point with the main rangebounding fault zone (Figure 4). This latter alluvial fault scarp decreases in height to the southeast and appears to die out completely; it does not appear to be simply covered by latest Holocene and historical alluvial deposits (Figure 4).

Minor scarplets offsetting early and mid Holocene alluvial deposits are visible northwest of stream 3 at the alluvial scarp/rangebounding strand intersection (Figure 5). They appear to have been formed by the imperfect transferral of slip across this releasing fault step. Another important aspect of deformation at this releasing or dilational corner includes the backtilting of geomorphic surfaces between the two northeast striking alluvial scarps, possibly indicating a listric nature for them. Also, the vertical rate of slip across these north-northeast striking, predominantly normal faults during the Holocene is probably greater than along the connected northwest striking oblique dextral scarps farther to the southeast. This seems to indicate that extension and stratal rotation are greatest along northeast striking normal faults, perpendicular to the length of the basin.

The eastern limit of thick late Quaternary sedimentary fill in the Laguna Salada basin in probably defined by the single main fault trace northwest of stream 3 and by the southwestern trace as mapped by major alluvial fault scarps offsetting Holocene geomorphic surfaces southeast of stream 3 (Figure 4). These scarps, which offset alluvial deposits, represent the locus of oblique-dextral slip across the width of the fault zone throughout at least the late Quaternary. A record of continual vertical offset across these scarps is visible as a series of progressively offset geomorphic surfaces of increasing late-Quaternary age (Figure 4). The morphology of many of these composite scarps attests to the recency of offset along them (Wallace, 1977; Bucknam and Anderson, 1979); vertical alluvial free faces in loose historical and latest Holocene alluvium are preserved along much of their length (Figure 4), and may have been created by a large magnitude earthquake on February 23,

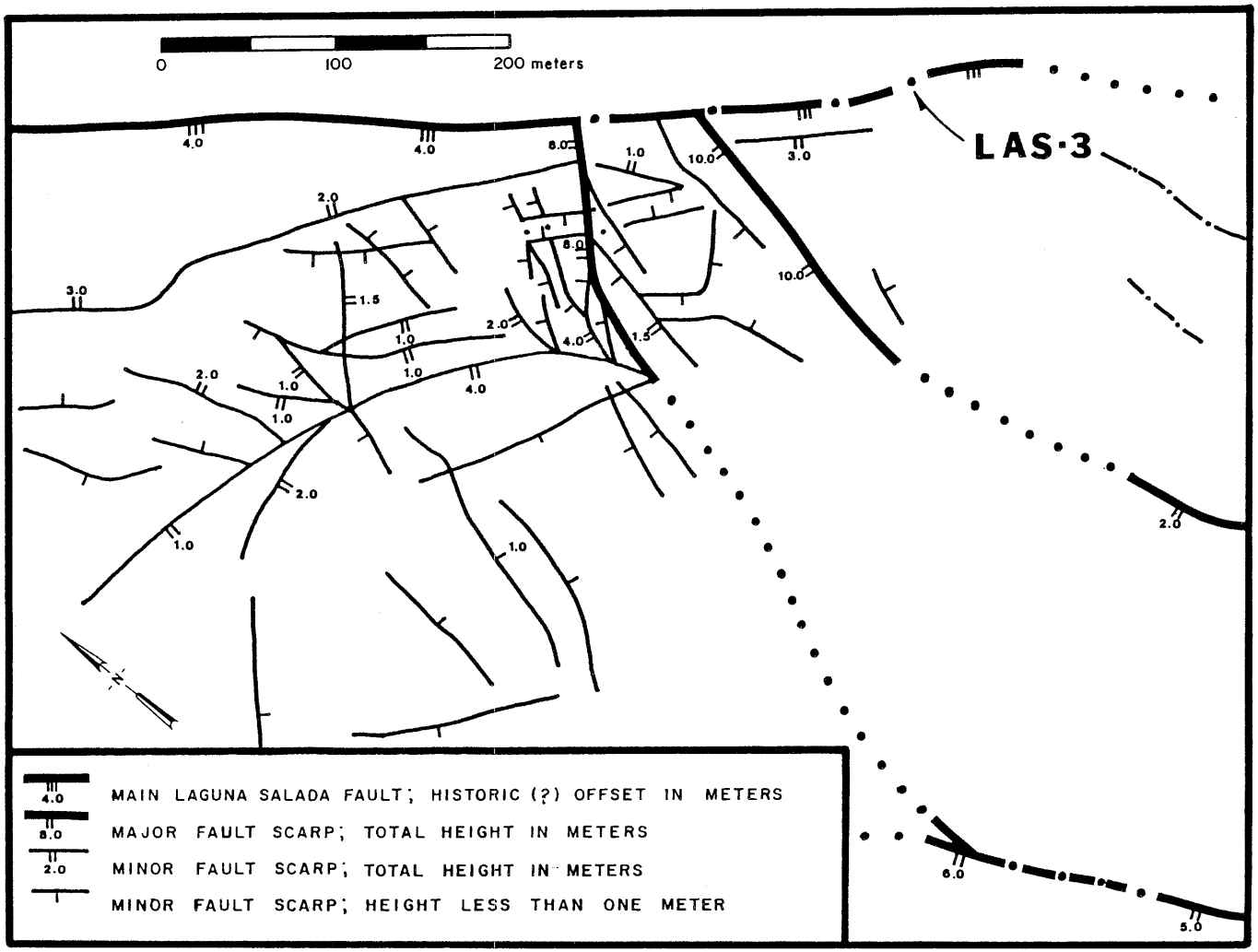

Figure 5. Field sketch of complex faulting offsetting Holocene alluvial deposits adjacent to a releasing right step in the Laguna Salada fault zone (at LAS-3 on Figure 4).

1892 (Strand, 1980). At present there are no known, temporally constrained geomorphic indicators of a lateral component of slip along these scarps (Mueller, 1984); recognition of offset stream channel walls and deflected streams is blurred by the large vertical component of slip across them. Good geomorphic indicators of lateral slip, such as offset walls of stream channels are generally not present because incision occurs only on the upthrown block, with rapid burial and deposition predominating on the down-thrown block. The geometry of the scarps in relation to the Canon Rojo fault along with easily identifiable linear kinematic indicators visible on the recently exposed Laguna Salada fault surface near its juncture with the Canon Rojo fault indicate that the ratio of vertical to horizontal slip along the Laguna Salada fault during the Holocene has been about 1.4:1 (Figure 6).

Although the present level of exposure indicates only two obvious fault strands southeast of stream 3, evidence for a number of others was found in channels incised into Pleistocene fan deposits (Figure 4). Here, individual slices of underlying igneous rocks and bounding gouge zones provided compelling evidence for the penetrative aspect of deformation across the zone. The kilometer wide width of the Laguna Salada fault zone thus contains many individual fault strands, whose periods of activity have varied since the inception of the zone.

The abrupt termination of the oblique-dextral line of fault scarps offsetting late-Quaternary alluvial deposits occurs about 10 kilometers southeast of its intersection with the rangebounding fault strand at stream 3 (Figure 4). This termination marks its intersection with the northeast striking, normal, Canon Rojo fault zone. Striations on the bedrock fault surface of the Canon Rojo fault, exposed during the 1892

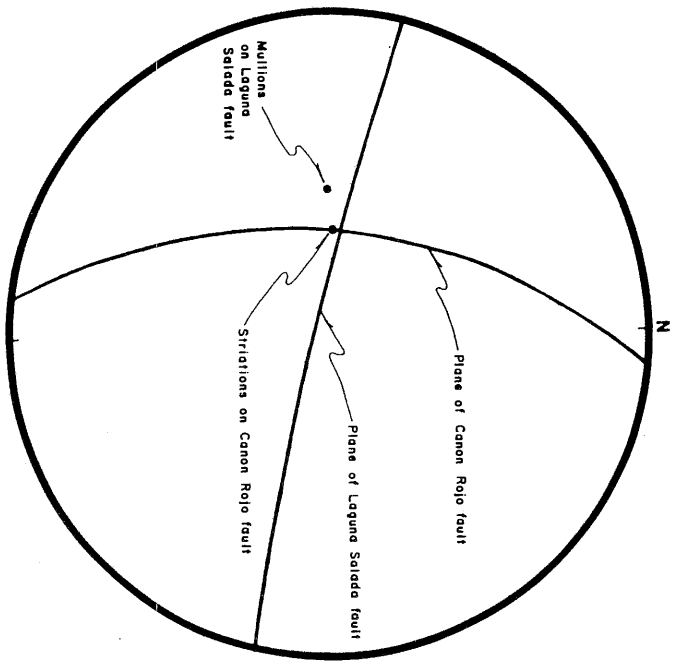

Figure 6. Stereoplot of fault surfaces and associated striations and mullions exposed at the intersection of the active strands of the Laguna Salada and Canon Rojo faults.

earthquake have 90° rakes that indicate the purely normal sense of slip along that fault (Figure 6). An inactive extension of the Canon Rojo fault zone extends another 600 meters to the northeast where it abuts the now inactive, predominantly strike-slip northeastern strand of the Laguna Salada fault zone (Figure 4). Offset alluvial deposits across this short 600 meter section of the Canon Rojo fault zone indicate no more than 140 meters of slip since mid-Pleistocene time. The mullions and striations, respectively visible on the active oblique-dextral Laguna Salada and normal Canon Rojo fault strand and the line formed by their intersection, are all essentially identical in orientation (Figure 6). This then gives a good representation of the late Quaternary direction or slip vector of pull-apart in this portion of the Laguna Salada basin. It also indicates the simple transferral of dextral slip from the Laguna Salada fault across the Canon Rojo fault to the oblique-dextral Chupamiertos fault lying to the southwest (Figure 3).

The morphology of the fault scarps defining this corner indicates that the most recent, possibly historical seismic event ruptured around it and extended approximately 2.5 kilometers to the southwest along the Canon Rojo fault (Figure 4). This geometry is consistent with other active dilational fault jogs within the Salton Trough which indicate that rupture propagation during seismic events is impeded at corners created at fault steps (Sibson, 1986).

Soil Stratigraphy and Slip Rate Estimates

It is possible to separate Holocene from Pleistocene age soils based on their morphological and chemical characteristics, related to variations in the soil forming environment or climate during the late Quaternary. Alluvium isolated from further deposition since the end of the Pleistocene contains soils corresponding to the more arid Holocene

climate. At Laguna Salada, the Holocene soils tend to be an order of magnitude thinner than the Pleistocene soils making for fairly rapid differentiation between the two. The time of this change in climate ranges from 7800-12,000 ybp, based on packrat midden data from the Sonoran and Mojave deserts (Wells, 1976; Van Devender, 1977; Burrows, 1979; Galloway, 1983). The lack of radiocarbon dates from the chronosequence, however, does not permit precise determination of the age of individual Holocene fans and the slip rate estimates, which are based on maximum ages, are therefore minimum rates.

The vertical rate of slip along the Laguna Salada fault zone is greatest where individual strands are oriented normal to the northwest-southeast extensional axis of the basin. The largest recorded scarps, located several hundred meters northwest of stream 3, display a minimum Holocene offset of 18 meters, and thus a minimum vertical slip rate of 1.5-2.3 mm/yr. Calculation of the lateral slip rate along the fault zone is not well-defined since the high vertical component of slip accelerates erosion of stream terrace and alluvial fan edges, or geomorphic piercing points. However, because the direction of Holocene slip at the junction of the Laguna Salada and Canon Rojo faults is well-defined, inferences can be drawn about the minimum lateral slip rate along the active Laguna Salada strand, based on the measured vertical displacement. Thus, the minimum lateral rate of Holocene slip along this strand 1.7 km northwest of the Canon Rojo fault is 0.70 ± 0.15 mm/yr based on 9.0 meters of vertical displacement and a slip vector of 54°, $N84^{\circ}W$. The corresponding minimum vertical slip rate at this point is 1.0 ± 0.2 mm/yr. It should be emphasized that the calculated slip rates are

minimums and should not be considered absolute; offset geomorphic surfaces may actually be as much as several times younger than the single 7,800 - 12,000 ybp age constraint.

Basin development

Basin development within Laguna Salada appears to be intimately related to the active oblique-dextral and normal fault zones exposed along the western margins of the Sierra de los Cucapas and Sierra Mayor. Gravity studies by Kelm (1971), using detailed gravity data (Figure 7), interpreted these faults to define the very steep northeastern walls of the basin. The southwestern side of the basin appears to be formed in analogous manner, although the faults defining it do not have a surficial representation due to repeated late Holocene inundation, except those farther to the south which define the northern end of the Sierra Pinta (Gastil, 1968; McEldowney 1970).

The sense of slip as provided by these bounding fault zones and the geophysically inferred shape of deep sedimentary fill in Laguna Salada leads to the suggestion that the basin has been created by extension or pull-apart between right-stepping oblique-dextral fault zones (Figure 7). Four individual sub-basins, have been delineated and have apparently coalesced with ongoing strike-slip to form a single, surficially continuous basin during at least the late Quaternary.

The depth of sedimentary fill within the northernmost sub-basin has been geophysically inferred to exceed five kilometers (Figure 8a) (Kovach et. al., 1962; Biehler, et. al., 1964; Kelm, 1971). Fill within the other three pull-aparts differs (based on gravity data) and may be due to either variable amounts of extension within individual sub-basins or the

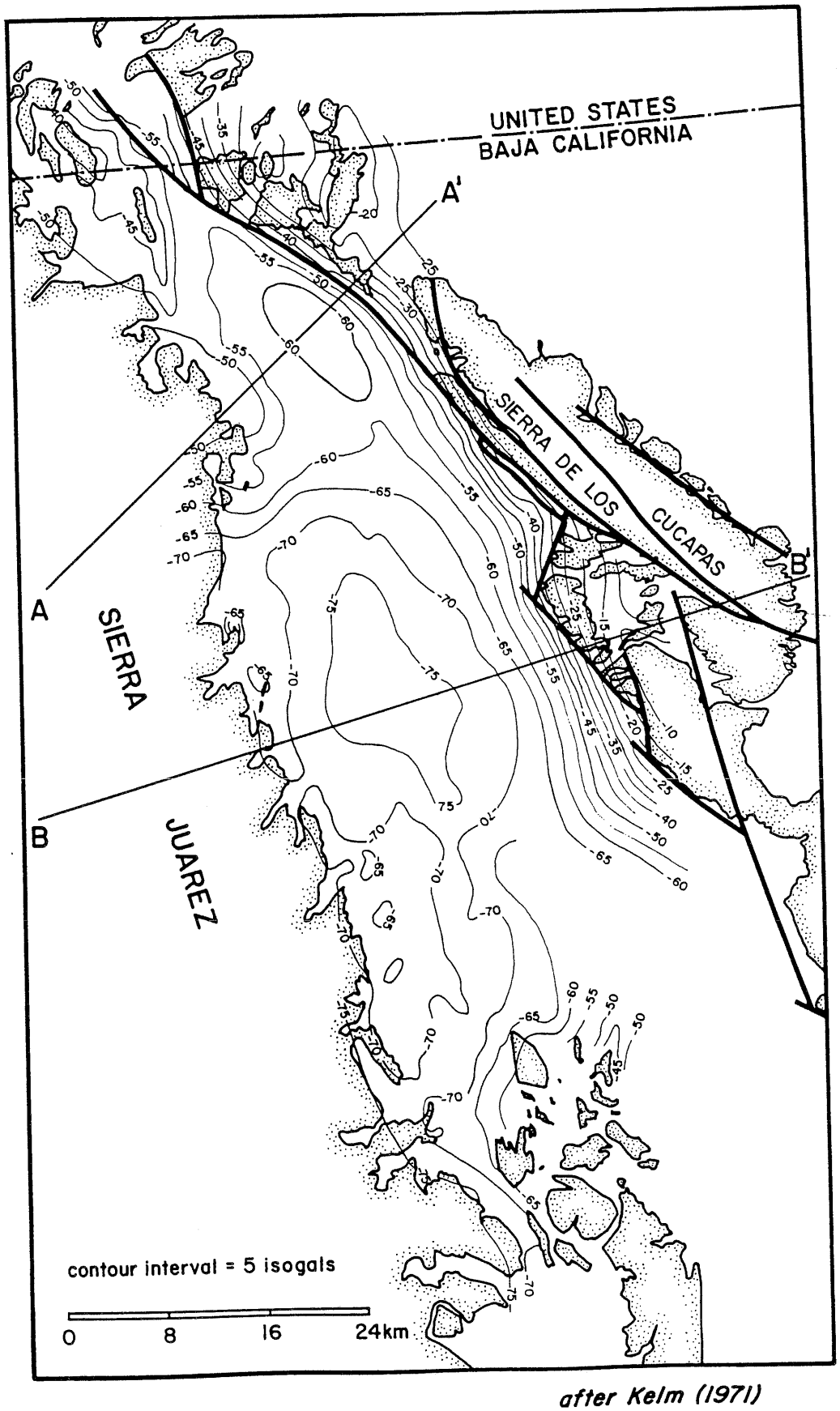

Figure 7. Gravity map from Kelm, 1971 showing en-echelon gravity lows in the Laguna Salada basin.

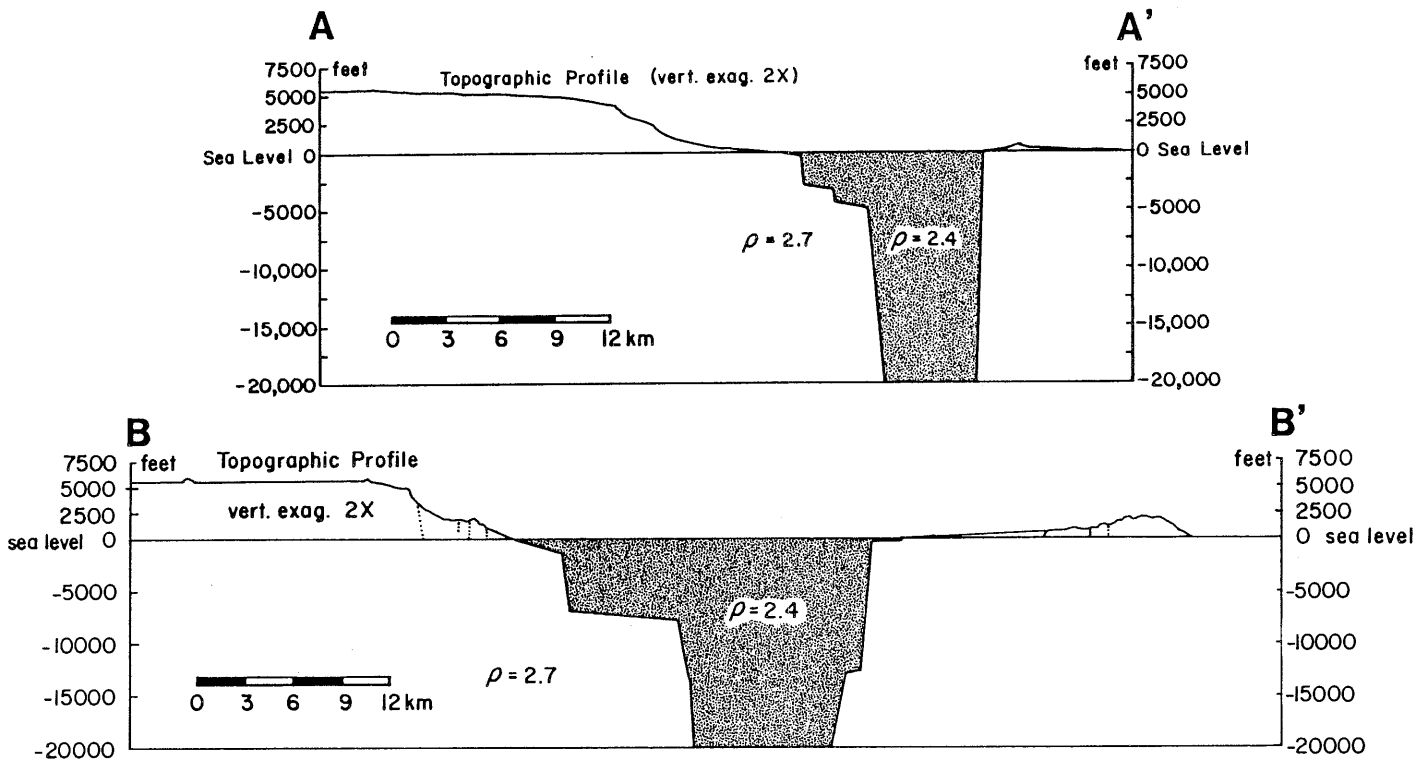

after Kelm (1971)

Figure 8a. Cross section from Kelm, 1971 showing basin shape derived from gravity data in the northern Laguna Salada basin. 8b Cross section from Kelm, 1971 showing basin shape derived from gravity data in the central Laguna Salada basin (section cuts across two coalesced pull-aparts; see Figure 7 for section locations). These cross-sections, derived from gravity surveys provide only a gross picture of basin shape in this area. Additional subsurface data should provide a more detailed picture of basin gravity, itself a product of complex, long term fault interactions along Laguna Saladas eastern margin.

specific manner in which extension was accommodated (Figure 8b). Based on the deep and elongate, highly evolved shape of individual sub-basins (Mann, et. al., 1983) the cumulative amount of dextral slip along the northwest striking oblique-dextral faults is considerable, possibly on the order of several tens of kilometers.

Although little is known about the early development of the Laguna Salada basin, the late Quaternary history of slip along the basins eastern margin is better constrained. Inferences can therefore be drawn about the late Quaternary basin development of this portion of Laguna Salada based on the geomorphic evidence of faulting activity in the study area.

Latest Pleistocene and Holocene slip across the Laguna Salada fault zone indicates active pull apart and basin subsidence, centralized along the Canon Rojo fault zone. This differs from previous ideas of pull-apart basin development which viewed extension as being localized in the center as opposed to one end of the basin (Crowell, 1974b; Mann, et. al., 1983). This style of faulting has not been constant throughout the late Quaternary, however. Geomorphic evidence for a late(?) Pleistocene cessation in vertical uplift across both the Laguna Salada and Canon Rojo faults is provided by extensive lacustrine terrace development across the footwall blocks of both fault zones (Figure 4). A substantial period of time is believed to have been required to cut these terraces, considering the material they cut across and their width. The cessation of vertical uplift may have been created by either a period of pure strike-slip along the Laguna Salada fault zone with little transferral of dextral slip across the Canon Rojo fault to the Chupamiertos fault (Figure 9); or an extended seismic gap along the Laguna Salada fault.

Prior to this period, pull-apart was probably active for much of the Pliocene and early Pleistocene, based on the steep range front of the

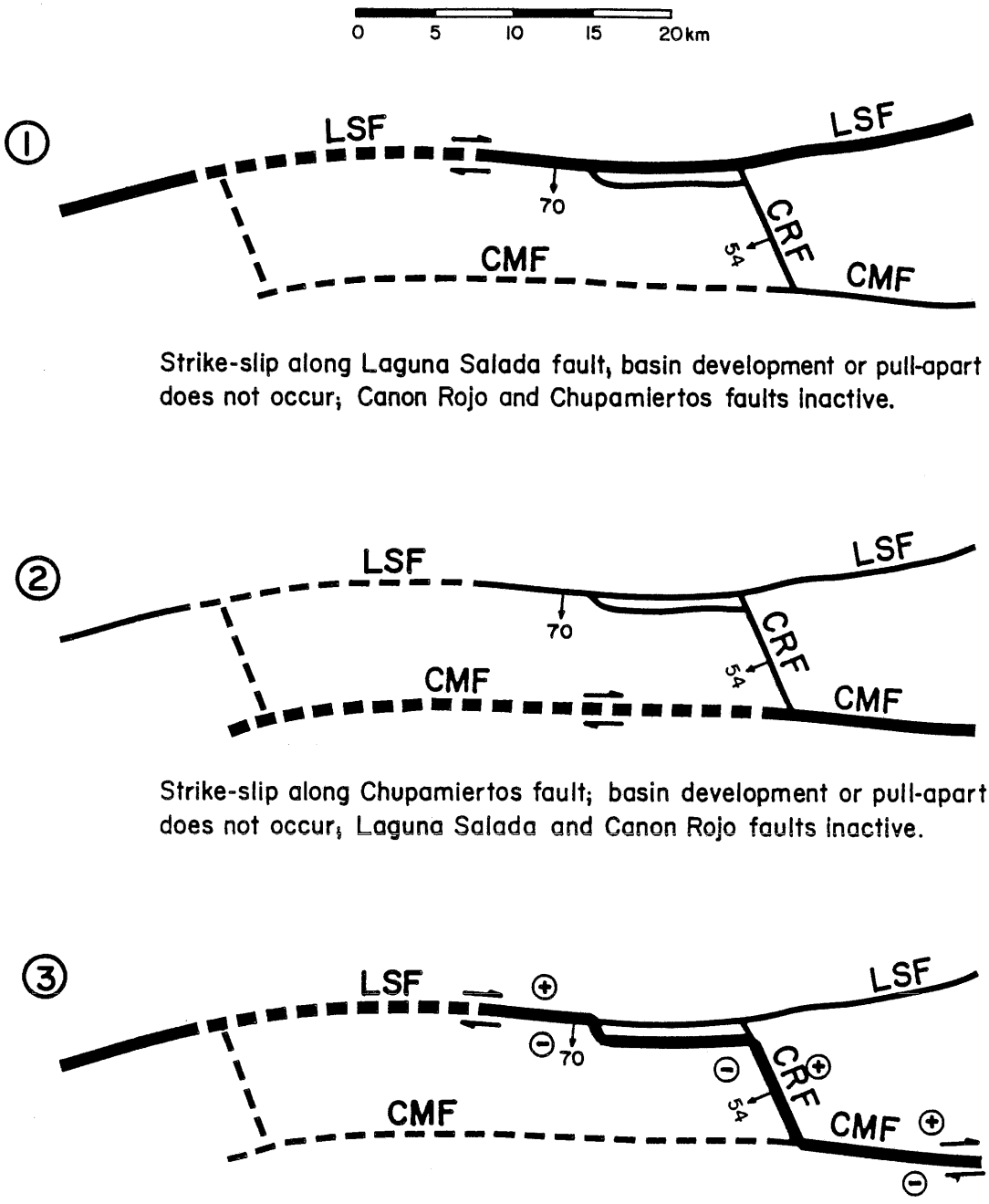

Figure 9. Diagram relating possible scenarios of faulting activity in the northernmost pull-apart and its affect on the late Quaternary basin development in that section of Laguna Salada.

Sierra de los Cucapas, and the depth of fill and the length of the individual sub-basins in Laguna Salada. Fault generated petrofabrics presently exposed along some sections of the range-bounding fault zone north of stream 3 may have been created at an upper mid-crustal level and thus also indicate a long history of oblique dextral slip. Therefore, basin development appears to be intermittent and is dependent upon the rates and senses of slip along bounding oblique-dextral fault zones.

Considering the amount of extension required to form the coalesced pull-apart basins in Laguna Salada, underlying crust of continental (Peninsular Ranges Province) affinity may have been thinned or attenuated. This may account for the extremely high heat flow in the basin, currently being defined by the drilling of geothermal exploration wells by the Mexican government. Laguna Salada therefore may be a precursor to the more highly evolved Imperial and Mexicali Valleys and may eventually experience enough crustal attenuation to initiate spreading and the formation of crust of an oceanic affinity.

The evolution of Laguna Salada and its relationship to the rest of Salton Trough (i.e., the Imperial and Mexicali Valleys) may provide some insight into the ongoing deformation within the Gulf of California. Ongoing widening and development of the Salton Trough has isolated individual blocks of continental affinity (i.e., the Sierra de los Cucapas). The mechanism of branching rifts or pull-aparts (i.e., the Mexicali Valley and Laguna Salada basin) may therefore be an intrinsic part of rift development as widening oceanic crust "captures" and assimilates enclosed continental crust.

REFERENCES

Alexander, E.B., and Nettleton, W.D., 1977, Post-mazama natrargids in Dixie Valley, Nevada: Soil Sciences, v. 41, p. 1210-1212.

Allen, C.R., 1957, San Andreas fault zone in San Gorgonio Pass, Southern California: Geological Society of America Bulletin, v. 68, p. 315-350.

Barnard, F.L., 1968, Structural geology of the Sierra de los Cucapas, Northeastern Baja California, Mexico and Imperial County, California (Ph.D. dissert.): Boulder, Colorado, University of Colorado at Boulder, 157 p.

Beal, C.H., 1948, Reconnaissance of the geology and oil possibilities of Baja California, Mexico: Geological Society of America Memoir 31, 138 p.

Biehler, S., Kovach, R.L., and Allen, C.R., 1964, Geophysical framework of northern end of Gulf of California strucutural province, in van Andel, T. H., and Shor, G., eds. Marine geology of the Gulf of California: American Association of Petroleum Geologists Memoir 3, p. 126-143.

Bischoff, J.L., Merriam, R., Childers, W.M., and Protsch, R., 1976, Antiquity of man in America indicated by radiometric dates on the Yuha burial site: Nature, v. 261, p. 128-129.

Brown, L.G., 1978, Recent fault scarps along the eastern escarpment of the Sierra San Pedro Martir, Baja California (M.S. Thesis): San Diego, California, San Diego State University, 108 p.

Bucknam, R.C., and Anderson, R.E., 1979, Estimation of fault-scarp ages from a scarp-height-slope-angle relationship: Geology, v. 7, p. 11-14.

Burrows, C.J., 1979, A chronology for cool-climate episodes in the Southern Hemisphere 12,000-1,000 yr. B.P.: Palaeogeography, Palaeoclimatology, Palaeoecology, v. 27, p. 287-347.

Clark, M.M., 1972, The Borrego Mountain earthquake of April 9, 1968: United States Geological Survey Professional Paper 787, p. 55-86.

Clark, M.M., Grantz, A., and Rubin, M., 1972, Holocene activity of the Coyote Creek fault as recorded in sediments of Lake Cahuilla: United States Geological Survey Professional Paper 787, p. 112-1300.

Crowell, J.C., 1952, Probable large lateral displacement on the San Gabriel fault, southern California: American Association of Petroleum Geologists Bulletin, v. 36, p. 2026-2035.

Crowell, J.C., 1962, Displacement along the San Andreas fault, California: Geological Society of America Special Paper no 71, 61 p.

Crowell, J.C., 1974a, Sedimentation along the San Andreas fault, California, in Dott, R.J., Jr., and others, eds., Modern and ancient geosynclinal sedimentation: Society of Economic Paleontologists and Minerologists Special Publication no. 19, p. 292-303.

Crowell, J.C., 1974b, Origin of late Cenozoic basins in southern California, in Tectonics and Sedimentation: Society of Economic Paleontologists and Minerologists Special Publication no. 22, p. 190-204.

Crowell, J.C., 1975, The San Andreas fault in southern California, in Crowell, J.C., ed., San Andreas fault in southern California: California Division of Mines and Geology, Special Report 118, p. 7-27.

Crowell, J.C., and Baca, B., 1979, Sedimentation history of the Salton Trough, in Crowell, J.C., and Sylvester, A.G., eds., Tectonics of the juncture between the San Andreas fault system and the Salton Trough, southeastern California: Guidebook for the Annual Geological Society of America meeting, San Diego, California, p. 101-110.

Crowell, J.C., and Sylvester, A.G., 1979, Introduction to the San Andreas-Salton Trough Juncture, in Crowell, J.C., and Sylvester, A.G., eds., Tectonics of the juncture between the San Andreas fault system and the Salton Trough, southeasternn California: Guidebook for the Annual Geological Society of America meeting, San Diego, California, p. 1-14.

Curtis, C.M., 1963, Sedimentology of the northern half of the Laguna Salada, Baja California (M.S. Thesis): Los Angeles, California, University of Southern California, 191 p.

Dibblee, T.W., Jr., 1954, Geology of the Imperial Valley region, California, in Geology of Southern California: California Division of Mines Bulletin, v. 1, p. 21-28.

Dibblee, T.W., Jr., 1977, Strike-slip tectonics of the San Andreas fault and its role in Cenozoic basin development: in Late Mesozoic and Cenozoic Sedimentation and Tectonics in California: San Joaquin Geological Society Short Course, p. 26-38.

Elders, W.A., Rex, R.W., Meidav, T., Robinson, P.T., and Biehler, S., 1972, Crustal spreading in southern California: Science, v. 178, p. 15-22.

Elders, W.A., and Biehler, S., 1975, Gulf of California rift system and its implications for the tectonics of western North America: Geology, v. 3, p. 85-87.

Fuis, G.S., Friedman, M.E., and Hileman, J.A., 1977, Preliminary catalog of earthquakes in southern California, July 1974-September 1976: United States Geological Survey Open File Report 77-181, 107 p.

Fuis, G.S., Money, W.D., Healey, J.H., McMechan, G.A., and Lutter, W.J., 1982, Crustal structure of the Imperial Valley region, United States Geological Survey Professional Paper 1254, p. 25-50.

Fuis, G.S., Mooney, W.D., Healy, J.H., McMechan, G.A., and Lutter, W.J., 1984, A seismic refraction survey of the Imperial Valley Region, California: Journal of Geophysical Research, v. 89, no. B2, p. 1165-1189.

Galloway, R.W., 1983, Full glacial southwestern United States, mild and wet or cold and dry: Quaternary Research, v. 19, p. 236-248.

Gastil, R.G., 1968, Fault systems in northern Baja California and their relation to the origin of the Gulf of California, in Dickinson, W.R., and Grantz, A., eds., Proceedings in a conference on geologic problems of the San Andreas fault system: Stanford University Publications in Geological Sciences, v. 11, p. 283-286.

Gastil, R.G., Phillips, R.P., and Allison, E.C., 1971, Reconnaissance geologic map of the State of Baja California: Geological Society of Americia Memoir 140, 170 p.

Gastil, G., Krummenacher, D., and Minch, J., 1979, The record of Cenozoic volcanism around the Gulf of California: Geological Society of America Bulletin, v. 90, p. 839-857.

Gile, L.H., 1975, Holocene soils and soil-geomorphic relations in an arid region of southern New Mexico: Quaternary Research, v. 5, p. 321-360.

Gile, L.H., Peterson, I.F., and Grossman, R.B., 1960, Morphological and genetic sequences of carbonate accumulation in desert soils: Soil Science, v. 101, p. 347-360.

Gile, L.H., and Grossman, R.B., 1968, Morphology of the argillic horizon in desert soils of southern New Mexico: Soil Science, v. 106, p. 6-15.

Hileman, J.A.,, Allen, C.R., and Nordquist, J.M., 1973, Seismicity of the southern California region, 1 January 1932 to 31 December 1972: Seismological Laboratory of the California Institute of Technology, Pasadena, 486 p.

Kelm, D.L., 1971, A gravity and magnetic study of the Laguna Salada area, Baja California, Mexico (M.S. thesis): San Diego,California, San Diego State University, 103 p.

Kovach, R.L., Allen, C.R., and Press, F., 1962, Geophysical investigation of the Colorado Delta region: Journal of Geophysical Research, v. 67, p. 2845-2871.

Lindgren, W., 1888, Notes on the geology of Baja California, Mexico, California Academy Science Proceedings, second series, v. 1, p. 173-196.

Lomnitz, C., Mooser, F., Allen, C.R., Brune, J.N., and Thatcher, W., 1970, Seismicity and tectonics of northern Gulf of California region, Mexico, Preliminary results: Geofisica Internacional, v. 10, no. 2, p. 37-48.

Mann, P., Hempton, M.R., Bradley, D.C., and Burke, K., 1983, Development of pull-apart basins: Journal of Geology, v. 91, 250 p. 529-554.

McEldowney, R.C., 1970, Geology of the northern Sierra Pinta, Baja California, Mexico (M.S. Thesis): San Diego, California, San Diego State University, 74 p.

Mueller, K.J., 1984, Neotectonics, Alluvial History and Soil Chronology of the southwestern margin of the Sierra de los Cucapas, Baja California Norte (M.S. Thesis): San Diego, California, San Diego State University, 363 p.

Muffler, L.J.P., and White, D.E., 1969, Active metamorphism of upper Cenozoic sediments in the Salton Sea geothermal field and the Salton Trough, southeastern California: Geological Society of America Bulletin, v. 80, no. 2, p. 157-181.

Robinson, P.T., Elders, W.A., and Muffler, L.J.P., 1976, Quaternary volcanism in the Salton Sea geothermal field, Imperial Valley, California: Geological Society of America Bulletin, v. 87, no. 3, p. 347-360.

Schlemon, R.J., 1976, Quaternary soil stratigraphy, southeastern Mojave Desert, California and Arizona, in Mahaney, W.C., ed., Quaternary Soil Symposium: York University, Toronto, p. 53-56.

Schlemon, R.J., and Purcell, C.W., 1976, Geomorphic reconnaissance, southeastern Mojave Desert, California and Arizona: San Diego Gas and Electric Company Early Site Review Report Sundesert Nuclear Power Project, Appendix 2.5 M, San Diego, Californiaa.

Sharp, R.V., 1967, San Jacinto fault zone in the Peninsular Ranges of southern California: Geological Society of America Bulletin, v. 788, p. 706-730.

Sharp, R.V., 1981, Variable rates of late Quaternary strike slip on the San Jacinto fault zone, southern California: Journal of Geophysical research, v. 86, no. B3, p. 1754-1762.

Sharp, R.V., 1982, Tectonic setting of the Imperial Valley Region: United States Geological Survey Professsional Paper 1254 p. 5-14.

Sibson, R.H., 1986, Rupture interaction with fault jogs: American Geophysical Union, Geophysical Monograph No. 37, p. 157-167.

Strand, C.L., 1980, Pre-1900 earthquakes of Baja California and San Diego County (M.S. thesis): San Diego, California, San Diego State University, 320 p.

Van Devender, T.R., 1977, Holocene woodlands in the southwestern deserts: Science, v. 198, no. 4313, p. 189-192.

Walker, T.R., 1967, Formation of red beds in modern and ancient deserts: Geological Society of America Bulletin, v. 78, p. 353-368.

Walker, T.R., Ribbe, P.H., and Honea, R.M., 1967, Geochemistry of hornblende alteration in Pliocene red beds, Baja California, Mexico: Geological Society of America Bulletin, v. 78, p. 1055-1060.

Wallace, R.E., 1977, Profiles and ages of young fault scarps, northcentral Nevada: Geological Society of America Bulletin, v. 88, p. 1267-1281.

Wells, P.V., 1976, Macro fossil analysis of wood rat (Neotoma) middens as a key to the Quaternary vegetational history of arid America: Quaternary Research, v. 6, p. 223-248.

HOLOCENE ACTIVITY OF THE ELSINORE FAULT IN THE COYOTE MOUNTAINS SOUTHERN CALIFORNIA

by

Thomas Rockwell
With Field Assistance From Andy Thomas and Greg Unruh
San Diego State University
San Diego, CA 92182

INTRODUCTION

The Elsinore-Laguna Salada fault zone can be divided into a number of discrete segments based on the continuity of strands within a reach of the fault zone as well as termination of strands at major steps or jogs (Figure 1)(Wesnousky, 1986; Rockwell, 1987 or 1988). The Coyote Mountain reach is the southernmost segment of what is mapped as the Elsinore fault zone, with the Laguna Salada fault beginning just north of the U.S./Mexico international border and continuing southeastward into northern Baja California. The region between the Coyote Mountain and Laguna Salada strands is characterized by a complex system of northeast-trending cross faults (Rockwell and others, this volume) which display left-lateral separation and slip. To the northwest, the Coyote Mountain segment ends where it steps left across the front of the Tierra Blanca Mountains. This northern end is also in an area of intersecting northeast-trending faults.

The youthfulness of faulting along the Elsinore fault in the Coyote Mountains has been known for some time based on the recognition of abundant geomorphic indicators of recent activity such as sags, shutter and pressure ridges, deflected and offset drainages, hillside benches and scarps in canyon bottom alluvium (Clark, 1975). Pinault (1984) and Pinault and Rockwell (1984) demonstrated that many of these displaced features are Holocene in age based on the relative expression of the soil profiles developed in those deposits in comparison to dated deposits in other arid regions. That work has now been continued with a detailed study of the soils in the Alverson and Fossil Canyon areas (Goodmacher and Rockwell, this volume; Goodmacher, M.S. thesis in prep.), and it is clear that the youngest displaced deposits are late Holocene in age. Work continues on better resolving the age of the displaced Holocene and Pleistocene deposits using a combination of ^{14}C dates on pedogenic carbonate (samples have been submitted), Thermoluminescence (TL) dating of fissure fillings in the fault zone (with Steve Foreman), and cation ratio dating of the rock varnish (with Charles Harrington at Los Alamos).

Pinault and Rockwell (1984) and Rockwell and Pinault (1986) also suggested that the past several earthquakes along the Coyote Mountain segment produced an average of about 1.5 m of strike- slip in the Alverson Canyon area. Their work was focused along a 1 km

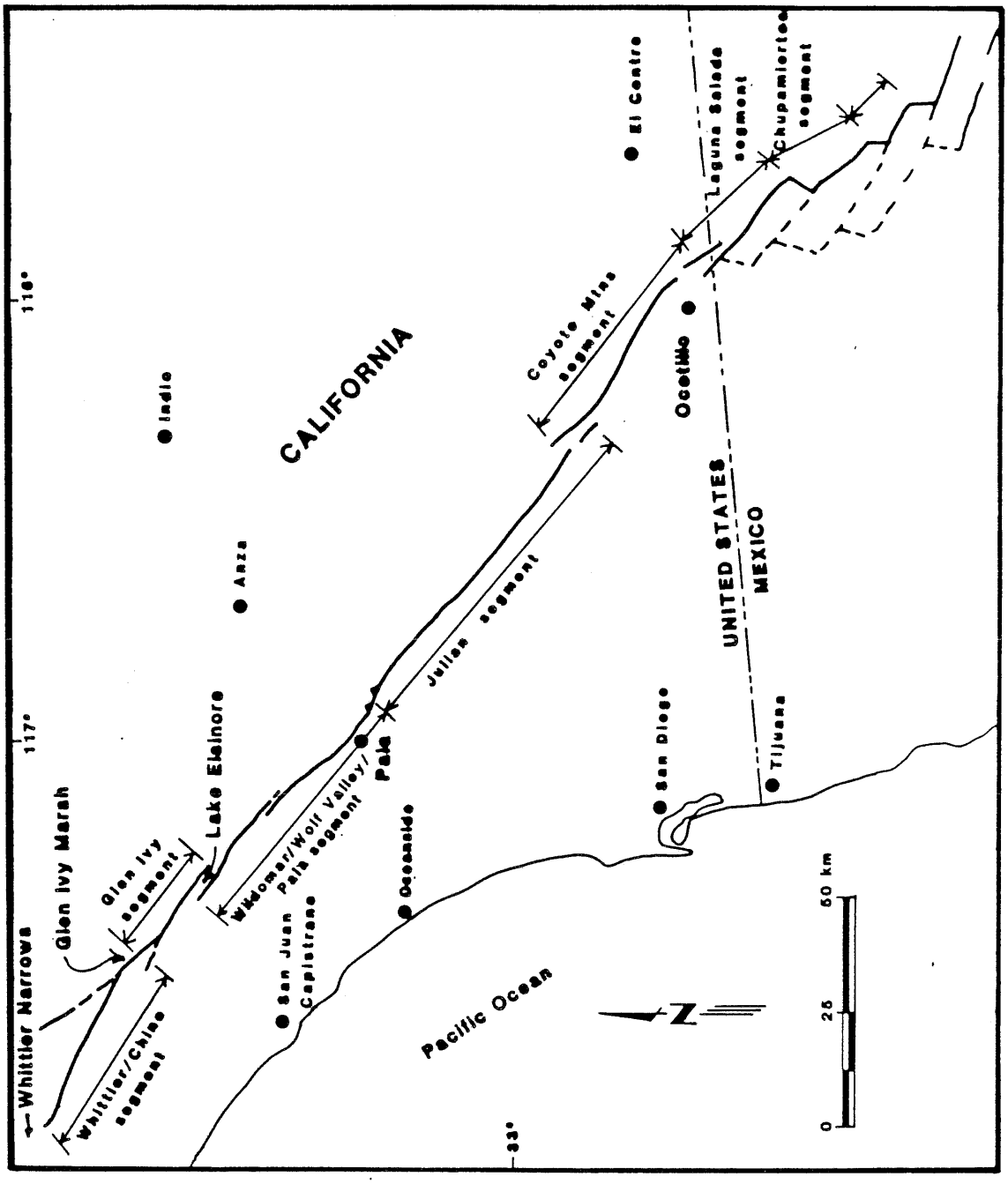

Figure 1. Map showing fault segments along the Elsinore fault zone.

section of the fault where they measure several dozen offset geomorphic features (channels, alluvial bars, channel walls, erosional headscarps, rills, and talus cones) and grouped the offsets by magnitude of displacement. Further work in separating the late Holocene deposits based on their soil development, pavement development and varnish development now allows for the delineation of deposits of similar age in the many different canyon bottoms along much of the length of the fault. Therefore, it is now possible to directly measure displacements of similar age along much of the length of the Coyote Mountains and to determine the distribution of slip for the past several earthquakes where evidence is preserved.

The focus of this paper is on the new mapping that has been done to resolve displacement per event for the Coyote Mountain segment. The fault zone was field mapped on aerial photographs at a scale of 1:5000 (1 inch = about 400 feet), thus allowing for fairly great detail. These data were then transferred to a 1:12000 scale topographic map (Plate 1). The mapping provides the data base for the conclusions presented here. The next step will be to make large scale topographic maps of many of the offset features by surveying with a Wild Total Station, which will be completed prior to final publication. Thus, the field measurements presented in this paper should be considered preliminary, although they are not expected to vary much (< 10%) from the final results.

STRUCTURAL CHARACTERISTICS

The character of faulting along most of the length of the Coyote Mountain segment is dominantly transpressive (Plate 1), probably due largely to the more westerly trend of this part of the Elsinore fault (Fig. 1). The fault generally dips shallowly to steeply to the north, although southerly dips are locally present along the southeastern portion of the segment. Several major strands comprise the Coyote Mountain segment, and either step or bend left (restraining jog) along the range front. A vertical (reverse) component of faulting usually is present in areas where the fault makes a substantial step or bend, but in all cases the horizontal component of slip is dominant by a factor of five or more. Along the straighter reaches of the fault, the slip is almost entirely horizontal with areas of minor valley-side-up separation (normal or reverse depending on the fault dip) locally present.

For most of the length of the Coyote Mountains, each major substrand is, in turn, comprised of multiple, closely spaced active fault strands. Where there are only one or two active strands present, and they are within a couple of meters of each other, it was usually possible to measure the displacement on individual channel features (alluvial bar or channel) across both strands. For over half of the length of this segment, several active substrands are present (three or more), and these may be up to several tens of meters apart. Thus, the fault slip is distributed in these areas and displacement measurements were generally low for individual events.

The minor, mountain-side up vertical component of slip measured for much of the length of the Coyote Mountains is consistent with the physiographic expression of the range. Sediments of the Miocene/Pliocene Imperial Formation are present in the highest parts of the range (Christianson, 1957) and attest to substantial longterm uplift. Nevertheless, it is clear from the mapping of the active strands that the strike-slip component is far larger than the dip-slip component and that vertical slip along this segment of the Elsinore fault zone is due primarily to the local trend of the fault.

One interesting aspect of the deformation in the Coyote Mountains is that although the range has sustained substantial Quaternary uplift, the sediments of the Imperial Formation are not strongly folded. Rather, the overlying sedimentary cover has ridden on the underlying crystalline rocks which have behaved brittlely. Thus, both the Paleozoic-Mesozoic basement rocks and the overlying Miocene and Pliocene units are complexly faulted and only openly folded, even where the mechanical characteristics of the Mio-Pliocene sediments would favor a more plastic deformational style (such as the thick mudstone section of the Imperial Formation). Conversely, southwest of the Elsinore fault, sediments of the Imperial and Palm Spring formations are strongly folded near the fault. This may be due to either decoupling from the basement at depth or a much thicker sedimentary section south of the fault or both.

SUMMARY OF THE CHRONOLOGY USED IN DETERMINING SLIP DISTRIBUTION

With the recognition and delineation of several distinct late Holocene deposits within many of the major canyon bottoms, it is possible to identify and measure displacements on deposits or features of similar age. For this study, the terminology will follow that of Goodmacher and Rockwell (this volume) where Q1 are modern channel deposits and Q2 through Q7 are deposits of increasing age. The Q1-Q4 deposits are all Holocene in age whereas the Q5-Q7 are Pleistocene. Another unit (or two) was recognized in the central part of the range as having been deposited between the deposition of the Q4 and Q5 deposits (based on soil and varnish development), and that unit is designated as Q4-5.

The Q2 deposits are very late Holocene in age and are chemically indifferentiable (as determined from laboratory analysis) from the Q1 deposits, although there is a minor accumulation of secondary carbonate visible in field exposures. They are distinguished by a very weak and indistinct patina or coloration developed on the clast surfaces. Chuck Harrigton and I were unable to find any clasts with recognizable varnish in hand samples but the clasts do exhibit coloration, presumably due to minor surface oxidation and incipient varnish formation. In all cases, the Q2 deposits are faulted where they are present across the active fault strands.

Similarly, the Q3 deposits cannot be distinguished from modern alluvium based on chemical analysis, nor is there significant difference between the soil characteristics of the Q2

and Q3 deposits. However, clasts on the Q3 surfaces have distinctly more coloration than those of the Q2 deposits, and there is a recognizable (although weak) varnish.

The Q4 deposits have distinct, although weak, calcic horizons and some clasts on the surface have a substantial varnish (still considerably less so than the older deposits). A preliminary TL date on a fissure filling associated with the 3rd or 4th slip event back (post Q4) yielded a preliminary age of 2000±500 years (1 sigma)(Steve Foreman, oral communication) which should approximate a minimum age for this deposit. The maximum age is about one recurrence interval older, or about 3 ka, assuming the TL date to be valid. At this point, however, it should be noted that this is preliminary data.

Similarly, the Q4-5 deposits exhibit still better varnish and soil characteristics. In all of the above deposits, the original bar and swale topography is well-preserved on the surface and only the Q4-5 surfaces are beginning to show any degradation or smoothing.

Q5 surfaces have substantial varnish formation and are showing significant smoothing of the bar and swale topography. The soils developed in the Q5 deposits have Stage I+ to II calcic horizons with carbonate clearly deeper than the present (Holocene) maximum depth of wetting. These characteristics, along with their other soil properties suggest a late Pleistocene age (Goodmacher and Rockwell, this volume).

The Q6 and Q7 deposits are readily distinguished by their surface morphology (nearly flat), stage II+ and stage III carbonates (respectively), and other soil characteristics (see Goodmacher and Rockwell, this volume). An interesting feature to point out is that clasts on the Q6 surface are well-varnished whereas clasts on the Q7 surface (as well as older, Q8, surfaces farther up the range to the northwest) appear to have been sandblasted smooth and a second generation of varnish has now formed. It is not clear what to attribute this factor to, but it appears to be consistent on all Q7 and Q8 surfaces that have been examined. Speculatively, the Q7 and Q8 deposits are all pre-last interglacial (consistent with their soil morphology and characteristics) and the sandblasting occurred during the last interglacial when conditions were dryer and sand may have been easily mobilized.

RECOGNITION OF INDIVIDUAL EVENTS AND ESTIMATION OF THEIR SLIP DISTRIBUTION AND SIZE

With the above chronology, the entire length of the fault along the Coyote Mountains was mapped and displacements of deposits were measured according to their relative age (Plate 1). No Q1 deposits were noted as being offset whereas all Q2 and older deposits were, where they crossed active strands of the fault. Mapping of the offset features based on their relative age allows, then, for a direct assessment of slip distribution as a function of the age of displaced deposits.

Nearly a hundred displacements of alluvial features were

measured in the field on the various fault strands (Plate 1). It was found that in virtually all areas of several active fault strands, measured slip is lower than along the straighter, simpler reaches of the fault, even when slip across substrands is summed (Figure 2). Also, there is low slip along the fault where their is a substantial thrust component. This latter aspect may be due to either complex strain release in areas of thrusting (coseismic folding of the bedrock) or masking of the strike-slip by the vertical component. In either case, the recognizable surface slip is not believed to represent slip at depth.

Lateral slip reaches a maximum of about 2.8 m for the most recent event (Event 1; in Q2 deposits) in the central portion of the range. This is considerably more than that estimated by Rockwell and Pinault (1986) near Alverson Canyon where slip is only about 1.5 m. The magnitude of lateral slip decreases farther to the northwest to below a meter near Canon Sin Nombre. Displacement of Q2 deposits could not be clearly recognized farther to the northwest towards the Tierra Blanca Mountains, although much of the distance is either active wash (Carrizo Wash with only Q1 deposits of historical age) or steep terrain.

Southeast of Alverson and Fossil Canyons, about 3 km of fault is in an area of extreme mechanical disturbance due to quarry operations. Southeast/east of Shell Canyon Road, the fault is again mappable but motorcycle activity has obliterated much of the evidence of recent slip for another couple of kilometers.

The Q3 deposits show a similar distribution of slip (Event 2), ranging from about 2.7 m near Alverson Canyon to a maximum measured value of 4.2 m about 4 km to the northwest. No Q3 deposits are preserved in the area where the Q2 displacement values reach their maximum, so an estimate of maximum slip was probably not measured for this event. In the area of 4.2 m of slip on the Q3 deposits, Q2 deposits are offset only 2.3 m, lower than the Q2 maximum value. Based on this, a maximum Q3 offset of about 4.5-5 m is inferred.

Displacements of Q4 deposits (Event 3? or 4) are less common and are best preserved in the southeastern and northwestern parts of the range. Similar to the Q3 offsets, the maximum lateral displacement of the Q4 alluvium (7.1 m) occurs about 4 km northwest of Alverson Canyon; Q4 alluvium is not preserved in the area of maximum Q2 displacement.

Pinault (1984) and Rockwell and Pinault (1986) measured three displacement values that fall in between those measured for the Q3 and Q4 deposits in the Alverson Canyon area. They suggested that there was an event between the Q3 and Q4 offsets described above (their event 3). However, none of the three offset features were alluvial bars that could be definitely associated with a particular age of deposit. Further, they are all erosional features that could have been modefied after their initial formation. Based on the mapping of this study, it is not clear whether those measurements on erosional features (two offset channel walls and a deflected small channel), represent local areas of higher slip during the penultimate event or whether there was another event between the deposition of the Q3 and Q4 deposits. Displacements were measured for both Q3 and Q4 alluvial bars in the same area,

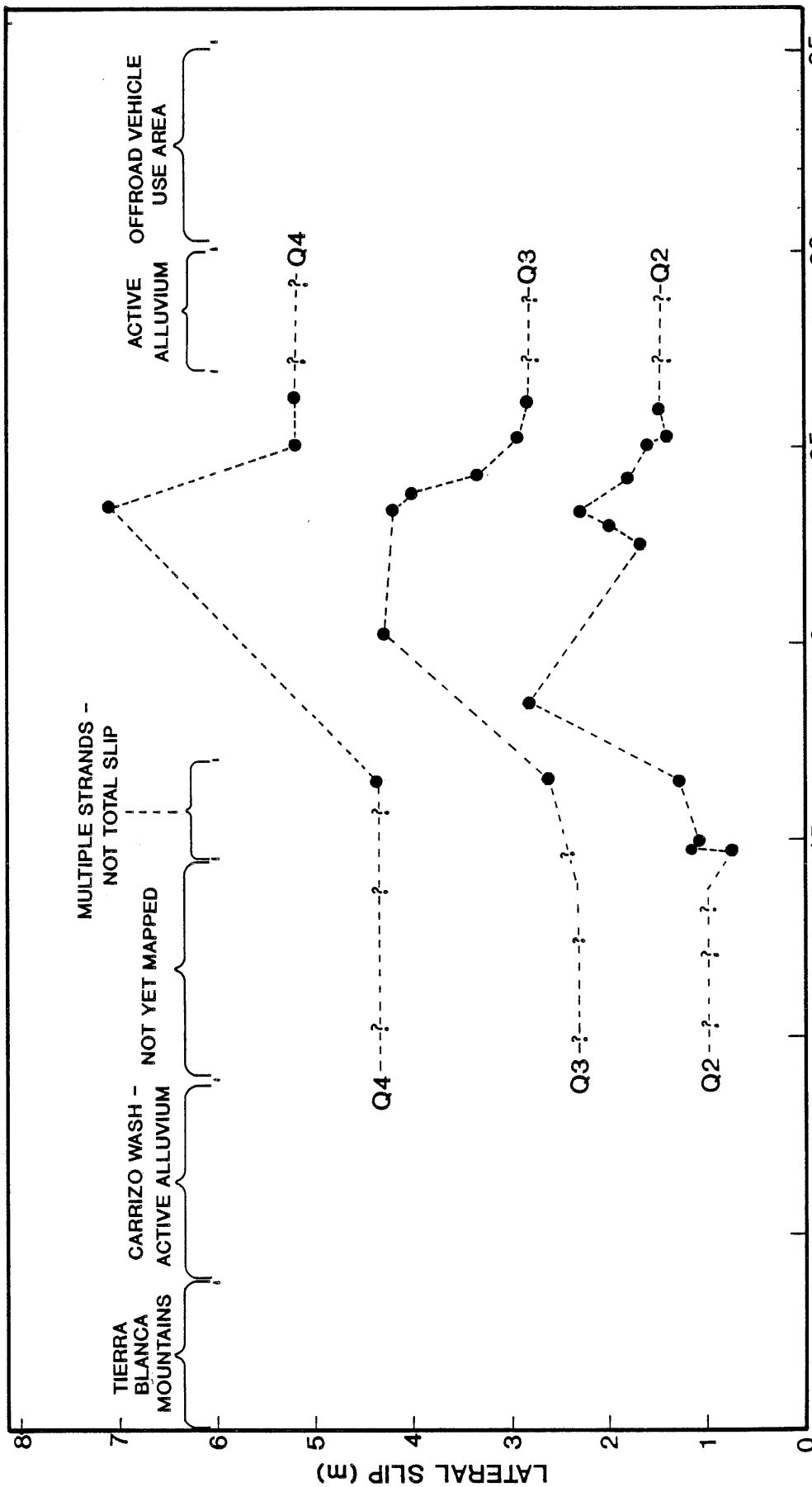

Figure 2. Slip distribution for the past three (or four?) earthquakes in the central Coyote Mountains. Note that multiple fault strands along portions of the fault result in minimum slip estimates.

which were displaced lesser and greater amounts, respectively, which supports the possibility of another event.

Finally, there are several displacements in Q4, Q4-5 and Q5 deposits that show considerably greater displacement than what can be attributed to event 3. It is clear that their are elements of the Q4 and Q4-5 deposits which span a considerable age range that is somewhat greater than the recurrence interval for earthquakes along the Coyote Mountain segment.

Based on the distribution of slip measured on the Q2 deposits, which appear to be a result of only one event, an estimate can be made of the size of the last earthquake. It is assumed that the entire segment ruptured from the Tierra Blanca Mountains to the Yuha desert, but due to the presence of active alluvium for much of the northwestern third of the segment, it is not clear how much slip was sustained in that area. For the purposes of this discussion, a value of 1 m is used for that northern portion, which is similar to values measured along the northern range front. The highest values along the straight portions of the fault along the range front are assumed to be representative for their respective portions of the fault and were used for this calculation. Finally, the southeasternmost part of the fault was also assumed to have about a meter of slip, although folding at the surface clearly accomodates some of this. This slip distribution is summarized in figure 3 and, using a depth of locked crust of 12 km and assuming that the fault steepens to near vertical with depth (many exposures along the range front, especially to the southeast, show very steep or near vertical dips of the fault surface), an estimated moment of about 1.8×10^{26} dyn-cm is yielded. This value roughly corresponds with an M^S 6.8 earthquake for the Coyote Mountain segment.

TIMING OF FAULTING

The ages of the past several slip events is poorly constrained at the present time. It is hoped that continued work, along with the aquisition of results of samples already submitted for analysis, will constrain the timing of events to within several hundred years. As a first approximation, the following discussion will focus on what is presently known about the ages of the Q2-Q4 deposits and the recency of the last event.

Free Faces along Scarps - Free faces on low fault scarps (less than 0.5 m high) in unconsolidated alluvium (generally Q2 and Q3 deposits) are preserved for short stretches over much of the length of the Coyote Mountains, although less than 5% of the total length of the scarps have free faces. The presence of free faces suggests a very young age for the most recent event (Wallace, 1977; Bucknum and Anderson, 1979). Profiling of several scarps will be done when the offset deposits are surveyed so as to estimate the scarp ages. At this stage, it is reasonable to assume that these scarps, and the last event, are no more than several hundred years old.

The historical record of seismicity for the Salton Trough region is poor prior to the instrumental record (circa 1932), and

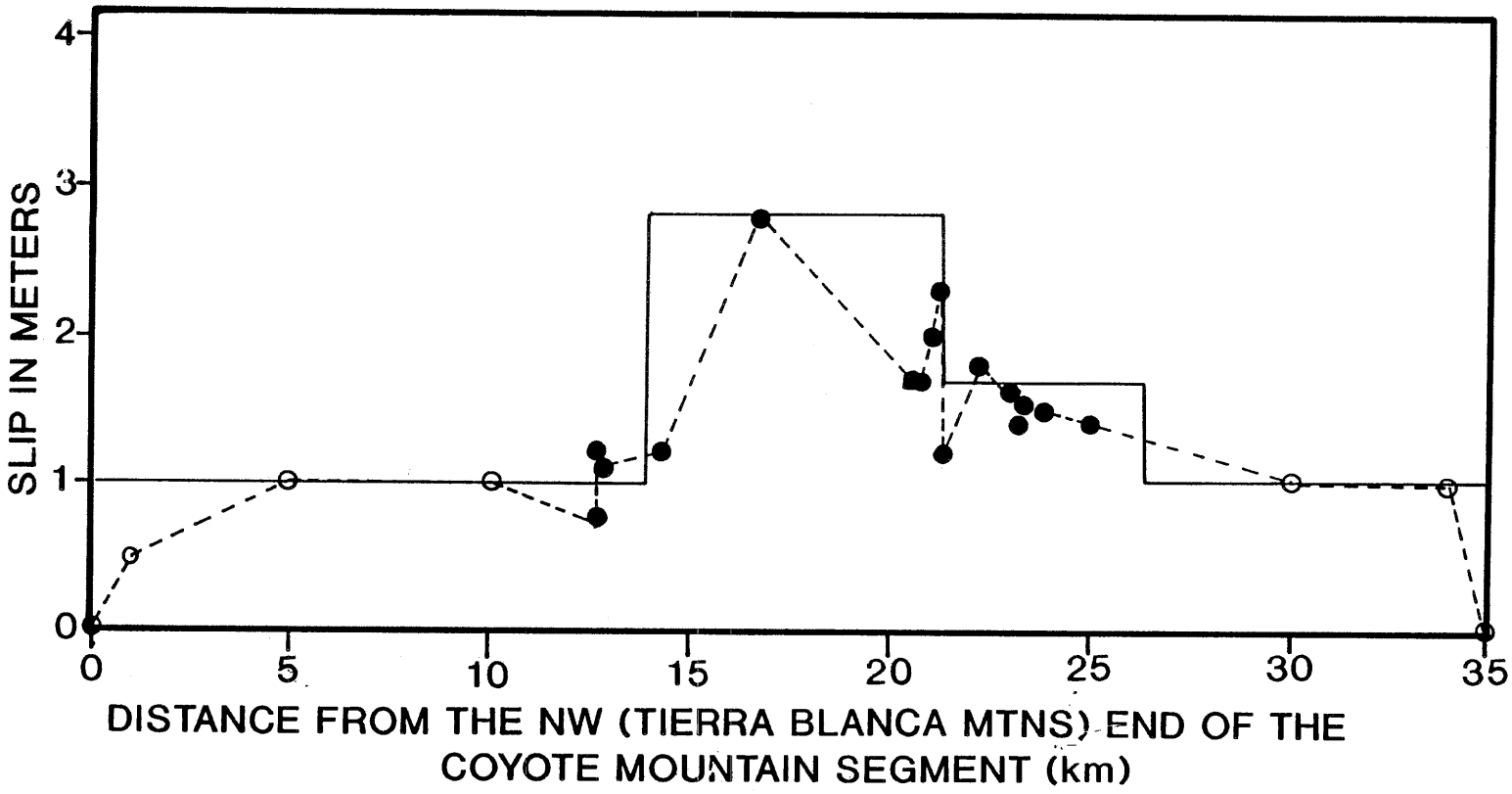

Figure 3. Slip distribution (dashed line) for the most recent slip event that displaces Q2 deposits (solid circles). Open circles are in areas covered by active channel alluvium and are hypothetical. Horizontal lines represent slip used to estimate the moment for this event. Note that many of the areas of low slip are along parts of the fault with multiple strands and total slip was probably not measured. Therefore, this moment estimate is probably a minimum.

most early historical earthquakes are poorly located. Even post 1932 events may be poorly located and understood (the 1942 M6.5 Carrizo Mountain event for one). There are many M6-M7 earthquakes in the Salton Trough region that have been noted for the 50 year period prior to 1932, many of which probably occurred south of the international border in the Colorado Delta region (Strand, 1980; Toppozada and Parke, 1982; Toppozada and others, 1981). None of these earthquakes have been attributed to the southern Elsinore fault except perhaps the Feb. 23, 1892 event (Toppozada and others, 1981), although Strand (1980) and Mueller and Rockwell (this volume) place that earthquake farther to the south on the Laguna Salada fault. It is possible that the Coyote Mountain segment has sustained historical surface rupture, based on the presence of preserved free faces, but there are no specific events that can be attributed to it.

Another indication of the recency of displacement is the apparently young age of the Q2 deposits which are faulted. These deposits are chemically indifferentiable from modern alluvium, but then so are the Q3 deposits. The presence of secondary carbonate, however, suggests that the Q2 deposits are not historical. I have examined low gravelly terraces that incise bar deposits of the most recent high stand of Lake Cahuilla (circa 1660 A.D.: Sieh, 1986) on the east side of the Fish Creek and Santa Rosa Mountains, and several terrace deposits have Q2 type soils developed in them with 1-2 cm thick A_v horizons and very weak stage I carbonates. This suggests, although doesn't prove, that the Q2 deposits can be younger than 300 years old.

In summary, Event 1 could be as young as early historical in age but is more likely 200-300 years old. It is hoped that a combination of ^{14}C analysis of secondary carbonate, TL analysis of the fault fissure fillings (with Steve Foreman), and analysis of the catio ratios of the desert varnish will further constrain the age of Event 1 as well as the earlier events.

DISCUSSION AND CONCLUSIONS

The maximum slip for the most recent earthquake (Event 1) is measured at about 2.8 m near the central portion of the segment in the Coyote Mountains. Based on slip measurements from the several kilometer long reach of the fault northwest from Alverson Canyon, Event 2 was roughly 80% the size of Event 1. Event 3 (if represented by the difference in displacement between the Q3 and Q4 deposits), using data from the same reach of the fault, may have been about 50% larger than Event 1, although it is not clear whether there was another slip event separating events 2 and 3, as suggested by Rockwell and Pinault (1986). If so, then the third event back (Event 3a?) was relatively smaller than Event 1 by about 50% and Event 3b (or 4) was similar in size to Event 1. These uncertainties make it difficult to establish the repeatability of a specific sized event although from these data, it is clear that there is some variability. Rockwell (1989) suggested about a factor of two degree of variability, but part of this hinges on the existence of Event 3a. Further work will hopefully resolve this

issue.

A repeatable or characteristic event would not be surprising for the Coyote Mountain segment because it is bound on the south by a region of complex cross-faulting and it is doubtful that rupture overlap from events to the south is possible. This relationship is very similar (although reversed) to the Superstition Hills segment of the San Jacinto fault zone in that the 1987 rupture appears to be bound at its northwestern end by the northeast-trending Elmore Ranch fault zone. Lindvall and others (1989) suggest that the 1987 slip was characteristic for the Superstition Hills fault, based on the similar distribution of slip for the past two or three events.

Alternatively, the segment of the Elsinore fault to the northwest may occasionally break with the Coyote Mountain segment, producing greater slip values. At this point, there is still uncertainty in the slip distribution for the older events so this question may not be resolvable, especially since the northern third of this segment is largely underlain by active alluvium with no preserved surface rupture features.

ACKNOWLEDGEMENTS

This work was supported by U.S. Geological Survey Grant No. 14-08-0001-G1669. I wish to thank Andy Thomas and Greg Unruh for assistance in completing the fieldwork.

REFERENCES CITED

Bucknum, R.C. and Anderson, R.E., 1979, Estimation of fault-scarp ages from a scarp-height-slope-angle relationship: Geology, v. 7, p. 11-14.

Clark, M.M., 1975, Character and distribution of recent movement along the southeastern part of the Elsinore fault zone, southern California: Geological Society of America, Abstracts With Programs, p. 304.

Christiansen, A.D., 1957, Part of the geology of the Coyote Mountain area, Imperial County, California: unpub. M.S. thesis, University of California, Los Angeles, 188 p.

Goodmacher, J. and Rockwell, T.K., 1990 this volume, Properties and inferred ages of soils developed in alluvial deposits in the southwestern Coyote Mountains, Imperial Valley, California.

Lindvall, S.C., Rockwell, T.K., and Hudnut, K.W., 1989, Evidence for prehistoric earthquakes on the Superstition Hills fault from offset geomorphic features: Seismological Society of America Bulletin, v. 79, no. 2, p. 342-361.

Mueller, K.J. and Rockwell, T.K., 1990 (this volume and in press for the AAPG Memoir on the Gulf of California), Late Quaternary structural evolution of the western margin of the Sierra de los Cucapas, Baja California Norte.

Pinault, C.T., 1984, Structure, tectonic geomorphology and neotectonics of the Elsinore fault zone between Banner Canyon and the Coyote Mountains, southern California: unpub. M.S. thesis, San Diego State University, 231 p.

Pinault, C.T. and Rockwell, T.K., 1984, Rates and Sense of Holocene faulting on the southern Elsinore fault; Further constraints on the distribution of dextral shear between the Pacific and North American Plates: Geological Society of America, Abstracts with Programs, v. 16, no. 6, p. 624.

Rockwell, T.K., 1989, Behavior of individual fault segments along the Elsinore-Laguna Salada fault zone, southern California and northern Baja California:Implications for the characteristic earthquake model: U.S. Geological Survey Redbook on Fault Segmentation and the Earthquake Generation Process: U.S. Geological Survey Open File Report.

Rockwell, T.K. and Pinault, C.T., 1986, Holocene slip events on the southern Elsinore fault, Coyote Mountains, southern Californai: in Guidebook and Volume on Neotectonics and Faulting in Southern California (P. Ehlig, ed.), Cordilleran Section, Geological Society of America, p. 193-196.

Rockwell, T.K., Blom, R., Crippen, R., Klinger, R.E., Stinson, A., and Thomas, A., 1990, this volume, Recognition, extension and significance of northeast trending faults between the Elsinore and San Jacinto fault zones using combined SPOT and LANDSAT imagery.

Sieh, K.E., 1986, Slip rate across the San Andreas fault and prehistori earthquakes at Indio, California: EOS v. 67, no.44, p. 1200.

Strand, C., 1980, Pre-1900 earthquakes of Baja California and San Diego County: unpub. M.S. thesis, San Diego State University, 320 p.

Toppozada, T.R. and Parke, D.L., 1982 , Areas damaged by California earthquakes: 1900-1949: California Division of Mines and Geology Open File Report 82-17, Sacramento, California.

Topozzada, T.R., Real, C.R., and Parke, D.L., 1981, Preperation of isoseismal maps and summaries of reported effects for pre-1900 California earthquakes: California Division of Mines and Geology Open File Report 81-11 SAC, 182 p.

Wallace, R.E., 1977, Profiles and ages of young fault scarps, north-central Nevada: Geological Society of America Bulletin, v. 88, p. 1267-1281.

Wesnousky, S.G., 1986, Earthquakes, Quaternary faults, and seismic hazard in California: Journal of Geophysical Research, v. 91, no. B12, p. 12,587-12,631.

PROPERTIES AND INFERRED AGES OF SOILS DEVELOPED IN ALLUVIAL DEPOSITS IN THE SOUTHWESTERN COYOTE MOUNTAINS, IMPERIAL COUNTY, CALIFORNIA

by
Jonathan Goodmacher and Tom Rockwell
Dept. of Geological Sciences
San Diego State University
San Diego, CA. 92182

Introduction

One of a number of models used in explaining soil development is the state factor model first enunciated by Jenny (1941). This model theorizes that soil formation results from the interactions of five state factors: (1) climatic conditions (cl); (2) organic or biotic factors (o); (3) topographic relief (r); (4) parent materials (pm); and (5) the passage of time (t). These relationships are summarized by the equation: $S = f(cl, o, r, p, t)$. In this equation S may denote the soil as a whole or any single property of the soil. Holding the effects of each of the state factors constant or negligible, with the exception of time, results in the following derivation: $\partial S = \partial t$. This is the equation for the soil chronosequence, wherein time becomes the major independent variable affecting development of the soil profile or the development of any properties of the soil. A soil chronosequence is thus a series of soils of different ages forming in the same climate, hosting similar vegetation communities, on topographically similar slopes, and from similar parent materials.

This study is a chronosequence investigation of soils in the Fossil and Alverson Canyon area of the Coyote Mountains, Imperial County, California (Fig. 1). This investigation had several goals: (1) to develop an understanding of the soil developmental processes in this region; (2) to understand how these soil developmental processes proceed over time; (3) to evaluate the Soil Development Index (Harden,1982) as a tool in the quantitative analysis of soil field data in this arid region; and (4) to determine the role of aeolian deposition in the development of the geochemistry and mineralogy of soils in this area.

Although Mueller (1984) included a soil chronosequence in his study of the Laguna Salada fault, this investigation is the the first detailed chronosequence study undertaken in the southern Salton Trough region. Other detailed chronosequence studies have focused on soils of the southwestern United States, yet none of these have focused on soils in the Salton Trough region (Gile, 1975; Bachman and Machette, 1977; Gile et al, 1981; McFadden, 1982).

The Soil Development Index (Harden, 1982; Harden and Taylor, 1983) was used to analyze morphological changes in these soils. The Soil Development Index has proven to be a useful tool in the quantification of rates and processes of soil development in chronosequence studies in other regions (Harden and Taylor, 1983; Busacca, 1987; Reheis et al, 1989). However, it has not been previously applied to soil studies in the Salton Trough.

Finally, several authors (McFadden, 1981; Machette, 1985; Reheis et al, 1989) have attributed soil development in the arid

Fig. 1 - Fault map showing study area location vis a vis major right-lateral strike-slip faults of southern California.

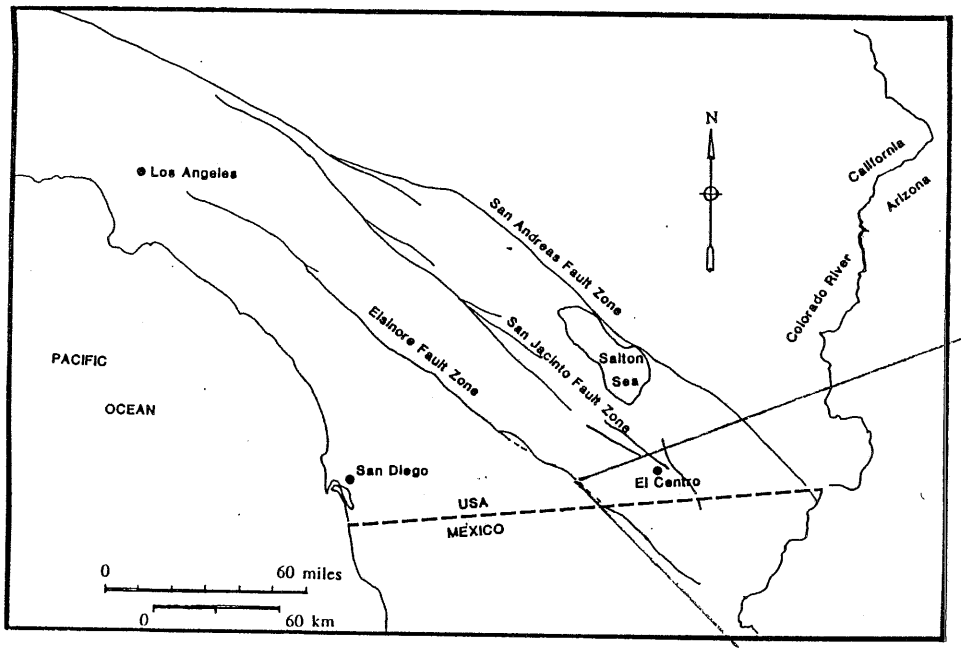

Inset map - Map of alluvial fan deposits in Alverson and Fossil Canyon study area.

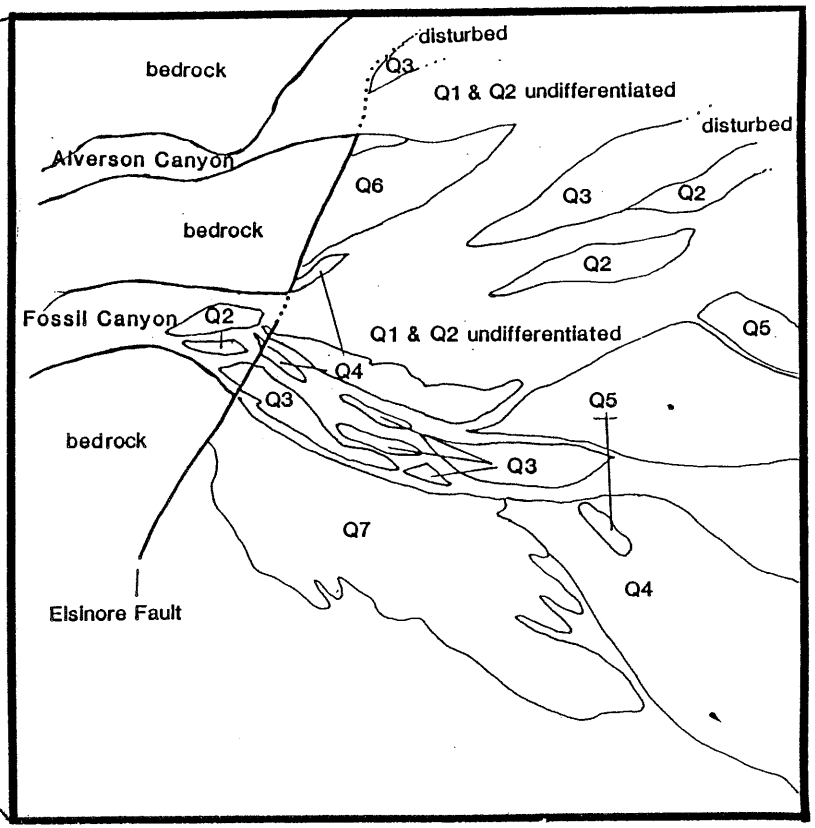

southwest United States to the deposition and accumulation of aeolian dust. Aeolian dust, in this region, has been shown to be dominantly composed of silt and clay, carbonates, gypsum, and other soluble salts (Reheis, pers. comm.). This investigation was undertaken to determine the validity of this model of soil development.

Description of the Study Area

The field area is located on the southwestern margin of the Coyote Mountains, approximately 5 km from the town of Ocotillo, California. Geomorphic surfaces hosting soil development are alluvial, channel bar and stream terrace deposits which have been offset from their sites of deposition at the mouths of Fossil and Alverson Canyons by tectonic activity on the right-lateral Elsinore fault. Seven distinct geomorphic surfaces were identified and sampled in the course of this study. These surfaces were designated Q1 through Q7, with Q1 and Q7, respectively, being the youngest and oldest such deposits (Fig. 1, inset).

Geology

The Coyote Mountains have provided the alluvial detritus which is the parent material of these soils. The Coyote Mountains are comprised of a number of highly deformed Paleozoic metasedimentary rocks, Mesozoic igneous and metaigneous rocks, Neogene volcanic and sedimentary rocks, and Quaternary alluvial and aeolian deposits.

The Elsinore fault bounds the Coyote Mountains on their southwestern margin. In the Alverson and Fossil Canyon area the Elsinore fault consists of a single dominant strand (Pinault, 1984; Rockwell and Pinault, 1986).

Vegetation

Plant species on these surfaces are typical of the Creosote Bush scrub community. Common species are Creosote Bush (*Larrea divaricata*), Ocotillo (*Fouquirea splendens*), Burrobush (*Franseria dumosa*), Brittle Bush (*Encelia farinosa*), minor amounts of Cholla Cactus (*Opuntia sp.*), and forbs. Smoke Trees (*Parosela spinosa*), Cat's Claw (*Acacia greggi*) and Palo Verde (*Cercidium floridum*) trees are found in the washes.

Climate

The study area is within a hyperthermic, arid climatic regime. Mean annual air temperatures are approximately 22-23° C. Mean January and July temperatures are 13-14° C and 33-34° C respectively. Precipitation falls as rain and mean annual precipitation is approximately 75 mm (U.S. Dept of Commerce, 1960-1987). This rainfall has a nonsymmetrical distribution, with approximately 40% of it falling during the summer due to monsoon conditions in the Gulf of California. Because so much of the rain falls during the hottest months it is quickly lost to evapotranspiration and therefore may not be effective as a chemical weathering agent.

Methodology

Field Methods

Field methods utilized in this study included mapping of the lithologic contacts in the Fossil Canyon and Alverson Canyon areas, identification and mapping of Quaternary geomorphic surfaces, and descriptions of soil profiles. Field mapping was performed on 1:6000 scale aerial photographs and U.S.G.S. topographic maps. To minimize the effects of variability in the soil, replicate soil profiles were described on each of the identified geomorphic surfaces. Variance among the soil profiles of any single surface was calculated and these calculations were included in the analysis of the quantified field data. A total of thirty three soil profiles were described and sampled in hand-dug pits and bulldozer trenches.

Site selection in the field involved the identification of geomorphic surfaces characterized by both minimal evidence of human alteration and minimal evidence of post-depositional erosion. Activities at gravel quarries in the vicinity have destroyed a number of potential investigation sites. Offroad vehicle use has disrupted an additional number of potential study sites.

In order to identify geomorphic surfaces of different ages in the study area a number of geomorphic relative age indicators were utilized. These included observations of changes in the microtopography of the surfaces, the development of desert varnish coatings on rock clasts, the development of reddened

clast undersides, and qualitative examinations of rock shattering and pitting.

The Soil Development Index

A modified version of the Soil Development Index (Harden, 1982) was used in quantifying soil field data. Calculation of the Soil Development Index (SDI) involves the conversion of observed field properties to numeric data. The goal of this process is to allow an evaluation of the development of a soil profile relative to both its possible maximal state of development and to the state of the unaltered parent material. Quantification of soil field data provides a statistical basis for comparisons of soil development between soils in different regions and/or soils of a given chronosequence.

Briefly, the SDI works by assigning points to each soil property investigated in the field. Points are assigned on the basis of the development of a property. These points are then normalized on a scale of 0 to 1 with 0 indicating no development and 1 indicating maximal development. Points for each property in a horizon are then multiplied by horizon thickness and the points for each horizon are summed for each soil profile examined. This summary quantity is the profile development index (PDI). Additionally, each property of the soil may be separately and similarly examined. These are the various profile property indices, e.g. carbonate morphology, rubification, etc. Two approaches were adopted in the calculation of the profile development index. Initially the PDI was calculated following the procedure outlined above. A second calculation of the PDI was

then made in which all soil profiles were uniformly described to a depth of 2 m. This technique is designed to remove the effects of depth bias in the calculations of the profile development indices (after Rockwell, 1983).

Laboratory Methods

In order to more fully understand the processes behind soil formation in the Coyote Mountains a number of geochemical and laboratory investigations were included in this study. These were analyses of: (1) the particle size distribution of the <2 mm size fraction of the soil; (2) the accumulation and distribution of carbonates, gypsum, and soluble salts; (3) soil pH; and (4) the mineralogy of the <2 mm size fraction of the soil.

Results of Field and Laboratory Analysis

Field Observations

Field observations indicate that the Q1-Q4 soils are minimally developed. They show little evidence of accumulations of secondary carbonate or of translocation of silt and clay from their upper horizons. Taxonomically these soils are Typic Torriorthents (Soil Survey Staff, 1975).

On the other hand the Q5-Q7 soils display significant and progressive evidence of pedogenic alteration. Progressive in that these properties are better manifested in the Q7 deposit soils than the Q5 deposit soils. These soils have well developed horizons of carbonate accumulation, are redder with increasing age, and are finer textured with increasing age. In addition to the general trends noted above, there seems to be a consistent increase in the thickness of the Av horizon of the soil. The

development of a calcic horizon, a diagnostic horizon of soil development, is reflected taxonomically in the classification of these soils as Typic Calciorthids.

In summary, the field data suggests that, over time, these soils: (1) became increasingly finer textured; (2) reached higher stages of carbonate morphology; (3) developed reddened B horizons (Bw horizons); and (4) develop thicker Av horizons. Taxonomically these changes are reflected in the classification sequence: Typic Torriorthent >>> Calciorthidic Typic Torriorthent >>> Typic Calciorthid (Soil Survey Staff, 1975). Soils on Q1 through Q4 surfaces classify as Typic Torriorthents, soil on Q5 through Q7 surfaces classify as Typic Calciorthids. Some intermediate soils were classed as Calciorthidic Typic Torriorthents. The designation of a soil as a Typic Torriorthent indicates that it is only minimally developed and lacks diagnostic soil horizons. Designating a soil as a Typic Calciorthid indicates that the major morphological change, taxonomically, is the development of a calcic horizon.

Soil Development Index Data

Three profile properties were useful in differentiating soils from geomorphic surfaces of different ages. These properties were carbonate morphology, rubification, and textural class change. The category of secondary calcium carbonate morphology reflects directly the increasing morphological buildup of carbonate in calcic horizons in these soils. Rubification is a measure of the reddening of the soil color with increasing soil age. Textural class change reflects the increasing accumulation

of fines in these soils with increasing age. Table 1 summarizes the results of this portion of our investigation. The data presented in Table 1 represents the average value of the soil properties for all of the soils of any single geomorphic surface. The PDI values, for both calculation methods, are also average values for all of the soils on any single geomorphic surface.

As the data in Table 1 indicates there are progressive increases in the PDI values (calculated by both methods), and in the profile property, carbonate morphology. The profile properties soil rubification and textural classification do not readily fit into these observed trends.

Table 1 - Summary data of PDI and selected profile property indices.

Quaternary Surfaces	PDI* (desc.)	PDI# (2 m)	Carb. Morph.	Rubi-fication	Text. Class.
Q2 Soils	1.08	3.20	12.5	3.28	9.46
Q3 Soils	3.13	7.15	35.79	12.94	0.37
Q4 Soils	5.83	9.13	34.60	2.13	3.44
Q5 Soils	10.69	15.09	61.29	27.57	28.53
Q6 Soils	14.08	18.11	68.78	31.09	34.30
Q7 Soils	19.42	20.40	90.24	32.57	34.20

* = Profile Development Index calculated to the soil depth described in the field.

= Profile Development Index calculated to a uniform depth of 2 m for each soil.

The profile properties, textural classification and rubification, most likely obtain their differences from the

extremely variable initial nature of these deposits. This inherited variability is partially a function of whether the soil is forming on a bar or a swale. Removing soils which are forming in swales, which thus have a much finer parent material than soils forming in bars, from the analysis and recalculating the average values for the the soil properties rubification and textural classification yields the data summarized in Table 1a. In Table 1a, a similar pattern of progressive increase is noted for each of these soil properties, textural classification and rubification, as well as the PDI.

Table 1a - Summary data of PDI and selected recalculated profile property indices.

Quaternary Surfaces	PDI* (desc.)	PDI# (2 m)	Carb. Morph.	Rubi-fication	Text. Class.
Q2 Soils	1.08	3.20	12.5	0.76	0.00
Q3 Soils	3.13	7.15	35.79	2.76	0.37
Q4 Soils	5.83	9.13	34.60	2.13	3.44
Q5 Soils	10.69	15.09	61.29	27.57	28.53
Q6 Soils	14.08	18.11	68.78	31.09	34.30
Q7 Soils	19.42	20.40	90.24	32.57	34.20

* = Profile Development Index calculated to the soil depth described in the field.

= Profile Development Index calculated to a uniform depth of 2 m for each soil.

The data summarized in Table 1a was statistically evaluated to test the validity of using PDI values and/or profile property values to differentiate between soils on the different geomorphic surfaces. An equality of means test was applied to

test the degree of overlap of these indices. Soils which are considered to be statistically nonunique have overlapping values at a single standard deviation. The results of this analysis are summarized in Table 2. Soils which are statistically indistinguishable from one another are bracketed together.

This summary of the data demonstrates that, statistically, the properties of the Q5 through Q7 soils are very different from those of the Q1 through Q4 soils. This is in an accord with the observed field data, which qualitatively grouped these soils in an identical fashion. These qualitative observations differentiated these soils into Typic Torriorthents (Q1-Q4 soils) and Typic Calciorthids (Q5-Q7 soils).

Table 2 - Results of equality of means test on profile development index and selected profile property values.

PDI (desc.)	PDI (2 m)	Carbonate Morphology	Adjusted Rubif.	Adjusted Text.Class.
Q2	Q2	Q2	Q2	Q2
Q3	Q3	Q3	Q3	Q3
Q4	Q4	Q4	Q4	Q4
Q5	Q5	Q5	Q5	Q5
Q6	Q6	Q6	Q6	Q6
Q7	Q7	Q7	Q7	Q7

Laboratory Results

Particle size analysis was undertaken to test the observed morphological trend towards a finer grained soil with increasing

age. Analysis of the accumulation and distribution of calcium carbonate was undertaken to evaluate the observed trend towards increasingly higher stages of carbonate morphology with increasing soil age.

Analyses of the accumulation and distribution of soil calcium carbonate, gypsum, and soluble salts were also included. These analyses were undertaken to determine how the differences in solubility of these soil components might be reflected in their distribution. These data could lead to inferences regarding the effects of past climates on soil development. The soil salts are listed in increasing order of solubility: calcium carbonate, gypsum, and other soluble salts. Soluble salts is a catchall category consisting most likely of sodium carbonates, halite, etc.

Soil pH values reflect the ionic concentration and content of the soil, as well as, the exchangeable cation complex adsorbed to colloidal surfaces (Birkeland, 1984). Common ions present in the soil are Ca^{2+}, Mg^{2+}, K^{+}, Na^{+}, H^{+}, Cl^{-}, NO_3^{-}, CO_3^{2-}, HCO_3^{-}, and OH^{-}. The relative proportion of these ions determines soil pH (Birkeland, 1984). Additionally, soil pH is affected by the relative strength of the bases or acids formed (Birkeland, 1984). Analyses of soil pH were therefore undertaken in order to determine the distribution and possibly the type of charged species in the soils.

X-ray diffraction analysis of the <2 μm size fraction of the soil was used in order to determine the role of weathering in the apparent trend towards increasingly finer textured soil over time. If chemical weathering processes are important in the

development of these soils, then the mineralogy and distribution of clays in the soil would be affected (Plaster and Sherwood, 1971; Kronberg, et al, 1979).

Particle size analysis indicates that there is an increase in the volume of total fines in the soil with increasing soil age (Table 3). The coefficient of variability (C.V.) calculations are included in Table 3 (C.V. = (st.dev./average)*100). The coefficient of variability is a measure of how dispersed a statistical grouping is, the lower the C.V. the more tightly its values are clustered about the given average value. This analysis is included to make the equality of means test accessible to the reader. For the purpose of this analysis, total fines are defined as the sum of the silt- and clay-size particles. This observation is in agreement with the observed field data and adjusted SDI calculations.

Table 3 - Summary of particle size analysis

Geomorphic Surface	Total Fines (g/cm^2)	Clay Volume (g/cm^2)	Total Fines (C.V.)	Clay Volume (C.V.)
Q1 Soils	36.83	13.30	41.3%	25.9%
Q2 Soils	45.09	15.96	27.9%	27.5%
Q3 Soils	32.88	12.33	18.8%	22.6%
Q4 Soils	44.53	16.66	10.0%	17.4%
Q5 Soils	71.04	22.80	25.3%	24.7%
Q6 Soils	76.81	26.74	15.3%	9.6%
Q7 Soils	65.03	24.35	8.4%	18.3%

As was true of the Soil Development Index calculations, two statistical clusterings of data occur. One of these clusterings is

the Q1-Q4 soils. The second clustering is of the Q5-Q7 soils. The equality of means tests show that within these clusters the soils are statistically indistinguishable from one another.

The soil calcium carbonate, gypsum, and soluble salts accumulation data are presented in Table 4. Listed with each of the analyses is the coefficient of variance for the particular geochemical property investigated. These data do not fall into statistically similar groups in the manner of the SDI and particle size data.

Table 4 - Summary of $CaCO_3$, gypsum, and soluble salts analyses.

Geomorphic Surface	$CaCO_3$ Volume (g/cm^2)/C.V.	Gypsum Volume (g/cm^2)/C.V.	Soluble Salts Volume (g/cm^2)/C.V.
Q1 Soils	25.15 / 11.6%	0.31 / 74.2%	6.46 / 48.5%
Q2 Soils	29.38 / 9.4%	0.22 / 13.6%	3.99 / 20.1%
Q3 Soils	28.14 / 10.3%	0.20 / 40.0%	5.49 / 57.6%
Q4 Soils	23.99 / 9.1%	0.13 / 76.9%	6.79 / 34.0%
Q5 Soils	15.94 / 27.0%	4.08 / 94.4%	89.72 / 43.0%
Q6 Soils	28.47 / 13.1%	1.34 / 57.5%	57.92 / 83.4%
Q7 Soils	20.09 / 21.3%	1.37 / 48.2%	46.30 / 40.1%

The calcium carbonate accumulation results are unexpected for two reasons. One, these data do not fall into two separate statistical groups, as did the particle size data and the SDI data. Instead, the equality of means test indicates that these soils are statistically indistinguishable at the level of one standard deviation. Secondly, this result is contrary to the expectations

raised by the field data. Recall that both the observed and the calculated soil field data indicated that distinct accumulations of secondary calcium carbonate develop with increasing soil age. These accumulations were represented by well defined calcic horizons and/or by increases in the stages of calcium carbonate morphology. Despite the development of higher levels of carbonate morphology and of calcic horizons the average total volume values of calcium carbonate in the soil column is not any greater in the Q7 soils than it is in the Q1 soils.

The soil gypsum accumulation data is similarly unexpected. However, clustering into groups did occur. One group is composed of the soils on the Q1-Q4 surfaces, a second group is composed of the soils on the Q6 and Q7 surfaces. The Q5 soils are independent of both of the statistically recognized groups or clusters. As expected the older soils (Q6-Q7) have higher accumulations of gypsum than the youngest soils (Q1-Q4). However, the Q5 soils have up to several times the gypsum accumulation of the Q6 and Q7 soils. These observations did not change following application of the equality of means test. These data suggests that Q5 soils tended to accumulate gypsum at a much higher rate than the Q6 and Q7 soils.

The pattern of the soluble salts accumulation data are very similar to the pattern of the gypsum accumulation data. These data, again, cluster into two distinct groups, the Q1-Q4 soils versus the Q6-Q7 soils. As was the case with the gypsum accumulation data the Q5 soils are statistically independent of

both of these groupings. The application of equality of means test did not change these results.

Soil pH analysis indicates that these are generally basic soils, with values ranging from pH 6.7 to pH 8.4, and a mean value of approximately pH 8.0 (Appendix B). General trends in soil pH development are towards slightly more acidic soil profiles with increasing age. The general trend in young soils (Q1-Q4) is towards a more basic soil with increasing depth in the profile. In the older soils (Q5-Q7) the opposite trend is observed, that is the soils become more acidic with depth.

Preliminary mineralogical analysis, using XRD analysis of the < 2μm fraction, indicates that there are not significant changes in the mineralogy of these soils with increasing age (Fig. 2). These results are qualitative observations and will be further investigated quantitatively. These observations are therefore somewhat speculative.

Summary of Field, Statistical and Laboratory Results

With increasing age, the percentage of soil fines increases, there is an increase in the stage of carbonate morphology, the quantities of gypsum and soluble salts increase, and the soils become redder. These changes are reflected in the taxonomy of the soils, the Soil Development Index, and in the soil property indices.

Taxonomically these changes result in the sequence: Typic Torriorthents >>> Calciorthidic Typic Torriorthents >>> Typic Calciorthids (Soil Survey, 1975). Q1-Q4 surface soils classify as Typic Torriorthents, Q5-Q7 surface soils are Typic Calciorthids.

Fig. 2 X-ray diffractograms from first horizon under the Av horizon of soils from Q2, Q4, and Q7 deposits. Exception is Active Channel deposit, this is a surface sample. This demonstrates the similarity in the mineralogy of each of the soils sampled. X-ray diffractograms were taken following exposure of the sedimented slides to ethylene glycol.

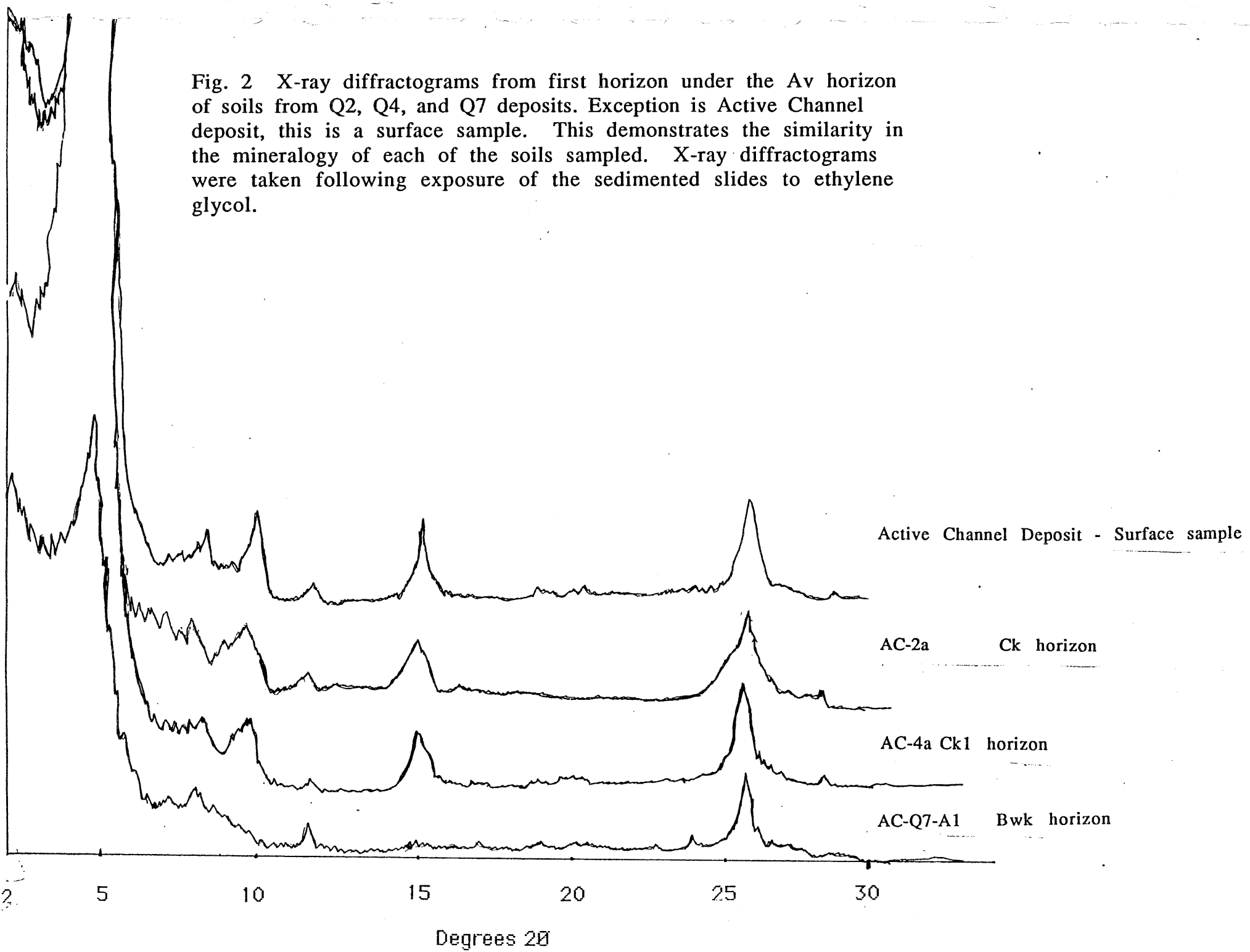

Some intermediate soils are classified as Calciorthidic Typic Torriorthents.

Geochemical and laboratory analyses demonstrate that there are trends towards increasing accumulations of fines, gypsum, and soluble salts in these soils. The particle size accumulations are progressive with increasing soil age. However, the accumulations of gypsum and soluble salts are not progressive but are lowest in the Q1-Q4 soils, highest in the Q5 soils, and intermediate in the Q6 and Q7 soils. Additionally, preliminary x-ray analysis indicates that the clay mineralogy of these soils is not significantly changing with time.

Trends in Soil Development

Quantification of soil development rates requires the assignment of age parameters to the geomorphic surfaces hosting soil development. This assignment places an upper limit to the age of the soils forming on those surfaces. The most precise and readily applied methods of assessing the age of geologic materials are based on changes, with time, in accumulations of the radioactive isotopes of carbon, uranium, potassium, and argon. The use of isotopic dating techniques is impractical for this study for two reasons: (1) a lack of datable material; and (2) a lack of precision and resolution. Carbonaceous materials, such as plant remains, are readily oxidized in this arid environment and are not available for dating. Furthermore, the young, overlapping ages of these surfaces could not be resolved satisfactorily using U-series, or other isotopic techniques.

This constraint is not unique to this study. It is generally the case with other soil studies in the arid southwest. Previous workers have utilized soil carbonate accumulations and the stages of soil carbonate morphology to assign rough ages to Quaternary soils in the desert southwest (Machette, 1985). This technique is based on the assumption that secondary carbonate accumulations in the soil result primarily from aeolian influx. These secondary accumulations are then divided by the aeolian carbonate flux rate to yield rough ages for the soils being studied (Machette, 1985). A review of the data presented in Table 4 demonstrates that this approach clearly would not work for this study. The carbonate volume data is too scattered and overlapping for this method to yield usable data.

Estimated Ages

Since we were unable to utilize any of the above methods we have instead estimated the ages of each of the geomorphic surfaces (Table 5). Estimated ages are based on: (1) comparisons to similar soils, with age control, that are documented in the literature (Reheis, 1989; Sowers, 1985); and (2) literature on the rate of accumulations of desert varnish (Dorn et al, 1986; Dethier et al, 1988). It should be strongly noted that these estimated ages have errors of 50% or greater. Therefore, I have included estimated minimum and maximum ages for these surfaces.

Table 5. - Estimated Ages of Geomorphic Surfaces.

Q Surfaces	Probable Age (yrs)	Minimum Age (yrs)	Maximum Age (yrs)
Q1 Surfaces	$<0.25 \times 10^2$	0.10×10^2	0.5×10^2
Q2 Surfaces	2.0×10^2	1.0×10^2	4.0×10^2
Q3 Surfaces	1.0×10^3	5.0×10^2	2.0×10^3
Q4 Surfaces	3.0×10^3	1.5×10^3	5.0×10^3
Q5 Surfaces	1.2×10^4	0.9×10^4	2.0×10^4
Q6 Surfaces	3.5×10^4	2.0×10^4	7.5×10^4
Q7 Surfaces	1.75×10^5	1.0×10^5	2.5×10^5

Reheis (1989) estimates that soils forming in the area of the Silver Lake playa, southern California, in alluvial deposits, with similar vegetation communities and under a hyperthermic, arid climatic regime require approximately 35 ka to develop stage II to II+ carbonate morphology. These soils approximate the Q6 soils of this study in their development. Further, Sowers (1985) documents that approximately 50 ka are required to develop stage III to stage IV carbonate morphology in the Kyle Canyon, Nevada area. These soils are forming in carbonate parent materials, but under similar climatic conditions to those of the Coyote Mountains. Because large amounts of carbonate materials are present in the Kyle Canyon deposits prior to soil formation it is probable that carbonate morphology would develop more quickly in those soils than in the Coyote Mountain soils. Therefore, I have used these data to place a lower age boundary on the development of similar properties in the Coyote Mountains.

This stage of carbonate morphology correlates approximately to the oldest soils (Q7 soils) of this study.

Previous work (Dorn, 1986; Dethier et al, 1988) indicates that the formation of desert varnish is initiated within a few hundred years after exposure of a rock clast at the surface. Incipient desert varnish formation is developed on the Q3 deposits. These data are used to constrain the ages of the younger surfaces in the study area.

Developmental Trends with Increasing Soil Age

Soil Development Indices, soil property indices and soil geochemistry were regressed against estimated soil ages. These analyses are presented in Table 6. The data presented in Table 6 is an average value for the given statistic for the soils on a given geomorphic surface.

Two regression models used for these calculations. These models were: (1) $y = a + bX$ and (2) $y = a + (b \log X)$ (after Bockheim, 1980). In these models Y represents the soil or any property of the soil and X is time. These regressions, using both logarithmic and linear correlations, were deemed to be statistically significant if they yielded r^2 values greater than .500.

Table 6 - Regression of Soil Properties vs. estimated age for Coyote Mountains soils.

Soil Property	Probable Age		Maximum Age		Minimum Age	
	lin r^2	log r^2	lin r^2	log r^2	lin r^2	log r^2
Profile Index#	.642	.817	.688	.859	.673	.726
Profile Index@	.435	.720	.480	.780	.468	.647
Carbonate Morphology	.460	.662	.484	.678	.505	.602
Rubification	.275	.563	.309	.588	.300	.506
Adj. Textural Classification	.432	.589	.439	.521	.506	.647
Carbonate Vol.	.111	.221	-----	-----	-----	-----
Gypsum Vol.	.028	.162	-----	-----	-----	-----
Adj. Soil Fines	.175	.612	.217	.577	.225	.672
Sol. Salts Vol.	.081	.366	-----	-----	-----	-----

*lin = linear regression; +log = logarithmic regression.
= calculated to the described field depth; @ = calculated to a uniform depth of 2 m.
r^2 values underlined if > .500.

The profile index represents the summation, for each soil profile, of the soil properties examined. The profile index value, indicated with a # sign, is calculated on the profile only to the depth that profile is described in the field. The second profile index value above, indicated with a @ symbol, is calculated to a uniform 2m depth for each soil. Although the linear and log correlations between the profile index and time are deemed to be statistically significant the log relationship between time and the profile indices is stronger than the linear relationship between time and the profile indices (Fig. 3a and 3b). Those soil properties statistically correlating most significantly with

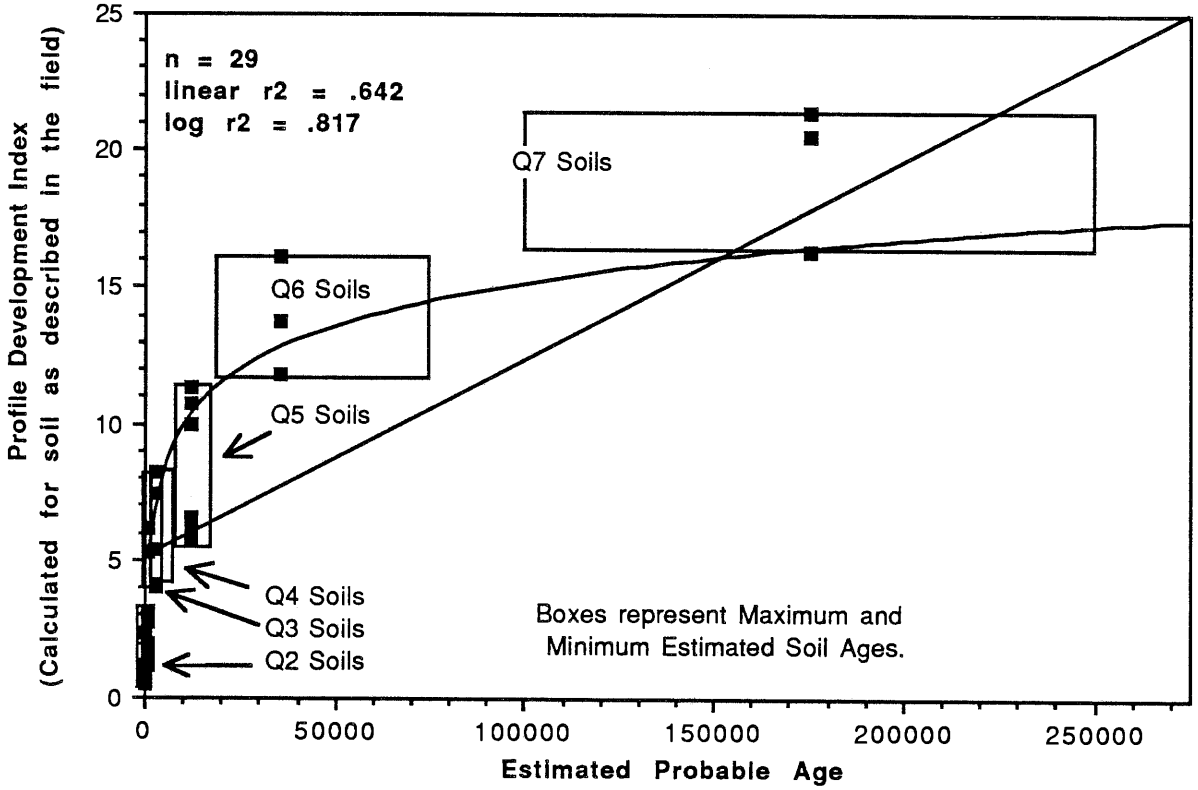

Fig. 3a - Graph of Profile Development Index vs. Estimated Soil Age.

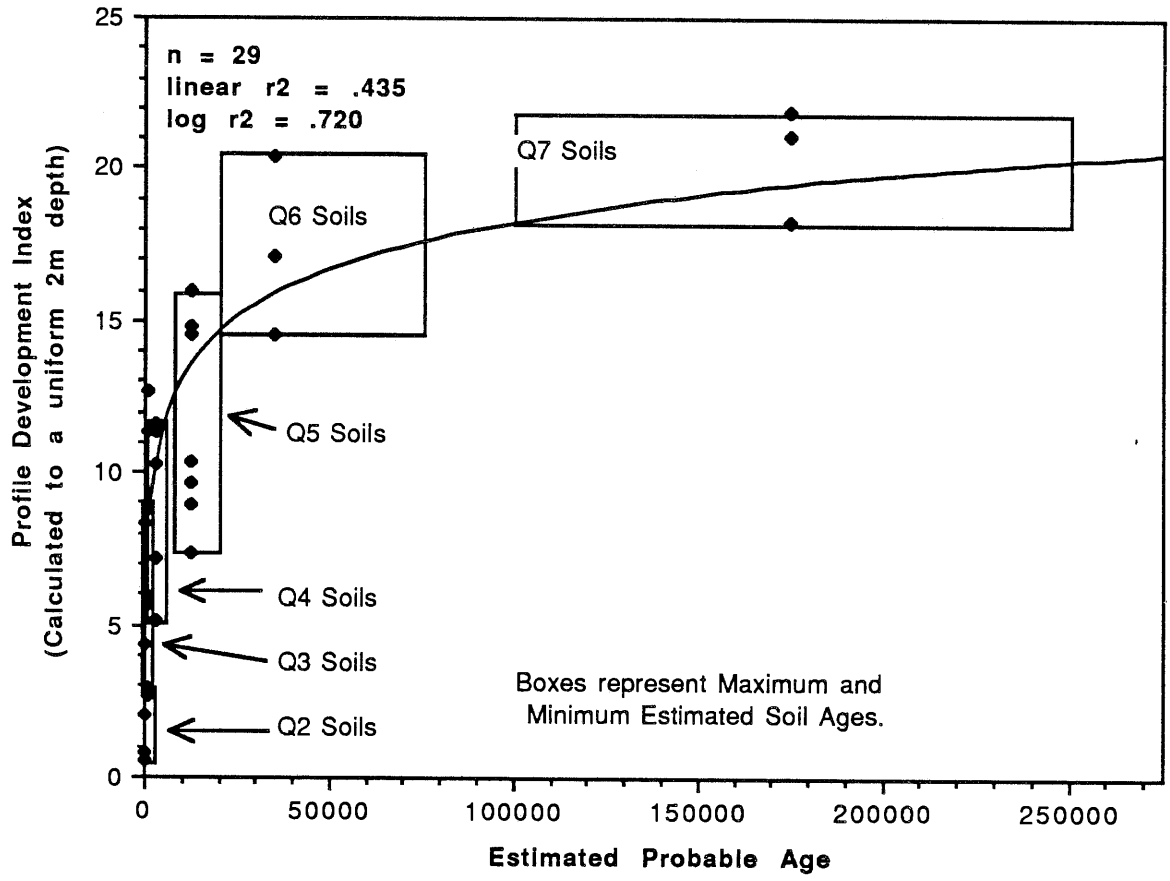

Fig. 3b - Graph of Profile Development Index vs. Estimated Soil Age.

increasing soil age are carbonate morphology, rubification, and adjusted textural classification.

As previously discussed one of the major developmental changes in these soils is the formation of a calcic soil horizon. Increasing amounts of soil carbonates are reflected in the soil by progressive increases in carbonate morphology. r^2 values for increasing carbonate morphology indicate that a significant relationship exists between carbonate morphological development and log time (Fig. 4).

Rubification, soil reddening, is a function of oxidation in the soil (Schwertmann and Taylor, 1977). This reddening was especially evident in the older soils where it appears as a pink or light brown (7.5YR 7/4d or 6/4d) Bw horizon characterized by accumulations of fines. Statistically, r^2 values for the regression of rubification against log time are significant, .563 against estimated probable soil age (Fig. 5).

Textural classification changes reflect the presence of increasing amounts of fines in these soils. As per the previous discussions of the soil textural classification I removed the soil profiles the Q2 and Q3 soils forming on swales from this analysis. Using these adjusted textural classification values, r^2 values for textural change are considered to be statistically significant. The resultant r^2 is .563 against estimated probable soil age (Fig. 6).

Particle size analysis, carbonate volume, gypsum volume, and soluble salts volume were also regressed against estimated soil ages. These analyses are presented in Table 6. Again, for the

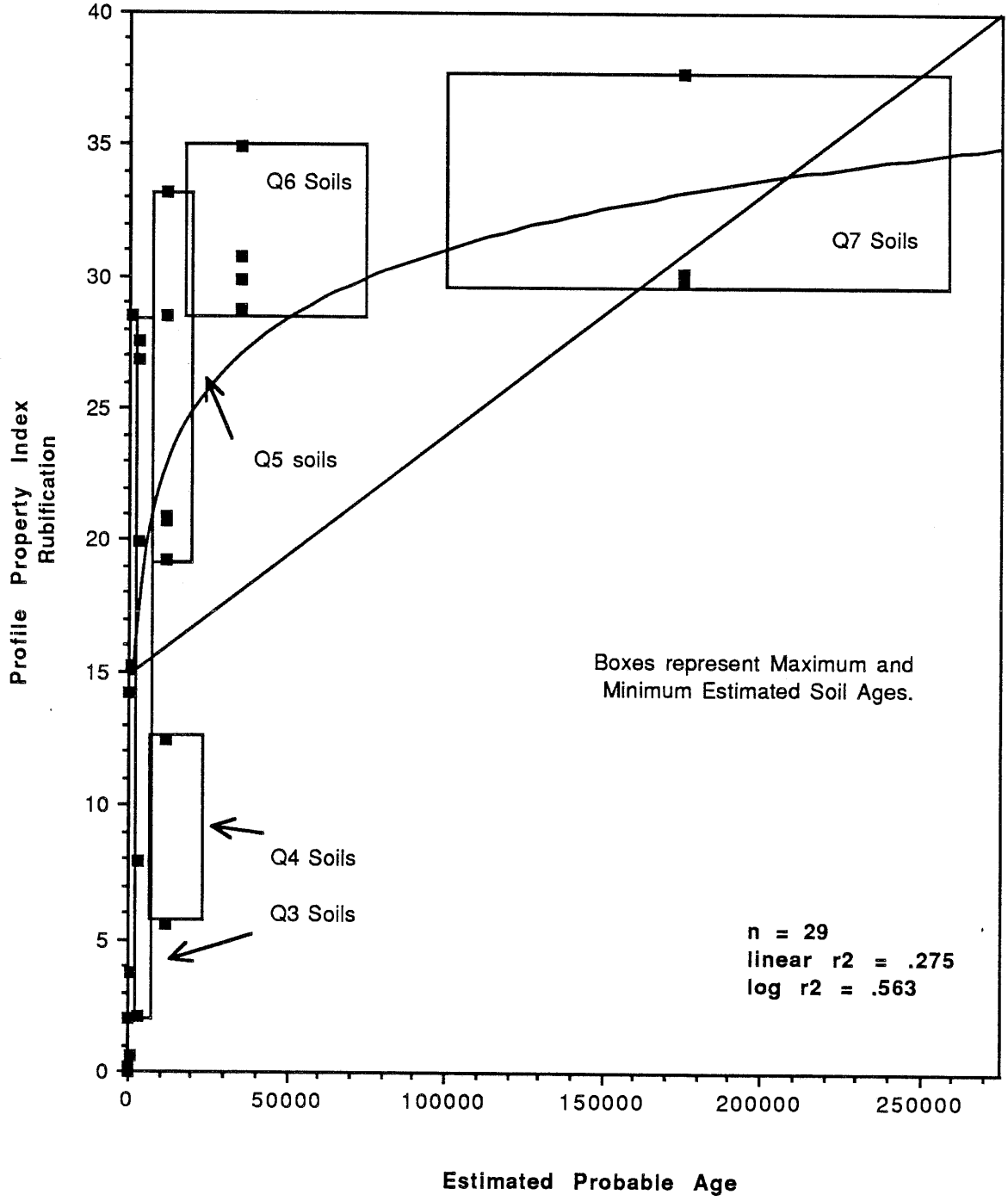

Fig. 5 - Graph of Rubification vs. Estimated Soil Age.

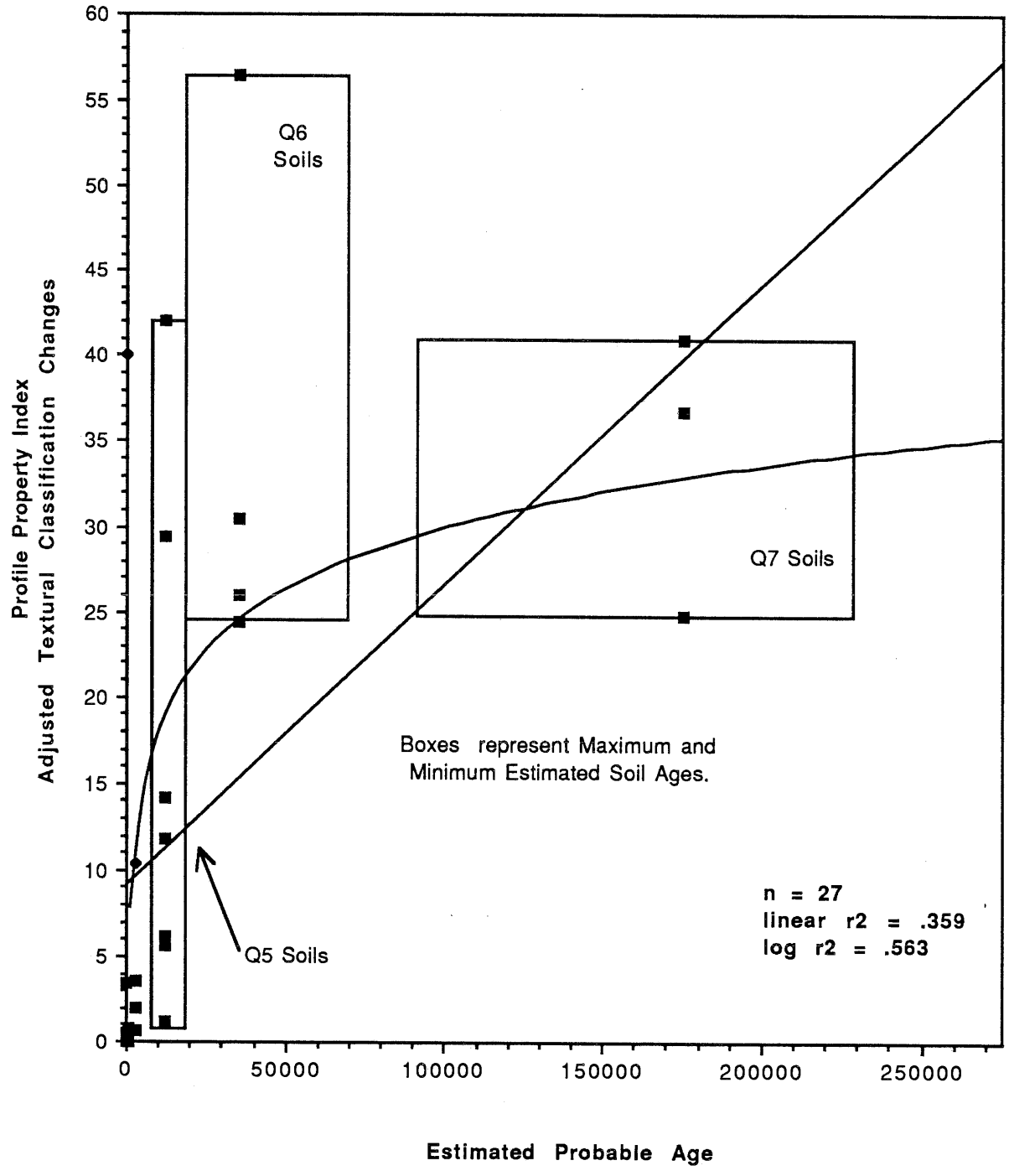

Fig. 6 - Adjusted Textural Classification vs. Soil Age.

property, Adjusted Fines, the Q2 and Q3 soils forming in swales were removed from this analysis. The logarithmic regression of adjusted soil fines volume against estimated probable soil age was deemed to be statistically significant, .589 (Fig. 8).

In summary, statistical analysis of the Soil Development Index values reveals that significant correlations exist between the soil as a whole and certain soil properties (carbonate morphology, rubification, and adjusted textural classification) versus log time. Additionally, a similar statistical analysis was performed on the laboratory determined accumulations of soil fines, carbonates, gypsum, and soluble salts (Figs. 7, 9 and 10, carbonates, gypsum and soluble salts). A significant correlation was observed to occur between the volume of soil fines and logarithmic time (Fig. 8).

Discussion

A number of lines of evidence seem to be converging to indicate that the primary motive force behind soil development in this region is the deposition and accumulation of aeolian dust. This dust is dominantly composed of silt and clays, carbonate, gypsum, and soluble salts (M. Reheis, pers. comm.). Support for this contention can be derived from three lines of evidence: (1) quantities of each of the chemical species investigated (carbonates, gypsum and soluble salts) are not initially present in the parent material alluvial deposits in quantities approaching those present in the well-developed soils; (2) preliminary X-ray diffraction analysis indicates weathering is not a major contributing factor in the increase in the relative percentage of

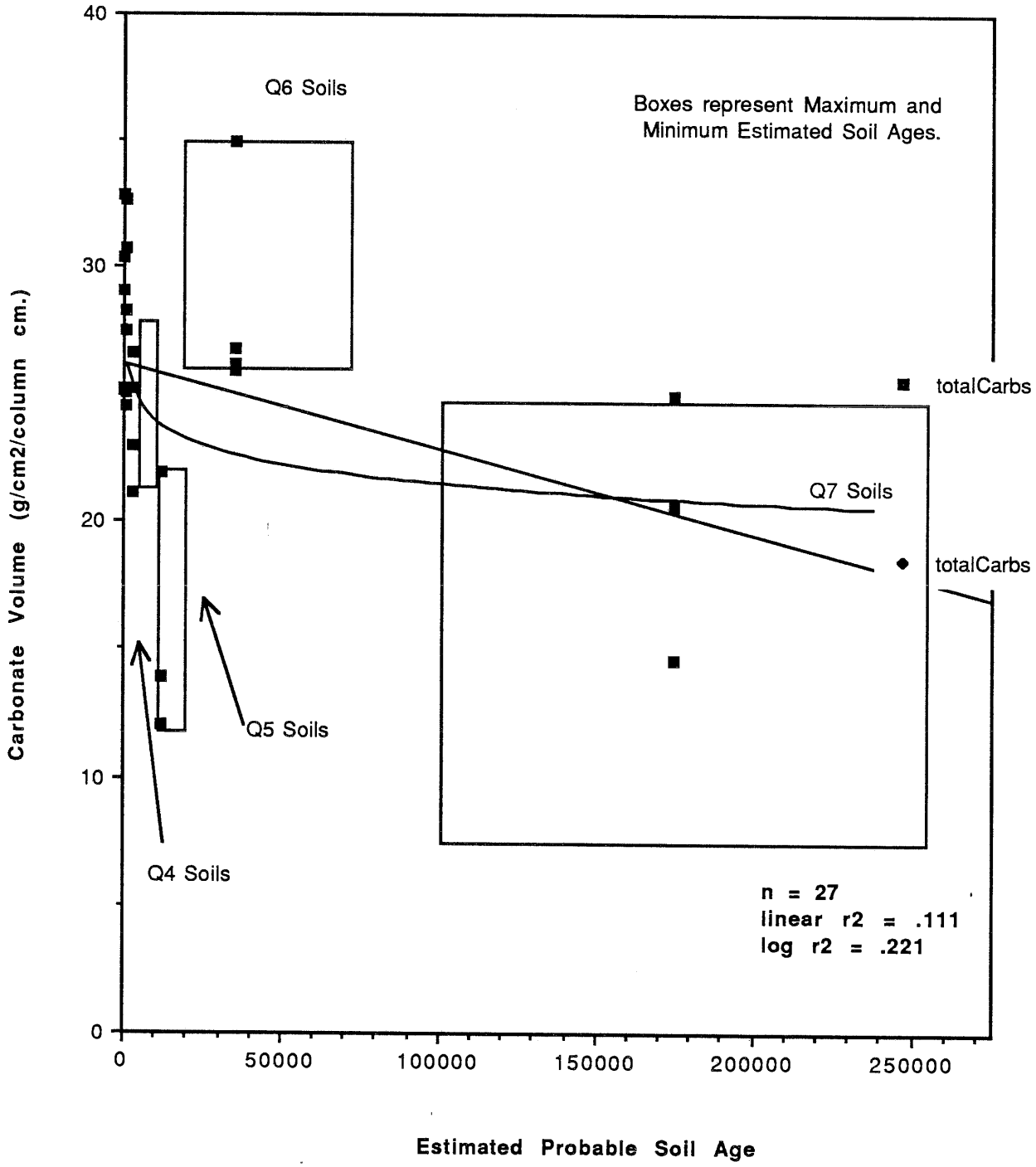

Fig. 7 - Carbonate Volume vs. Estimated Soil Age.

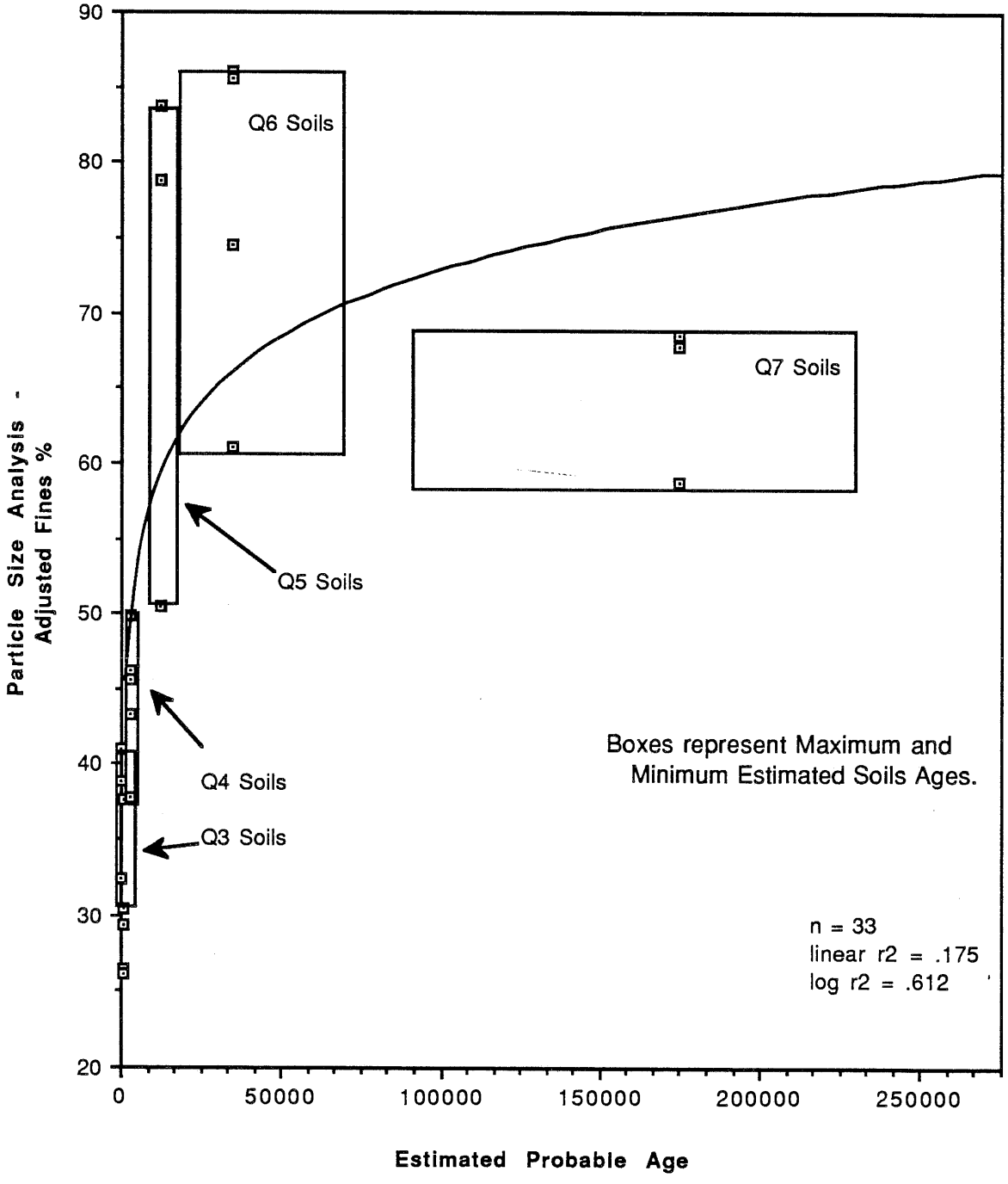

Fig. 8 - Graph of Adjusted Particle Size Analysis vs. Estimated Soil Age.

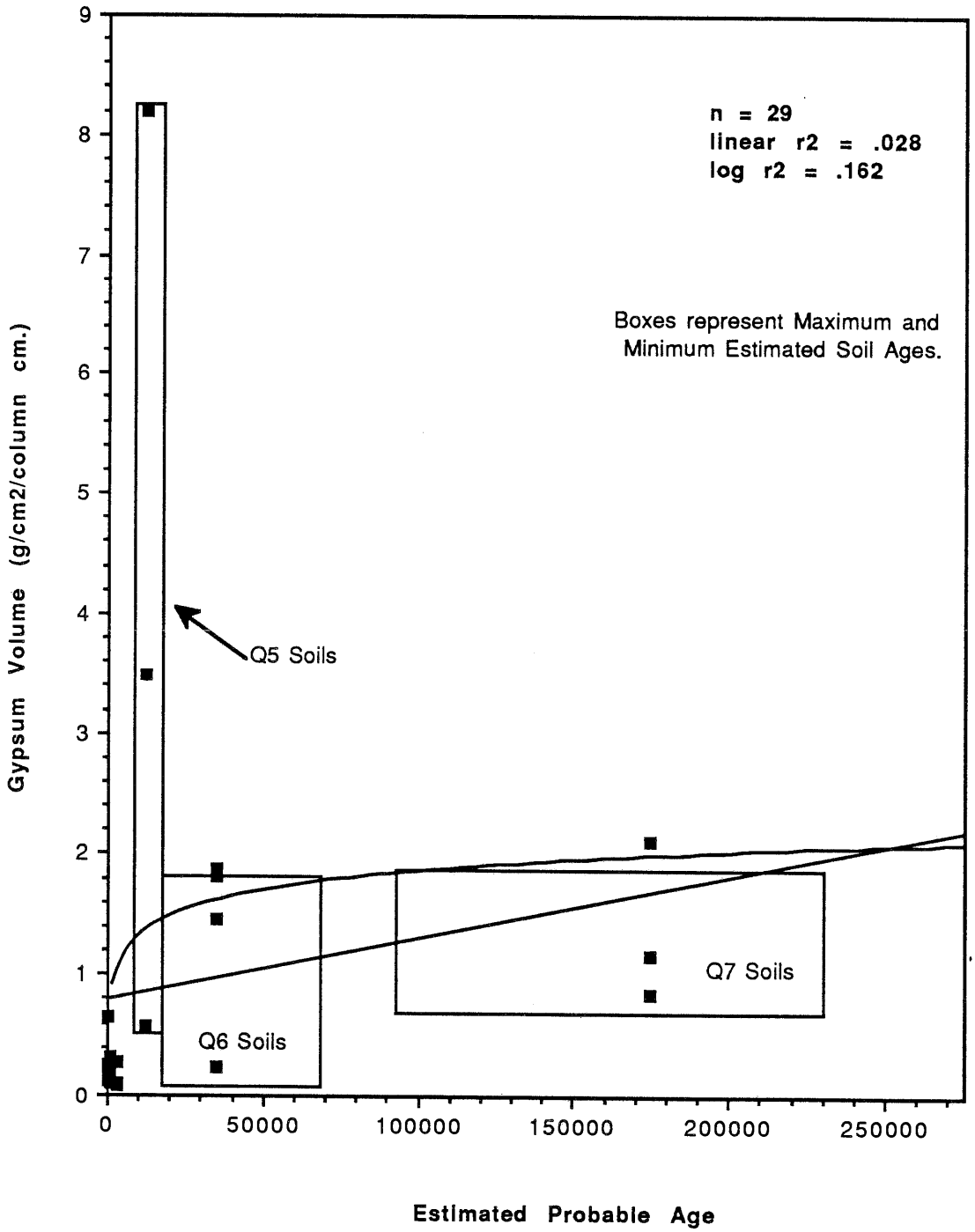

Fig. 9 - Gypsum Volume vs. Estimated Soil Age.

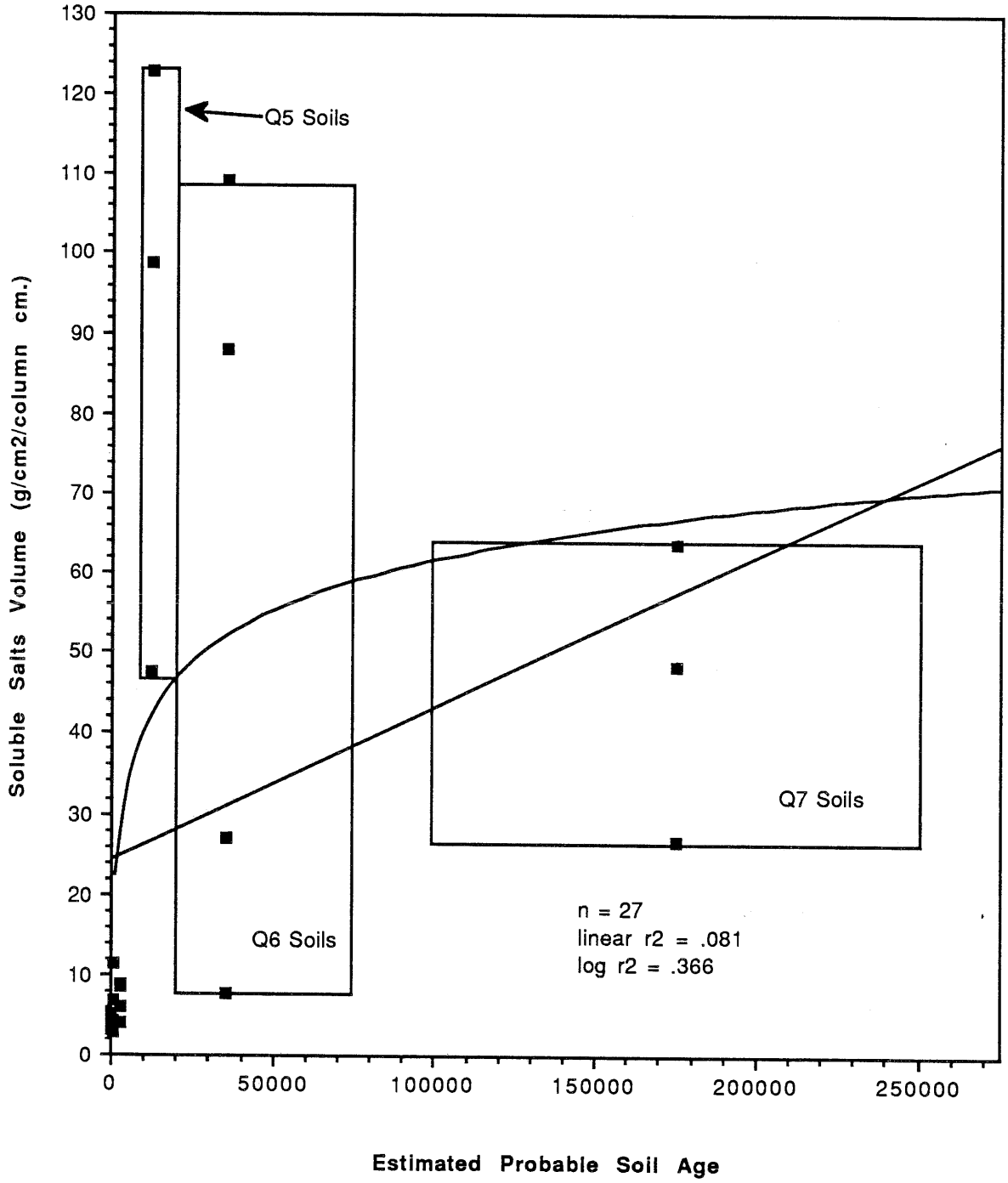

Fig. 10 - Soluble Salts Volume vs. Estimated Soil Age.

fines, in the soil, with time; and (3) the increase in thickness of the Av horizon (Fig. 11), coupled with the previous evidence, further supports the contention that aeolian inputs are the most reasonable sources for the fines in these soils.

The major field observations, that increasing development in these soils is manifested by an increase in the stage of carbonate accumulation, by reddening of the upper soil horizons, and by increases in the amount of soil fines are reflected in the SDI data. Additionally the profile development index, the summary of the profile properties, shows that overall soil development increases with increasing age. These data validate the use of the SDI as a tool in the quantitative analysis of soil field data.

Qualitative observations of the Coyote Mountains soils indicated that these soils fall into two broadly defined groups. The Q1-Q4 were classified as Typic Torriorthents, Q5-Q7 soils classified as Typic Calciorthids. These qualitative observations were supported by the SDI analyze. Statistically the same broad groups of soils occur both for the profile development index and for the profile property indices, carbonate morphology, rubification, and adjusted textural classification.

These divisions or groupings of the soil data apply also to the particle size analysis data. That is, the Q1-Q4 soils are statistically indistinguishable from one another and the Q5-Q7 soils are similarly indistinguishable from one another. The general trend, from the first group to the second group, is towards increasing accumulations of fines. This is further

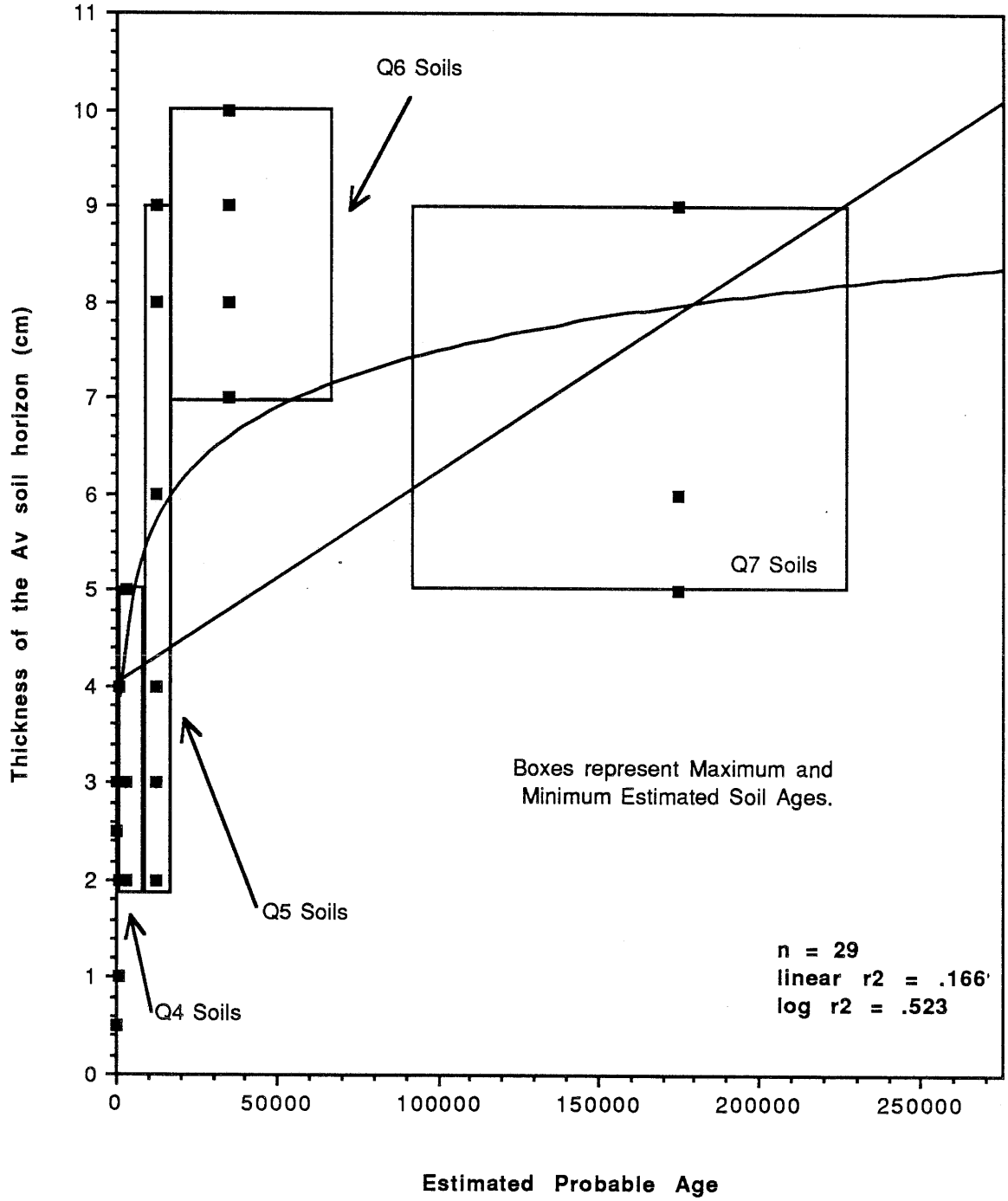

Fig. 11 - Av horizon thickness vs. Estimated Soil Age.

support for the contention that aeolian depositional processes lead to increased soil development in these soils. Within each of the two groups the coefficient of variability decreases from the youngest to the oldest soils. This might be indicative of a reduction in variability with increasing soil age. However, this observation is speculative and would require more data collection before such a blanket statement can be accepted.

Total accumulations of calcium carbonate, gypsum, and soluble salts were not observed to fit into the discussed statistical trend. The average values of calcium carbonate volume, for soils on a given geomorphic surface, do not increase with increasing soil age. As previously stated this is contrary to the expectations raised by field observations. The general trend derived from the field data, the SDI data, and the particle size data is towards increasing accumulations of soil fines with increasing age, again most likely due to aeolian deposition of these materials.

Because total carbonate volume can reasonably be expected to reflect a similar trend, of increasing accumulation with increasing age, the inference may be drawn that calcium carbonates have been removed from the soil system. This withdrawal may reflect the dissolution of these materials from the soil and their repre-cipitation elsewhere in the fan system. This withdrawal is most likely a function of the effects of groundwater and infiltrating precipitation. Furthermore, if this speculation is true then the more soluble soil constituents, gypsum and soluble salts must also have been removed from the

soil system in a similar fashion. It is interesting to note that the analysis of the distribution of these soil constituents, gypsum and soluble salts, supports this speculation.

Analysis of the gypsum and soluble salt accumulation data demonstrates that there are three statistically significant groups or clusterings of soils. Q1 through Q4 soils cannot be statistically separated from one another. Q6 and Q7 cannot be statistically distinguished from each other. Soils from the Q6 and Q7 deposits have several times greater accumulations of both gypsum and soluble salts than the Q1-Q4 deposit soils. Q5 soils, however, have much greater accumulations than Q6 and Q7 soils and so constitute the third unique statistical clustering.

Assuming that the arguments above regarding the loss of calcium carbonate, gypsum, and soluble salts are accepted, then their current accumulations must reflect recharge since the dissolution events. The most likely candidate for these events is during a slighter wetter Pleistocene. Therefore, we suggest that this is further evidence that the Q5, Q6, and Q7 deposits predate the Pleistocene-Holocene transition.

If these soils are indeed forming primarily by the deposition and translocation of aeolian dust and given that the accumulations of gypsum and soluble salts are aeolian in origin why is it that the Q5 deposits have much greater accumulations of these constituents than the Q6 and Q7 soils, which are considered to have been recharged simultaneously during the dryer Holocene?

A plausible answer to this question is that the Q5 deposits are more effective at trapping aeolian dust than the Q6 and Q7 deposits. Consider that the Q5 deposits display subdued bar and swale microtopography and an incipient desert pavement whereas the Q6 and Q7 deposits have nearly planar surfaces and well developed desert pavements. The net effects of these differences are to reduce the surface roughness of the older deposits, a reduction that would have a negative effect on the retention of aeolian dust and perhaps precipitation. A reduction in surface roughness of the deposit would allow more aeolian infall to be blown off readily and possibly for some precipitation to run off as sheet flow.

The data summarized in Table 6 indicates that the relationship between soil profile development and increasing age is best described by a logarithmic function rather than a linear function. Further, in studying soil development as a function of time it is apparent that a number of individual soil properties show a similar logarithmic relationship to increasing soil age. In the Coyote Mountains chronosequence, those soil properties whose increasing development correlate most strongly with soil age are carbonate morphology, rubification, and changes in textural classification.

If aeolian influx is the primary process leading to the increasing development of these soils, why does a log function best explain the relationship between increasing soil development and soil age? Theoretically, aeolian flux rates in this area have remained fairly constant about a relatively steady-

state equilibrium value for the last several thousand years. Yet both Soil Development Index calculations and soil laboratory data indicate that a log function yields the most significant correlation between soil age and each of the parameters investigated.

Two possible reasons exist to explain this apparent discrepancy: (1) the rough age estimates are biased in such a way that the analysis yields this result or (2) soil development is truly related logarithmically to soil age. It is clear that these age estimates are imprecise and probably inaccurate (at least for the mean values) but we believe them to be adequate for the examination of developmental trends.

Chemical weathering has been show to be related logarithmically to time (Colman, 1981) yet it has also been demonstrated that chemical weathering is not responsible for the development of these soils. Decreases in geomorphic surface roughness, with time, can be used to explain the logarithmic relationship between soil age and soil development for this study. Recall that several factors were utilized initially to differentiate the Quaternary units in this study. Among these factors, the development of two of them would have a strong negative influence on the surface roughness of the deposit. One, the planation of the original bar and swale microtopography and secondly, the increasing development of a desert pavement. It is probable that these factors are working to lower the surface roughness of these deposits with time. This reduction in surface roughness would lower both the adhesion of particles to the

surface and decrease the ability of precipitation to enter the surface. Both the lack of adhesion and the reduction in infiltration would serve to lower the rate of accumulation of aeolian particles without requiring that significant changes in the aeolian flux rate have occurred.

Summary

Increasing soil development in the Coyote Mountains soils is manifested in several ways. Laboratory and geochemical analyses reveal that there are significant increases in accumulations of: (1) silt and clay-sized materials; (2) carbonates; (3) gypsum; and (4) soluble salts with increasing soil age. These accumulations are translocated through the soil profile by infiltrating precipitation and contribute strongly to the morphological changes that occur in these soils. Increasing soil age is morphologically evidenced by the development of a reddened B horizon (Bw), by the development of the various stages of carbonate accumulation morphology, and by thickening of the Av soil horizon. The Soil Development Index provides a mechanism for the evaluation of these changes.

However, these investigations suggest that these soils are not accumulating fines, carbonates, gypsum, and soluble salts linearly with time. Instead a number of factors have intervened to make the rates of accumulation of these materials difficult to determine and decipher. These factors seem to be a function of (1) flushing of these materials from the soil system at some point in the past (or present) and (2) the efficiency of these deposits in retaining aeolian dust for later translocation into the

soil. Therefore soil development rates in the Coyote Mountains are best described by the equation $y = a + (b \log X)$, where y is the soil and X is time.

Finally, increasing soil development in the Coyote Mountains soils is attributable to accumulations of aeolian dust with time. This aeolian dust is dominantly composed of carbonates, gypsum, other soluble salts, silt, and clay. The sources for these aeolian materials lie in the surrounding Salton Trough region. Reheis (pers. comm.) has documented that high aeolian flux rates exist both on a local and a regional scale for each of these materials.

References

Bachman, G.O., and Machette, M.N., 1977, Calcic soils and calcretes in the southwestern United States: U.S. Geological Survey Open-File Report 7-794, 163 p.

Birkeland, P.W., 1984, Soils and geomorphology: Oxford University Press, 216 p.

Bockheim, J.G. 1980, Solution and use of chronofunctionsin studying soil development: Geoderma, v. 24, p. 71-85

Busacca, A.J., 1987, Pedogenesis of a chronosequence in the Sacramento Valley, California, U.S.A., I. Application of a Soil Development Index: Geoderma, v. 41, p. 123-148

Dethier, D.P., Harrington, C.D., and Aldrich, M.J., 1988, Late Cenozoic rates of erosion in the western Espanola basin, New Mexico: Evidence from geologic dating of erosion surfaces: Geological Society of America Bulletin, v. 100, p. 928-937

Dorn, R.I.,and Oberlander, T.M., 1981, Rock varnish origin, characteristics, and usage: Zeitschrift f■ Geomorphologie Supplement, v. 25, p. 420-436

Dorn, R.I., Bamforth, D.B., Cahill, T.A., Dohrenwend, B.D., Turrin, D.J., Donahue, D.J., Jull, A.J.T., Long, A., Macko, M.E., Weil, E.B., Whitley, D.S., and Zabel, T.H., 1986, Cation-ratio and accelerator radiocarbon dating of rock varnish on Mojave artifacts and landforms: Science, v. 231, p. 830-833

Gile, L.H.,1975, Holocene soils and soil-geomorphic realtions in an arid region of southern New Mexico: Quaternary Research, v. 5, p. 321-360

Gile, L.H., Peterson, F.F., and Grossman, R.B., 1966, Morphological and genetic sequences of carbonate accumulation in desert soils: Soil Science, v. 101, p. 347-360

Gile, L.H., Hawley, J.W., and Grossman, R.B., 1981, Soils and geomorphology in the Basin and Range area of southern New Mexico-Guidebook to the desert project: New Mexico Bureau of Mines and Mineral Resources Memoir 39, 222 p.

Harden J., 1982, A study of soil development using the geochronology of Merced River Deposits, California: Ph.D. thesis: Berkeley, University of California, Berkeley, 237 p

Harden, J.W., and Taylor, E.M., 1983, A quantitative comparison of soil development in four climatic regimes: Quaternary Research, v. 20, p. 342-359

Jenny, H., 1941, Factors of Soil Formation: New York, McGraw-Hill Book Co., Inc., 221 p.

Kronberg, B.I., Fyfe, W.S., Leonardos, O.H., and Santos, A.M., 1979, The chemistry of some Brazilian soils: Element mobility during intense weathering: Chemical Geology, v. 24, p. 211-229

Machette, M.N., 1985, Calcic soils of the southwestern United States *in* Weide, D.L., ed., Soils and Quaternary geology of the southwestern United States: Geological Society of America Special Paper 203

McFadden, L.D., 1982, The impacts of temporal and spatial climatic changes on alluvial soils genesis in southern California: Ph.D. thesis Tucson, University of Arizona, 430 p.

Mueller, K., 1984, Tectonic geomorphology of the southwestern Sierra de las Cucapas, Baja California Norte: Master's thesis, San Diego State University, 436 p.

Pinault, C.T., 1984, Structure, tectonic geomorphology and neo-tectonics of the Elsinore Fault Zone between Banner Canyon and the Coyote Mountains, southern California: Master's thesis,San Diego State University, 231 p.

Plaster, R.W., and Sherwood, W.C., 1971, Bedrock weathering and residual soil formation in central Virginia: Geological Society of America Bulletin, v. 82, p. 2813-2826

Reheis, M.C., Harden, J.W., McFadden, L.D., and Shroba, R.R., 1989, Development rates of Late Quaternary soils, Silver Lake playa, California: Soil Science Society of America Journal, v. 53, p.1127-1140

Rockwell, T.K., 1983, Soil chronology, geology, and neotectonics of the north central Ventura Basin, California: Ph.D. thesis Santa Barbara, University of California, Santa Barbara, 424 p.

Rockwell, T.K. and Pinault, C.T., 1986, Holocene slip events on the southern Elsinore fault, Coyote Mountains, southern California: *in* Ehlig, P., ed., Neotectonics and Faulting in Southern California, Geological Society of America Fieldtrip Guidebook for the Cordilleran Section Meeting in Los Angeles, p. 167-176

Schwertmann, U., and Taylor, R.M., 1977, Iron oxides *in* Dixon, J.B., and Weed, S.B., eds., Minerals in soil environments: Soil Science Society of America

Soil Survey Staff, 1975, Soil Taxonomy: United States Department of Agriculture Handbook No., 436, 754 p.

Sowers, J., 1985, Ph.D. thesis: Berkeley, University of California, Berkeley

Wells, P.V., 1976, Macrofossil analysis of wood rat (Neatoma) middens as a key to the Quaternary vegetation history of arid America: Quaternary Research, v. 6, p. 223-248

Appendix A -. Summary of Geochemical Analysis of Coyote Mour

Soil Profiles	pH	CaCO3 %	Gypsum %	Soluble Salts %
Q1 Geomorphic Surfaces				
AC-Q1-A1	8.1	8.97	0.26	0.51
	8.2	8.79	0.26	0.69
	8.1	7.21	0.17	1.52
	8.2	6.82	0.08	0.19
	8.2	5.94	0.06	2.00
FC-Q1-A1	7.1	6.87	0.05	3.45
	7.8	7.19	0.06	4.41
	7.8	7.65	0.05	2.89
FC-Q1-A2	7.9	6.55	0.01	1.49
	8.1	6.03	0.08	1.20
FC-Q1-A3	8.1	7.44	0.02	1.08
	8.1	7.97	0.03	1.07
Q2 Geomorphic Surfaces				
FC-Q2-A1	7.9	8.05	0.08	1.88
	8.1	6.88	0.06	1.26
	8.1	9.32	0.05	0.81
FC-Q2-A2	7.7	7.62	-----	1.59
	7.9	7.27	0.05	0.95
	8.0	8.01	0.06	1.24
	7.7	8.08	0.07	1.10
FC-Q2-B1	7.7	7.14	0.06	1.96
	7.8	6.51	0.07	1.77
	8.0	8.57	0.05	0.92
FC-Q2-B2	7.5	6.85	0.09	2.65
	7.6	6.33	0.08	1.38
	7.9	7.02	0.07	1.39
Q3 Geomorphic Surfaces				
AC-Q3-A1	8.4	6.85	0.05	0.37
	8.3	8.42	0.03	2.97
	8.2	8.07	0.01	2.35
	7.8	8.48	0.02	1.96
	8.3	8.61	0.03	3.60
AC-Q3-A2	7.9	5.79	0.15	2.47
	7.9	6.13	0.03	1.23
	8.0	6.90	0.04	0.79
	8.2	8.37	0.07	3.18
	8.3	8.34	0.01	0.48
FC-Q3-A1	7.7	6.30	0.09	1.17
	7.9	7.42	0.07	0.79
	7.9	15.71	0.07	1.10
	8.0	8.73	0.06	1.17
FC-Q3-A2	7.1	7.29	0.09	1.22
	8.1	7.00	0.05	0.80
	7.7	8.37	0.06	1.00
	7.9	6.67	0.05	0.74
FC-Q3-A3	7.7	7.59	0.08	1.25

Appendix A -. Summary of Geochemical Analysis of Coyote Mour

Soil Profiles	pH	CaCO3 %	Gypsum %	Soluble Salts %
	7.8	7.79	0.07	0.91
	7.8	7.91	0.06	1.56
	8.0	7.16	0.05	0.75
	7.8	6.58	0.07	1.25
FC-Q3-A4	7.7	4.58	0.08	1.09
	7.8	8.67	0.08	1.02
	7.3	7.52	0.09	2.02
Q4 Geomorphic Surfaces				
AC-Q4-A1	8.4	4.25	0.09	4.40
	8.0	6.02	0.01	1.59
	8.0	6.05	0.10	2.27
	8.2	8.45	0.01	2.25
	8.2	5.21	0.02	1.29
AC-Q4-A2	8.1	6.15	0.17	2.49
	8.0	6.29	0.01	0.78
	7.8	6.55	0.02	1.37
	7.6	8.06	0.01	1.54
	7.8	7.63	0.02	1.05
AC-Q4-B1	8.1	7.48	0.15	1.90
	7.8	6.61	0.06	1.32
	7.8	5.13	0.09	1.75
	8.0	6.88	0.01	1.92
Q5 Geomorphic Surfaces				
AC-Q5-A1	8.1	3.33	0.07	2.83
	8.0	1.74	0.02	1.79
	7.7	1.53	0.11	3.35
	7.9	3.66	0.01	3.40
	7.5	4.13	0.06	18.46
	7.5	3.79	0.29	20.72
AC-Q5-A2	7.9	4.72	0.10	2.85
	7.9	3.07	0.06	4.20
	7.5	3.19	2.23	27.23
	7.7	3.90	2.75	45.23
	7.5	4.03	2.53	33.75
AC-Q5-B1	8.3	3.81	1.78	3.56
	8.0	2.79	0.03	1.45
	7.9	4.73	0.02	5.05
	7.4	7.00	1.71	38.41
	7.5	6.43	1.14	37.33
	7.5	6.86	0.99	32.73
Q6 Geomorphic Surface				
FC-Q6-A1	6.8	7.88	0.52	- - - - -
	7.1	6.74	0.28	66.44
	6.7	13.88	0.26	59.17
	7.3	8.09	1.22	42.14
	7.7	11.84	0.50	11.57
	7.5	8.62	0.23	23.50

Appendix A -. Summary of Geochemical Analysis of Coyote Mour

Soil Profiles	pH	CaCO3 %	Gypsum %	Soluble Salts %
FC-Q6-A2	8.1	4.36	0.03	0.47
	8.2	2.52	0.02	1.66
	8.0	9.02	0.48	11.72
	7.9	10.18	0.30	10.07
	7.6	12.97	0.14	15.60
	8.0	5.85	0.24	4.54
FC-Q6-A3	8.0	8.42	0.11	3.21
	8.0	4.89	0.11	2.73
	7.8	8.64	0.22	7.41
	7.3	8.68	1.33	57.08
	7.3	9.43	0.56	55.08
	7.5	6.06	0.32	26.43
FC-Q6-A4	8.1	7.20	0.07	2.07
	8.0	5.87	0.06	1.69
	7.9	7.97	0.06	2.62
	8.0	13.96	0.06	1.78
	8.3	6.69	0.11	1.88
	8.5	6.20	0.05	2.30
Q7 Geomorphic Surfaces				
AC-Q7-A1	8.0	4.82	0.14	3.45
	7.7	11.02	0.08	8.58
	7.6	4.97	0.23	21.14
	7.5	12.88	1.38	33.89
	7.6	4.39	0.08	15.44
	7.8	4.00	0.07	12.70
AC-Q7-B1	8.0	3.71	0.05	3.51
	7.9	3.73	0.08	3.04
	7.8	4.49	0.04	7.34
	8.0	14.75	0.05	1.87
	7.9	5.26	0.04	4.92
	7.6	8.42	1.88	22.44
	8.1	4.45	0.52	14.18
AC-Q7-B2	8.0	3.81	0.08	2.23
	7.9	1.81	0.04	1.59
	7.9	2.33	0.05	1.38
	7.7	6.25	0.34	4.86
	7.5	3.90	0.86	13.61
	7.3	5.57	1.88	22.33
	7.5	4.06	0.17	20.28

Soil Description - Coyote Mountains Chronosequence

Classification: sandy-skeletal, mixed (calcareous), hyperthermic, Typic Torriorthent
Identifier: AC-Q1-A1
Geomorphic Surface: Q1 surface
Location: Mouth of Alverson Canyon
Geographic Coordinates: NE 1/4 of NE 1/4 of S15 T16S,R9E San Bernardino Base Meridian; Carrizo Mountain 7.5' Quadrangle
Landform: Channel incised into alluvial fan
Parent Material: Gravelly alluvium derived from Coyote Mountains
Slope: <3%
Elevation: 660 ft.
Vegetation: Smoke Trees (Parosela spinosa), desert scrub vegetation
Collected by: J. Goodmacher
Described by: J. Goodmacher
Exposure: Soil pit - excavated by hand

Horizon	Depth (cm)	Description
C1	0-5	Brown (10YR 5/3m, 10YR 6/3d); sand; single grain; loose, non-sticky, non-plastic; violently effervescent in dilute HCl; abrupt, wavy boundary
C2	5-10	Grayish Brown (10YR 5/2m, 10YR 6/2d) silt or fine sand; single grain; loose, non-sticky, non-plastic; violently effervescent in dilute HCl; few fine roots; abrupt, wavy boundary
C3	10-19	Brown (10YR 5/3m, 10YR 6/3d); coarse sand; single grain; loose, non-sticky, non-plastic; violently effervescent in dilute HCl; few fine and medium roots; abrupt, wavy boundary
C4	19-39	Brown (10YR 5/3m, 10YR 6/3d); sand; single grain; loose, non-sticky, non-plastic; violently effervescent in dilute HCl; abrupt, wavy boundary
C5	39-49+	Brown (10YR 5/3m, 10YR 6/3d); sand; single grain; loose, non-sticky, non-

plastic; violently effervescent in dilute HCl

NOTES-

1. Depositional stratigraphy provides a basis for division into horizons. Changes occur in both stoniness of materials and in coarseness of sand fraction.
2. Surface with prominent bar and swale topography; no desert varnish development; clasts not shattered; no reddening on clast bottoms.
3. Estimated gravel content:

C1	70%
C2	10-20%
C3	60%
C4	80%
C5	60-70%

Soil Description - Coyote Mountains Chronosequence

Classification: sandy-skeletal, mixed (calcareous), hyperthermic, Typic Torriorthent
Identifier: FC-Q2-A1
Geomorphic surface: Q2 surface
Location: Near mouth of Fossil Canyon
Geographic Coordinates: SE 1/4 of SE 1/4 of S10 T16S,R9E San Bernardino Base Meridian; Carrizo Mountain 7.5' Quadrangle
Landform: Abandoned intermittent stream channel
Parent Material: Gravelly alluvium derived from Coyote Mountains
Slope: <3%
Elevation: ~ 650 ft.
Vegetation: Smoke Tree (Parosela spinosa), Brittle Bush (Encelia farinosa), Burrobush (Franseria dumosa)
Collected by: J. Goodmacher
Described by: J. Goodmacher
Exposure: Stream cut - excavated by hand

Horizon	Depth (cm)	Description
Av	0-4	Dark Grayish Brown (10YR 4/2m; 10YR 6/2m); loamy sand; single grain; loose, non-sticky, non-plastic; few, fine roots; violently effervescent in dilute HCl; common medium inped vesicular pores; gradual, smooth boundary
Ck1	4-12	Brown (10YR 4/3m; 10YR 6/3d); loamy sand; single grain, non-sticky, non-plastic; violently effervescent in dilute HCl; very weak carbonate accumulations on the undersides of some clasts; abrupt, wavy boundary
Ck2	12-26	Brown (10YR 4/3m; 10YR 6/3d); sand; single grain, non-sticky, non-plastic; very weak carbonate accumulations on clasts, violently effervescent in dilute HCl; abrupt, wavy boundary

C	26-51+	Grayish Brown (10YR 5/2m;10YR 6/2d); sand to coarse sand; single grain; loose, non-sticky, non-plastic; violently effervescent in dilute HCl

NOTES-

1. Carbonates are extremely weak stage I on clasts, none in matrix.
2. Bar and swale topography is well preserved; very faint varnish development on only some clasts; no clast shattering; no reddening on undersides of clasts.
3. Estimated gravel content by horizon.

Av	50%
Ck1	50%
Ck2	75%
C	75%

Soil Description - Coyote Mountains Chronosequence

Classification: sandy-skeletal, mixed (calcareous), hyperthermic, Typic Torriorthent
Identifier: FC-3
Geomorphic surface: Q3 surface
Location: Near mouth of Alverson Canyon
Geographic Coordinates: NW 1/4 of NW 1/4 of S15 T16S,R9E San Bernardino Base Meridian; Carrizo Mountain 7.5' Quadrangle
Landform: Abandoned intermittent stream channel
Parent Material: Gravelly alluvium derived from Coyote Mountains
Slope: <3%
Elevation: ~ 650 ft.
Vegetation: Ocotillo (Fouquiera splendens), desert scrub vegetation
Collected by: J. Goodmacher
Described by: J. Goodmacher
Exposure: Stream cut - excavated by hand

Horizon	Depth (cm)	Description
Av	0-1	Brown (10YR 4.5/3m; 10YR 6/3d) loamy sand; medium platy; soft, very friable, slightly sticky, non-plastic; moderately effervescent in dilute HCl
Ck1	1-12	Brown (10YR 4.5/3m; 10YR 5/3d); sand; single grain; loose, loose, non-sticky, non- plastic; slightly effervescent in dilute HCl; weak stage I carbonate accumulating on bottoms of some clasts
Ck2	12-22	Brown (10YR 4.5/3m; 10YR 6/3d); loamy sand; single grain; loose, loose, non-sticky, non-plastic; slightly effervescent in dilute HCl; very weak stage I carbonate
C	22-30	Dark Grayish Brown (10YR 4.5/2m; 10YR 7/2d); sand; single grain; loose, loose, non-sticky, non-plastic; very slightly effervescent in dilute HCl

Ck3	30-50+	Dark Grayish Brown (10YR 4.5/2m; 10YR 6/3d); sand; single grain; loose, loose, non-sticky, non-plastic; slight effervescence in dilute HCl; weak stage I carbonate similar to Ck1

NOTES -
1. weak varnish development
2. unweathered clasts, no surface pitting
3. schists, plutonics and andesites have a thin rust-brown patina, carbonates very slightly etched.

Soil Description - Coyote Mountains Chronosequence

Classification: sandy-skeletal, mixed, hyperthermic, Typic Calciorthid
Identifier: AC-Q4-A2
Geomorphic surface: Q4 surface
Location: Near mouth of Alverson Canyon
Geographic Coordinates: SE 1/4 of SE 1/4 of S10 T16S,R9E San Bernardino Base Meridian; Carrizo Mountain 7.5' Quadrangle
Landform: Abandoned intermittent stream channel
Parent Material: Gravelly alluvium derived from Coyote Mountains
Slope: <3%
Elevation: ~ 650 ft.
Vegetation: Ocotillo (Fouquiera splendens), desert scrub vegetation
Collected by: J. Goodmacher
Described by: J. Goodmacher
Exposure: Stream cut - excavated by hand

Horizon	Depth (cm)	Description
Av	0-3	Brown (10YR 4/3m; 10YR 7/3d); sandy loam; moderate medium platy breaking to single grain; soft, very friable, slightly sticky, non-plastic; violently effervescent in dilute HCl; common medium vesicular pores; abrupt, smooth boundary
Ck1	3-28	Grayish Brown (10YR 5/2m; 10YR 7/2d); sand; single grain; loose, non-sticky, non-plastic; violently effervescent in dilute HCl; few fine and medium roots; stage I carbonate on clasts; gradual, wavy boundary
Ck2	28-52	Brown (10YR 5/3m; 10YR 7/2d); sand; single grain; loose, non-sticky, non-plastic; violently effervescent in dilute HCl; common fine to medium roots; stage I carbonate development on clasts; gradual, wavy boundary

Ck3	52-72	Grayish Brown (10YR 5/2m; 10YR 6/2d); coarse sand; single grain; loose, non-sticky, non-plastic; violently effervescent in dilute HCl; stage I carbonate on clasts; abrupt, wavy boundary
Ck4	72-89+	Grayish Brown (10YR 5/2m; 10 YR 7/2d); coarse sand; single grain; loose, non-sticky, non-plastic; violently effervescent in dilute HCl; stage 1 carbonates on clasts

NOTES-

1. Geomorphic indicators are minimally developed.
2. Gravel contents by horizon
   - Av ---
   - Ck1 25-30%
   - Ck2 60-70% (stony)
   - Ck3 60-70%
   - Ck4 negligible

Soil Description - Coyote Mountains Chronosequence

Classification: sandy-skeletal, mixed, hyperthermic, Typic Calciorthid
Identifier: AC-Q5-B1
Geomorphic surface: Q5 surface
Location: Near mouth of Alverson Canyon
Geographic Coordinates: SE 1/4 of SE 1/4 of S10 T16S,R9E San Bernardino Base Meridian; Carrizo Mountain 7.5' Quadrangle
Landform: Alluvial fan deposit
Parent Material: Gravelly alluvium derived from Coyote Mountains
Slope: <3%
Elevation: ~ 650 ft.
Vegetation: Desert scrub vegetation
Described by: J. Goodmacher
Collected by: J. Goodmacher
Exposure: Stream cut - excavated by hand

Horizon	Depth (cm)	Description
Av	0-9	Brown (10YR 5/3m; 10YR 7/2d); sandy loam; weak subangular blocky breaking to single grain; soft, very friable, slightly sticky, non-plastic; violently effervescent in dilute HCl; few fine roots; few fine inped vesicular pores; abrupt, wavy boundary
Bw	9-28	Dark Yellowish Brown (10YR 4/4m; 10YR 6/4d); sandy loam; single grain; loose non-sticky, non-plastic; strongly effervescent in dilute HCl; common fine and medium roots; stage I carbonate development; clear wavy boundary
Ck1	28-48	Dark Yellowish Brown (10YR 4/4m; 10YR 5/3d); loamy sand; weak subangular blocky breaking to single grain; soft, very friable, non-sticky, non-plastic; violently effervescent in dilute HCl; few medium roots; stage I carbonate accumulations occurring as soft, pendant masses on undersides of some clasts; clear, wavy boundary

Ck2	48-74	Dark Brown (10YR 4/3m; 10YR 6/3d); loamy sand; weak subangular blocky breaking to single grain; soft, very friable, non-sticky, non-plastic; violently effervescent in dilute HCl; few fine roots; stage I+ carbonate, soft, pendant masses on undersides of clasts and thin filaments in matrix; gradual, wavy boundary
Ck3	74-111	Brown (10YR 5/3m; 10YR 7/2d); loamy sand; single grain; loose, loose, non-sticky, non-plastic; violently effervescent in dilute HCl; stage I+ carbonates with local stage II, carbonate pipes are present as weak to strongly cemented masses; gradual, wavy boundary
Ck4	111-136+	Brown (10YR 5/3m; 10YR 7/2d); loamy sand; single grain; loose, loose, non-sticky, non-plastic; violently effervescent in dilute HCl; stage I+ carbonates, local stage II, carbonate pipes are present as weak to strongly cemented masses; gradual, wavy boundary

NOTE -

1. Geomorphic indicators - desert varnish covering most clasts; reddening on undersides of clasts is becoming more apparent; bar and swale topography is no longer apparent; there is moderate desert pavement development
2. Gravel content by horizon.
   - Av 60%
   - Bwk 60-70%
   - Ck1 65-75%
   - Ck2 50-60%
   - Ck3 70-80%
   - Ck4 60-70%
3. Division into separate horizons of Ck3 and Ck4 is done on basis of gravel content.

Soil Description - Coyote Mountains Chronosequence

Classification: sandy, mixed, hyperthermic, Typic Calciorthid
Identifier: FC-Q6-A2
Geomorphic surface: Q6 surface
Location: Immediately northwest of the mouth of Fossil Canyon
Geographic Coordinates: SE 1/4 of SE 1/4 of S10 T16S,R9E San Bernardino Base Meridian; Carrizo Mountain 7.5' Quadrangle
Landform: Alluvial fan deposit
Parent Material: Gravelly alluvium derived from Coyote Mountains
Slope: <3%
Elevation: ~ 650 ft.
Vegetation: Brittle brush (Encelia farinosa), sparse desert shrubs
Collected by: J. Goodmacher
Described by: J. Goodmacher
Exposure: Soil pit - excavated by hand

Horizon	Depth (cm)	Description
Av	0-8	Yellowish Brown (10YR 5/6m; 10YR 7/3d); sandy loam; weak, fine platy breaking to single grain; soft, very friable, slightly sticky, non-plastic; violently effervescent in dilute HCl; common fine inped vesicular pores; abrupt, wavy boundary
Bwk	8-14	Yellowish Brown (10YR 5/4m; 10YR 7/4d); sandy loam; weak subangular blocky breaking to single grain; soft, very friable, non-sticky, non-plastic; violently effervescent in dilute HCl; abrupt, wavy boundary
Ck1	14-38	Brown (10YR 5/3m; 10YR 7/2d); sandy loam; weak, subangular blocky breaking to single grain; soft, non-sticky, non-plastic; violently effervescent in dilute HCl; stage II carbonate development, thick on clasts and in matrix; clear, wavy boundary

Ck2	38-70	Brown (10YR 4/3m; 10YR 7/3d); loamy sand; weak subangular blocky breaking to single grain; soft, very friable, non-sticky, non-plastic; violently effervescent in dilute HCl; stage II carbonates, thickest on clast bottoms, throughout matrix; abrupt, wavy boundary
Ck3	70-128	Brown (10YR 5/3m; 10YR 7/3d); loamy sand; weak, subangular blocky breaking to single grain; soft, non-sticky, non-plastic; violently effervescent in dilute HCl; stage II+ carbonate accumulations, thick around clasts, throughout matrix with prominent carbonate pipes; clear, wavy boundary
Ck4	128-148+	Brown (10YR 4/3m; 10YR 6/3d); sand; single grain; loose, non-sticky, non-plastic; violently effervescent in dilute HCl; stage I carbonate accumulating around clasts but not in matrix materials

NOTES-

1. Geomorphic indicators- subdued microtopography, moderately well developed desert pavement surface; beginnings of incision of pavemented surface; thick varnish development; moderate to strong development of reddened surfaces on clast bottoms; clast shattering is strongly developed on limestones and andesitic materials.

Soil Description - Coyote Mountains Chronosequence

Classification: sandy-skeletal, mixed, hyperthermic, Typic Calciorthid
Identifier: AC-Q7-B2
Geomorphic surface: Q7 surface
Location: Immediately northwest of Alverson Canyon outlet
Geographic Coordinates: NW 1/4 of NW 1/4 of S15 T16S,R9E San Bernardino Base Meridian; Carrizo Mountain 7.5' Quadrangle
Landform: Alluvial fan deposit
Parent Material: Gravelly alluvium derived from Coyote Mountains
Slope: <3%
Elevation: ~ 650 ft.
Vegetation: Brittle Bush (Encelia farinosa), desert scrub vegetation
Collected by: J. Goodmacher
Described by: J. Goodmacher
Exposure: Stream cut - excavated by hand

Horizon	Depth (cm)	Description
Av	0-9	Yellowish Brown (10YR 6/4m; 10YR 8/4d); sandy loam ; weak, medium subangular blocky breaking to single grain; soft, very friable, slightly sticky, non-plastic; violently effervescent in dilute HCl; common fine and medium inped vesicular pores; few, fine roots; abrupt, wavy boundary
Bwk	9-29	Brown (10YR 4/4m; 10YR 6/4d); sandy loam; weak subangular blocky breaking to single grain; soft, very friable, non-sticky, non-plastic; violently effervescent in dilute HCl; few fine and very fine roots; weak stage I powdery carbonate accumulations on clast bottoms; clear, wavy boundary

Bk	29-48	Brown (10YR 4/4m; 10YR 6/4d); loamy sand; weak, subangular blocky breaking to single grain; soft, non-sticky, non-plastic (except matrix w/weak cementation by $CaCO_3$; violently effervescent in dilute HCl; few fine, medium and coarse roots; stage I to I+ carbonate accumulations on clasts, occurring as soft pendant masses on undersides of clasts; clear, wavy boundary
Ck1	48-64	Pale Brown (10YR 6/3m; 10YR 7/2d); loamy sand; weak, subangular blocky breaking to single grain; hard, non-sticky, non-plastic; violently effervescent in dilute HCl; few, fine and medium roots; stage II to local stage III carbonate accumulations; abrupt, wavy boundary
Ck2	64-111	Brown (10YR 5/3m; 10YR 6/3d); sand (bouldery); weak, subangular blocky breaking to single grain; soft, non-sticky non-plastic; violently effervescent in dilute HCl; few fine and medium roots; stage I to I+ carbonate accumulations on clasts; gradual, wavy boundary
Ck3	111-142	Brown (10YR 6/3m; 10YR 7/3d; sand; weak, subangular blocky breaking to single grain; soft, non-sticky, non-plastic; violently effervescent in dilute HCl; stage I+ to II carbonates accumulations on clasts; gradual, wavy boundary
Ck4	142-169+	Brown (10YR 4/3m; 10YR 6/3d); loamy sand; weak subangular blocky breaking to single grain; soft, very friable, non-sticky, non-plastic; violently effervescent in dilute HCl; few, fine roots; stage I carbonates occurring on clasts as soft pendant masses on the undersides of pebbles, none in matrix

NOTES-

1. Geomorphic indicators- strong desert varnish development on nearly all clasts; increasing incision of surface is apparent; well-developed desert pavement; strong reddening apparent on undersides of most rock clasts; complete shattering of limestone clasts, advanced shattering of schists.
2. Carbonate pipes are present in all horizons from approximately 80 cm. depth and deeper into the soil.

RECOGNITION, EXTENSION AND SIGNIFICANCE OF NORTHEAST TRENDING FAULTS BETWEEN THE ELSINORE AND SAN JACINTO FAULT ZONES USING COMBINED SPOT AND LANDSAT IMAGERY

by

Thomas Rockwell[1], Ronald Blom[2], Robert Crippen[2], Ralph Klinger[1], Amy Stinson[1], and Andy Thomas[1]

1 Department of Geological Sciences
San Diego State University
San Diego, CA 92182

2 Jet Propulsion Laboratory
California Institute of Technology
4800 Oak Grove Drive
Pasadena, CA 91109

ABSTRACT

Analysis of separate and digitally combined images from SPOT (HRV/PAN) and Landsat (TM) satellite data display previously mapped, short and discontinuous northeast-trending faults between the Elsinore and San Jacinto fault zones as throughgoing structures which likely control deformation between these two important fault zones in southern California. Field and airphoto study of two of the northeast trending structural zones reveals they are faults with dominantly left-lateral separation and slip. Such motion could accommodate the late Quaternary rotation of sedimentary rocks in the Carrizo Badlands that has been determined paleomagnetically. The northeast trending faults are seismically active, have sustained late Quaternary surface rupture as indicated by scarps in alluvium, and may have broken in at least one historical earthquake.

The through-going nature of the northeast trending faults is more obvious on the satellite images than in airphotos or on the ground. This is due to the synoptic view and the display of spectral information from wavelengths longer than the visible in the Landsat Thematic Mapper data. Rocks and soils are more spectrally distinct in this spectral region than in the visible, enhancing detectablility of fault features.

The continuity and activity of these northeast-trending structures indicates that they are likely important in distributing dextral shear between the northwest-trending Elsinore and San Jacinto faults. This observation may impact the interpretation of geodetic data well as in assessing the seismic hazard of faults in the western Salton Trough.

INTRODUCTION

Northeast-trending faults have long been recognized between the Elsinore and San Jacinto fault zones, but they were generally mapped as short, discontinous bedrock features of limited and unknown significance (Fig. 1) (Dibblee 1954; Strand 1962; Rogers 1965; Jennings 1975; Allison 1978; Christensen 1957). Utilizing enhanced co-registered Landsat Thematic Mapper (TM) and SPOT (Systeme Probatoire d'Observation de la Terre) HRV (High Resolution Visible Panchromatic or 'PAN') satellite images, and enhanced TM images alone, we demonstrate that at least two of these faults are laterally continuous, displace mid to late Quaternary deposits, and interconnect the northwest-trending Elsinore and San Jacinto faults. Field mapping, guided in part by the satellite images, along the Split Mountain and Yuha Wells faults, demonstrates their surface continuity and recency of activity. Other through-going features on the images of similar expression to those investigated in the field await study, but are likely through-going faults as well. Analysis of historical seismicity demonstrates that many of these faults are seismically active, and some may be capable of producing significant earthquakes.

The presence and activity of these faults requires that structural models for the western Salton Trough account for them and their relationship to the northwest-trending Elsinore and San Jacinto faults. Paleomagnetic work indicates up to 30 degrees of clockwise rotation of the Carrizo Badlands in the past 900 ka (Johnson et al. 1983). Some of this rotation may have been accommodated by these northeast-trending structures, and determination of which faults are presently active may be useful in delineating the domain boundaries of the rotation cells. Further, the seismic hazard of this area needs to consider both the northeast and northwest-trending faults, especially in light of the 1987 Ms 6.2 earthquake that occurred on the northeast-trending Elmore Ranch fault and triggered the main shock in the Superstition Hills earthquake sequence (Hudnut et al. 1989a, b). Finally, interpretation of regional geodetic data must consider the active elements of this complex fault system. In this paper, we present evidence of the continuity, activity and possible significance of these faults based on interpretation of the satellite images, and field studies along two of the faults.

METHODS

The images used in this study are from the Thematic Mapper (TM) instrument on the Landsat 5 satellite (scene 50203-17462, 20 September 1984) and from the HRV sensor on the French SPOT satellite (scene 1- 546283-880207-183719-1P, 7 February 1988). Landsat TM records radiance in 6 visible and near infrared bands from 0.45 to 2.35 micrometers, and one thermal infrared channel at 10 micrometers. A full TM scene represents an area 180 by 180 km. Each Landsat TM picture element (pixel) depicts an area 28.5 by 28.5 meters on the ground. A SPOT scene represents an area of 60 by 60 km on the ground. The SPOT image depicts visible-wavelength (0.51-0.73 micrometer), broadband panchromatic (black and white) information at a pixel size representing 10 X 10 meters on the ground.

The Landsat Thematic Mapper image was processed by "directed band ratioing" (Crippen et al. 1988). This technique uses 5 of the 7 spectral bands available by displaying the ratios of reflectivity of bands 3/1, 5/4, and 5/7, displayed in blue, green, and red, respectively. These ratios result in greatest discrimination among lithologic materials in well exposed areas (Crippen et al. 1989). The spectral information lacks sufficient spectral resolution to identify individual minerals or rock types; however, the ratios chosen display presence of, and relative abundances of, iron and hydroxyl bearing minerals. In the displayed color scheme, for most geological materials, blue (ratio 3/1) represents ferric iron while green (ratio 5/4) represents ferous iron, and red (ratio 5/7) represents hydroxyl bearing minerals. Healthy vegetation is also displayed in red in this color scheme.

Normally, properly computed band ratio images display no topography, which is a great handicap in geologic studies. The directed band-ratioing technique preserves the topograhpic information as achromatic brightness variations, while the spectral information is displayed in color. The complete image processing procedure is described in Crippen, et al. (1988).

The black and white SPOT image was enhanced by use of a "high-pass" spatial filter to improve detection of fine detail. This high pass filtered image was used individually in much the same way as an airphoto except with regional (60 by 60 km) areal coverage; however a much more effective use of SPOT data is to combine it with the Landsat TM spectral information.

The SPOT image and the Landsat TM image were merged by finding tiepoints (points of known equivalence) and geometrically distorting the SPOT image slightly to precisely correspond to the space oblique mercator projection of the Landsat image. A Landsat TM ratio image was generated in which atmospheric and sensor contributions to the recorded radiances were adjusted for (Crippen, 1987). As previously mentioned, such an image displays essentially no topographic information, only spectral. However, we reintroduce the topography by multiplying each ratio image (one per color displayed-red, green and blue) by the co-registered SPOT black and white image. The SPOT image contains essentially no spectral information but relatively high spatial resolution topographic detail. Multiplying the images together pixel by pixel thus exploits the strengths of both systems. A relatively high spatial resolution is combined with geologically useful spectral information not otherwise available. This image processing procedure is described in detail in Crippen (1989).

The images produced were enlarged to appropriate map scales. The merged SPOT/TM image can easily be enlarged to 1:24,000 (experimentation indicates the image breaks down at about 1:6,000 or so). These images were analyzed in essentially the same manner as monoscopic study of airphotos. Locations of known faults and other lineaments and were compared to published geologic maps (Figs. 1 and 2). Two of the structures which are through-going on the images were studied in the field to evaluate their surface continuity, recency of activity, and sense of slip. These field investigations give us confidence in our ability to interpret other similar features seen in the image, and will help guide future work.

COMPARISON OF THE SPOT/LANDSAT IMAGERY WITH PREVIOUSLY PUBLISHED GEOLOGIC MAPS

Comparison of the location and lateral extent of faults on previously published geologic maps (Fig. 1) with the lineaments identified from the satellite images (Figs. 2, 3 and 4) shows that most of the previously mapped faults are recognizable on the images. Further, discontinuously mapped structures commonly

appear as through-going lineaments, many of which interconnect the San Jacinto and Elsinore fault zones. In the imagery, not only can the faults be identified by their geomorphic expression, such as scarps in alluvium, alignment of ridges, shadows, or other linear geomorphic features, but several of them are also delineated by color contrasts. Most of these color contrasts come from spectral information at wavelengths longer than the eye can see and thus not expressed on airphotos and difficult for the geologist to see in the field (the field geologist, of course, has an extremely high spatial resolution imaging system with a limited field of view). Some of the features discussed will be difficult to detect in the black and white reduced scale photos accompanying this manuscript.

There are also several prominent lineaments that were not previously mapped. One of these lineaments, the Yuha Wells fault as expressed in Fig. 4, was studied on the ground and found to be a well developed sinistral fault, as discussed below. Others likely represent primary structural features, but confirmation awaits future field mapping.

Interestingly, a few previously mapped faults are poorly expressed or not recognizable on the images. Even portions of the Coyote Creek strand of the San Jacinto fault that ruptured in 1968 with the Borrego Mountain earthquake (Clark 1972) are difficult to delineate (Fig. 5). Part of this difficulty relates to the orientation of the mid-morning sun illumination during image acquisition, which is parallel to these northwest-trending faults. These observations indicate the value of the images yet also confirm the absolute necessity of field investigations.

FIELD STUDY ALONG TWO OF THE IMAGE LINEAMENTS

Split Mountain Fault - The Split Mountain fault was chosen for field study because of its prominence on the merged SPOT/TM image as a complex system of fault features such as the presence of scarps in alluvium along part of its length (Fig. 2 and 3). The combination of the SPOT and TM data is particularly useful because the fault is expressed both as a series of geomorphic features, and in some areas as subtle spectral contrasts. Furthermore, this fault is of particular interest because the epicenter of the October, 1942 Ms 6.5 earthquake, previously attributed to the San Jacinto fault zone, was relocated by Sanders (1986) onto the northeasterly projection of this fault. This is futher discussed below.

The fault is well-expressed in the field both in the bedrock as a 1-4 m wide gouge zone that juxtaposes different lithologic units, and in alluvium as an alignment of scarps up to several meters high (Fig. 6). The linearity of Split Mountain Gorge is likely related to the fault which is discontinously exposed. The fault displays left-lateral separation of bedrock units and stream channels (Fig. 6), as well as left-lateral offset of the channel wall of Split Mountain Gorge itself. Fault surface kinematic

indicators of slip direction, such as striae and mullions, indicate dominantly lateral slip. Based on these observations and its northeast trend, the Split Mountain fault is interpreted to be a sinistral fault, similar to the Elmore Ranch fault that ruptured with the first shock (Ms 6.2) of the Superstition Hills earthquake sequence on November 24, 1987 (Hudnut, et al. 1989). In that earthquake sequence, the Elmore Ranch fault rupture was followed about 12 hours later by a larger (Ms 6.6) shock and surface rupture on the northwest-trending Superstition Hills fault (Hudnut, et al. 1989).

Fault scarps in young alluvium occur along the Split Mountain fault where late Quaternary deposits are preserved, and nowhere is the fault overlain by unbroken pre-Holocene deposits. Although the analysis is not complete, work to date indicates that it is likely that the 1942 earthquake may have ruptured the Split Mountain fault with sinistral slip, and did not rupture a strand of the San Jacinto fault zone as previously believed. This interpretation is supported by the presence of about half of Sanders' (1986) relocated aftershocks aligning along the fault (Fig. 7). The other epicenters, with the exception of two, also fall in the region between the Elsinore and San Jacinto faults. Of the two exceptions, one occurred several kilometers south of the Elsinore fault whereas the other occurred several kilometers north of the San Jacinto fault, neither apparently associated with the probable rupture surface.

Yuha Wells Fault - The Yuha Wells fault (Fig. 8) is part of a set of northeast-trending sinistral faults in the Yuha desert between the northern Laguna Salada and Superstition Mountain faults (see Fig. 1 for location). On the Landsat TM image enhanced by the directed band ratioing method, the fault zone is expressed as a continous set of diffuse geomorphic features such as aligned drainages, and subtle spectral contrasts (changes in image color) whose linearity suggests a tectonic origin. The Yuha Wells fault was mapped from near Highway 98 near the northern terminus of the Laguna Salada fault zone northeastward to the Holocene Lake Cahuilla shoreline. Field mapping of reveals faults which display left-lateral separation, based on displaced stratigraphy, and rupture all but the youngest (late Holocene) deposits. It is likely that the Yuha Wells fault continues a few kilometers farther to the northeast to the southern mapped extent of the Superstition Mountain fault, which is one of the principal strands of the San Jacinto fault zone in the Salton Trough. Following the Superstition Hills earthquake in November 1987, the Yuha Basin region experienced a burst of microseismic activity that extended through the summer of 1988 (Fig. 9). Many of these earthquakes appear to align in a northeasterly fashion, and probably represent activity of the sinistral faults. The temporal association of this microearthquake swarm immediately following a major earthquake along the San Jacinto fault zone supports a relationship.

DISCUSSION

The coregistered TM/SPOT image, and to a lesser degree the Landsat TM alone, provide sufficient spectral and spatial detail to recognize and map tectonically produced structural features in the western Salton Trough region. Some of the features detected are poorly and discontinously expressed on the ground and on airphotos. The continous nature of the faults on the satellite images is due to the synoptic view and additional information provided by the longer wavelength spectral data. The lateral continuity of many of the faults, along with their demonstrated activity based on their seismicity and scarps in late Quaternary deposits, indicate that these are important structural elements of the region that must be considered when assessing tectonic models, geodetic data, or seismic hazards. In the following discussion, the importance of each is elucidated.

Tectonic Models - Northeast-trending cross faults had been suggested to play an important role in the structural development of the Salton Trough (Nicholson et al. 1986; Bogen and Seeber 1986). The Superstition Hills earthquake sequence brought these ideas to center stage among workers in this region because the first shock, a Ms 6.2 earthquake on the northeast-trending Elmore Ranch fault zone, was accompanied by left-lateral surface rupture on several discrete fault strands (Hudnut et al. 1989a). That event probably triggered the Ms 6.6 Superstition Hills earthquake about 12 hours later (Hudnut et al. 1989a and b). Bogen and Seeber (1986) suggest the area between the dominant dextral faults undergoes tectonic clockwise rotation, and recent work supports this in the Superstition Hills (Ken Hudnut, oral communication). The Carrizo badlands is in an area where there are many northeast-trending faults (Fig. 2), with at least the Split Mountain fault known to exhibit sinistral slip. We suggest that the rotation of up to 30 degrees documented by Johnson et al. (1983) was accommodated in large part by the activity of the cross faults that interconnect the Elsinore and San Jacinto fault zones.

Geodetic Considerations - In the past, it was generally assumed that the major right-lateral faults accommodated most or all of the dextral shear across the Salton Trough, and that the blocks in between were generally stable away from the faults (Savage et al. 1979, Snay and Drew, 1988). This is apparently not the case in that a large number of cross faults now appear to interconnect all of the dextral faults. Future modeling should account for the presence of these structural features.

Seismic Hazard Considerations - Assessment of seismic hazards of the Salton Trough region must consider the left-lateral cross faults. Although the majority of well-located major earthquakes in this region have occurred on dextral faults, at least one (1987; Ms 6.2) and possibly another (1942; ML 6.5) have resulted from rupture of northeast-trending sinistral faults. If the 1942

earthquake was a sinistral fault rupture, then it is of interest because it was not immediately followed by a dextral fault rupture, as was the case in the 1987 sequence. More study is required to understand these types of events to see if they are often or rarely precursory to larger dextral events. In particular, might the next major earthquake (M 8) along the southern San Andreas fault be preceeded by a northeast-trending sinistral rupture? Certainly, if the 1987 event is not atypical, then relatively large sinistral ruptures may be important forewarnings of subsequent large dextral events.

CONCLUSIONS

Analysis of Landsat TM and combined TM-SPOT imagery provides a useful tool in studying the structure of the western Salton Trough region. In particular, short, discontinuous, previously mapped faults between the Elsinore and San Jacinto fault zones are seen to be laterally continuous fault zones that interconnect larger dextral faults. The combined images have sufficient spatial and spectral resolution that relatively minor scarps and other topgraphic disturbances in late Quaternary alluvium are observable, allowing for partial assessment of the faults' activity. In addition to detection of possible tectonic features of significance, the images help guide the necessary field work. Based on image analysis, field mapping and seismicity studies, it is clear that the northeast-trending faults are important in the structural development of the Salton Trough, and in the continued distribution of dextral shear across this region.

ACKNOWLEDGMENTS

The work of Blom and Crippen was performed at the Jet Propulsion Laboratory of the California Institute of Technology and supported by the National Aeronautics and Space Administration (NASA). Lisa Barge and Jan Yoshimizu assisted in the production of the images. We thank Ken Hudnut and Steven Day for valuable discussions on the geology and seismicity of the study area.

REFERENCES CITED

Allison, M.L., Whitcomb, J.H., Cheatum, C.E., and McEuen, R.B., 1978, Elsinore fault seismicity: The September 13, 1973, Agua Caliente Springs, California, earthquake series: Seismological Society of America Bulletin, v. 68, no. 2, p. 429-440.

Bogen, N.L. and Seeber, L., 1986, Neotectonics of rotating blocks within the San Jacinto fault zone, southern California: EOS, v. 67, no. 44, p. 1200.

Christensen, A.D., 1957, Part of the geology of the Coyote Mountain area, Imperial County, California: Masters Thesis, University of California, Los Angeles, 188 p.

Clark, M.M., 1972, Surface rupture along the Coyote Creek fault: in The Borrego Mountain Earthquake of April 9, 1968: U.S. Geological Survey Professional Paper 787, p. 55-87.

Crippen, R. E., 1987, The regression intersection method of adjusting image data for band ratioing: International Jour. of Remote Sensing, v. 8, 137-155.

Crippen, R.E., 1989, Image display of four components of spectral data. International Journal of Remote Sensing, submitted.

Crippen, R.E., Blom, R.G., and Heyada, J.R., 1988, Directed band ratioing for the retention of perceptually-independent topographic expression in chromaticity-enhanced imagery. International Journal of Remote Sensing: v. 9, no. 4, p. 749-765.

Crippen, R.E., Hajic, E.J., Estes, J.E., and Blom, R.G., 1989, Statistical band and band-ratio selection to maximize spectral information in color composite displays: International Journal of Remote Sensing, submitted.

Dibblee, T.W., Jr., 1954, Geology of the Imperial Valley region, California: in R.H. Jahns (ed.) Geology of Southern California: California Division of Mines Bulletin 170, chapter II, p. 21-28.

Jennings, C.W., 1975, Fault map of California: California Division of Mines and Geology, California Geologic Data Map Series, Map no. 1.

Johnson, N.M., Opdyke, N.D., Woodard, G.D., Zeitler, P.K., and Lindsay, E.H., 1983, Rates of late Cenozoic tectonism in the Vallecitos-Fish Creek basin, western Imperial Valley, California: Geology, v. 11, p. 664-667.

Hudnut, K.L., Seeber, L., Rockwell, T.K., Goodmacher, J., Klinger, R., Lindvall, S., and McElwain, R., 1989a, Surface ruptures on cross-faults in the 24 November 1987

Superstition Hills, California, earthquake sequence: Seismological Society of America Bulletin, in press.

Hudnut, K. L., Seeber, L., and Pacheco, J., 1989b, Cross-fault triggering in the November 1987 Superstition Hills earthquake sequence, southern California: Geophysical Research Letters, v. 16, p. 199-202.

Nicholson, C., Seeber, L., Williams, P., and Sykes, L.R., 1986, Seismic evidence for conjugate slip and block rotation within the San Andreas fault system, southern California: Tectonics, v. 5, no. 4, p. 629-648.

Rogers, T.H., 1965, Santa Ana Sheet, Geologic Map of California, Olaf P. Jenkins Edition: California Division of Mines and Geology.

Sanders, C., 1986, Seismotectonics of the San Jacinto fault zone and the Anza seismic gap: Ph.D. dissertation, California Institute of Technology, 180 p.

Savage, J. C., Prescott, W.H., Lisowski, M., and King, N., 1979, Deformation across the Salton Trough, California, 1973-1977: Journal of Geophysical Research, v. 84, no. B6, p. 3069-3079.

Snay, R. A., Drew, A. R., 1988 (in press), Supplementing geodetic data with prior information for crustal deformation in the Imperial Valley, California: Technical Report Series, Geodetic Institute, University of Stuttgart, Stuttgart, Federal Republic of Germany.

Strand, R.G., 1962, San Diego-El Centro Sheet, Geologic Map of California, Olaf P. Jenkins Edition: California Division of Mines and Geology.

FIGURE CAPTIONS

Figure 1. Compiled map of previously recognized faults in and between the Elsinore and San Jacinto fault zones (after Rogers, 1965, and Strand, 1962). Note the short, discontinuous nature of most of the northeast-trending faults.

Figure 2. Map displaying both the faults from figure 1 (thin lines) and the faults identified on the satellite imagery (thick lines) for a portion of the region between the San Jancinto and Elsinore Fault zones. Note that many of the previously mapped short, discontinuous faults are mappable as continuous structures across the alluvial areas using the satellite imagery.

Figure 3. Digitally combined SPOT-Landsat TM image of the region between and including the Elsinore and San Jacinto fault zones. The image covers approximately the same area as the map in Figure 2. Faults are expressed both geomorphically and spectrally (color changes). Note in particular the scarps along several of the faults in the Carrizo badlands area (bottom center of photo).

Figure 4. Sketch map (left) and Landsat TM image (right) of the Yuha desert area showing the northeast-trending Yuha Wells and related faults, and the northwest trending Laguna Salada (LSF) and Elsinore (EF) faults.

Figure 5. Sketch map (left) and Digitally combined SPOT-Landsat TM image (right) of the Coyote Creek fault. The extent of rupture during the 1968 earthquake is indicated (after Clark, 1972). The fault is tracable on the image to the Superstition Mountain fault, but its expression is weak and poorly defined. This is due in part to the sun illumination being parallel to the fault trace.

Figure 6. Geologic map of the central part of the Split Mountain fault in Split Mountain Gorge. Note the presence of scarps where the fault traverses late Quaternary alluvium.

Figure 7. Map showing the location of the Split Mountain fault with respect to the relocated main shock and four prominent aftershocks of the 1942 Ms 6.5 earthquake (relocations by Sanders, 1986). CCF=Coyote Creek Fault, SMF=Superstition Mountain Fault, Sp Mtn F=Split Mountain Fault, EF=Elsinore Fault.

Figure 8. Map of the Yuha Wells fault zone in Yuha Basin. Insert shows detail of offset of minor stratigrahic units.

Figure 9. Map showing the seismicity of the Yuha Basin region following the 1987 Superstition Hills earthquake sequence.

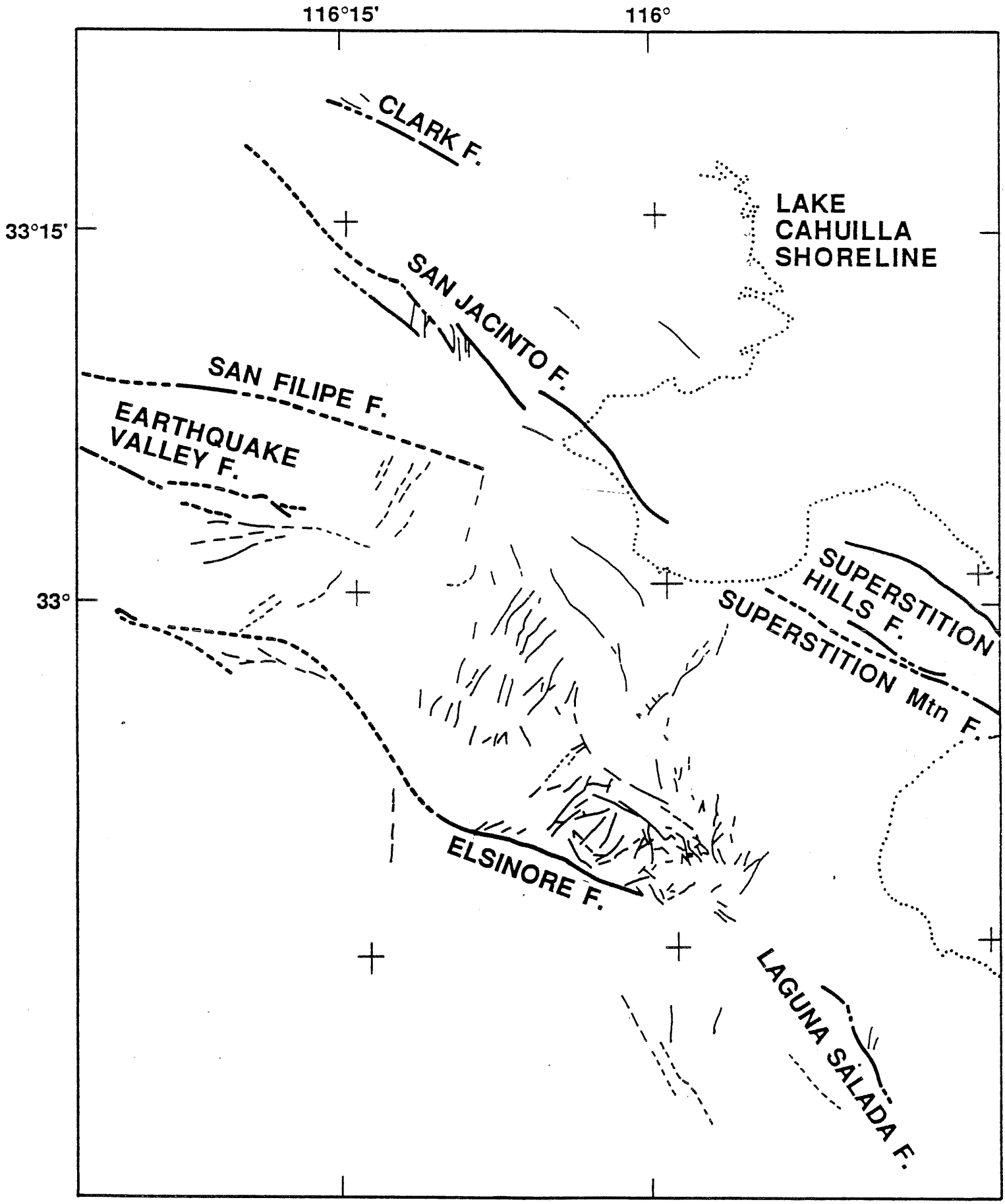
116°15'
116°
33°15'
33°
CLARK F.
LAKE
CAHUILLA
SHORELINE
SAN JACINTO F.
SAN FILIPE F.
EARTHQUAKE
VALLEY F.
SUPERSTITION
HILLS F.
SUPERSTITION Mtn F.
ELSINORE F.
LAGUNA SALADA F.

Fig. 1

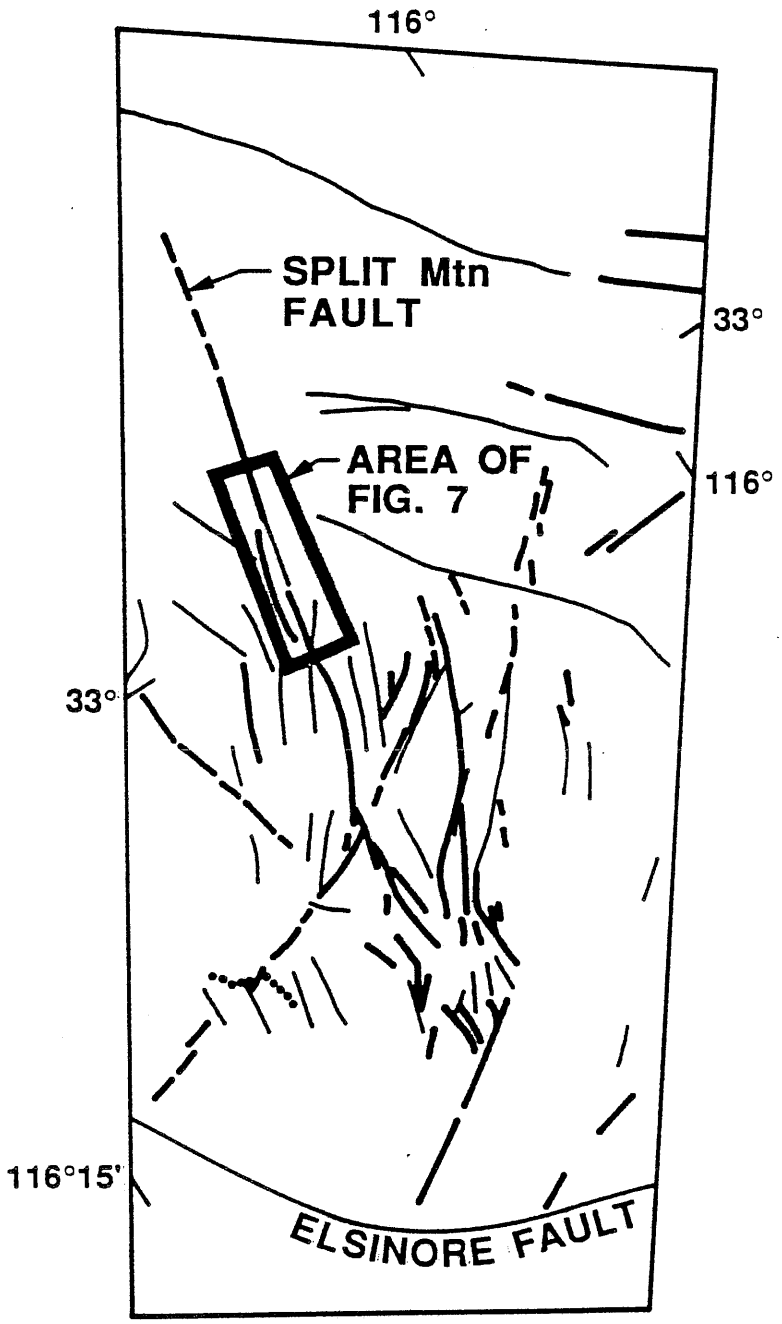
116°
SPLIT Mtn
FAULT
33°
AREA OF
FIG. 7
116°
33°
116°15'
ELSINORE FAULT

Fig 2.

Fig 3

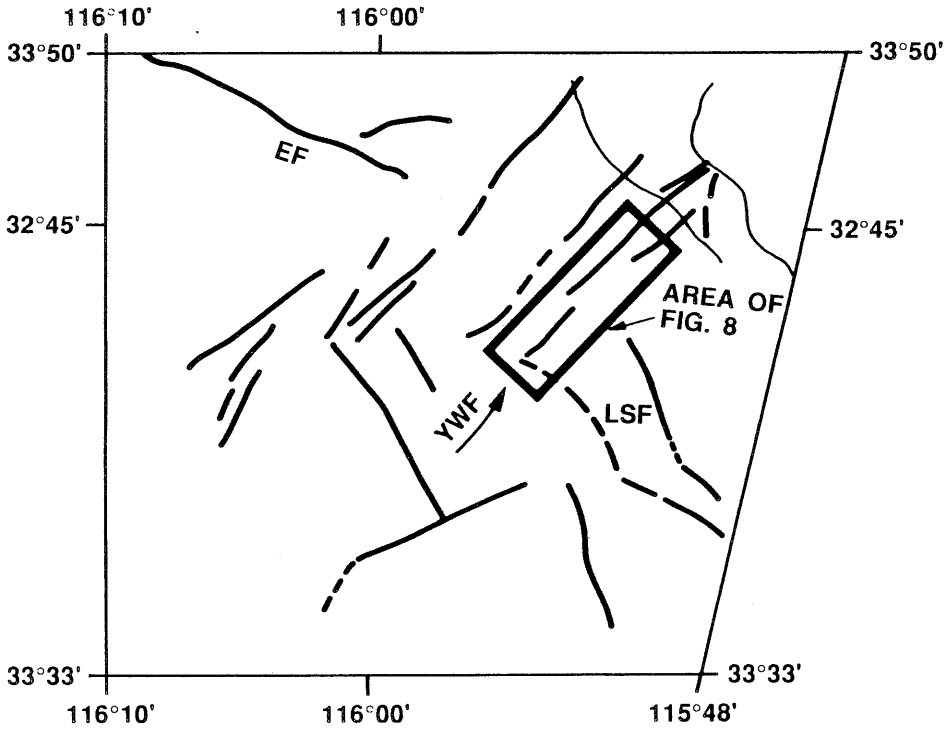

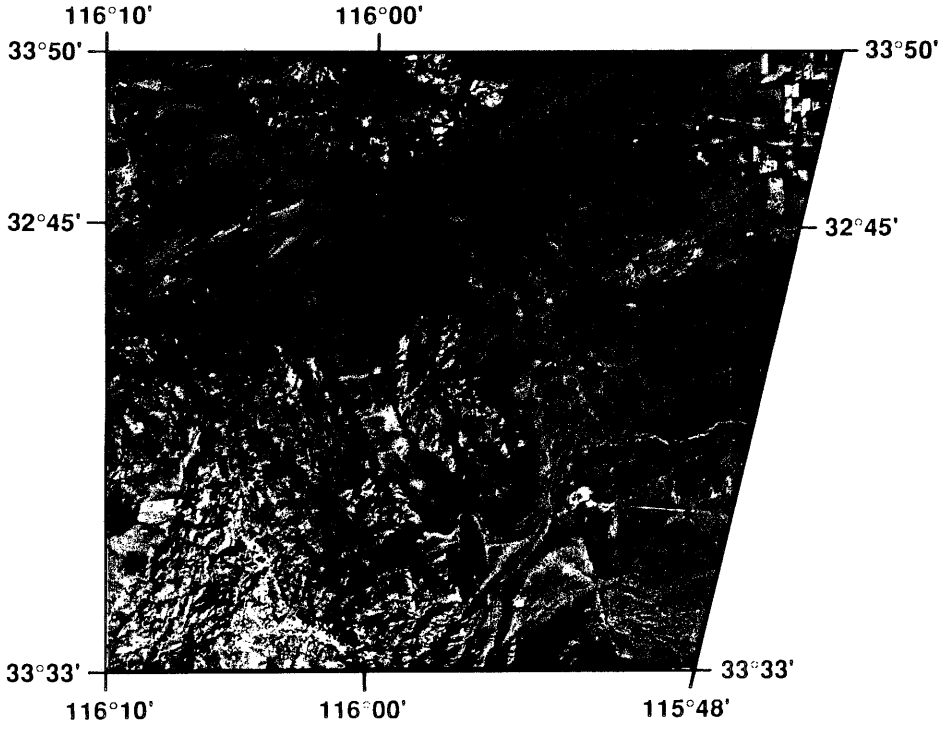

Figure 4
Review copy only

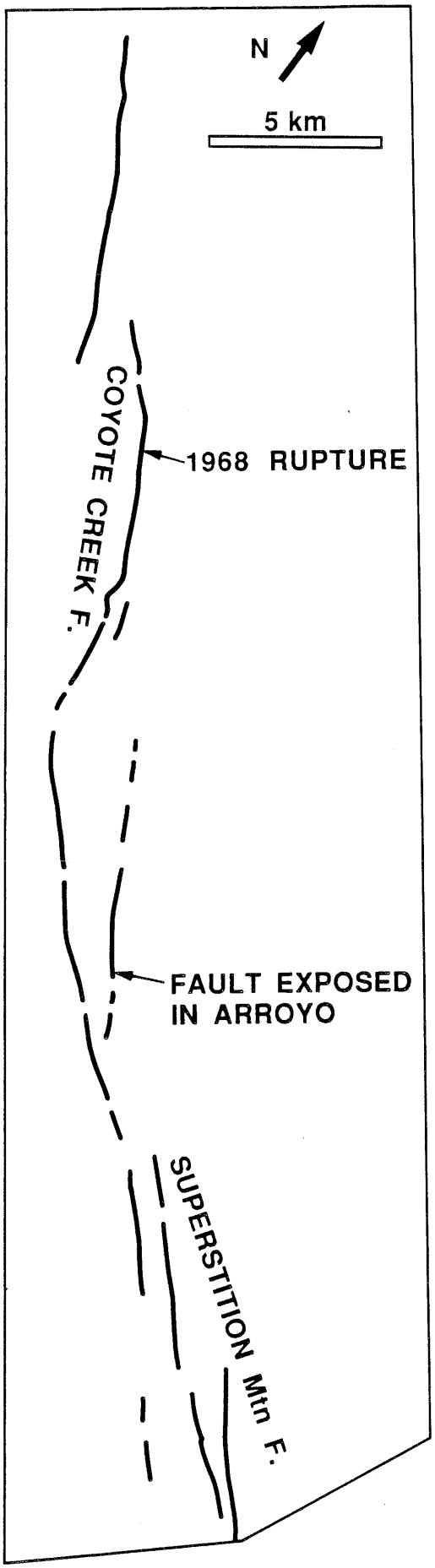

Fig. 5
Review copy only

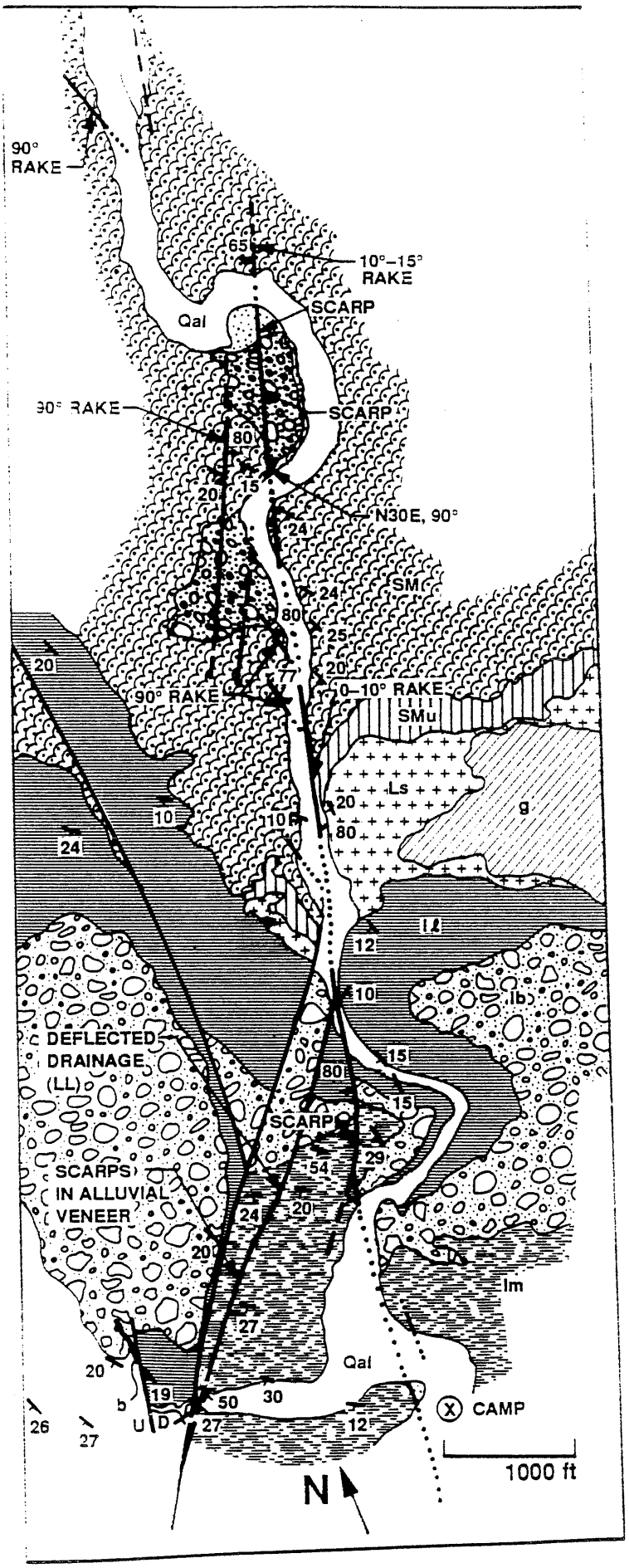
90°
RAKE
65
10°–15°
RAKE
SCARP
Qal
30° RAKE
SCARP
80
20
15
N30E, 90°
24
SM
24
80
25
20
77
90° RAKE
0–10° RAKE
SMu
20
Ls
20
10
10
80
g
24
12
10
lb
DEFLECTED
DRAINAGE
(LL)
80
15
15
SCARP
29
54
SCARPS
IN ALLUVIAL
VENEER
24
20
20
lm
27
Qal
20
19
b
50
30
CAMP
26
27
U
D
27
12
1000 ft
N

Fig. 6

KEY

MIOCENE-PLIOCENE (?)

SPLIT MOUNTAIN FORMATION

UPPER MEMBER – SPLIT MOUNTAIN FORMATION

GRANITIC LANDSLIDE (?)

FISH CREEK GYPSUM

BASAL MEMBER – IMPERIAL FORMATION

BRECCIA MEMBER IMPERIAL FORMATION

MUDSTONE MEMBER IMPERIAL FORMATION

FAN

TERRACE

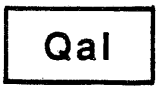

ACTIVE CHANNEL

Fig 6 key

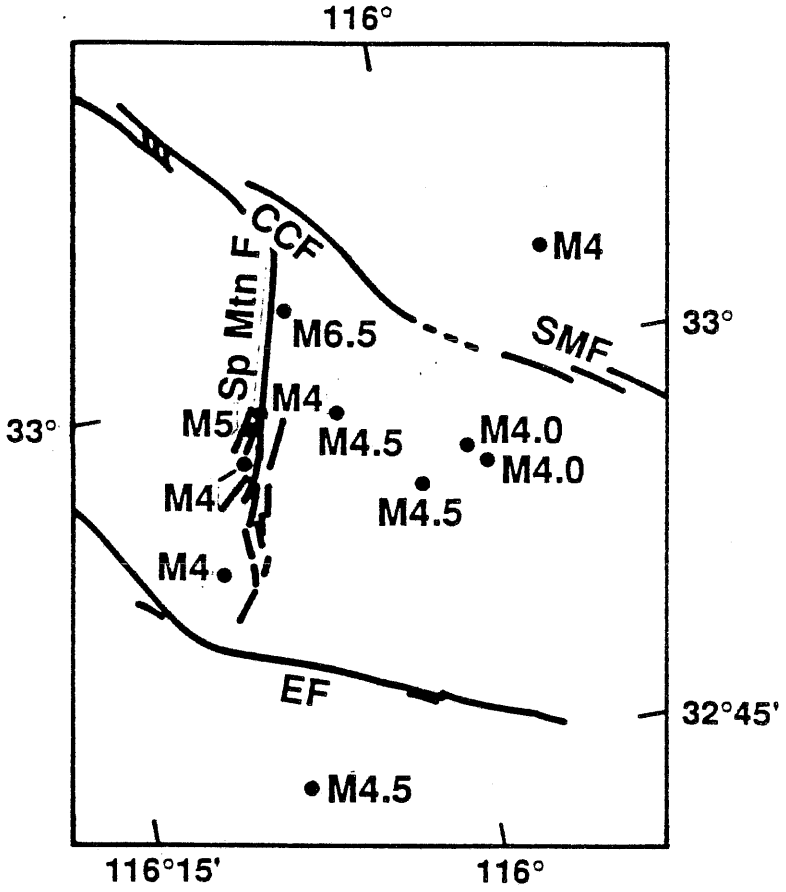
116°
33°
33°
32°45'
116°15'
116°
CCF
Sp Mtn F
SMF
EF
M4
M6.5
M4
M5
M4.5
M4.0
M4.0
M4
M4.5
M4
M4.5

Fig. 7

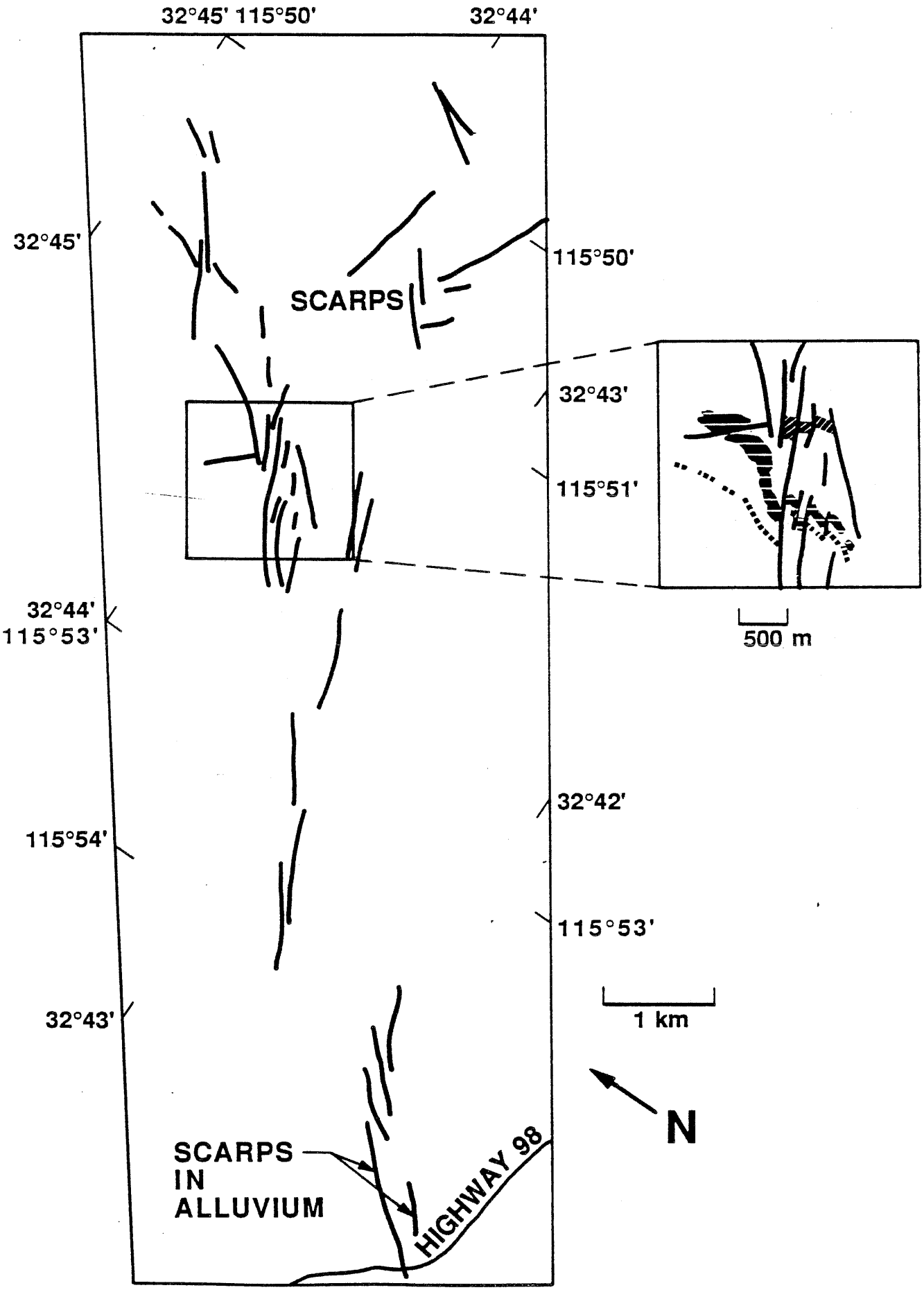
32°45' 115°50'
32°44'
32°45'
115°50'
SCARPS
32°43'
115°51'
32°44'
115°53'
500 m
32°42'
115°54'
115°53'
32°43'
1 km
N
SCARPS
IN
ALLUVIUM
HIGHWAY 98

Fig. 9

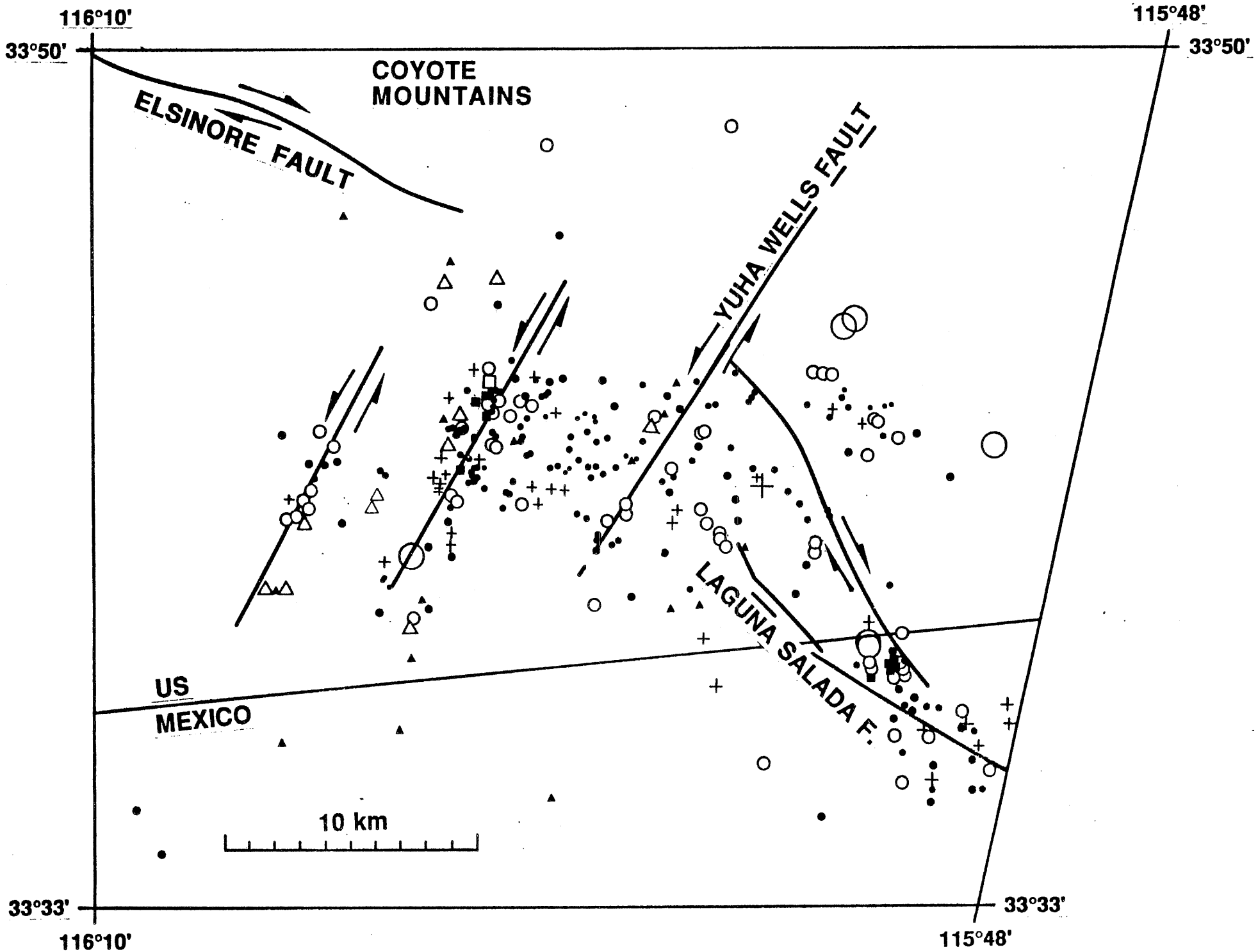
116°10'
115°48'
33°50'
33°50'
COYOTE
MOUNTAINS
ELSINORE FAULT
YUHA WELLS FAULT
LAGUNA SALADA F.
US
MEXICO
10 km
33°33'
33°33'
116°10'
115°48'

Northeast Striking Faults of the Yuha Desert southwestern Salton Trough, southern California

Andy Thomas, Amy Stinson

ABSTRACT

This study describes the recently recognized Yuha Wells fault in the Yuha Desert area of the western Salton Trough, southern California. The fault is comprised of a complex zone of anastamosing strands with an average strike of N35E located between the northern terminus of the Laguna Salada fault and the southern end of the Elsinore Fault. Young geomorphic features such as scarps and left-laterally deflected drainages, suggest recent sinistral movement. The Superstition Hills earthquake sequence of November, 1987 demonstrates the significance of northeast-striking faults as important tectonic structures associated with the San Jacinto and San Andreas fault systems. Northeast-striking faults, including the Yuha Wells and numerous others farther north in the Carrizo Badlands, display the same style of tectonic deformation that has been documented between the San Jacinto and San Andreas faults.

The occurrence of the Superstition Hills earthquake sequence, warrants a reevaluation of the seismic hazard for the western Salton Trough related to the northeast striking faults. Additional geodetic studies of the Yuha Wells fault and other northeast striking faults are needed to quantify the slip distribution in the fault zone. This information could document actual historic rotation of structures due to the tectonics of rigid block rotation and its relation to slip activity of the Elsinore / Laguna Salada fault system in this area.

INTRODUCTION

The Salton Trough in southern California has historically been a region of high seismic activity. Tectonics of the trough are explained as a complex oblique pull-apart basin occurring between right-stepping major right-lateral faults: the San Andreas, the San Jacinto, and the Laguna Salada / Elsinore Fault zones (Figure 1) (Crowell, 1974). These three major fault zones are recognized as the dominant tectonic structures that comprise the San Andreas Fault transform system continuing northwest towards the Los Angeles area. Between the northwest-striking faults of the western Salton Trough, smaller,

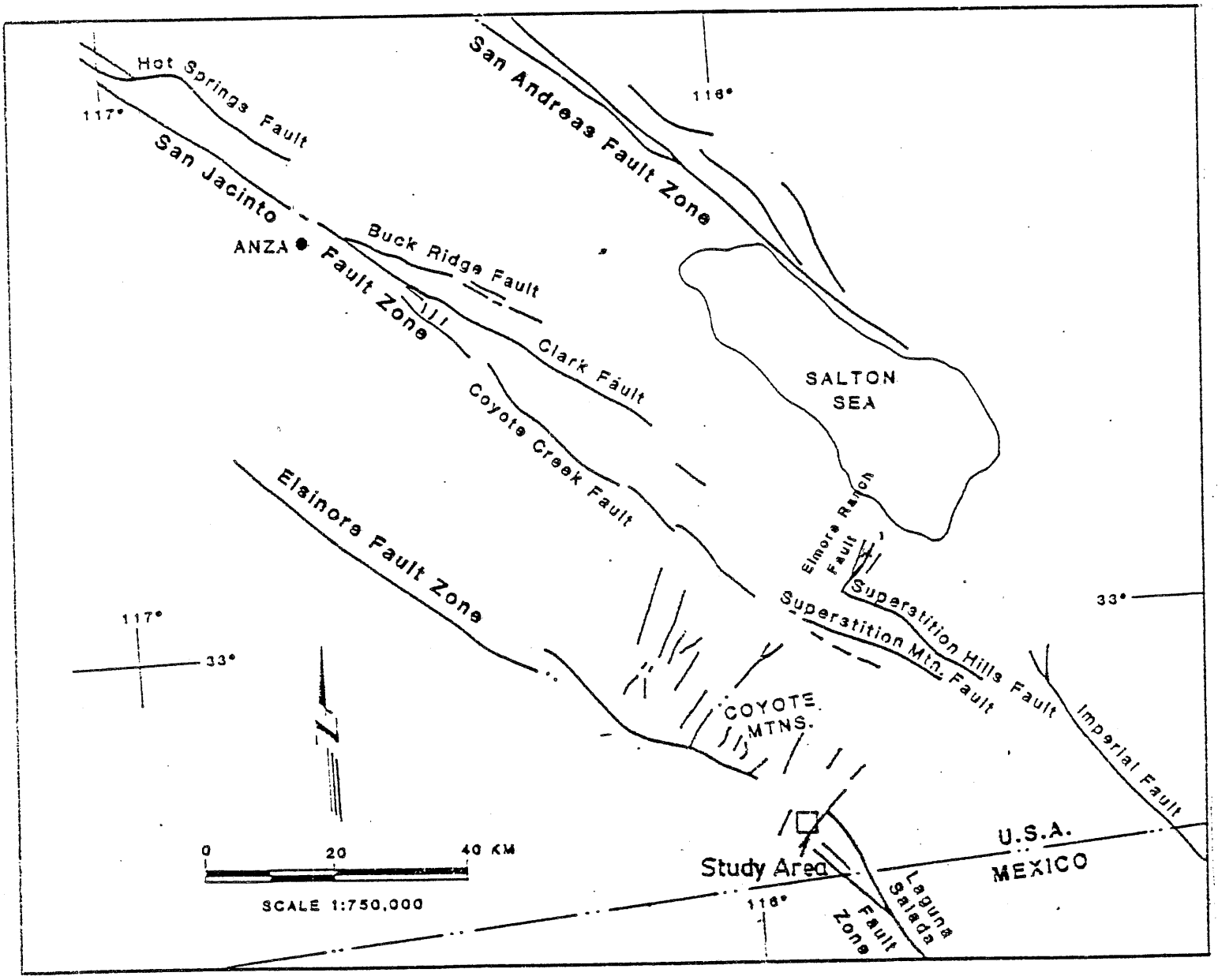

Figure 1. Location Map of Study Area

Modified from (Rockwell, unpublished)

discontinuous north to northeast striking faults have been mapped that display sinistral slip (Dibblee, 1954, 1984). Until recently, the role of these faults in the regional tectonic picture has probably been underestimated.

The seismic hazard associated with northeast-striking faults was not appreciated until the Superstition Hills earthquake couplet in Nov., 1987 (Figure 2). A M_S 6.2 earthquake with sinistral slip on the Elmore Ranch, and adjacent northeast-striking faults was followed 11.4 hours later by a M_S 6.6 earthquake on the nearby right-lateral Superstition Hills fault (Hudnut and others, 1989). The epicenter of the second event was located at the point of intersection between the Elmore Ranch and Superstition Hills faults. This earthquake sequence clearly displayed the relationship between northwest-striking right-lateral faults and northeast-striking left-lateral cross faults in the central Salton Trough. Subsequent reevaluation of several other large seismic events like the 1979 Imperial Valley earthquake for example, suggests a similar relationship (Nicholson and others, 1986).

Previously mapped, discontinuous, and seemingly minor northeast-striking faults in the Salton Trough can now be understood as important tectonic features capable of generating moderate magnitude events or initiating moderate to large magnitude earthquakes on adjacent northwest-striking faults. Attention was drawn to the Yuha desert for study because of the sudden increase in microseismicity following the Superstition Hills earthquake sequence (Figure 3). Left-lateral faults appear to be important structural entities in the western Salton Trough based on the surface expression of the Yuha Wells Fault trace and several other northeast-striking faults documented with satellite images (Rockwell and others, this volume), and the microseismicity associated with these features.

LOCATION OF STUDY AREA

The study area is in the northern portion of the Yuha Desert on the western edge of the Salton Trough, southeast of Ocotillo, California (Figure 1). The area is bounded on the north by Interstate 8 and on the south by Highway 98, and is approximately 10 kilometers north of the International Border. Eight kilometers of the Yuha Wells fault zone was mapped. Access to the field area was made easy by numerous dirt roads and offroad race tracks. (Whose

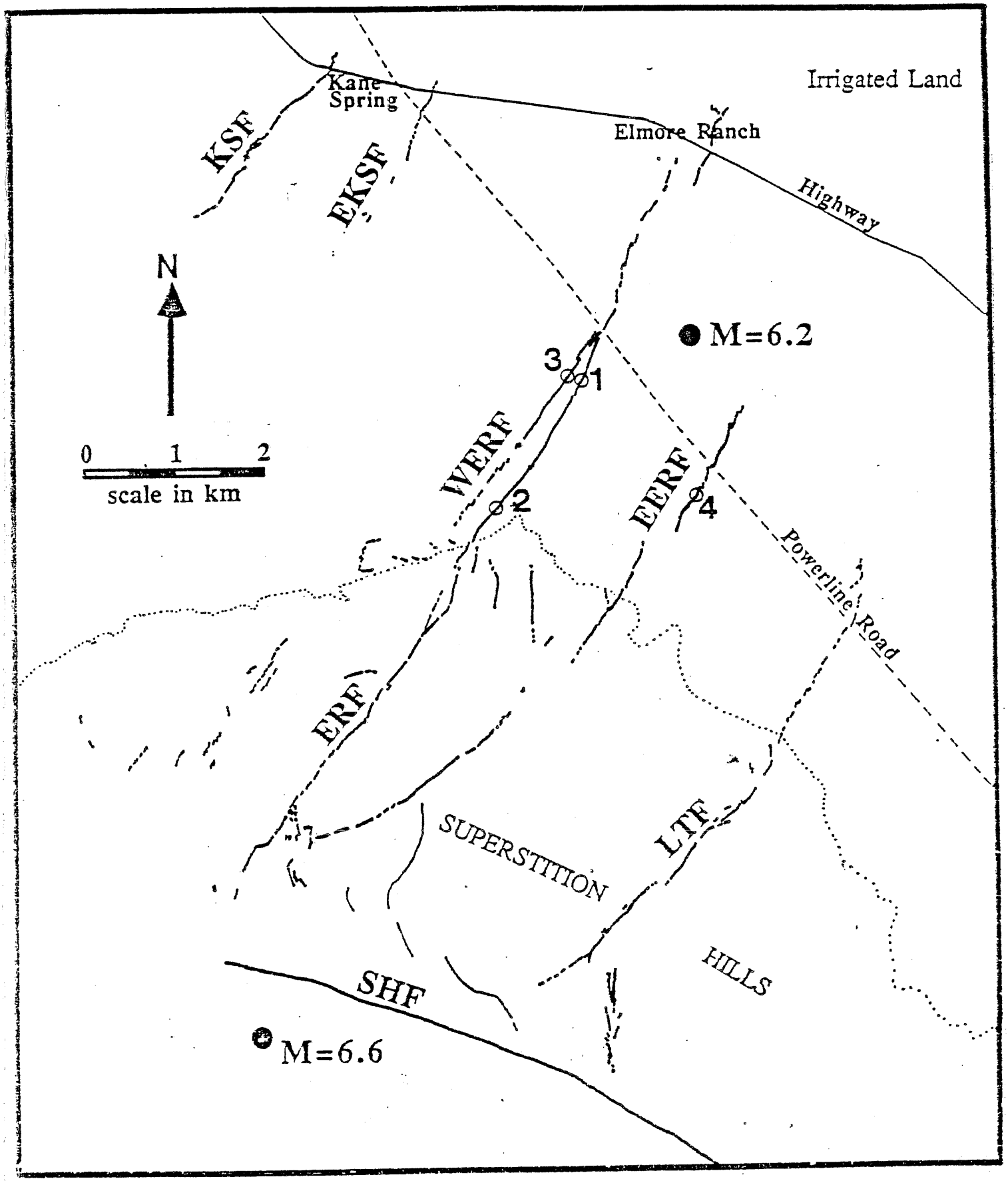

Figure 2. Map of Surface Break of 1987 Superstition Hills Earthquake

(Hudnut and others, 1989b)

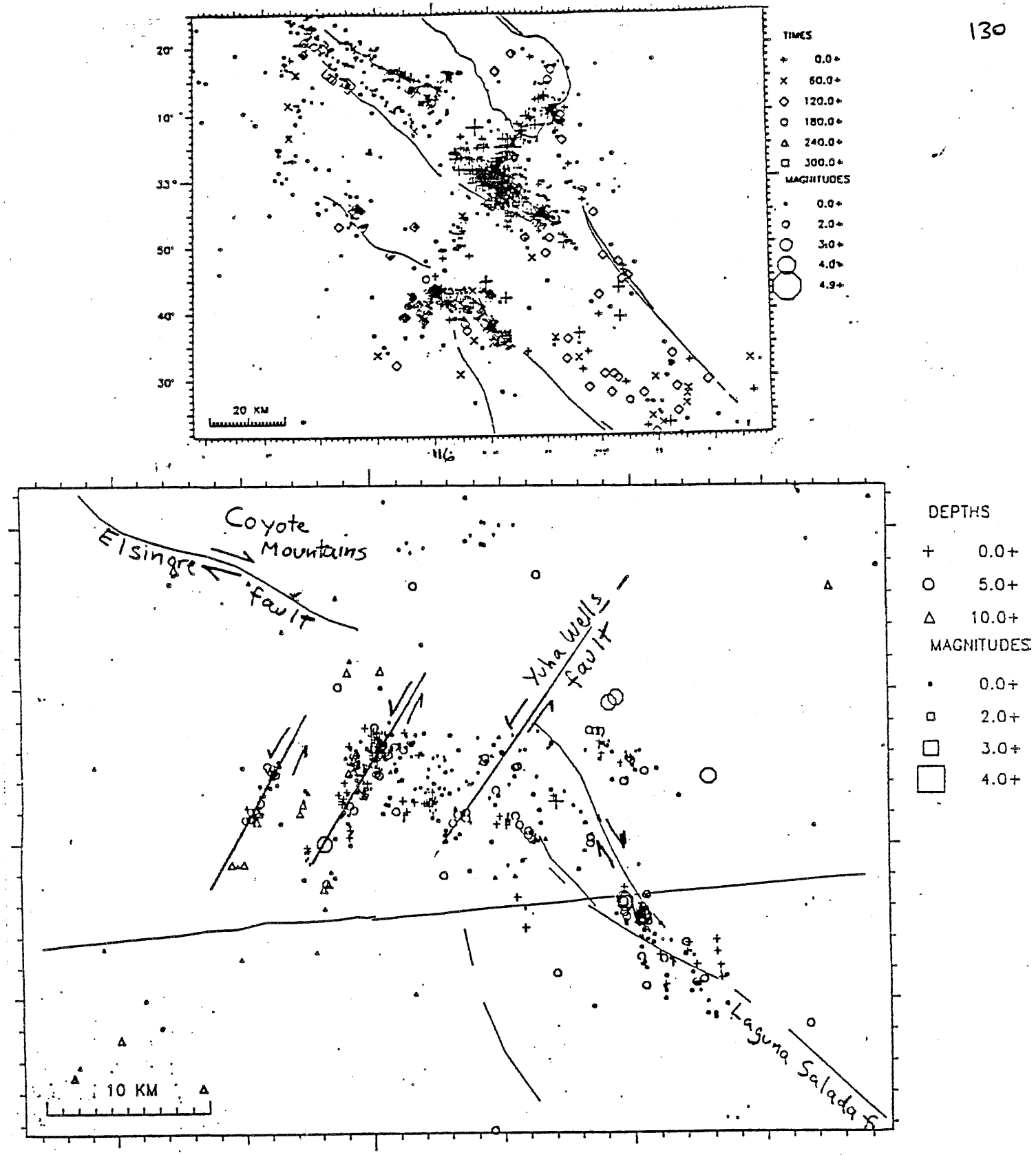

Figure 3. Seismicity of the southern California region from the November 24 Superstition Hills sequence through July, 1988. Note the abundant earthquake epicenters along the southern Elsinore-Laguna Salada fault trend. The lower diagram shows a detail of the southern Elsinore-Laguna Salada fault area. Note the northeast-trending seismicity trend at the north end of the Laguna Salada fault, at lea t one of which corresponds to a northeast-trending left-lateral fault.

Figure 3. Seismicity Map of the Yuha Wells Area, 1988.
(Hutton & others, for figure)
(Initial geological interpretation by K. Hudnut, additional modifications by T. Rockwell)

sole purpose is the destruction of valuable desert habitat for enjoyment of humanity)

REGIONAL GEOLOGY

The Yuha Desert is a structural basin filled with up to five kilometers of marine and poorly lithified clastic fluvial sediments overlying the basement (Dibblee, 1954). The stratigraphy exposed in the badlands-type topography of the Yuha Desert consists of the Imperial Formation overlain by the Palm Spring Formation and was initially named by Woodring (1931). These units are often obscured by Holocene alluvium and the lacustrine deposits of the prehistoric Lake Cahuilla. Dibblee (1954) described the Imperial Formation as a gray-yellow colored claystone interbedded with buff colored sandstone and oyster reefs. The formation is generally poorly-lithified and fine grained. There is abundant gypsum that is locally concentrated along cracks and fractures. The faunal assemblages suggest a shallow marine depositional environment indicative of a Miocene to Pliocene age (Dibblee, 1954).

The Imperial Formation grades into the overlying Palm Spring Formation, which can be recognized in the field by the reddish mudstones and yellow well-indurated concretionary sandstones. Mudstones in both the Imperial and Palm Spring formations exhibit an expansive popcorn-like fissile texture. The Palm Spring Formation was deposited in a fluvial-deltaic environment at the margins of the paleogulf. The sediment source came from the rising southern California Batholith in the west and the Colorado River (Dibblee, 1954).

The Yuha Desert has been locally uplifted within the Yuha Wells fault zone. Mudstones of the Palm Spring and Imperial formations are easily erodible, and typically are expressed topographically as badlands within this zone of uplift. Deformation along the northeast-striking Yuha Wells fault system has extensively sheared the sediments. Numerous faults and fractures exposed in the badlands contain a distinctive pinkish-brown colored clay gouge. Rapid weathering of the friable mudstone results in poor fault surface preservation.

PREVIOUS WORK

The stratigraphy and structure of the Yuha Basin was documented by Dibblee (1954; 1984) during reconnaissance mapping of the western Salton Trough . He noted the presence of numerous northeast-striking sinistral faults between the Elsinore / Laguna Salada, and San Jacinto fault systems. Dibblee (1954) attributes the northeast-striking structures to possible clockwise block rotation between the Elsinore and San Jacinto faults. Paleomagnetic studies of the Neogene stratigraphy in the Salton Trough suggest up to 35 degrees of clockwise rotation has occurred in some areas since the sediments were deposited (Luyendyk and others, 1985; Johnson and others, 1983; Christie-Blick and others, 1985).

Issacs (1986) mapped the surface expression of the northern portion of the Laguna Salada fault system which extends into the southern portion of the Yuha Basin. She describes a complex zone of faulting and deformation at the northern terminus of the Laguna Salada Fault. Crisman (M.S. in progress) is developing a soil chronosequence on the Pleistocene and Holocene Lake Cahuilla shorelines in the Plaster City area.

METHODS

USDA black and white 1 : 20,000 aerial photographs flown in 1953 were used as a base for field mapping. The most prominent lineaments were field checked for indications of recent tectonic activity. Orientations of fractures, faults, and bedding were measured where possible. Offset microchannel walls were measured using a metric tape parallel to the the fault trace.

DATA

The Yuha Wells fault is expressed geomorphically at its southwest end adjacent to highway 98 as a double fault scarp that cuts across surface alluvium forming a low mesa and graben. One of the scarps is approximately 5 meters high and slopes gently down to the southeast. On this scarp, left-lateral separation of microchannels were observed. Several faint strands, noticeable only on aerial photographs are parallel to this strand.

Holocene stream microchannels display pervasive left-lateral separation across this fault (See Table 1). The average offset of seven measured offsets is about 25 cm. Accurate determination of

the amount of separation is unfortunately compromised. Lateral erosion of the channel walls after fault movement introduce channel wall correlation ambiguities. Local changes in channel wall shape are due to variations in scarp morphology and the presence of small bushes that deflect the channels. Even though the data is not conclusive, the measurements certainly suggests that recent left-lateral slip has occurred.

The fault zone becomes progressively more complex to the northeast where uplift of an older alluvial surface has occurred and is presently being eroded into badlands topography. Several conjugate strands appear to splay off in many directions in a complicated and diffuse manner.

To the northeast in the central part of the Yuha Basin, a spectacular set of drag folds are observed within the Yaqui Wells fault zone which clearly display left-lateral separation of sandstone beds across the fault of at least 60 meters (See Figure 8.). Even though these folds are in strata of probable Pliocene age and do not necessarily indicate recent activity, the sharp expression of the faults suggest that recent movement has likely occurred. The fault zone then splays into several major strands that have cut the stratigraphy into several slivers that show block rotation on a small scale of less than one kilometer.

Several kilometers south of Plaster City at the northeast end of the study area , few lineaments or fault related features are discernable from airphotos and none were observed on the ground. The paucity of geomorphic evidence at the northeast end of the fault zone could be due to a decreasing amount of slip in this area, or the obscuring of the fault trace by alluvium recently reworked by the prehistoric Lake Cahuilla. Associated with the lake are a series of shorelines and beach berms that do not display significant left-lateral separation where the berms cross the trend of the fault zone. Examination of the youngest dated beach berm 1680 +- 40 A.D. shows no apparent offset (Sieh, 1986).

Other unnamed northeast-striking faults and fold structures indicate the existence of a pervasive northeast oriented tectonic fabric in the Yuha desert (Isaacs, 1987). Approximately 3 km north of the Yuha Wells fault on Highway 98, a low hill has been dissected by one of these faults. Air photos clearly display sinistral offset of the hill. The lateral extent of that fault is presently unknown.

DISCUSSION

The Yuha Wells fault orientation, location, and complicated expression can partially be explained by two models. One model, termed the block rotation model (e.g. Nicholson and others, 1986), has developed from the structural relationships of cross faults to the dominant northwest-trending faults. This model suggests that detached portions of the crust are rotating along strike-slip faults. It is supported by other lines of evidence such as documented rotation of sediments and the distribution of seismicity in the Salton Trough. A second model, the wrench fault model of Wilcox and others (1973), predicts the orientation of conjugate faults in a stress field along a basement wrench fault.

The Wilcox model predicts the angular relationships between two sets of secondary conjugate faults (sympathetic and antithetic faults) occurring within the main wrench fault zone (Wilcox and others, 1973) (Figure 4). Sympathetic faults occur at low angles (12 degrees) to the main wrench fault and have the same sense of slip. Of particular interest are the antithetic faults. These faults have an opposite sense of slip to the master wrench fault, intersect the fault at a high angle between 60 to 70 degrees, and accommodate less shear then the dominant wrench fault.

The Yuha Wells fault therefore might be considered an antithetic fault to the Elsinore / Laguna Salada fault as predicted by the Wilcox model. It intersects the dominant wrench trend of the Elsinore / Laguna Salada at a high angle (greater than 60 degrees) and also has an opposite sinistral sense of slip to the main wrench zone. Though the Yuha Wells fault does intersect the general trend of the Elsinore / Laguna Salada Fault at an angle higher than predicted (90 degrees), the model predicts that external rotation due to regional simple shear adjacent to the wrench fault will occur with progressive deformation. The external rotation of the antithetic faults to higher angles will take them out of preferential orientation for slip. The very complicated expression of the central portion of the Yuha Wells fault zone could indicate that as the sediments rotate, they are continually refaulted at the preferred antithetic fault orientation to the master fault. This causes the slivering up of the sediments with faults occurring at many different orientations.

One prediction of this model, that creates problems on a regional scale is that new antithetic faults should be generated at the

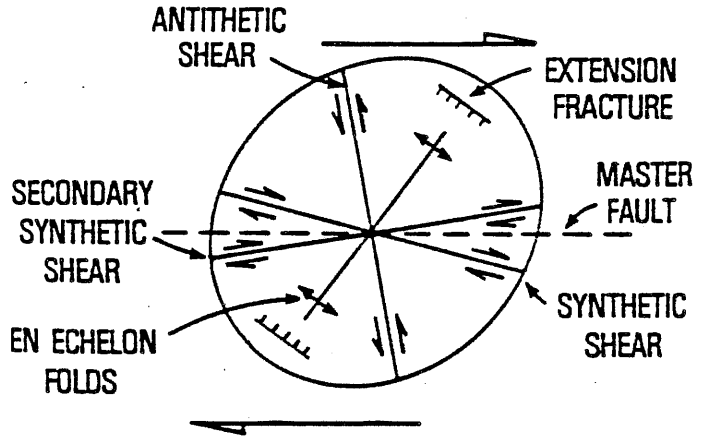

Figure 4. Angular Relationships of Wrench Fault Model

(Christie-Blick and others, 1985)

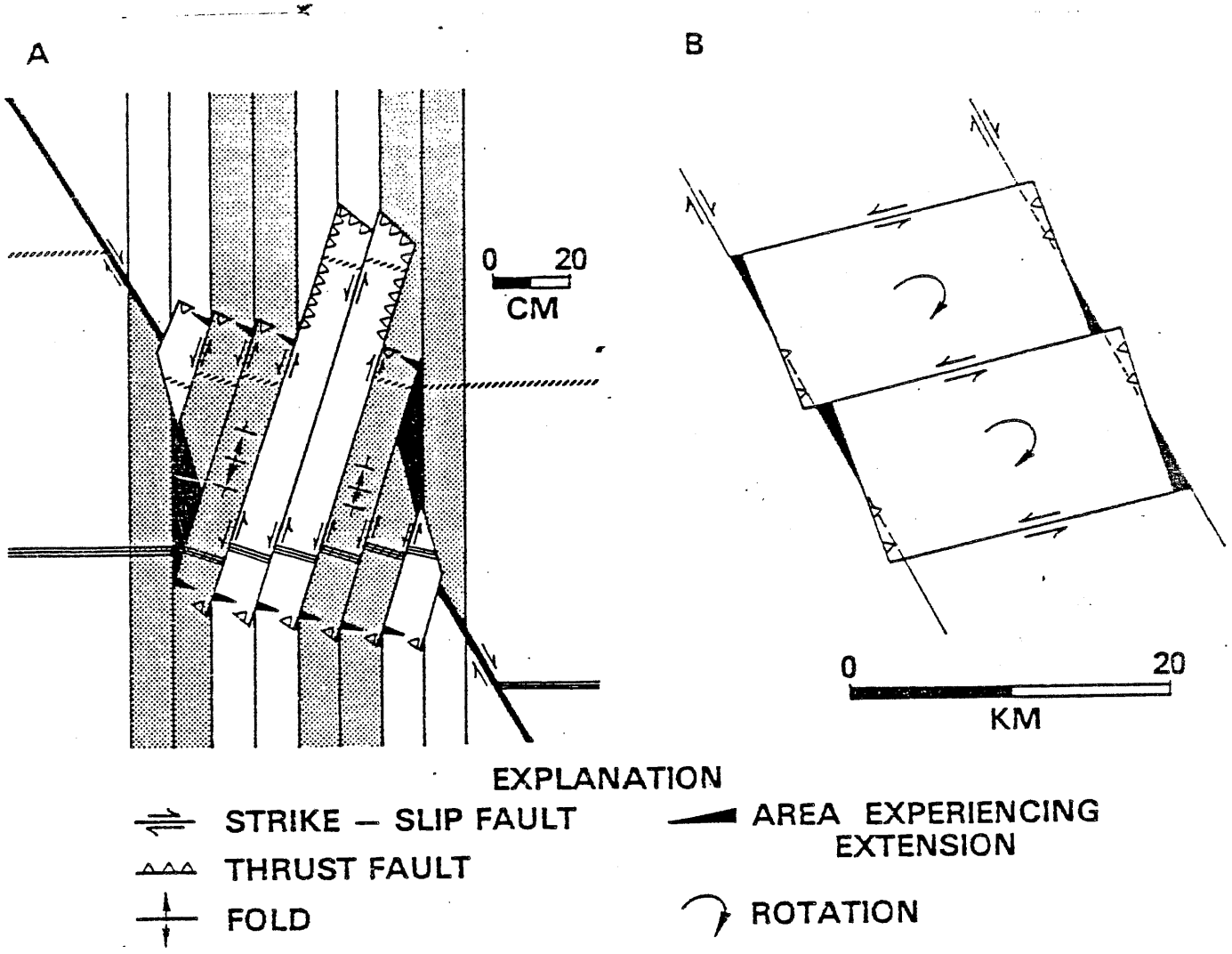

Figure 5. Models of Crustal Rotation

(Christie-Blick and others, 1985)

preferred orientations of 60 - 70 degrees during progressive external rotation along the wrench fault. It would seem reasonable that as the Yuha Wells "antithetic" fault is rotated out of preferred orientation, new antithetic faults should be generated and the rotated fault abandoned as an active structure (Wilcox, 1973). The recent microseismic activity aligned along the Yuha Wells fault associated with the active-looking geomorphic offset features documented in this study is therefore anomalous since the Yuha Wells fault intersects the Laguna Salada fault at approximately 90 degrees. Several other cross faults documented on Combined Thematic Mapper Spot Satellite images between the San Jacinto and the Elsinore Fault also show similar right-angle geometries (Rockwell and others, this volume).

The shallow crustal block rotation model provides an alternative explanation for the presence of northeast-striking faults in the Yuha Basin. Existence of the northeast striking sinistral faults between the San Jacinto and Elsinore faults was first discussed by Dibblee (1954), referring to the Carrizo Badlands. Based on structural interpretations, he suggests that they occur due to passive clockwise block rotation about a vertical axis between the Elsinore and San Jacinto faults (Dibblee, 1977) (Figure 6a). The north-northeast striking faults accommodate left-lateral motion between the individual blocks. The block geometry explains the preferred occurrence of cross faults at an angle of 90 degrees instead of the expected 60-70 degrees predicted by the Wilcox and others (1973).

There are several different lines of evidence that support the block rotation model. Paleomagnetic studies of sedimentary basins demonstrate large scale rotations occurring in southern California since the Neogene (Luyendyk and others, 1985; Johnson and others, 1983). Nicholson and others (1986) also document evidence for clockwise block rotation occurring between the San Andreas and San Jacinto faults in the Cajon Pass area. Detachment surfaces related to the east-west extension in the Miocene and the opening of the Gulf of California are exposed in the western perimeter of the Salton Trough as reported by numerous authors (Shultejahn, 1984; Wallace, 1982; Stinson, M.S in progress). Reactivation of these low-angle structures are postulated to have accomodated crustal block rotatations (Nicholson and others, 1986; Christie-Blick and others, 1985). Seismic profiles on the east side of the Imperial Valley document low-angle discontinuities attributable to detachment surfaces (Fuis and others, 1984). It is quite plausible that the low-angle

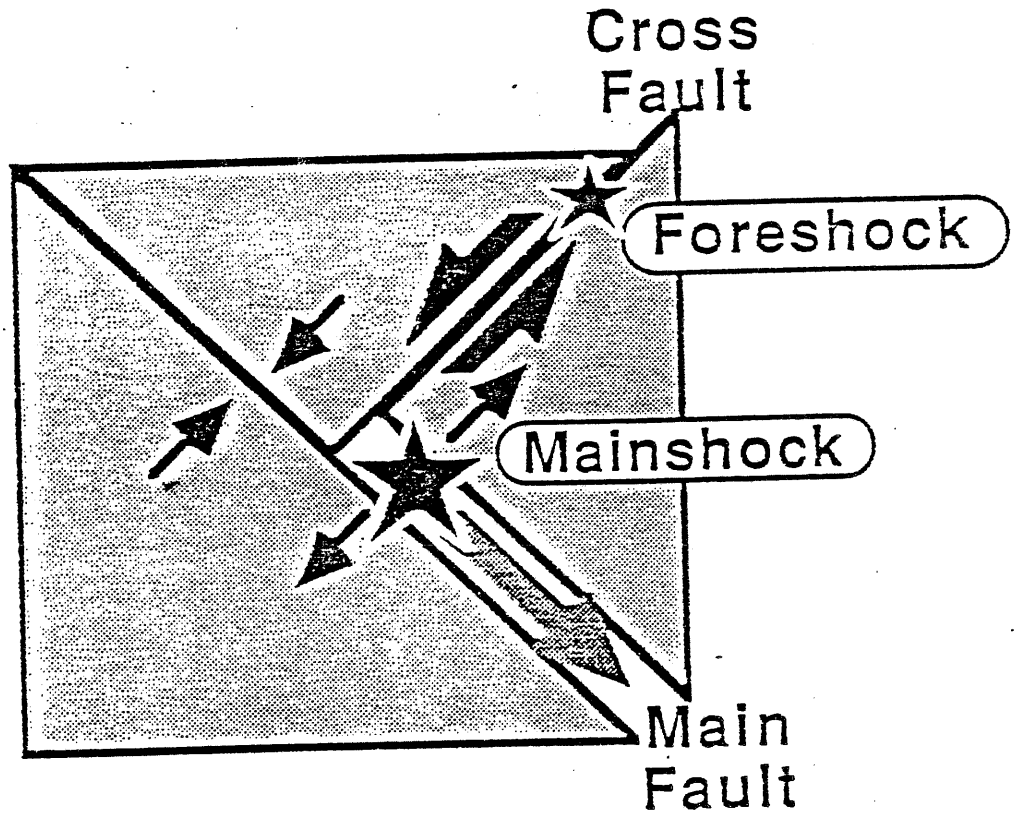

Figure 6. Geometric Interpretation of 1987 Superstition Hills Rupture (Hudnut and others, 1989a)

discontinuities were once continuous across the entire Salton trough (J. Bond, pers. comm.).

Microseismicity distribution in the Salton Trough is also persuasive evidence for the occurrence of ongoing block rotation. Examination of the microseismic epicenter maps over ten year time periods display northeast-trending seismic lineaments outlining possible blocks (Figure 5). This seismicity, located off the major northwest-striking faults, is probably associated with cross faults. It has a distinctly different character to that of the northwest-striking faults (Nicholson, 1986). Cross fault seismicity is usually of smaller magnitudes, occurs at depths of less than 10 kilometers, and exhibits sinistral motion. Nicholson and others (1986) argue that this seismicity is associated with clockwise block rotation occurring above detachment surfaces.

Alternating zones of compression and extension are predicted along the northwest-trending faults as the blocks rotate (Figure 5) (Nicholson, 1986). The seismicity of the major northwest-trending faults where cross faults intersect at the corners of the blocks should be affected by increasing or decreasing normal stress along the fault plane, thereby changing the shear strength of the fault. This mechanism may have caused the rupture of the Superstition Hills earthquake (Hudnut and others, 1989) (Figure 6). The left-lateral rupture of the Elmore Ranch Fault is believed to have reduced the normal stress across the northern Superstition Hills fault causing the rupture to initiate at the corner where the two faults intersect. The faulting behavior during major events such as the 1968 M_L 6.8 Borrego Mountain and the 1979 M_L 6.6 Imperial Valley earthquakes on northwest-striking faults show that triggered slip, aftershocks, and foreshocks to the main event occurred on northeast-striking faults (Nicholson, 1986). Sudden changes in seismic activity on these cross faults near the San Jacinto or San Andreas Faults could be important indicators of future rupture on the northwest-striking faults if cross-faulting precedes faulting on northwest-striking faults (Hudnut, 1989c).

Block rotation might also be a mechanism associated with shear distribution around transpressional bends of strike slip faults. Cross faults in the western Salton Trough commonly are associated with restraining bends (Nicholson and others, 1986). The Elsinore fault for example has two major transpressive steps at the Coyote Mountains and the Tierra Blanca Mountains. Just to the southeast of

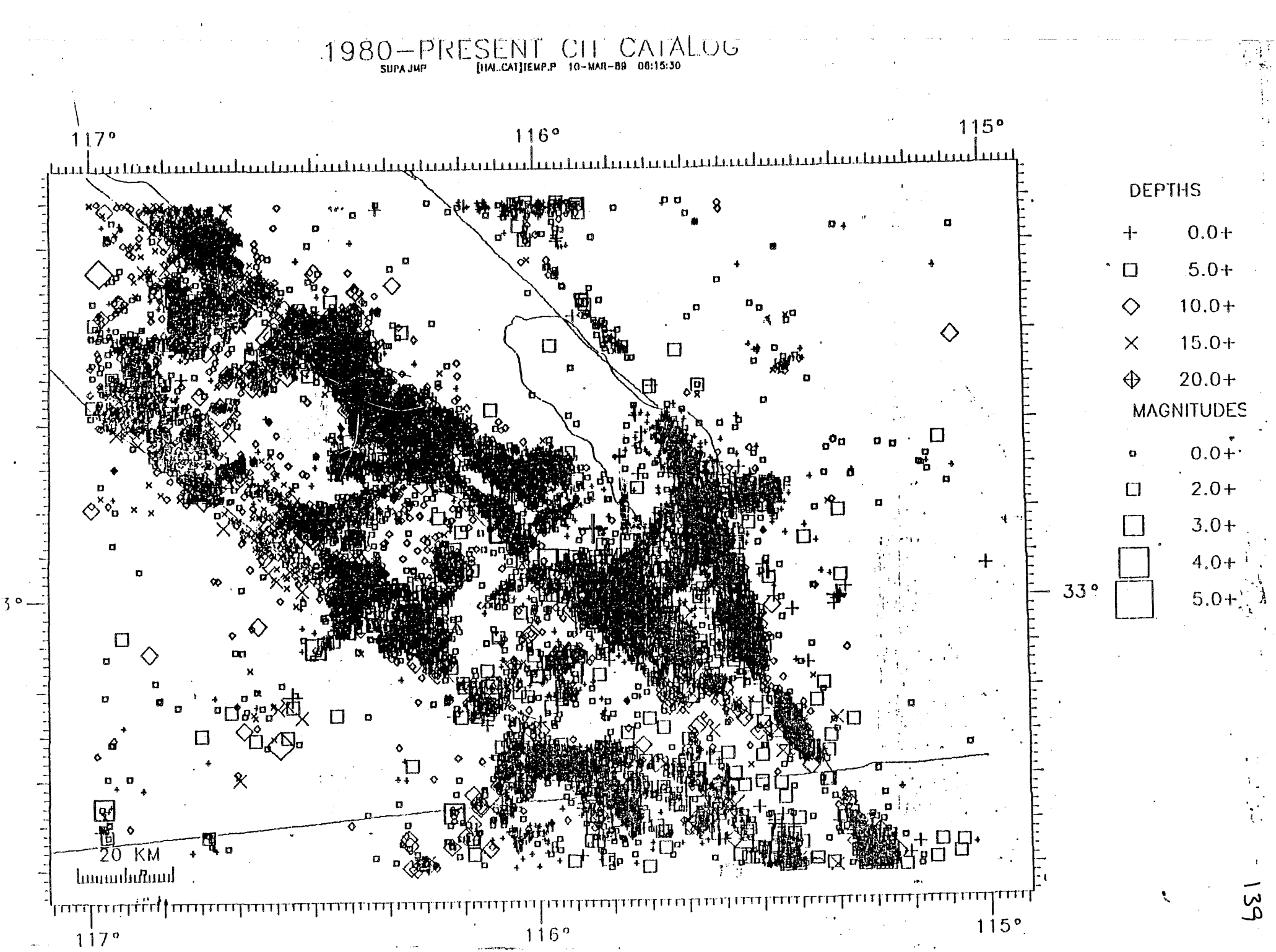

Figure 7. Microseimicity Map of The Salton Trough 1980 - 1989

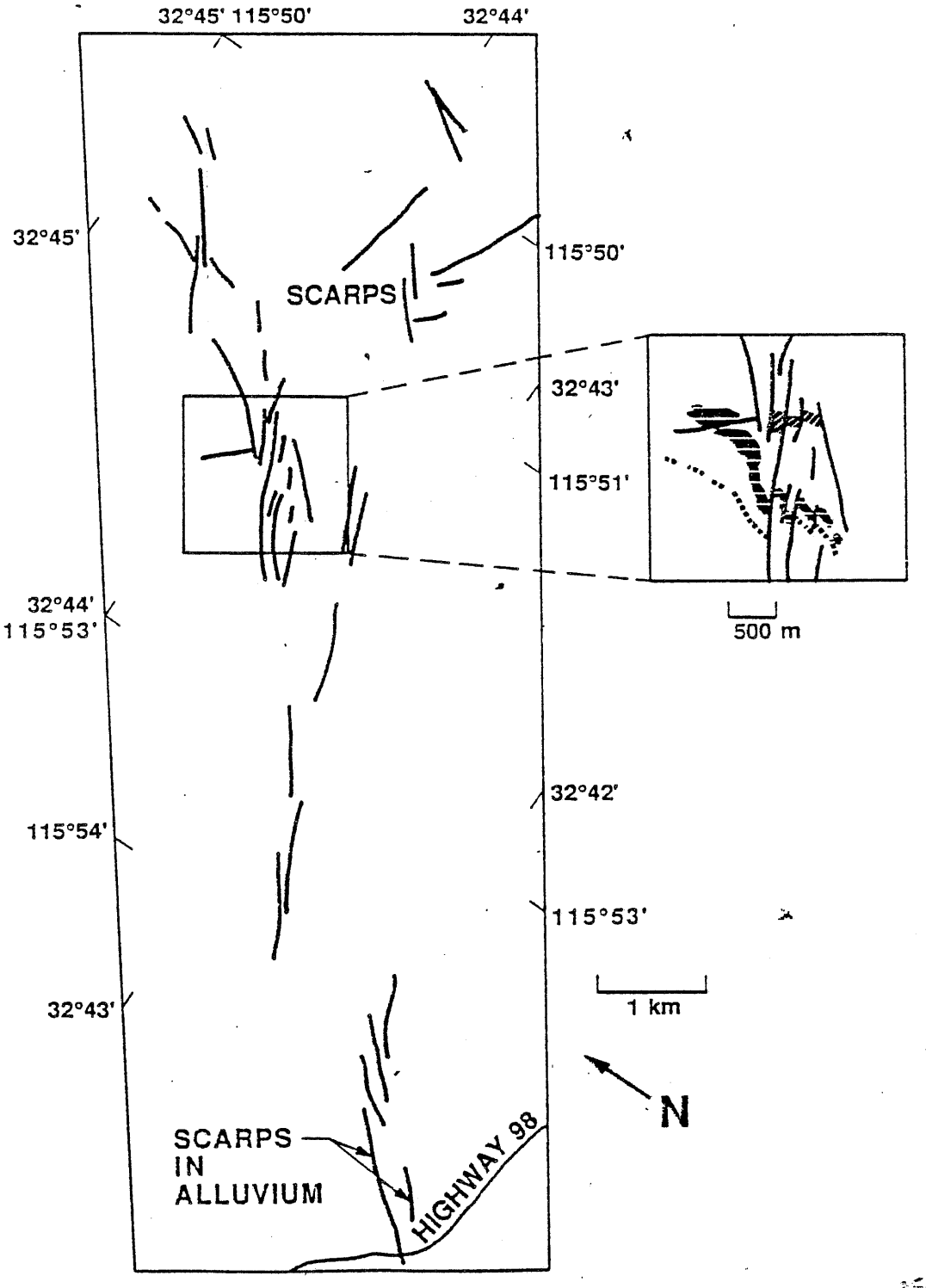

Figure 8. Map of Yuha Wells Area

these steps, the continuation of the Split Mountain and the Yuha Wells fault intersect respectively. The second variation of the block rotation model (Figure 4b) shows block rotation associated with a small transpressive step that was documented in a plowed field after the October 15, 1979 Imperial Valley, California earthquake (Terres and Sylvester, 1981). The dried parallel furrows of soil detached from the more moist subsurface and rotated as brittle blocks over the subsurface undergoing ductile deformation. Each of the blocks are bounded by left-lateral faults like a deck of cards being sheared. Nicholson (1986) has suggested that these faults might actually make the compressional bends larger on the northwest-trending faults by sinistral movement on northeast trending faults offsetting the dextral fault.

CONCLUSIONS

This study documents sinistral slip activity on the Yuha Wells fault. The strong geomorphic expression of the northeast-striking Yuha Wells fault, along with the many other cross faults in the western Salton Trough, suggests that the style of tectonic deformation that occurring in the central Salton Trough between the San Andreas and San Jacinto fault systems also operates in the western Salton Trough between the San Jacinto the and Elsinore Faults. Block rotation between northwest-striking faults over a regional detachment surface possibly explains the occurrence of widespread clockwise rotation of Neogene sediments. Paleomagnetic studies and the high seismic activity along cross faults supports this tectonic model.

There are probably components of both the block rotation and Wilcox models that at least partially explain the occurrence of these faults in the Salton Trough. Cross faults might originate as antithetic structures along major northwest-striking faults. These cross faults (including the Yuha Wells Fault) could accommodate rotational or antithetic shear mechanisms of both models: 1) Regionally, the left lateral motion due to block rotation; and, 2) Locally, the sinistral motion associated with the antithetic shear adjacent to the dominant northwest-striking fault.

Regardless of their origin, the activity of these sinistral faults is very important as active participants in moderate to large magnitude earthquake activity on associated dextral faults. The Superstition Hills earthquake sequence of 1987 demonstrates the importance of

these faults. The recent rise in microseismicity in the Yuha Desert centered along the well-expressed Yuha Wells Fault certainly warrants concern for possible future activity on the Laguna Salada / Elsinore Fault system or on the southern San Jacinto Fault system.

REFERENCES

Allison, M. L., Whitcomb, J.H., Cheatum, C.E., and McEuen, B.B., 1973, Elsinore Fault Seismicity: The September 13, 1973, Agua Caliente Springs, California, Earthquake Series: Bulletin of the Seismological Society of America, v. 68, no. 2, p. 429-440.

Christie-Blick, N, and Biddle, K.T., 1985, Deformation and Basin Formation Along Strike-Slip Faults, in Christie-Blick, N., and Biddle, R.T., eds.: SEPM Special Publication no. 37, p. 1-34.

Clark, M., 1987, The Borrego Mountain Earthquake of April 9, 1968: U.S. Geological Survey Professional Paper no. 787, p. 55-86.

Crowell, J.C., 1972, Origin of Late Cenozoic Basins in southern California, in A.G. Sylvester ed.: Wrench Fault Tectonics, 1984, AAPG Reprint n. 28, p. 195-209.

Dibblee, T.W., Jr., 1954, Geology of the Imperial Valley region, California, in R.H. Jahns, ed.: Geology of southern California, California Division of Mines Bulletin, v. 170, p. 21-28.

Dibblee, T.W., Jr., 1977, Strike Slip Tectonics of the San Andreas fault and its role in Cenozoic basin evolvement, in Late Mesozoic and Cenozoic Sedimentation and Tectonics in California: San Joaquin Geological Society Short Course, p. 26-38.

Dibblee, T.W., Jr., 1984, Stratigraphy and Tectonics of the San Felipe Hills, Borrego Badlands, Superstition Hills, and vicinity, in C.A. Rigsby, ed.: The Imperial Basin - Tectonics, Sedimentation, and Thermal Aspects, Pacific Section SEPM, p. 31-44.

Fuis, G.S., Mooney, W.D., Healy, J.H., McMechan, G.A., and Lutter, W.J., 1984, A Seismic Refraction survey of the Imperial Valley region, California: Journal of Geophysical Research, v. 89, p. 1165-1189.

Hudnut, K., Seeber, L., and Rockwell, T.,1989b, Slip On The Elmore Ranch Fault And Its Relation To Slip On The Superstition Hills Fault: Bulletin of Seismological Society of America, v.79, No.2, p. 330-341.

Hudnut, K., Seeber, L., Rockwell, T., Goodmacher, J., Klinger R., Lindvall S., and McElwain, R., 1989a, Cross-Fault Surface Ruptures In The November 23-24, 1987 Superstition Hills Earthquake Sequence, California: The Bulletin of Seismological Society of America, v. 79, No. 2, p. 282-296.

Hudnut, K., Seeber, L., and Pacheco, J., 1989, Cross-Fault Triggering In The November 1987 Superstition Hills Earthquake Sequence, southern California: Geophysical Research Letters, v. 16, No. 2, p.199-202.

Isaacs, S., 1987, Geology and Structure of the Yuha desert between Ocotillo, California, U.S.A. and Laguna Salada, Baja California, Mexico: Unpublished M.S. thesis, San Diego State University, San Diego California, 75 p.

Johnson, N.M., Officer, C.B., Opdyke, N.D., Woodard, G.D., Zeitler, P.K., and Lindsay, E.H., 1983, Rates of Cenozoic Tectonism in the Vallecito- Fish Creek basin, western Imperial Valley, California: Geology, v. 11, p. 664-667.

Langenkamp, D., and Combs, J., 1974, Microearthquake Study of the Elsinore Fault Zone, Southern California: Bulletin of the Seismological Society of America, v. 64, no. 1, p.187-203.

Lindvall, S., 1988, Evidence of Prehistoric Earthquakes On The Superstition Hills Fault, southern California and a Holocene Slip Rate of The San Andreas Fault at Gorman Creek, Southern California: Unpublished M.S. thesis, San Diego State University, San Diego California, 102 p.

Luyendyk, B.P., Kamerling, M.C., Terres, R.R., and Hornafas, J.S., 1985, Simple Shear of southern California During Neogene Time Suggested by Paleomagnetic Declinations: Journal of Geophysical Research, v. 90, n. B14, p. 12454-12466.

Nicholson, C., Seeber, L., Williams. P., and Sykes, L., 1986, Seismic Evidence For Conjugate Slip And Block Rotation Within The San Andreas Fault System, southern California: Tectonics, v. 5, no. 4, p. 629-648.

Pinault, T., 1984, Structure, Tectonic Geomorphology and Neotectonics of the Elsinore Fault Zone Between Banner Canyon and the Coyote Mountains, southern California: Unpublished M.S. thesis, San Diego State University, San Diego, California, 231p.

Rockwell, T.K. and Pinault, C.T., 1986, Holocene slip events on the southern Elsinore fault, Coyote Mountains, southern California in: Ehling, P.L. ed., Neotectonics and faulting in Southern California, Geological Society of America, Cordilleran Section Guidebook, p. 193-196.

Rockwell, T.K. Blom, R., Klinger, R., Stinson, A., and Thomas, A., (In Review), Recognition, Extension and Significance of Northeast-Trending Faults Between The Elsinore and San Jacinto Fault Zones Using Combined Spot and Landsat Imagery: this volume.

Rockwell, T.K., and R. Blom, Unpublished Preliminary Combined Thematic Mapper SPOT Satellite Image of the Western Salton Trough, California displaying recognized faults and lineaments: San Diego State University, San Diego, California.

Schultejahn, P., 1984, The Yaqui Ridge Antiform and Detachment Fault: Mid-Cenozoic Extensional Terrane West of the San Andreas Fault: Tectonics, v. 3, no. 6, p. 677-691.

Sieh, K., 1986, Slip Rate Across the San Andreas Fault and Prehistoric Earthquakes at Indio, CA: Eos, v.67, no.44, p. 1200.

Terres, R. R., and Sylvester, A.G.,1981, Kinematic Analysis of Rotated Fractures and Blocks in Simple Shear: Bulletin of the Seismological Society of America, v. 71, p. 1593-1605.

Wallace, R., 1982, Evaluation of Possible Detachment Faulting West of the San Andreas Fault, Southern Santa Rosa Mountains, California: unpublished M.S. thesis, San Diego State University, San Diego, California, 77 p.

Wilcox, R.E., Harding, T.P., Seely, D.R., 1973, Basic Wrench Tectonics: AAPG Bull., v. 57, no. 1, p.74-96.

Woodring, W.P., 1931, Distribution and age of the Tertiary deposits of the Colorado Desert: Carnegie Inst. Wash. Publ. 148, p.1-25.

Bulletin of the Seismological Society of America, Vol. 79, No. 2, pp. 342–361, April 1989

EVIDENCE FOR PREHISTORIC EARTHQUAKES ON THE SUPERSTITION HILLS FAULT FROM OFFSET GEOMORPHIC FEATURES

BY SCOTT C. LINDVALL,* THOMAS K. ROCKWELL, AND KENNETH W. HUDNUT

ABSTRACT

Offset geomorphic features along the Superstition Hills fault show evidence for at least one slip event prior to the 1987 surface rupture, and possibly as many as four to five earlier prehistoric earthquakes. We documented several geomorphic features that appeared offset by multiple events by making detailed topographic maps. Offset features were abundant along reaches of the fault with high topographic relief and large displacement. Slip distribution for the penultimate event, as recorded by offset rills, streams, and shrub-coppice dunes, is very similar to the slip distribution from the 1987 earthquake through April 1988. This similarity may prove to be fortuitous if afterslip from the 1987 event continues to increase the total slip for this earthquake. But if afterslip associated with the 1987 event ceases in the near future, then the past two earthquakes were nearly identical in slip, and the Superstition Hills fault may be expected to produce characteristic earthquakes of roughly magnitude $6\frac{1}{2}$.

INTRODUCTION

Paleoseismic studies of strike-slip faults have utilized offset streams and other features to determine the slip per event, length of rupture, and magnitude of prehistoric earthquakes (Wallace, 1968; Sieh, 1978; Sieh and Jahns, 1984; Rockwell and Pinault, 1986; Zhang *et al.*, 1987). Tectonically offset geomorphic features have enabled these and other workers to characterize a particular fault's prehistoric activity and assess its future seismic potential. Sieh (1978) measured stream offsets to show the slip distribution for the 1857 $M > 8$ earthquake on the San Andreas fault in south-central California. Rockwell and Pinault (1986), grouping offsets of similar amounts, determined the slip per event and estimated the magnitudes of prehistoric earthquakes on a segment of the Elsinore fault in the Coyote Mountains of southern California.

The Superstition Hills fault ruptured in the 24 November 1987 Superstition Hills earthquake ($M_s = 6.6$) (Sharp *et al.*, 1989). Displacements from the 1987 earthquake, as well as apparent offsets that appear to represent prehistoric slip events, have been recorded by offset rills, streams, and shrub-coppice dunes (mounds of aeolian sand accumulated at the base of a bush) along the Superstition Hills fault. Surface rupture from the November 1987 earthquake provided calibration for studying slip from past events, using offset geomorphic features.

The concept of similar amounts of slip per event or "characteristic" earthquakes was first implied by Wallace (1970) when he presented the idea of average recurrence intervals. The quotient of slip per event and the long-term slip rate, or recurrence interval, assumes that slip in an earthquake will be repeated by a similar amount in future events. Schwartz and Coppersmith (1984) have shown that some individual faults and fault segments produce repeated similar size earthquakes. Their charac-

* Present Address: Lindvall, Richter & Associates, 825 Colorado Blvd., Los Angeles, California 90041.

teristic earthquake model proposes that repeating or successive earthquakes have a narrow range of magnitudes at or near the maximum possible for any given fault, and is supported by several geologic observations. On the south-central San Andreas fault, displacement that occurred during the 1857 earthquake is approximately equal to the two previous events at Wallace Creek (Sieh and Jahns, 1984) and other localities.

This paper presents the results of our topographic mapping and analysis of offset geomorphic features along the Superstition Hills fault, and the implications regarding the characteristic earthquake model.

The Superstition Hills Earthquake Sequence and Regional Tectonics

The 24 November 1987 Superstition Hills earthquake sequence produced surface rupture along northeast-trending cross faults and the northwest-trending Superstition Hills fault (Hudnut *et al.*, 1989; Sharp *et al.*, 1989). On 24 November a M_s = 6.2 earthquake ruptured the northeast-trending, left-lateral Elmore Ranch fault oriented nearly perpendicular to the right-lateral Superstition Hills fault. This event apparently triggered the larger $M_s = 6.6$ event on the Superstition Hills fault approximately 12 hrs later (Hudnut *et al.*, 1989), which ruptured along its entire 23.5 km mapped length, as well as a several km long, previously unknown southern extension (Sharp *et al.*, 1989). Co-seismic slip and associated afterslip (through April 1988) from the larger earthquake produced a maximum total displacement of about 80 cm on the Superstition Hills fault.

The Superstition Hills fault is part of the seismically active San Jacinto fault zone of southern California (Fig. 1). As the Clark fault strand of the San Jacinto fault zone enters the western margin of the Salton trough, the zone splays into individual segments: the Coyote Creek fault, the San Felipe Hills fault, the Superstition Mountain fault, and the Superstition Hills fault. Farther to the southeast lies the Imperial fault, which trends more northerly than the San Jacinto fault zone. The San Andreas fault zone runs along the northeast margin of the Salton Sea. The seismically active Salton trough forms the transition region from the dextral strike-slip tectonics of the San Andreas fault system to the spreading regime of the East Pacific Rise in the Gulf of California.

The Superstition Hills is an uplifted area of relatively low relief comprised of a highly deformed section of the Plio-pleistocene Brawley Formation lacustrine sediments. The Superstition Hills fault extends from near the northwest end of the hills approximately 24 km southeast to where it marks the southern margin of the Superstition Hills uplift. Moderate-sized earthquakes in the Salton trough region have triggered surface slip on the Superstition Hills fault in the 1968 Borrego Mountain earthquake (Allen *et al.*, 1972), the 1979 Imperial Valley earthquake (Fuis, 1982), and the 1981 Westmorland earthquake (Sharp *et al.*, 1986). These three triggered slip events have cumulatively produced a maximum of nearly 4 cm of dextral slip on parts of the Superstition Hills fault (Sharp *et al.*, 1986).

Geomorphic Features

The sparsely vegetated Superstition Hills are subject to a hyper-arid climate and receive an average of less than 6 cm of rain annually (Waters, 1983; Clark, 1972) from thunderstorm activity. The soft and easily erodible Brawley Formation produces badland-type topography in areas of moderate to high relief within the hills. This locally dissected and deeply incised topography provides excellent geomorphic markers to record slip along the fault (Figs. 2 and 3). The low precipitation in this

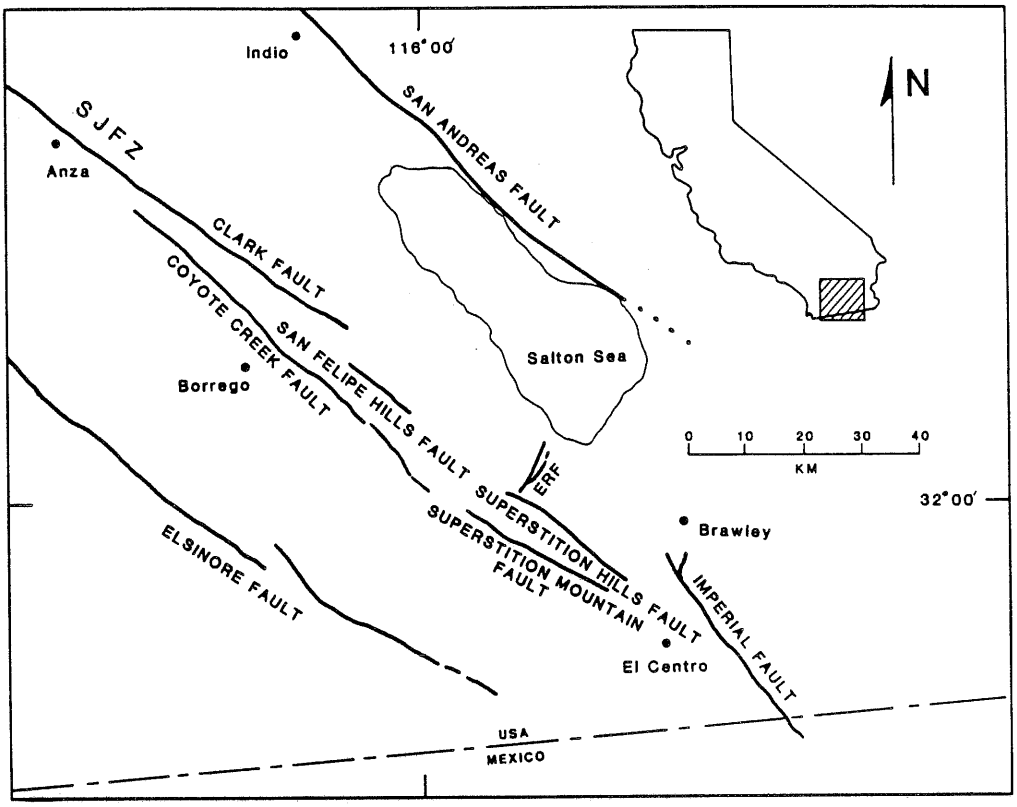

FIG. 1. Index map showing major faults of the Salton trough region. The highly segmented San Jacinto fault zone (SJFZ) consists of the Clark, Coyote Creek, San Felipe Hills, Superstition Mountain, and Superstition Hills faults. The Elmore Ranch fault (ERF) and the Superstition Hills fault ruptured in the 24 November 1987 earthquake sequence.

area has apparently enabled some of the geomorphic features to be preserved for hundreds of years.

A total of 38 offset geomorphic features, which express evidence of having been offset prior to the 1987 earthquake, were observed along the Superstition Hills fault. The offset geomorphic features that provided paleoslip data are rills, ephemeral streams, shrub-coppice dunes, and terrace risers. Fluvial features ranged in size from small rills with microdrainage basins of less than 2 square meters to small stream channels that drain basins in excess of hundreds of square meters. The channels in this region only carry water during and immediately following precipitation.

DATA ACQUISITION AND METHODS

Field Measurements

The majority of data collection for this study was conducted between the middle of March and the early part of May 1988. During this time, the 23.5 km length of the northern and central segments of the fault was traversed, with most portions of the fault examined two or more times. The southern segment (Sharp *et al.*, 1989) was not included in this study because displacements were small and the entire length of the segment lies topographically below the shoreline of ancient Lake Cahuilla. Further, most of the rupture along this segment occurred in tilled fields and, hence, older geomorphic features have been destroyed by plowing. Each offset

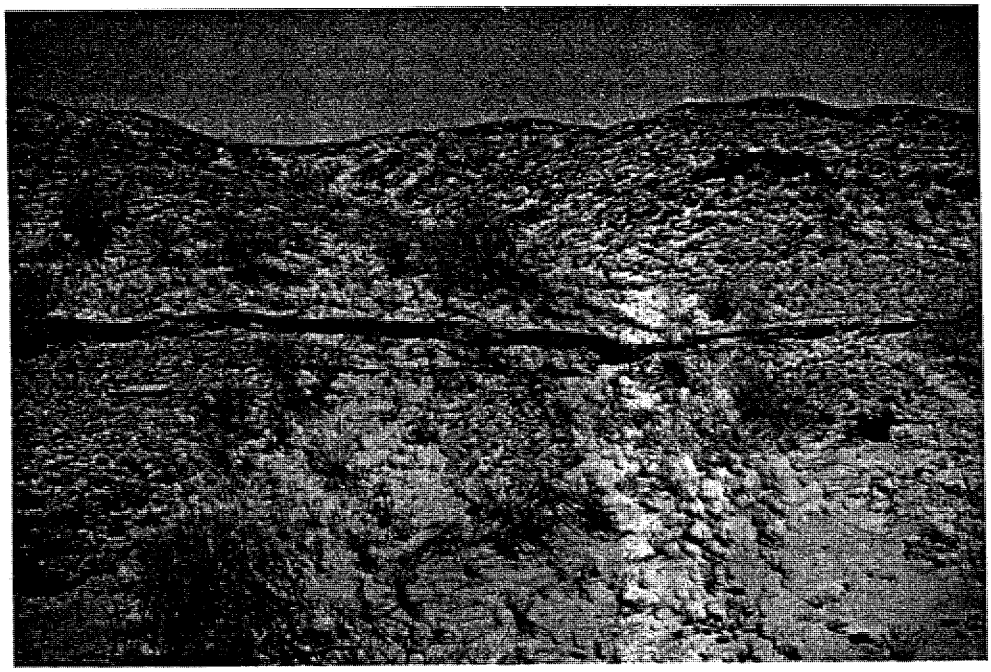

FIG. 2. Small beheaded stream channel at site 7. The beheaded channel on the left is offset 200 ± 30 cm from the active channel upstream from the fault. The channel on the right was offset 68 ± 5 cm in the 1987 earthquake. Clipboard in left center of photo for scale. See Figure 11 for contour map of this site.

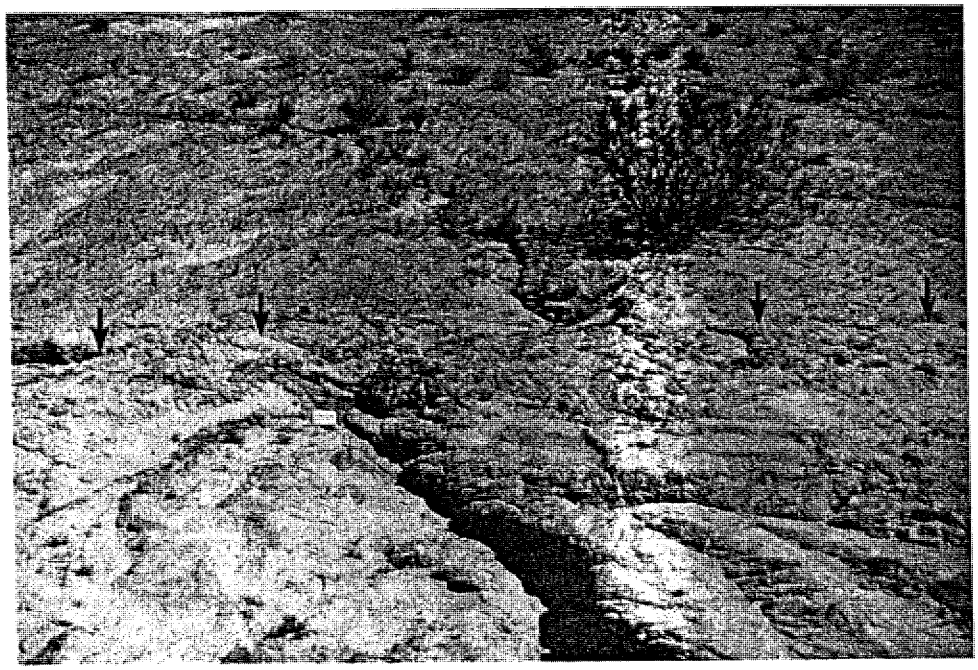

FIG. 3. Downstream view of the incised rill offset 146 ± 20 cm at site 24a. The 1987 rupture consists of a single strand through the center of the photo. The fault trace (denoted by arrows) is not readily seen in the photo since the scarp in the thick clay gouge zone degraded rapidly. White 3 by 5 inch card in the rill upstream from the fault for scale. See Figure 6 for contour map of this site.

was measured and documented by at least two of the co-authors, thus enabling valuable discussions and scrutiny and greatly reducing possible bias in the data collection.

In the field, sites of apparent multiple offsets and sites of 1987 slip measurement were located on postearthquake USGS aerial photographs (1:8000 scale) on which the November 1987 surface rupture was clearly visible. These locations were later transferred to the Kane Spring, Superstition Mountain, and Brawley NW 7.5 min topographic quadrangles (Fig. 4). Using a metric steel tape, offsets were measured by matching similar features such as channel centers or channel walls that were nearly perpendicular to and intersected the fault.

On channels that were rounded or otherwise lacking distinct piercing points, linear features of the channel morphology were projected to the fault and the offset was measured, as with all other features, along strike of the fault. This technique is used to restore the channel wall or center feature to its original configuration prior to subsequent rounding and was used for determining displacement at several sites.

Each offset was assigned a measurement error, and the quality of each measurement was rated as excellent, good, fair, or poor. An excellent offset is well preserved, prominent, and unambiguous, whereas an offset designated as poor may be poorly preserved, subtle, or yield ambiguous measurements and interpretations. Many poor quality apparent offsets, that could have been produced by other processes, were not included in this study. For instance, we commonly found but did not use rills that were deflected around plants or shrub-coppice dunes at the fault and channels that had been significantly altered during the postearthquake rains.

In addition to measuring large offsets that appear to have been produced during previous earthquakes, the slip distribution of the November 1987 rupture was developed from measurements collected at 100 points along the length of the northern and central segments of the Superstition Hills fault. The purpose of quantifying the recent rupture during the 8 week period from March to May 1988

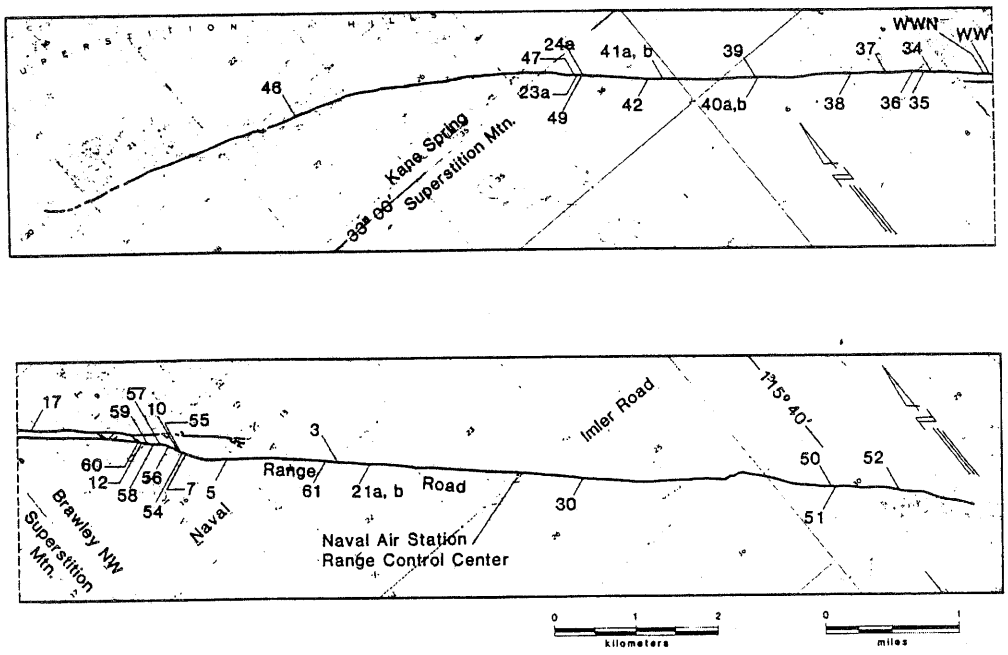

FIG. 4. Site locations of geomorphic features offset by multiple events along the 1987 Superstition Hills fault rupture. Trace of rupture modified from Kahle *et al.* (1988).

was to compile a data set that included co-seismic slip and afterslip for comparison with sites of apparent multiple offsets. Other studies of the November 1987 rupture (Williams and Magistrale, 1989; Sharp *et al.*, 1989) are presumably more detailed in scope and have better documented the slip in the areas of low displacements (at the ends of the fault and throughout the fault step-over). This is because small 1987 offsets, typically less than 15 cm, have been masked or significantly altered by water and wind during the period between November 1987 and March 1988. Most features that were used as piercing points to determine slip in the 1987 earthquake are the same type used to determine prehistoric slip such as rills, gullies, streams, and shrub-coppice dunes. Displaced road berms, tire tracks, and grass lines were also used to produce the 1987 slip distribution, but these constitute only about 5 per cent of the data.

Contour Maps

Detailed topographic maps were produced of selected sites with apparent multiple offsets using two related methods similar to plane table mapping. The sites chosen for detailed documentation were all of good to excellent quality, with most of the 1987 displacement along one or two discrete strands of the fault. Because most features were small and total offsets less than 3 m, accuracy and detail was a primary concern. Therefore, all maps were made using a theodolite mounted with an electro-optical distance measurer. The method used to construct contour maps of sites 23a, 24a, 39, WW, and 21 utilized a Zeiss Elta 4 surveying instrument, a Hewlett-Packard-41 calculator/data collector, and a standard single pen plotter. First the instrument was set up and a baseline and its azimuth established. Then between approximately 70 and 130 data points were shot using a rod-mounted reflector at each site. The data collector converted all distances and angles into XYZ coordinates and stored the data. Information from the data collector was downloaded and backed up on a laptop computer in the field before creating a plot of data points and elevations with the battery-driven plotter. The resulting plot of point locations and elevations was used as a base map for drawing the contours by hand.

Using the second method, maps of sites 38 and 7 were generated using a contouring program, after the distance and angle measurements were converted to XYZ coordinates with instrument-specific software. A WILD TC-2000 surveying instrument and a GRE-3 data collector were used to gather field data. Site 42 was not computer-generated, but rather hand-contoured using a plot of point locations and elevations. This was because the site's very low relief was difficult for the computer to depict. At sites where the WILD TC-2000 was used, the intent was to generate the maps by computer, and therefore between 170 (Site 38) and 290 (Site 7) data points were collected for each site. We felt more topographic control was necessary for the computer-generated plots than the maps contoured by hand in the field.

Observations of 1987 and Earlier Offsets

Data representing total offset of geomorphic features collected for this study are listed in Table 1. In general, the larger offsets correspond with the larger and more pronounced, and hence presumably older, rills and gullies along the fault. The smaller offsets are associated with smaller and presumably younger geomorphic features. The majority (over 70 per cent) of the dextral offsets fall between 100 and 200 cm. Spatially, most of the data are distributed between 6 and 16 km from the northwest terminus of the fault.

The smallest offsets, 31 and 50 cm, were found near the ends of the fault where

TABLE 1. Measurements of Offset Geomorphic Features Along the Superstition Hills Fault

SITE	TYPE OF FEATURE	TOTAL OFFSET (cm)	ERROR (+/-)	QUALITY RATING	DIST. ALONG FAULT (km)*	DATE MEASURED	1987 SLIP** (cm)	ERROR (+/-)
46	rill	31	8	poor	3.20	5-8-88	15	5
47	rill	105	30	fair	6.73	5-8-88	53	6
23a	large rill	250	45	excel.	6.75	3-27-88	60	4
24a	large rill	146	20	excel.	6.78	3-27-88	61	3
49	large rill	120	30	fair/poor	6.80	5-8-88	60	4
42	shrub-coppice dune	140	20	good	7.59	4-16-88	70	5
41a	large rill	190	30	good	7.79	4-16-88	60	3
41b	large rill	380	70	poor	7.79	4-16-88	60	3
39	beheaded rill	119	10	excel.	8.89	4-16-88	68	5
40a	rill	124	20	good/fair	8.91	4-16-88	65	3
40b	rill	190	50	poor	8.91	4-16-88	65	3
38	rill	140	20	good	10.10	4-16-88	76	4
37	channel and terrace	240	30	fair	10.45	4-16-88	80	3
36	terrace	420	100	poor	10.80	4-16-88	67	7
35	rill divide	102	15	good	10.90	4-16-88	67	7
34	rill	125	20	fair	11.05	4-16-88	67	7
WWN	rill	110	15	good	11.66	5-14-88	70	7
WW	2 rills	140	25	good/fair	11.69	5-14-88	70	2
17	rill and shutter ridge	290	100	poor	12.00	3-20-88	70	6
60	rill	170	20	good	13.33	5-14-88	44	4
12	large stream	156	30	good	13.35	3-19-88	44	4
59	beheaded rill	220	40	poor	13.41	5-14-88	44	4
58	rill	100	15	fair	13.50	5-14-88	48	3
57	rill	125	20	good	13.53	5-14-88	48	3
56	small stream	135	15	good	13.67	5-14-88	65	6
10	stream	220	35	good/fair	13.78	3-19-88	65	6
55	rill	110	15	good	13.80	5-14-88	65	6
54	rill	115	15	good	13.82	5-14-88	65	6
7	beheaded stream	200	30	good	13.90	3-19-88	68	5
5	rill	310	50	good	14.45	3-19-88	60	8
61	rill	135	25	fair	15.58	5-15-88	54	5
3	braided stream	120	15	poor	15.70	3-19-88	56	5
21a	stream	120	10	good	16.10	3-20-88	55	3
21b	stream	240	20	good	16.10	5-15-88	55	3
30	shrub-coppice dune	100	?	poor	18.68	4-16-88	55	4
50	terrace riser?	75	20	poor	21.70	5-7-99	34	3
51	stream channel divide	140	40	poor	21.74	5-7-88	34	3
52	channel wall?	50	6	poor	22.53	5-7-88	22	3

* From NW end

** Values represent 1987 slip (through April 1988) measured nearest to site.

slip dies out significantly. The largest offsets measured were 380 and 420 cm and are located along the reach of the fault that experienced the greatest amount of displacement in the 1987 event. The quality of both of these large offsets, however, was judged as poor. The lack of good quality, large (>350 cm) offsets may be a result of the degradation of these presumably old features with time. Few and poor quality data at the ends of the fault probably reflect the difficulty with which smaller magnitude offsets are preserved.

Two other factors that significantly influence the distribution of our data are

topography and the position of the 300 yr old Lake Cahuilla shoreline. Slopes traversed by the fault contain a large number of the offset features because they produce the linear, incised gullies that remain captured or contained between the channel's walls through time. Stream channels on the flat desert floor generally exhibit a high sinuosity, poorly defined channel walls, and little or no incision. This lack of distinct channel morphology may be one reason that slip was poorly preserved from events before 1987 in areas of low topographic relief. A more important factor is that areas of low relief only contain a few rills and gullies, and thus provide only a limited number of geomorphic features to record tectonic offset. Fault geometry, in some areas, is responsible for relief along the trace and is best illustrated approximately 4 km northwest of the Naval Air Station Range Control Center, where the fault makes a bend and step (Fig. 4).

The reach of the Superstition Hills fault southeast from Imler Road was repeatedly inundated by the waters of Lake Cahuilla over the past millennium (Sieh, 1987; Waters, 1983). It seems unlikely that very old offsets would be preserved along this part of the fault and, hence, we suspect the 140 cm offset at site 51 (judged as poor) may not represent a tectonic offset. Only the slip event prior to 1987 occurred after the lake receded (Hudnut and Sieh, 1989), enabling rupture from the penultimate event to be recorded in the present geomorphic regime. Of the 38 multiple offsets presented in Table 1, we studied several in detail, and documentation of eight of these sites follows.

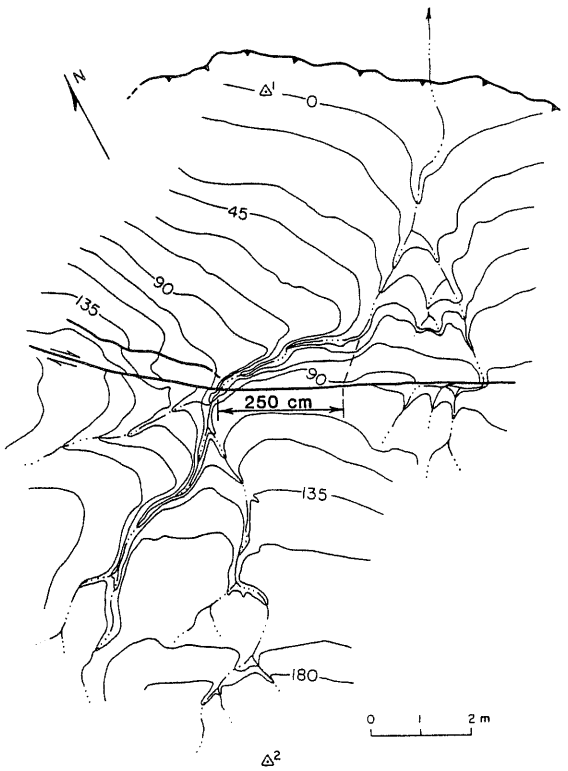

FIG. 5. Contour map of offset rill at site 23a. Contour interval is 15 cm. Linear portion of rill was projected into the fault in order to measure the offset of 250 ± 45 cm. A small triplet of rills to the right of the 250 cm multiple offset has recorded both a 120 cm offset and a 60 ± 4 cm offset from the 1987 earthquake. Triangular symbols on this and other contour maps represent benchmarks used for surveying.

Site 23a

A stream channel offset 250 ± 45 cm is located 6.75 km from the northwest end of the Superstition Hills fault. The channel drains a northeast-facing hillside of moderate to steep relief, which enabled the channel to develop a linear trend perpendicular to the fault. Tributary rills on the southwest side of the fault coalesce into a single channel that is offset about 250 cm by the fault (Fig. 5). The 250 cm dextral offset was produced by one principal fault strand. A minor thrust fault downstream from this offset produced only 1 to 2 cm of dip slip in 1987. The 1987 slip measured in April at the site was 60 ± 4 cm. The 250 cm offset is roughly four times larger than the slip at this site associated with the 1987 earthquake.

Another offset rill at same site exhibits a dextral displacement of 120 cm, about twice the amount of slip experienced in 1987. This can be seen on the northwestern most rill in a triplet of rills to the southeast of the larger offset (Fig. 5).

Site 24a

A very linear stream channel offset 146 ± 20 cm is located approximately 20 m southeast of site 23a. The channel at site 24a is oriented perpendicular to the fault and is fed by a number of incised tributaries on a northwest-facing hillside that converge into a single channel approximately 1 m upstream from the fault (Figs. 3 and 6). The stippled pattern in Figure 6 represents a strath terrace that probably formed after the November 1987 earthquake. In the postearthquake rains the

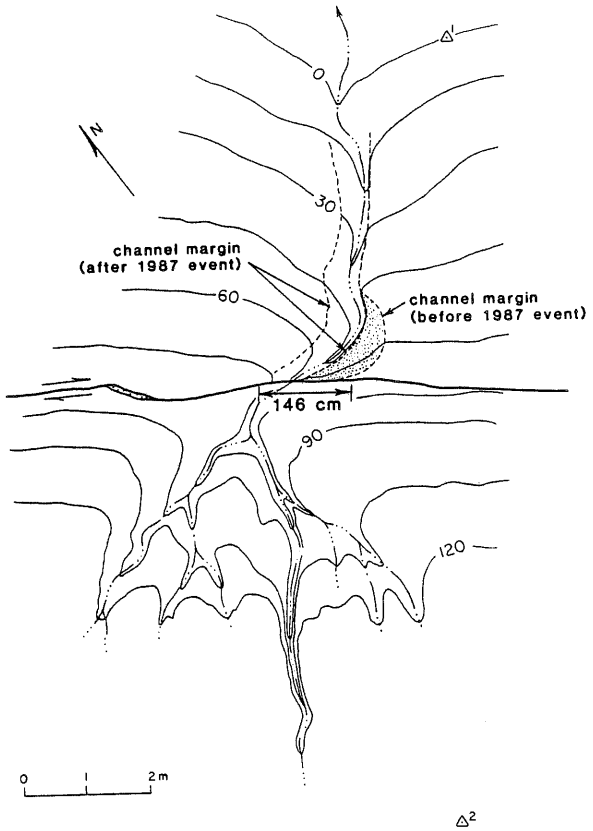

FIG. 6. Contour map of offset rill at site 24a. The incised rill is right-laterally offset 146 ± 20 cm. Contour interval is 15 cm. Downstream from the fault, a strath terrace (stippled area) apparently formed during postearthquake rains as a result of the right-lateral displacement from the 1987 event.

channel center apparently shifted from the southeast margin of the channel to its present incised position, attempting to straighten its course, leaving behind the flat terrace.

This shift in the thalweg of the channel is roughly equivalent to the 61 ± 3 cm displacement of November 1987 recorded on a rill less than 10 m from site 24a. The 146 ± 20 cm right-lateral offset represents the distance obtained by projecting a best-fit line of the linear upstream and downstream portions of the channel center into the fault. The channel at site 24a has been offset by more than one event; the 146 cm offset is between two and three times larger than the displacement that occurred from the 1987 earthquake.

Site 42

Two shrub-coppice dunes, located 7.5 km from the northwest end of the 1987 rupture, are offset by the fault. Along this reach of the fault, the 1987 rupture was confined to a single, linear strand that displaced both dunes. A well-defined dune with distinct margins was laterally displaced during the 1987 earthquake. Displacement of this feature as of April 1988 was measured as 70 ± 5 cm (Fig. 7). Another dune is offset 140 ± 20 cm, which is twice that of the dune displaced by only the 1987 earthquake (Fig. 7).

This presumably older dune is lower in topographic relief, larger in extent, and more diffuse around its perimeter than the younger, more morphologically distinct dune that is offset 70 cm. This difference in dune morphology is apparently a function of the plants about which the dunes are centered. Only the sparse, dead remains of a bush are present in the 140 cm offset dune that is now apparently being degraded. On the other hand, a living bush serves as the locus of active deposition of aeolian sand that comprises the 70 cm offset dune.

Site 39

Site 39 is located approximately 9 km from the northwest terminus of the fault on a gentle north-facing slope. The site consists of two small, shallow rills that have been offset by the fault (Fig. 8). Slip that occurred in 1987 has offset and beheaded

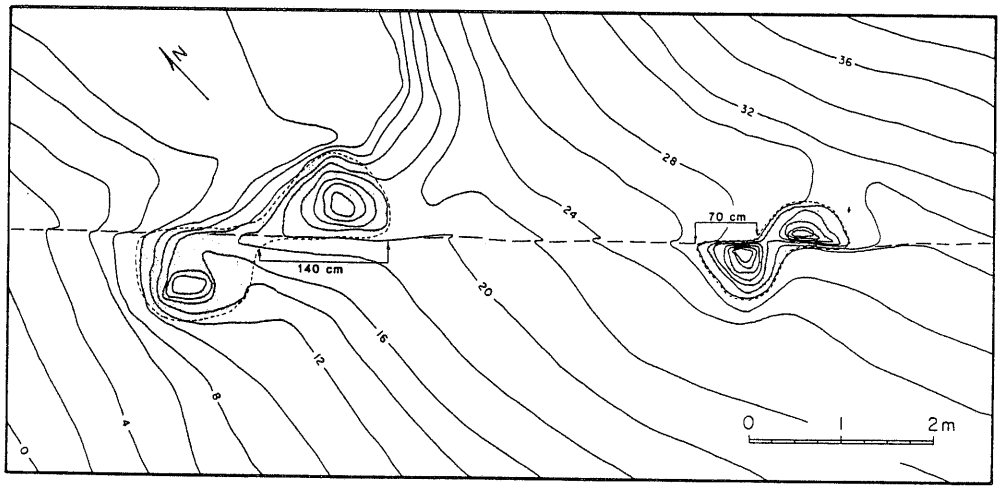

FIG. 7. Contour map of two shrub-coppice bush dunes (stippled areas) offset by the Superstition Hills fault (long-dashed line). Contour interval is 2 cm. The dune on the right was offset 70 ± 5 cm in the 1987 rupture event. The total offset of the dune on the left was measured as 140 ± 20 cm using the dune margins (short-dashed lines) as piercing points.

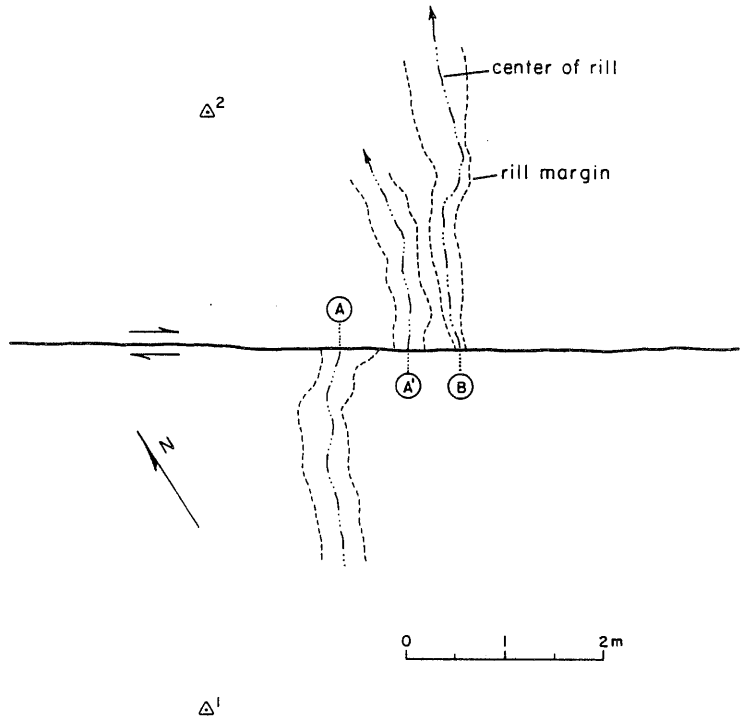

FIG. 8. Line drawing of beheaded rill at site 39. Positions of fault, rill centers, and rill margins were located with a surveying instrument. Offset A-A′ is 67 ± 5 cm from the 1987 event. Offset A-B is 119 ± 10 cm and is interpreted as cumulative slip from the 1987 event and the penultimate event.

the active rill by 67 ± 5 cm (offset A-A′ in Fig. 8). An older, more degraded rill appears to have been beheaded by the penultimate event and is now offset 119 ± 10 cm (offset B-A in Fig. 8). The north-facing aspect of the slope, along with the north-northeast trend of the rills apparently allowed for complete abandonment of the downslope reach of the rills after each earthquake.

Site 38

Located approximately 10 km from the northwest terminus of the fault, this site contains a channel with an apparent offset of 140 ± 20 cm across two strands of the fault. The amount of 1987 offset near this location was about 75 cm, about half of that recorded in the offset channel. The map of site 38 (Fig. 9) was contoured by computer at a contour interval of 5 cm. Figure 9a represents the topography after the 1987 earthquake. The small closed depression immediately upstream from the principal strand of the fault formed in response to a newly created shutter ridge and downdropping of the fault-bounded silver. The absence of abrupt offsets of contour lines at the fault is an artifact of the computer contouring. In Figure 9b, the map was cut and restored along the principal linear strand to reconstruct the original position of the small drainage. The best fit or reconstructed topography indicates a cumulative offset of 140 ± 20 cm.

Site WW

At this site, located 11.7 km southeast of the northwest end of the Superstition Hills fault, two small drainages that converge downstream of the fault appear to be offset approximately 140 cm (Fig. 10a). The offset of the southern drainage was measured between point A on Figure 10a (the intersection of the upstream channel

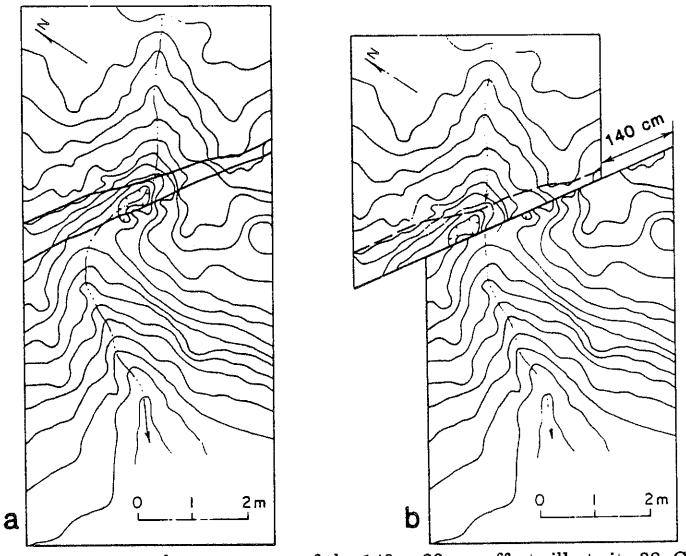

FIG. 9. a) Computer-generated contour map of the 140 ± 20 cm offset rill at site 38. Contour interval is 5 cm. b) 140 cm restoration of the offset rill along the linear, principal (southwestern) fault strand.

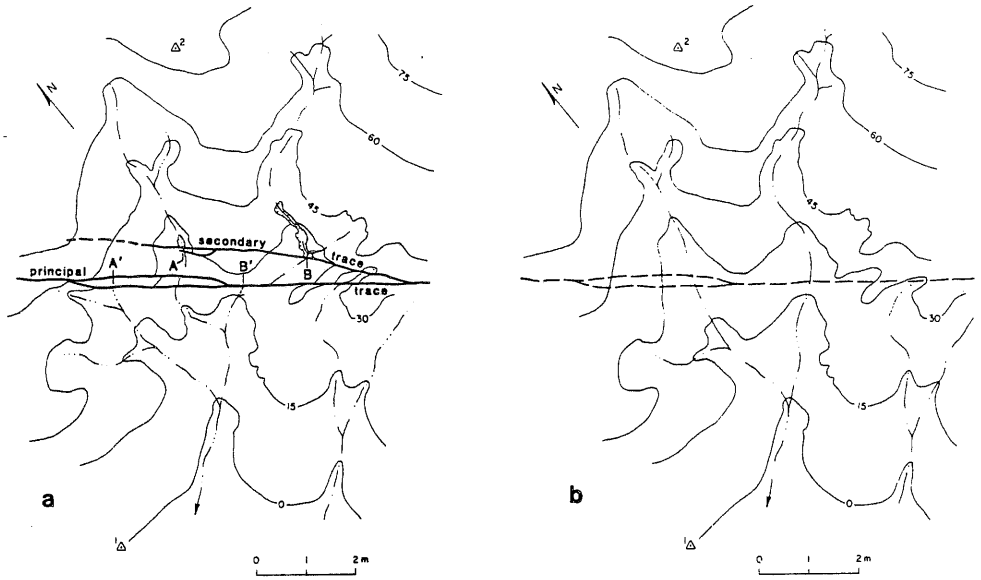

FIG. 10. a) Contour map of two offset rills at site WW. Contour interval is 15 cm. The rill on the left is offset 137 ± 20 cm (A-A′) and was judged as fair quality, whereas the rill on the right is offset 140 ± 25 cm (B-B′) and was judged as good/fair quality (center of rill at B′ required minor straightening). b) Reconstructed topography of site WW before the penultimate event. Map was restored 140 cm along the principal strand of the fault (long-dashed lines) and required only minimal modification of contour lines.

center and the secondary (northeastern) fault strand) and point A′ (the intersection of the projected downstream channel center and the principal fault strand) as 140 ± 25 cm. Another offset channel was measured between point B in Figure 10a (the intersection of the center of its channel with the secondary (northeastern) fault) and point B′ (the intersection of the beheaded channel and the principal fault strand) as 137 ± 20 cm.

Figure 10b shows the reconstructed topography of site WW after back-slipping the fault 140 cm and restoring the contours. The nearest measurement of 1987 slip, taken approximately 200 m southeast of site WW, was 70 ± 2 cm, approximately half of that suggested by the two offset channels.

Site 7

About 1 km northwest of where the Naval Range Road bends sharply to the west away from the fault (Fig. 4), a channel is apparently beheaded from the active channel upstream from the fault. These channels are separated by 200 ± 30 cm (Figs. 2 and 11). This site is located at a large bend in the fault that has resulted in the downdropping of the northeastern block and the formation of a prominent northeast-facing slope that contains several multiply offset gullies and channels oriented perpendicular to the fault. Site 7 contains two fault strands that slipped in 1987 with the easternmost or principal strand accommodating the majority of offset. The 1987 dextral slip summed across both strands at this site is 68 ± 5 cm. Displacement on the western strand was predominantly dip-slip, with as much as 12 cm of normal slip in the southern part of the computer-contoured map. The dip-slip component decreased to the north where the 2 strands become closely spaced and parallel. The 200 ± 30 cm apparent offset of the beheaded channel is larger than the 1987 slip by a factor of 3.

Site 21

About 16 km from the northwest end of the fault and approximately 2 km northwest of the Naval Range Tower at Imler Road, a single stream has apparent offsets of 120 ± 10 cm and 240 ± 20 cm (Fig. 12). This broad, flat-bottomed channel flows northeast at a low gradient in an area of very little topographic relief. The well-defined northern channel wall, which was used as the piercing point, is clearly offset 120 ± 10 cm with only very little rounding of the channel wall. This offset, which was recorded as of good quality, is similar to the total offset (through March 1988) obtained by Hudnut and Sieh (1989) for cumulative slip from both the 1987 and penultimate events at the Imler Road trench site, 2 km to the southeast.

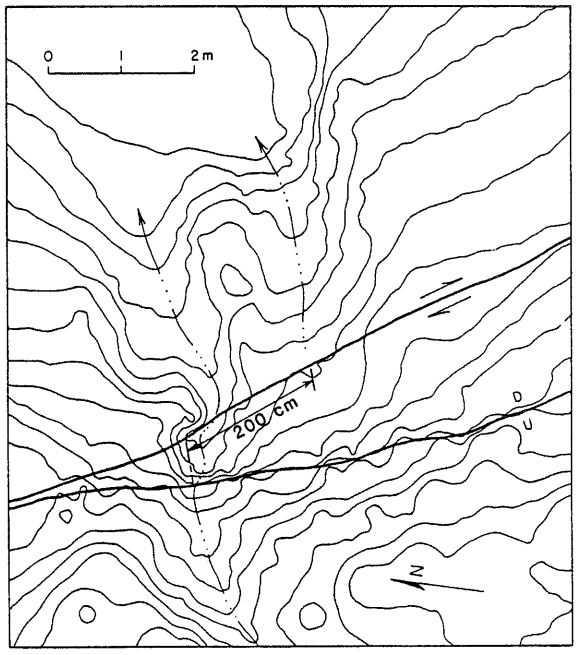

FIG. 11. Computer-generated contour map of the small beheaded stream at site 7. Contour interval is 5 cm. The offset of the beheaded channel is 200 ± 30 cm. Displacement of the active channel from the 1987 earthquake measured across both strands is 68 ± 5 cm.

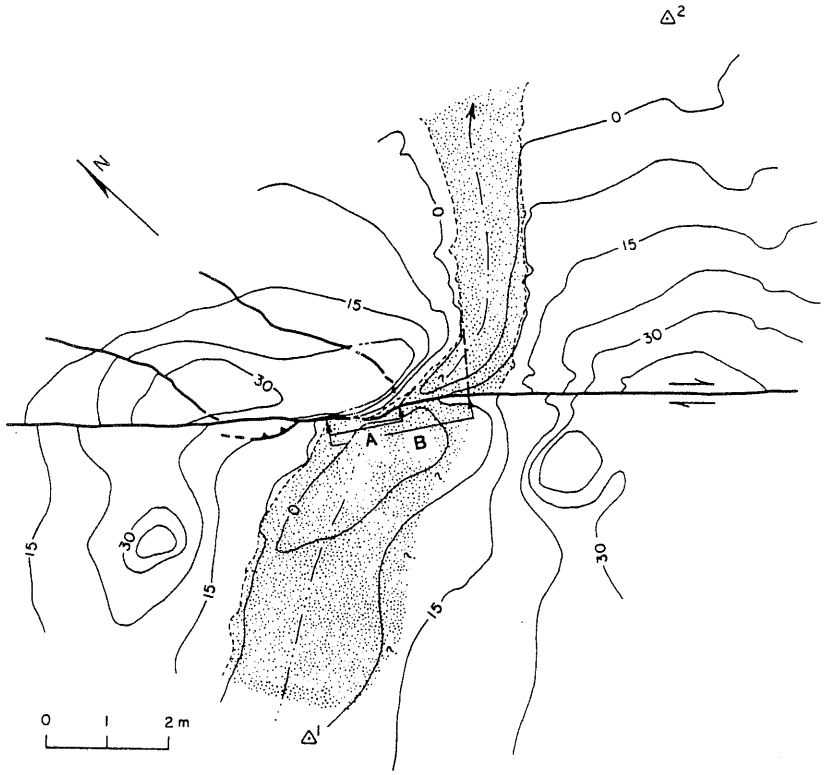

FIG. 12. Contour map of the offset stream at site 21. Contour interval is 7.5 cm. Stippled pattern represents the sand-covered channel bottom and short-dashed lines represent the base of the channel walls. Offsets A and B are 120 ± 10 cm and 240 ± 20 cm, respectively.

A portion of the northern channel wall is significantly rounded immediately downstream from the fault. Straightening of the downstream linear reach into the fault suggests 240 ± 20 cm of dextral offset. We feel that this is valid because the channel walls are linear both upstream and downstream from the fault (Fig. 12). Based on these observations, we classified this offset as of good quality. With 1987 slip values near site 21 ranging from 52 to 58 cm, the two offsets of about 120 and 240 cm are greater than the 1987 slip by factors of about 2 and 4, respectively.

DISCUSSION

The repeated offsets interpreted at sites along the 1987 surface rupture indicate that several prehistoric surface faulting events have occurred on the Superstition Hills fault. A few poor-quality offset values are five to six times greater than the amount of 1987 displacement, which may suggest that as many as a half dozen earthquakes can be recognized by study of offset geomorphic features along the Superstition Hills fault. In the following analysis, we assume that the full amount of lateral deflection and apparent offset expressed by each multiply offset geomorphic feature is of tectonic origin, and that we can use these values as accurate estimates of lateral slip within the stated uncertainties.

Nearly 40 per cent of the multiply offset geomorphic features are either exactly or approximately double that of the 1987 slip distribution (as measured in April 1988), suggesting a penultimate slip event with a similar slip distribution to that of 1987. This is consistent with Hudnut and Sieh's (1989) recognition of a prior slip event at their Imler Road site, which they argue was caused by an earthquake.

Characteristic Earthquake Model

Probabilistic analysis of earthquake hazards (Sykes and Nishenko, 1984; Wesnousky, 1986) relies, in part, on use of the characteristic earthquake model for recurrence (Schwartz and Coppersmith, 1984). Observations that either support or provide evidence of alternative types of fault behavior have both scientific and societal repercussions; therefore, it is of general interest to test this model against geologic observations. The Superstition Hills fault presents an opportunity to evaluate the characteristic earthquake model in a nearly ideal situation, in which ruptures overlapping along strike can perhaps safely be assumed not to occur (at least to the northwest). We take this opportunity to test the model for this fault to the extent allowed by our data. We also note that an independent test by Hudnut and Sieh (1989) challenges the characteristic earthquake model for this fault. Their results, discussed below, are based on study and evaluation of slip at a single site near the intersection of the Superstition Hills fault with Imler Road.

Testing the Model

We set up the characteristic earthquake model in its strict sense, that slip per event at any given point along the fault will not vary. Thus, we take as the predicted values the 1987 slip and afterslip through April 1988 (Fig. 13) multiplied by factors of 2, 3, and so on (Fig. 14). As observations, we take the values we obtained for total slip across multiply offset geomorphic features. This is illustrated on Figure 14, where integer multiples of the 1987 slip curve of Figure 13 are shown as dotted lines, and the multiple offsets are shown as open circles with error bars.

We then analyze the fit of our observations to curves predicted by the model. For each site, we subtracted integer multiples of 1987 slip from the total slip across

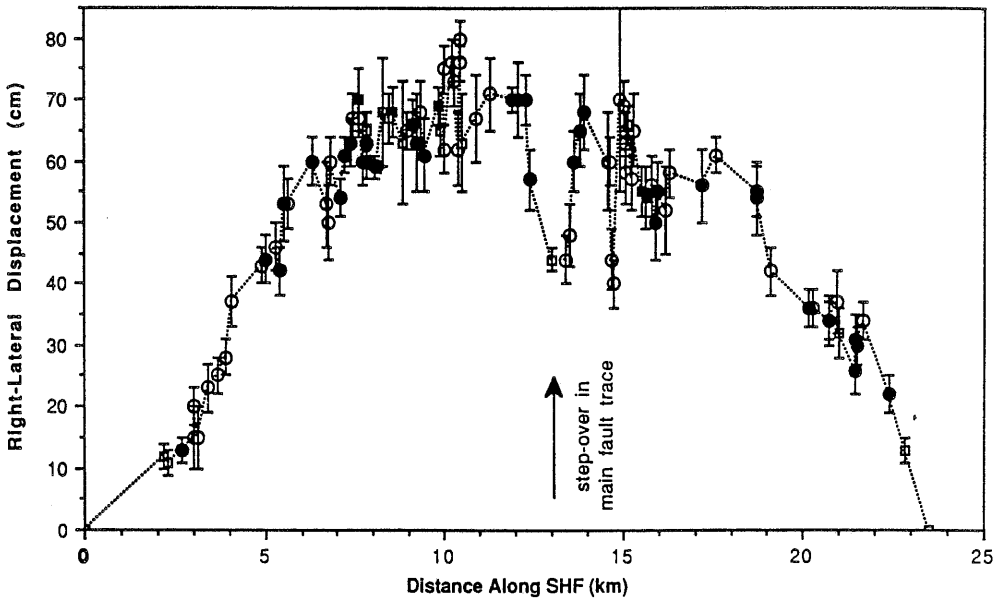

FIG. 13. Slip distribution along the Superstition Hills fault as of April 1988. This curve is defined mainly by data from features comparable to those used to measure pre-1987 offsets. Such features are rills, shown as open circles, and channel walls, shown as filled circles. These two categories comprise about 90 per cent of the data presented on this graph. In addition, offset dunes, lines of grass, and other shorter-lived geomorphic features are grouped as filled square symbols, and transient features such as pull-aparts, tire tracks, and road berms are grouped as open square symbols. Error bars were estimated for each offset in the field. A major stepover in the main trace of the fault is indicated at 13 km along the fault. This step actually spans from about 12.4 to 13.5 km.

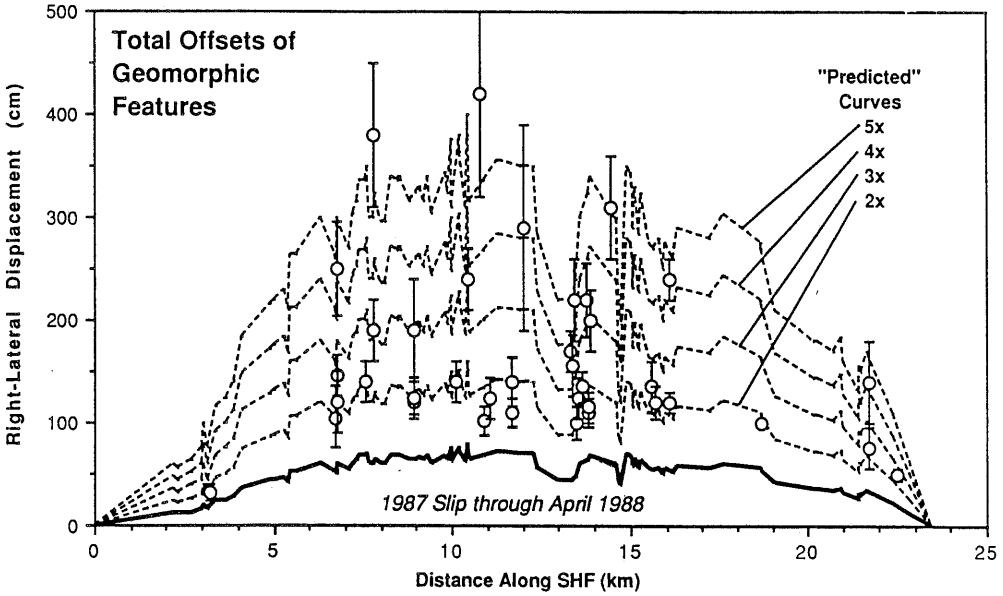

FIG. 14. Illustration of our test of the characteristic earthquake model. The 1987 slip curve presented on Figure 13 has been multiplied by integer factors, producing a family of "predicted" curves. Measurements of offset geomorphic features (open circles with error bars) from Table 1 are overlain upon this family of curves. If these data points fit any of the predicted curves, it suggests the model is correct. Because it is difficult to quantitatively analyze this simply by looking at this graph, we have computed residuals between observed and predicted values on Figure 15.

multiply offset features. For example, we first tested for a single event prior to 1987. The 1987 slip was multiplied by a factor of 2, generating a set of predicted values. These values were then subtracted from the observed total offsets across features at the same location. This produced the set of residual values shown in Figure 15.

Analysis of the Residuals

The test for a pre-1987 slip event identical to the 1987 event produces a strong concentration of residuals about the zero value, supporting the characteristic earthquake hypothesis for the penultimate event. These residuals are not normally distributed; instead there appears to be a weak second mode in the data centered about +70 cm. This may be expected because we mix values from the penultimate event with older events. The weak second mode centered at about +70 cm may reflect an event before the penultimate earthquake.

Because we multiplied the 1987 slip distribution strictly, minor variations in 1987 slip were amplified in the test for the residuals. This may have had the effect of scattering the residual plot to some degree. Alternatively, it may reflect real variability in slip per event at a given point along the fault.

The data are too sparse to conclusively test the characteristic earthquake hypothesis for any slip events earlier than the penultimate event. The suggestion of a prepenultimate event seems strong from the mode of residuals near +70 cm (Fig. 15). When the appropriate test (total slip − 1987 slip × 3) for this event was made, however, the apparent concentration broadened, so we are not confident that a characteristic prepenultimate earthquake is represented in the data.

Visual inspection of the distribution of the residuals should be sufficient to support the conclusion that one pre-1987 event did produce slip along the Superstition Hills fault that was very comparable to the slip in November 1987 and its related afterslip through April 1988.

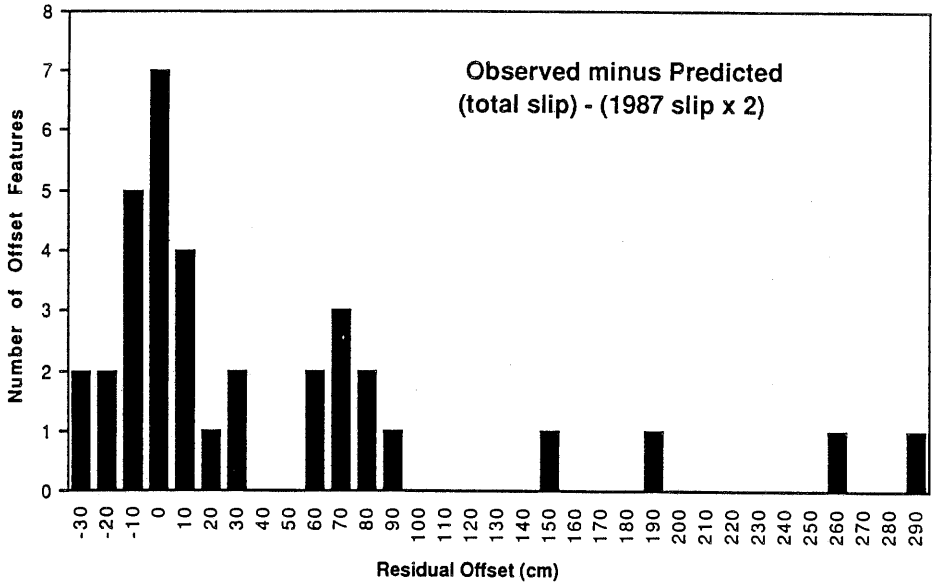

FIG. 15. Distributions of residuals between observed and predicted values for multiple offsets along the Superstition Hills fault. When predicted values for one pre-1987 event were subtracted from the total offsets, this plot of residuals resulted. It shows a strong concentration about the zero value, which would be expected if the model is correct. Also, a weak secondary mode is seen at about +70 cm, possibly indicating a prepenultimate event.

Consideration of the Imler Road Results

Although this analysis indicates a close correlation between co-seismic and afterslip of the 1987 event to total slip in the previous event, this does not completely resolve our test of whether the characteristic earthquake model is appropriate for this fault. Because afterslip continues to accumulate along most of the length of the Superstition Hills fault trace as of mid-1988, its long-term effects must be considered.

Hudnut and Sieh (1989) have established at their Imler Road excavations that total postlake slip before the 1987 event was about 60 cm. Total slip from the 1987 rupture plus afterslip, measured at about 50 cm in March 1988, will not reach 60 cm until about March 1989. Nonetheless, their extrapolation of aftercreep data 150 to 300 yrs into the future (one estimated recurrence interval) predicts that total slip from the 1987 rupture will reach about 120 cm at Imler Road. The implication of their result also applies to our test of whether the characteristic earthquake model is applicable to the Superstition Hills fault. If we assume that afterslip along the entire trace of the Superstition Hills fault will continue to accumulate in the future, then the close similarity we observe between 1987 slip (through April 1988) and the penultimate event slip may be fortuitous. Williams and Magistrale (1989) show abundant afterslip data suggesting that nearly the entire length of the fault can be expected to continue to creep, and that eventual slip accumulation along the fault may significantly increase the values obtained in April 1988, with maximum slip values along the central reach of the fault increasing to about 120 cm. Therefore, the same argument made by Hudnut and Sieh for their data at Imler Road likewise applies to our analysis, in that eventual total slip from the 1987 event may be significantly larger than that of the penultimate event.

The fault may continue to creep at our locations showing the multiple offsets. Although a strong correspondence exists between the April 1988 values and the

penultimate event slip values, this will be changed. The expected outcome would be that slip distribution along the entire fault caused by the 1987 event would be greater than the amounts caused at the same sites by the penultimate event. A rigorous evaluation of this effect will require consideration of afterslip data at locations documented in other studies in this issue. On our plot of residuals, however, a simple shift towards the left, and perhaps changes in the distributions of residuals, would be the anticipated changes.

If this occurs, the characteristic earthquake model is not applicable to this fault in a strict sense for its most recent behavior. It would support the hypothesis by Hudnut and Sieh (1989) that the 1987 event was larger than the previous event. Alternatively, Boatwright *et al.* (1989) used a damped power law for projection of afterslip into the future which suggests that most afterslip (greater than 95 per cent) will have occurred within the first few years after the earthquake. Their projected values are considerably less (<1 m) and suggest that the slip we measured from the 1987 earthquake (through April 1988) is not significantly different than the projected total slip for this event.

Our data provide constraints that Hudnut and Sieh (1989) could not address regarding variation in slip along strike and length of the penultimate rupture. We have shown that slip distribution as of April 1988 was similar to that in the penultimate event along the central portion of the fault. The length of the pre-1987 rupture is not well constrained by this study, but it is evident that at least the reach of the fault from about 6 to 16 km from the northwest end has experienced slip before the 1987 earthquake.

Triggered Slip

The historical occurrence of triggered slip on the Superstition Hills fault (Allen *et al.*, 1972; Fuis, 1982; Sharp *et al.*, 1986) was not included in our analysis. The total amount of triggered slip of nearly 4 cm (Sharp *et al.*, 1986) since the 1968 Borrego Mountain earthquake could easily be absorbed in the errors of our offset measurements and, therefore, would not alter our interpretations. If the features we observed were offset by a large accumulation of creep, we could not necessarily distinguish this from co-seismic offset. Hudnut and Sieh (1989) have argued for seismic slip in the penultimate event. Our observations suggest slip before the penultimate event, but we cannot say what percentage of this slip was seismic.

CONCLUSIONS

Documentation of offset geomorphic features along the Superstition Hills fault have helped constrain the slip distribution of one rupture event that occurred before the 1987 earthquake. Older and larger offsets less clearly show evidence for several other prehistoric events.

Along reaches of the fault where we have data, it appears that the penultimate event had a slip distribution similar to the 1987 total slip distribution as measured through April 1988. If afterslip on the Superstition Hills fault is arrested in the near future, our data will support the application of the characteristic earthquake model to this fault. However, if slip continues to accrue for the next 150 to 300 yrs until the next earthquake, as suggested by some workers, then afterslip is expected to increase the 1987 total slip to approximately twice that of the penultimate event. If this occurs, then either characteristic earthquakes exhibit a large degree of variability near their maximum magnitudes, or the model is not applicable to the Superstition Hills fault.

Continued monitoring of the 1987 event's afterslip will determine if total slip from this earthquake will stabilize or continue to increase with time. This will enable more accurate estimates of the size of past earthquakes on the Superstition Hills fault as well as provide checks on this test of the characteristic earthquake model for this fault.

ACKNOWLEDGMENTS

We are grateful to R. Wallace for his initial enthusiasm to pursue this study of the offset features along this fault. We thank D. Valentine at SDSU for helping with the surveying, T. Hanks at the USGS for providing us with new air photos, and P. Williams at L-DGO/C.I.T. for his discussions on afterslip. We especially thank D. Schwartz for his thoughtful review of our manuscript, which led to improvements and clarification of the presentation. This project was partially supported by USGS Grant no. 14-08-0001-G1330.

REFERENCES

Allen, C. R., M. Wyss, J. N. Brune, A. Grantz, and R. E. Wallace (1972). Displacements of the Imperial, Superstition Hills, and San Andreas faults triggered by the Borrego Mountain earthquake, in *The Borrego Mountain earthquake of April 9, 1968, U.S. Geol. Surv. Profess. Paper 787*, 87–104.

Boatwright, J., K. E. Budding, and R. V. Sharp (1989). Inverting measurements of surface slip on the Superstition Hills fault, *Bull. Seism. Soc. Am.* **79**, 411–423.

Clark, M. M. (1972). Surface rupture along the Coyote Creek fault, in *The Borrego Mountain earthquake of April 9, 1969, U.S. Geol. Surv. Profess. Paper 787*, 55–86.

Fuis, G. (1982). Displacement on the Superstition Hills fault triggered by the 1979 Imperial Valley earthquake, in *The Imperial Valley earthquake of October 15, 1979, U.S. Geol. Surv. Profess. Paper 1254*, 145–154.

Hudnut, K., L. Seeber, T. Rockwell, J. Goodmacher, R. Klinger, S. Lindvall, and R. McElwain (1989). Surface ruptures on cross-faults in the 24 November 1987 Superstition Hills, California, earthquake sequence, *Bull. Seism. Soc. Am.* **79**, 282–296.

Hudnut, K. and K. Sieh (1989). Behavior of the Superstition Hills fault during the past 330 years, *Bull. Seism. Soc. Am.* **79**, 304–329.

Kahle, J. E., C. J. Wills, E. W. Hart, J. A. Treiman, R. B. Greenwood, and R. S. Kaumeyer (1988). Preliminary report: surface rupture—Superstition Hills earthquakes of November 23 and 24, 1987, *California Geology* **41**, 75–84.

Rockwell, T. K. and C. T. Pinault (1986). Holocene slip events of the southern Elsinore fault, Coyote Mountains, southern California, in *Neotectonics and Faulting in Southern California: Geological Society of American Guidebook for the Cord. Sect. Meeting in Los Angeles*, 193–196.

Schwartz, D. P. and K. J. Coppersmith (1984). Fault behavior and characteristic earthquakes: examples from the Wasatch and San Andreas fault zones, *J. Geophys. Res.* **89**, 5681–5698.

Sharp, R. V., K. E. Budding, J. Boatwright, M. J. Ader, M. G. Ader, M. G. Bonilla, M. M. Clark, T. E. Fumal, K. K. Harms, J. J. Lienkaemper, D. M. Horton, B. J. O'Neill, C. L. Ostergren, D. J. Ponti, M. J. Rymer, J. L. Saxton, and J. D. Sims (1989). Surface Faulting along the Superstition Hills fault zone and nearby faults associated with the earthquakes of 24 November 1987, *Bull. Seism. Soc. Am.* **79**, 252–281.

Sharp, R. V., M. Rymer, and J. Lienkamper (1986). Surface displacement on the Imperial and Superstition Hills faults triggered by the Westmoreland, California earthquake of 26 April 1981, *Bull. Seism. Soc. Am.* **76**, 949–965.

Sieh, K. E. (1978). Slip along the San Andreas fault associated with the great 1857 earthquake, *Bull. Seism. Soc. Am.* **68**, 1421–1448.

Sieh K. E. (1987). Earthquake geology of the San Andreas and other faults in California: Annual Technical Report, Grant No. 14-08-0001-G1098, submitted to U.S. Geol. Surv., 12 November 1987.

Sieh, K. E. and R. Jahns (1984). Holocene activity of the San Andreas fault at Wallace Creek, California, *Geol. Soc. Am. Bull.* **95**, 883–896.

Sykes, L. R. and S. P. Nishenko (1984). Probabilities of occurrence of large plate rupturing earthquakes for the San Andreas, San Jacinto, and Imperial faults, California, *J. Geophys. Res.* **89**, 5905–5927.

Wallace, R. E. (1968). Notes of stream channels offset by the San Andreas fault, southern Coast Ranges, California, in *Proceedings of Conference on Geologic Problems of San Andreas Fault System*, Stanford University Publications, Geological Sciences, University Series 11, 6–21.

Wallace, R. E. (1970). Earthquake recurrence intervals on the San Andreas fault, *Geol. Soc. Am. Bull.* **81**, 2875–2890.

Waters, M. R. (1983). Late Holocene lacustrine chronology and archeology of ancient Lake Cahuilla, California, *Quat. Res.* **19**, 373–387.

Wesnousky, S. G. (1986). Earthquakes, Quaternary faults, and seismic hazards, *J. Geophys. Res.* **91**, 12587–12631.

Williams, P. L. and H. W. Magistrale (1989). Slip along the Superstition Hills fault associated with the 24 November 1987 Superstition Hills, California, earthquake, *Bull. Seism. Soc. Am.* **79**, 390–410.

Zhang, W., D. Jiao, P. Zhang, P. Molnar, B. C. Burchfiel, Q. Deng, Y. Wang, and F. Song (1987). Displacement along the Haiyuan fault associated with the great 1920 Haiyuan, China, earthquake, *Bull. Seism. Soc. Am.* **77**, 117–131.

DEPARTMENT OF GEOLOGICAL SCIENCES
SAN DIEGO STATE UNIVERSITY
SAN DIEGO, CALIFORNIA 92182
(S.C.L., T.K.R.)

LAMONT-DOHERTY GEOLOGICAL OBSERVATORY
PALISADES, NEW YORK 10964
AND DEPARTMENT OF GEOLOGICAL SCIENCES
COLUMBIA UNIVERSITY
NEW YORK, NEW YORK 10027
(K.W.H.)

Manuscript received 4 August 1988

Bulletin of the Seismological Society of America, Vol. 79, No. 2, pp. 297–303, April 1989

FLEXURAL-SLIP FOLDING ALONG THE EASTERN ELMORE RANCH FAULT IN THE SUPERSTITION HILLS EARTHQUAKE SEQUENCE OF NOVEMBER 1987

RALPH E. KLINGER AND THOMAS K. ROCKWELL

ABSTRACT

Co-seismic flexural-slip folding of a small anticline along the Eastern Elmore Ranch fault associated with the Superstition Hills earthquake sequence demonstrates that variations in left-lateral slip can be explained locally by folding. Surface rupture on the eastern branch of the Elmore Ranch fault was greatest to the northeast of the fold but decreased to zero across the southern limb. A kilometer long surface-slip gap exists just southwest of the fold, being bounded on the northeast with 75 mm of slip and to the southwest with about 60 mm of slip. Lateral slip continues southwesterly to the faults intersection with the Superstition Hills fault.

The gentle-to-openly folded, moderately plunging, upright asymmetric anticline experienced left-lateral slip on the northern limb and right-oblique slip on the southern limb with maximum documented lateral slip along bedding planes of 10 mm. Slip values were greatest on the limbs and decreased to zero at the fold hinge, which is consistent with the flexural-slip folding process. Secondary left-lateral faults ruptured both limbs of the anticline and bedding plane slip was not observed hingeward of these faults.

These data suggest that left-lateral strain associated with seismogenic fault rupture was continuous in the subsurface but was accommodated locally by folding at the surface.

INTRODUCTION

Surface slip on several left-lateral, northeast-trending faults that broke during the Superstition Hills earthquake sequence of 23 and 24 November 1987 (Fig. 1) displayed significant variations in slip magnitude along fault strike (Hudnut *et al.*, 1989). Some variation would be expected where the surface trace of a fault steps or bends and slip is distributed between several strands (Segall and Pollard, 1980; Sibson, 1986). Part of the variation seen along the Eastern Elmore Ranch fault can be explained by co-seismic flexural-slip folding at the surface (Fig. 2).

The flexural-slip process is commonly associated with parallel folds in well-stratified sedimentary rock of contrasting lithologies that are separated by distinct bedding surfaces (Curie *et al.*, 1962; Ghosh, 1968; Chapple and Spang, 1974). Flexural-slip folding produces simple shear between these layers with displacements parallel to the bedding (Ramsay and Huber, 1987) (Fig. 3).

The strata in the Superstition Hills are lacustrine silt and clay beds interstratified with sand and gravel units of the Pleistocene Brawley Formation (Dibblee, 1984). Specifically, the stratigraphy in the study area is comprised dominately of poorly endurated, lacustrine silty sand and claystone interbedded with thin, well-endurated sandstone.

During the mapping of the surface ruptures associated with the Superstition Hills sequence (presented in Hudnut *et al.*, 1989), it became clear that the amount of slip varied widely along strike of individual faults, particularly in the central portion of the Eastern Elmore Ranch fault. A kilometer long surficial-slip gap occurs just southwest of a major anticline (Figs. 1 and 4). Minor ruptures occurred and were

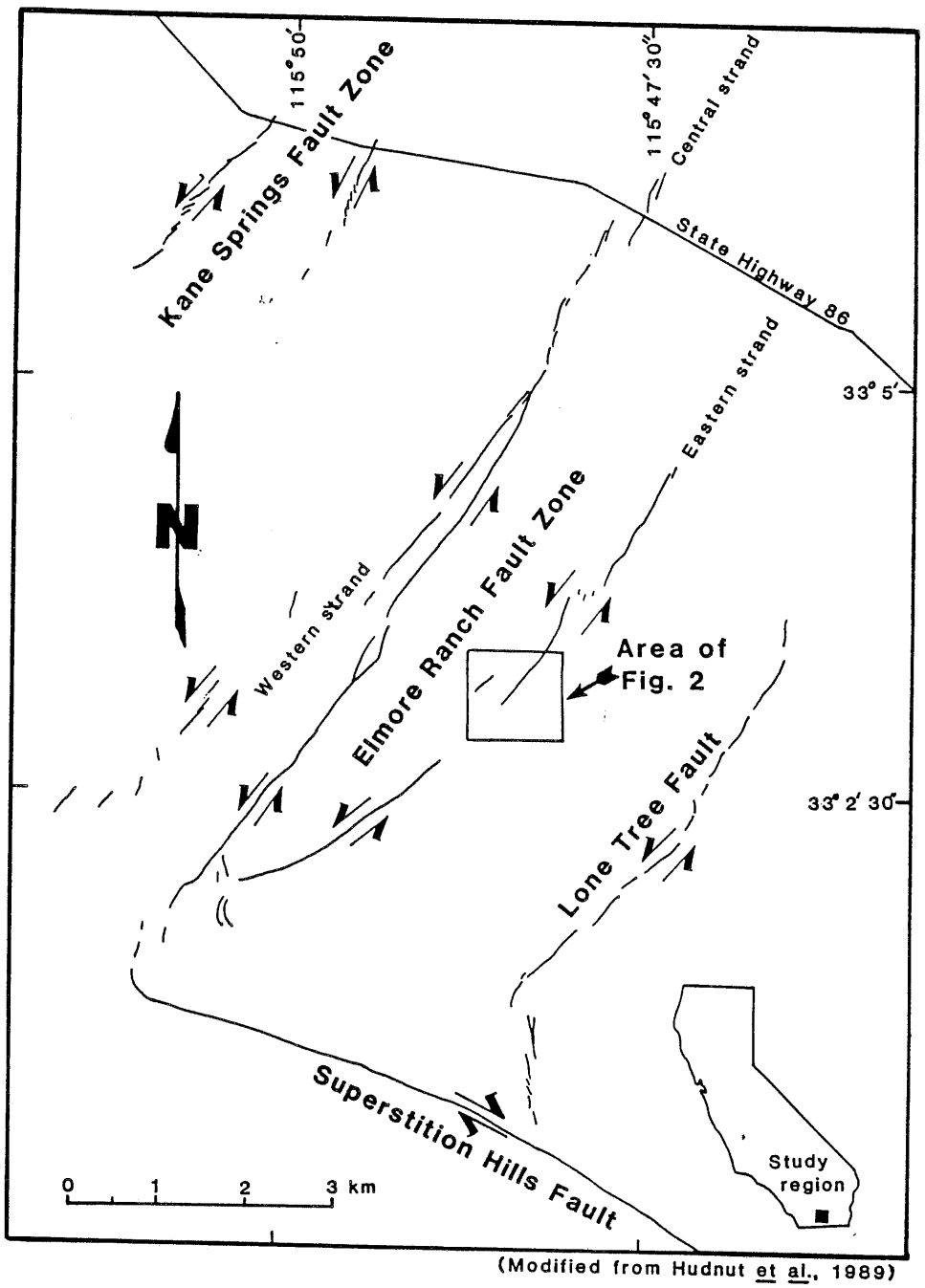

FIG. 1. Location map of the left-lateral surface ruptures associated with the 23 and 24 November 1987 Superstition Hills earthquake sequence. The box indicates the location of Willow Wash anticline and the area of detailed mapping in Figure 2 along the eastern strand of the Elmore Ranch fault. Notice the surficial-slip gap just southwest of Willow Wash anticline.

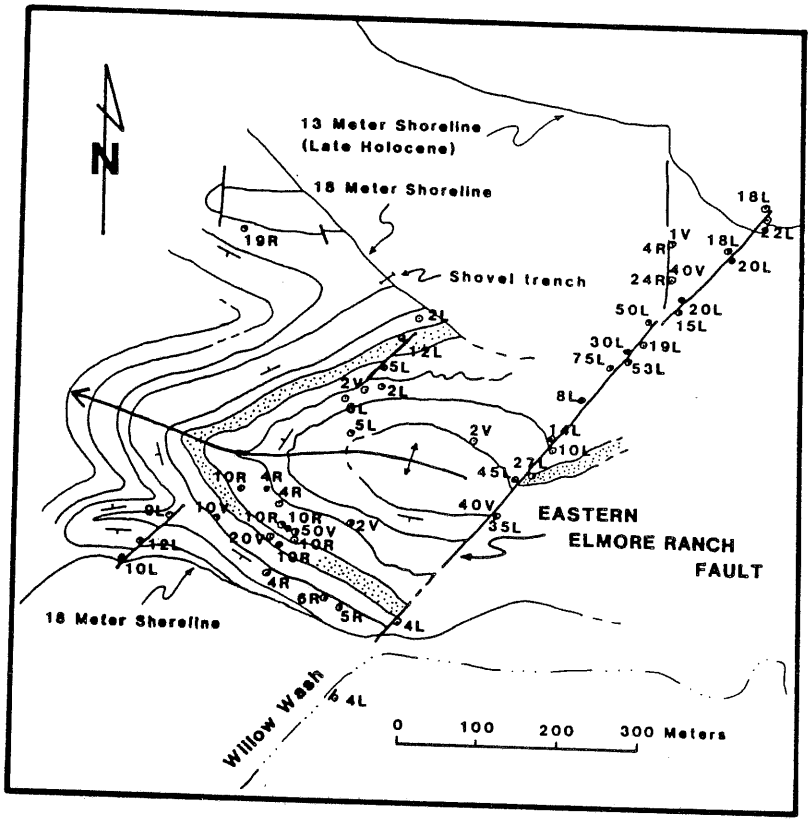

FIG. 2. Map of the Willow Wash anticline and the Eastern Elmore Ranch fault. Form lines represent contacts between distinct lithologic units, heavy lines are faults that ruptured, and dots are slip measurement locations. All values are in millimeters with V, R, and L representing vertical, right-lateral, and left-lateral separation, respectively. The stippled unit is a distinct light-colored, gravelly, very coarse sand bed that is highly visible both on aerial photographs and the ground.

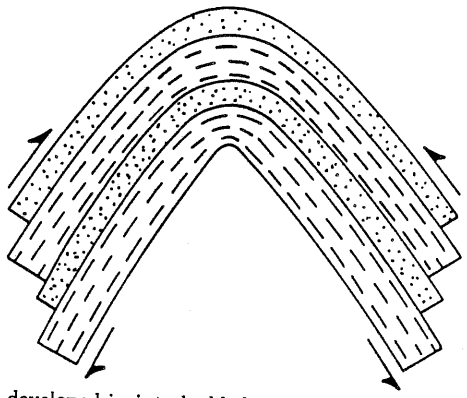

FIG. 3. Flexural-slip fold developed in interbedded competent (stippled) and incompetent (dashed) strata. Arrows indicate the direction and relative sense of bedding-parallel slip.

recognized along the bedding planes of many folds in the northeastern portion of the Superstition Hills. We present data from one fold, the Willow Wash anticline, that is truncated by the eastern branch of the Elmore Ranch fault at the northeast end of the surface-slip gap (Figs. 1 and 2). This anticline accommodated significant bedding-plane slip during the earthquake sequence.

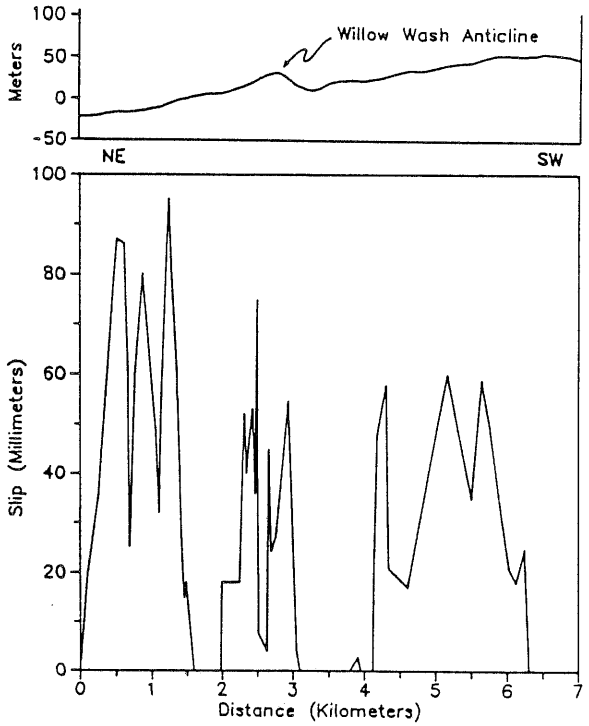

FIG. 4. Slip distribution diagram for the eastern strand of the Elmore Ranch fault. Distance is along strike, measured from the northeast end of the mapped rupture toward the intersection with the Superstition Hills fault. The topographic profile at the top is parallel to strike of the eastern branch of the Elmore Ranch fault. Note the absence of observable surface slip just southwest of the Willow Wash anticline.

WILLOW WASH ANTICLINE

The Willow Wash anticline, named herein for the major drainage just southeast of the fold, is a prominent feature on both aerial photographs and topographic maps. Using form lines mapped on aerial photographs that represent contacts between distinct lithologic units, the fold can be classified as a parallel fold (Fig. 2). The northern limb of the fold trends about N65°E, subparallel to the left-lateral Elmore Ranch fault, which trends N40°E at this location. The southern limb trends about N47°W, roughly perpendicular to the trend of the fault. An interlimb angle of 129° suggests that the anticline has been gently-to-openly folded (Fig. 5). The axial surface is upright with the hinge of the anticline trending N77°W and plunging moderately at 19° to the west (Figs. 2 and 5).

Willow Wash anticline was mapped in detail after the earthquake sequence when numerous small bedding-plane slips were noticed on both flanks of the fold with significantly different magnitudes and senses of slip occurring between the two limbs (Fig. 2). Of particular interest was the fact that the surface slip along the Elmore Ranch fault, which apparently nucleated the first shock of this double earthquake sequence, died out along the southern flank of the fold, whereas nearly 100 mm of slip to the northeast and 60 mm of slip to the southwest was apparent along strike of the fault (Figs. 1 and 4). Values of left-lateral slip on the Eastern Elmore Ranch fault were as high as 75 mm at the northern limb of Willow Wash anticline.

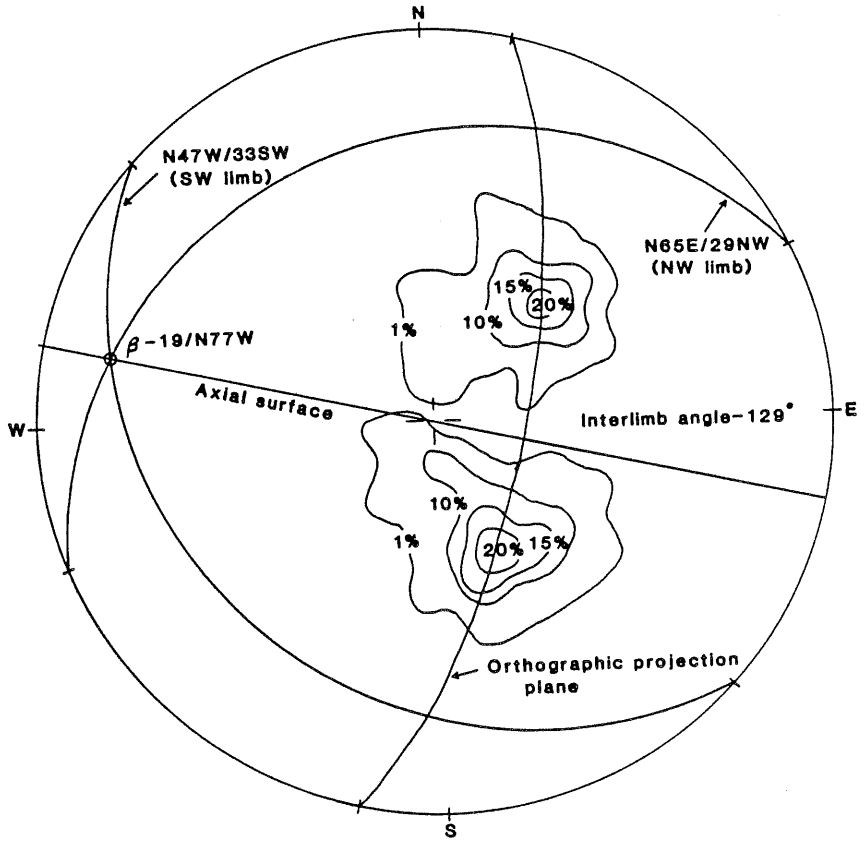

FIG. 5. Contoured π diagram for projections of poles to bedding, the statistical fold axis, orthographic projection plane, and great circles representing the mean attitude of the limbs of the Willow Wash anticline. Contours are expressed as the percentage of total points per 1 per cent area of the lower hemisphere equal area net. Mean attitudes were determined by visually fitting data to the best-fit great circle.

Flexural-slip folding should produce bedding-plane slip with an opposite sense of slip between the limbs of the fold (Ramsay and Huber, 1987). The northern limb of Willow Wash anticline experienced nearly pure left-lateral slip of up to 10 mm on individual bedding surfaces but only 2 mm or less of dip slip. The southern limb displayed a component of right-lateral slip with maximum values of about 10 mm, but dip slip was dominant and vertical movement ranged up to 50 mm. It should be noted these slip data were collected only where the magnitude and sense of movement could be determined by distinctly offset rills and disrupted surface crust.

Bedding-plane slip occurred dominately in the upper portion of the folded section, away from the core of the anticline. Slip was particularly visible at the contact between relatively more competent, well-endurated, $CaCO_3$-cemented, flaggy sandstone units and less competent lacustrine silty sand and claystone strata. Additionally, no slip was observed in or near the hinge region of the anticline (Fig. 2). These data are consistent with folding by the flexural-slip process.

Minor left-lateral faults parallel to the northeast-trending Eastern Elmore Ranch fault ruptured both limbs, but none of these cut through the core of the anticline (Fig. 2). No bedding-plane slip was observed hingeward from these minor faults. Slip along these minor faults experienced sinistral slip, with values ranging from 9

to 12 mm, that died out coincident with the 18 m shoreline. It is unclear if they are associated with the folding process or represent the end of a westerly strand of the Eastern Elmore Ranch fault in a transpressive step. The sense of slip and a lack of en-echelon folds to the southwest would suggest the latter. Evidence for a fault and a step southwest of the anticline was not observed, but may be obscured by recent sedimentation.

Discussion and Conclusions

The close spatial association between the cessation of surface slip on the eastern strand of the Elmore Ranch fault and the Willow Wash anticline, which clearly exhibited evidence of co-seismic folding, suggests that surface slip was locally accommodated by folding (Fig. 2). The geometry of the fold relative to the Eastern Elmore Ranch fault and the large dip-slip values on the southern flank of the fold are consistent with the flexural-slip process and a model where the surface sediments buckle at the end of a propagating rupture (Harland, 1971; Wilcox et al., 1973). The 1 km gap in the surface rupture on the Eastern Elmore Ranch fault does not mean that surface deformation did not occur. On the contrary, these data suggest through this area it was expressed at the surface by folding (Fig. 4). In turn, this suggests that the rupture, as it propagated through this region in the subsurface, probably sustained slip at depth of at least 60 to 75 mm.

If this relationship of slip at depth to deformation at the surface by folding is generally valid for other areas of low slip on the northeast-trending faults that broke in the November earthquake sequence, then it is probably valid to smooth out the slip distribution along individual faults. This is supported by the recognition that slip variation can be distributed across several strands in dilational steps or jogs. Likewise, slip deficits in the vicinity of transpressional steps or jogs can be explained by surface deformation such as flexural-slip folding. This would affect estimates of seismic moment and rupture length that are based on mapped surface-slip data. Moment estimates might increase by a factor of 2 or more if the slip distribution along a fault is more accurately represented by the local maximum values rather than inclusion of low slip values that result from co-seismic folding or dilation associated with steps and bends of the surface trace.

References

Chapple, W. M. and Spang, J. H. (1974). Significance of layer-parallel slip during folding of layered sedimentary rocks, *Geol. Soc. Am. Bull.* **75**, 1523–1534.

Currie, J. B., Patnode, H. W., and Trump, R. P. (1962). Development of folds in sedimentary rocks, *Geol. Soc. Am. Bull.* **73**, 655–674.

Dibblee, T. W., Jr. (1984). Stratigraphy and tectonics of the San Filipe Hills, Borrego Badlands, Superstition Hills and vicinity, in *The Imperial Basin—Tectonics, Sedimentation and Thermal Aspects*, C. A. Rigsby, Editor, Pacific Section, SEPM, 1–13.

Ghosh, S. K. (1968). Experiments of buckling of multilayers which permit interlayer gliding, Tectonophysics 6, 207–249.

Harland, W. B. (1971) Tectonic transpression in Caledonian Spitsbergen, Geological Magazine 108, 1, 27–42.

Hudnut, K., L. Seeber, T. Rockwell, J. Goodmacher, R. Klinger, S. Lindvall, and R. McElwain (1989). Surface ruptures on cross-faults in the 24 November 1987 Superstition Hills, California, earthquake sequence, *Bull. Seism. Soc. Am.* **79**, 282–296.

Ramsay, J. G. and M. I. Huber (1987). *The Techniques of Modern Structural Geology, Vol. 2, Folds and Fractures*, Academic Press, New York, 391 p.

Segall, P. and D. D. Pollard (1980). Mechanics of discontinuous faults, *J. Geophys. Res.* **85**, 4337–4350.

Sibson, R. H. (1986). Rupture interaction with fault jogs, in *Earthquake Source Mechanics*, American Geophysical Union Monograph **37**, Maurice Ewing 6, 157–167.

Wilcox, R. E., T. P. Harding, and D. R. Seely (1973). Basic wrench tectonics, *The American Association of Petroleum Geologists Bulletin* **57**, 1, 74–96.

DEPARTMENT OF GEOLOGICAL SCIENCES
SAN DIEGO STATE UNIVERSITY
SAN DIEGO, CALIFORNIA 92182

Manuscript received 16 September 1988

Bulletin of the Seismological Society of America, Vol. 79, No. 2, pp. 282–296, April 1989

SURFACE RUPTURES ON CROSS-FAULTS IN THE 24 NOVEMBER 1987 SUPERSTITION HILLS, CALIFORNIA, EARTHQUAKE SEQUENCE

BY K. HUDNUT, L. SEEBER, T. ROCKWELL, J. GOODMACHER, R. KLINGER, S. LINDVALL, AND R. MCELWAIN

ABSTRACT

Left-lateral slip occurred on individual surface breaks along northeast-trending faults associated with the 24 November 1987 earthquake sequence in the Superstition Hills, Imperial Valley, California. This sequence included the M_s = 6.2 event on a left-lateral, northeast-trending "cross-fault" between the Superstition Hills fault (SHF) and Brawley seismic zone, which was spatially associated with the left-lateral surface breaks. Six distinct subparallel cross-faults broke at the surface, with rupture lengths ranging from about $1\frac{1}{2}$ to 10 km and maximum displacements ranging from 30 to 130 mm. About half a day after the M_s = 6.2 event, an M_s = 6.6 earthquake nucleated near the intersection of the cross-faults with the SHF, and rupture propagated southeast along the SHF. Whereas right-lateral slip on the SHF occurred dominantly on a single trace in a narrow zone, the cross-fault surface slip was distributed over several stands across a 10-km-wide zone. Also, whereas afterslip accounted for a large proportion of total slip on the SHF, there is no evidence for afterslip on the cross-faults. We present documentation of these surface ruptures. A simple mechanical model of faulting illustrates how the foreshock sequence may have triggered the main rupture. Displacement on other cross-faults could trigger an event on the southern San Andreas fault by a similar mechanism in the future.

INTRODUCTION

Faults that trend northeast between bounding northwest-trending faults with right-lateral slip are important tectonic elements of the Salton trough. It has recently been found that these faults, here termed "cross-faults," are dominantly strike-slip faults with left-lateral motion. This implies that the present kinematic role of these faults is different than that proposed by studies that have considered these normal faults. Seismic ruptures of these faults also can be followed by larger ruptures on the main bounding faults, as seen in the Superstition Hills sequence. This sequence provided the first example on these cross-faults of surface ruptures; we document these with mapping and data analysis.

The Imperial Valley historically has been one of the most seismically active regions in California. Located near the southern termini of the San Andreas fault and San Jacinto fault zones, it is a region of tectonic transition from the Gulf of California "ocean rifting" regime to the southern California "continental transform" regime. The Brawley seismic zone, between the San Andreas fault and Imperial fault, is generally considered the northernmost ridge segment of the ridge/transform system in the Gulf of California (Lomnitz *et al.*, 1970). Detailed studies (Johnson and Hutton, 1982; Fuis *et al.*, 1984) show a complex structure, however, and the mechanism by which spreading is taking place in the Salton trough remains controversial.

Within this region, some of the prominent and seismically active faults trend northeast, roughly perpendicular to the strike of the main bounding faults (Fig. 1). These cross-faults are oriented normal to the inferred spreading direction, and were thought in some cases to be normal faults (Fuis *et al.*, 1984). A large aftershock of

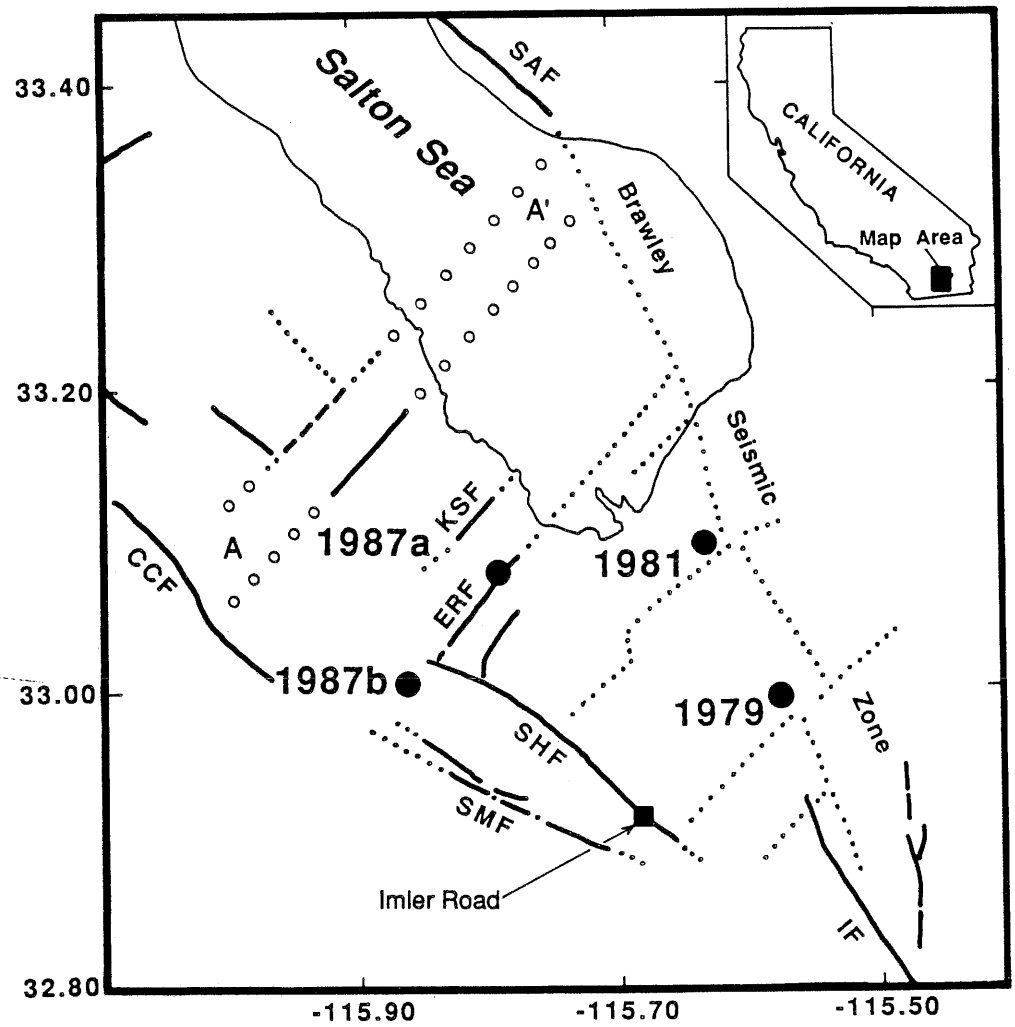

FIG. 1. Major known faults, faults inferred from seismicity (dotted lines), incompletely mapped (dashed lines), and inferred (open circles) in the region between the southern termini of the San Andreas fault and San Jacinto fault zone, including the Brawley seismic zone. Fault names are abbreviated as follows: SAF, San Andreas fault; IF, Imperial fault; CCF, Coyote Creek fault; KSF, Kane Spring fault; and ERF, Elmore Ranch fault. Epicenters related to the cross-fault rupturing 1979 aftershock and 1981 Westmorland event, and the two large earthquakes that occurred in November 1987 are shown. Aftershocks show the 1987 rupture of the ERF extended from the SHF to the Brawley seismic zone. Note the zone of cross-faults northwest of the Superstition Hills, labelled A-A′, that we name the Extra fault zone. Inset map shows the location of this study area in California.

the 1979 Imperial Valley earthquake (Johnson and Hutton, 1982), and the main shock of the 1981 Westmorland earthquake (Nicholson *et al.*, 1986) instead showed focal mechanisms indicating dominantly left-lateral slip. Seismological study of cross-fault events in the November 1987 sequence again showed left-lateral slip. Surface rupture on cross-faults in that sequence yields the first unambiguous geological evidence that the predominant present-day movement on these cross-faults is left-lateral strike-slip. Basement morphology (Fuis *et al.*, 1984) suggests dip-slip motion may have dominated in the past. The present-day kinematic role of the cross-faults remains unresolved.

Seismicity

The first large event, M_s = 6.2, occurred at 0154 on 24 November 1987 (GMT) and was co-located with several foreshocks of its own about 10 km northeast of the Superstition Hills fault (Fig. 2). Epicenters during the 10 hr following the Elmore Ranch earthquake (M_s = 6.2) showed a northeast trend extending from the Superstition Hills fault to the Brawley seismic zone (L. Jones and D. Given, personal comm., 1987). Early epicentral locations from the CIT/USGS network guided our efforts during the surface rupture mapping. Subsequent relocations of these earthquakes confirmed that the rupture was on a northeast-trending fault zone (Magistrale *et al.*, 1989). Aftershock patterns indicate that this event probably propagated bilaterally to the northeast, to the Brawley seismic zone, and to the southwest, toward its zone of intersection with the northwestern end of the Superstition Hills fault surface rupture.

At 1315 on 24 November the main shock of the sequence (M_s = 6.6) occurred. Within location errors, this event was located close to the northwestern terminus of the SHF, near its intersection with the Elmore Ranch fault surface rupture zone. Aftershock locations of this event formed a northwest-southeast trending zone, roughly paralleling the Superstition Hills fault, but several kilometers southwest of the surface trace of the fault, and concentrated near the intersection of the cross-faults with the SHF.

Surface-Rupture Chronology

At 1030 (GMT) on 24 November no new surface rupture was observed on the Superstition Hills fault at Imler Road (Fig. 1) following the Elmore Ranch earthquake, but rupture was observed on the SHF half an hour following the main event (Kahle *et al.*, 1988). Unfortunately, no northeast-trending surface ruptures were observed until after the main shock had already occurred. Thus, while the temporal correlation between the main shock on the SHF and its related surface rupture is strong, such a correlation for the Elmore Ranch event is uncertain.

Significant afterslip on the SHF was observed shortly after the main earthquake; afterslip is continuing (at much slower than initial rates) as of October 1988. Slip on the main fault surface ruptures are approaching 90 cm, including afterslip, along some parts of the fault (Sharp *et al.*, 1989; Williams and Magistrale, 1989). We found no evidence for afterslip on any of the cross-faults. Small amounts of surface slip, possibly triggered, were observed on parts of both the Imperial fault (Sharp, 1989; McGill *et al.*, 1989) and the Coyote Creek fault (Hudnut and Clark, 1989).

The set of northeast-trending, left-lateral fault breaks (Fig. 2) nearly parallel the trend of the foreshock sequence epicenters (Magistrale *et al.*, 1989). The seismic moment of the largest foreshock is in the size range for which surface ruptures usually occur in California. There were no field observations on these faults between the times of the foreshock sequence and main shock. Despite this caveat, we associate the cross-fault surface ruptures with the foreshock sequence.

METHODS

Displacements were measured across features such as the edges of fractures, tire tracks, and linear features on the soil surface that could be matched reliably on either side of the fault. Care was taken that the along-strike component of strike-slip was measured. In some instances, dip slip and extension across the cracks were

also measured. Most measurements were across single fault strands, though some were made over multiple strands at a single site. Most offset determinations represent the largest offset of several measurements at one locality, though usually the slip was consistent at each locality. All of the fault breaks we mapped were examined on foot for their entire lengths. Deviation from even sampling along the faults usually was because of ground shattering, or otherwise nontectonic slumping that obscured the rupture trace. Many, but not all, offset features were documented with photographs. Aerial photographs were used as base maps for plotting surface faulting in the field, and final data transfer from the field photos to $7\frac{1}{2}$ min topographic quadrangles was done using a zoom transfer scope.

A WILD® TC-2000 surveying instrument was used to obtain accurate locations of the mapped faults and displacement measurement sites. The instrument was used for spot-checking mapping done soon after the earthquakes, and for station locations concurrent with field mapping later on. We field checked much of our mapping with the instrument. The instrument was most useful for correcting mapping discrepancies, and for removing the distortion inherent in airphoto-based mapping.

Our afterslip markers were spray-painted lines and tire tracks. We have especially monitored the Kane Spring fault and Elmore Ranch fault (Fig. 2), through October 1988. Beginning in March 1988, slip on the Elmore Ranch fault has been monitored with alinement arrays.

Cross-Fault Surface Ruptures

Description

All of the 1987 surface ruptures were on pre-existing faults displacing consolidated and deformed strata of the Pleistocene Brawley Formation. Moreover, in places these faults exhibit geomorphic expression of prior slip such as scarps, en-echelon folds (forming subtle topographic highs), and linear ridges or sags. The majority of surface ruptures were confined to faults that had been previously mapped along at least part of their lengths (Dibblee, 1984; unpublished maps by Sharp and Lienkaemper, and by Hudnut). Several of the previously mapped faults in this area did not show surface slip in this earthquake sequence, while some ruptures occurred on previously unmapped faults. Although their past slip orientations may have been different, the 1987 surface rupture shows these northeast-trending faults are all dominantly left-lateral faults.

Names used here (see Fig. 2) for each of the six fault strands that ruptured are, from southeast to northwest, the Lone Tree fault (after Lone Tree Wash), the Eastern, Central, and Western Elmore Ranch faults (after Elmore Desert Ranch), and the Eastern and main Kane Spring faults (after Kane Spring). Cracking and possibly minor slip was also noted on the Extra fault (after benchmark EXTRA; fault zone is labelled A-A′ in Fig. 1) to the northwest of the Kane Springs fault. The three strands of the Elmore Ranch fault were treated as a single fault zone because each of the strands either joins or branches from the central strand somewhere along the length of their ruptures (Fig. 2).

The cross-fault surface ruptures typically consisted of short en-echelon breaks that in places stepped to the left or right, producing small areas of extension or shortening. Some of the rupture segments, particularly those associated with larger amounts of surface slip on strands of the ERF zone did exhibit continuous breaks for tens to hundreds of meters long.

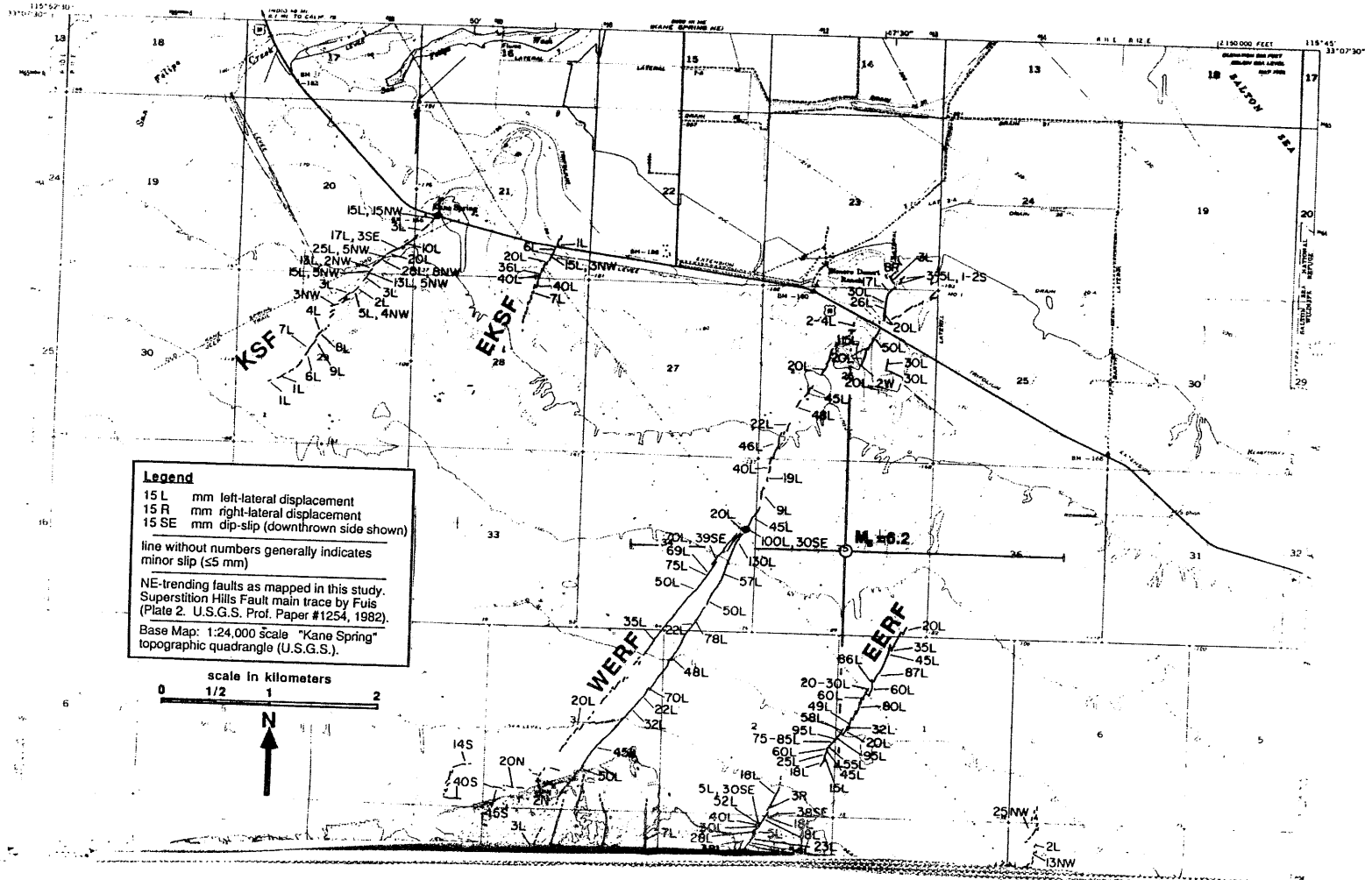
KSF
EKSF
WERF
EERF
M_s 6.2
I-25
Legend
15 L mm left-lateral displacement
15 R mm right-lateral displacement
15 SE mm dip-slip (downthrown side shown)
line without numbers generally indicates minor slip (≤5 mm)
NE-trending faults as mapped in this study. Superstition Hills Fault main trace by Fuis (Plate 2. U.S.G.S. Prof. Paper #1254, 1982).
Base Map: 1:24,000 scale "Kane Spring" topographic quadrangle (U.S.G.S.).
scale in kilometers
0 1/2 1 2
N

SURFACE RUPTURES ON CROSS-FAULTS

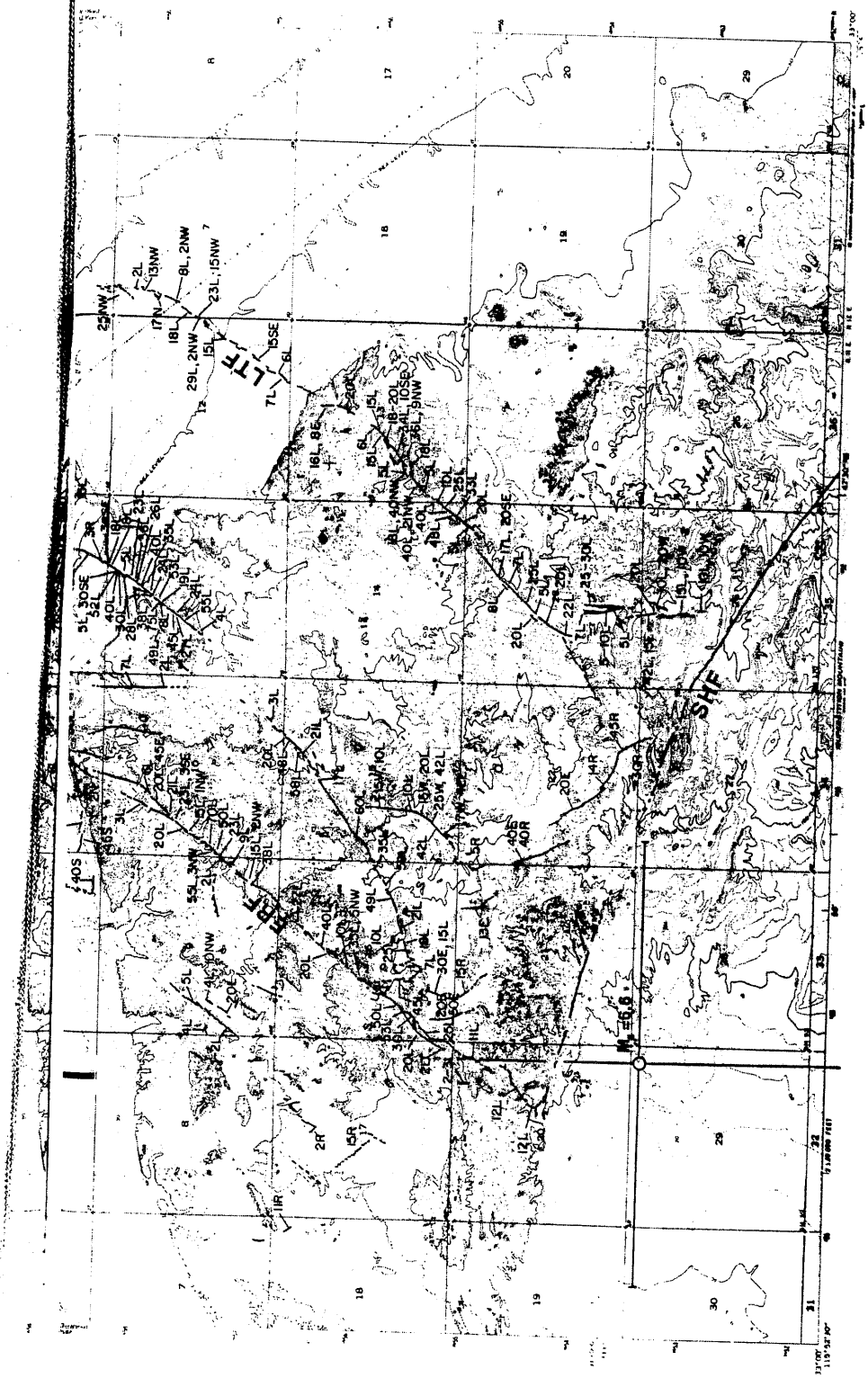

FIG. 2. Map of surface ruptures along cross-faults and surface slip data, also showing proposed names for the cross-faults. The names are: KSF, Kane Spring fault; EKSF, Eastern Kane Spring fault; WERF, Western Elmore Ranch fault; ERF, Elmore Ranch fault; EERF, Eastern Elmore Ranch fault; LTF, Lone Tree fault. Epicenters of the largest events in the November 24, 1987 Superstition Hills earthquake sequence are shown, with ±2 km error bars (our estimate of the absolute location error). Base map is the Kane Spring (7½ minute topographic) quadrangle. Minor ruptures occurred on the Harper's Well quadrangle to the west. A map of these breaks, full-scale copies of the Kane Spring quadrangle mapping, and a key map to station locations with accompanying data listings, are available from the authors by request. Filled circles on the Kane Spring fault at the highway, and Elmore Ranch fault at the power line road, are stations where no afterslip has yet been observed.

Figures 3a and 3b show that cumulative displacement over multiple strands of the Elmore Ranch fault zone was up to nearly 200 mm of left-lateral slip. The main strand had up to 130 mm, the western strand had a maximum of 75 mm, and the eastern strand had as much as 95 mm of left-lateral slip. The Lone Tree, Kane Springs, and Eastern Kane Springs faults had maximum left-lateral displacements at the surface of 48, 28, and 40 mm, respectively. Maximum surface displacements on the Elmore Ranch fault strands occurred a few kilometers southwest of the epicentral location for the Elmore Ranch earthquake, whereas slip maxima on the Kane Spring strands were within a kilometer of the epicenter as projected onto the distance axes in Figure 3.

Terminations of Cross-Fault Breaks

At their northeastern ends, surface breaks on the Kane Spring fault, Elmore Ranch fault, Eastern Elmore Ranch fault, and Lone Tree fault terminated at fault bends and/or step-overs associated with anticlines. At their southwestern ends, near their intersections with the Superstition Hills fault, surface breaks on both the Elmore Ranch fault zone and the Lone Tree fault splayed into multiple strands. Surface breaks on the Elmore Ranch fault followed a nearly straight course to within a short distance of its intersection with the Superstition Hills fault. Left-lateral slip decreased to a few millimeters within 100 m of the intersection. Some of the slip apparently was distributed on nearly north-south trending normal faults (in the eastern quadrant of the fault intersection); displacement was down on the east side, with up to 50 mm of dip slip. These normal faults are arcuate in map view, concave eastward, with multiple splays. A component of left-lateral slip occurred on the northeast-striking splays, and a component of right-lateral slip occurred on the southeast-striking splays. Splays of these dominantly normal faults merged into right-lateral faults paralleling the Superstition Hills fault.

In contrast, the main surface break on the Lone Tree fault did not maintain a straight trend toward its intersection with the Superstition Hills fault. At a distance of about one kilometer northeast of the intersection, the northeast trend of surface breaks on the Lone Tree fault changed into a nearly north-south trend. The point of change in trend of the surface trace roughly coincides with the north-dipping limb of a major anticline. A minor break, with cracking but no measurable offset, splayed from this point towards the west, along the limb of the fold. The main break continued towards the Superstition Hills fault, showing dominantly left-lateral slip, and terminated near a fault that parallels the Superstition Hills fault, but did not rupture in the 1987 sequence.

MOMENT CALCULATIONS

Most surface ruptures on the cross-faults showed highly variable slip along-strike (Fig. 3a). In other well-studied examples of nearby earthquakes, slip versus distance

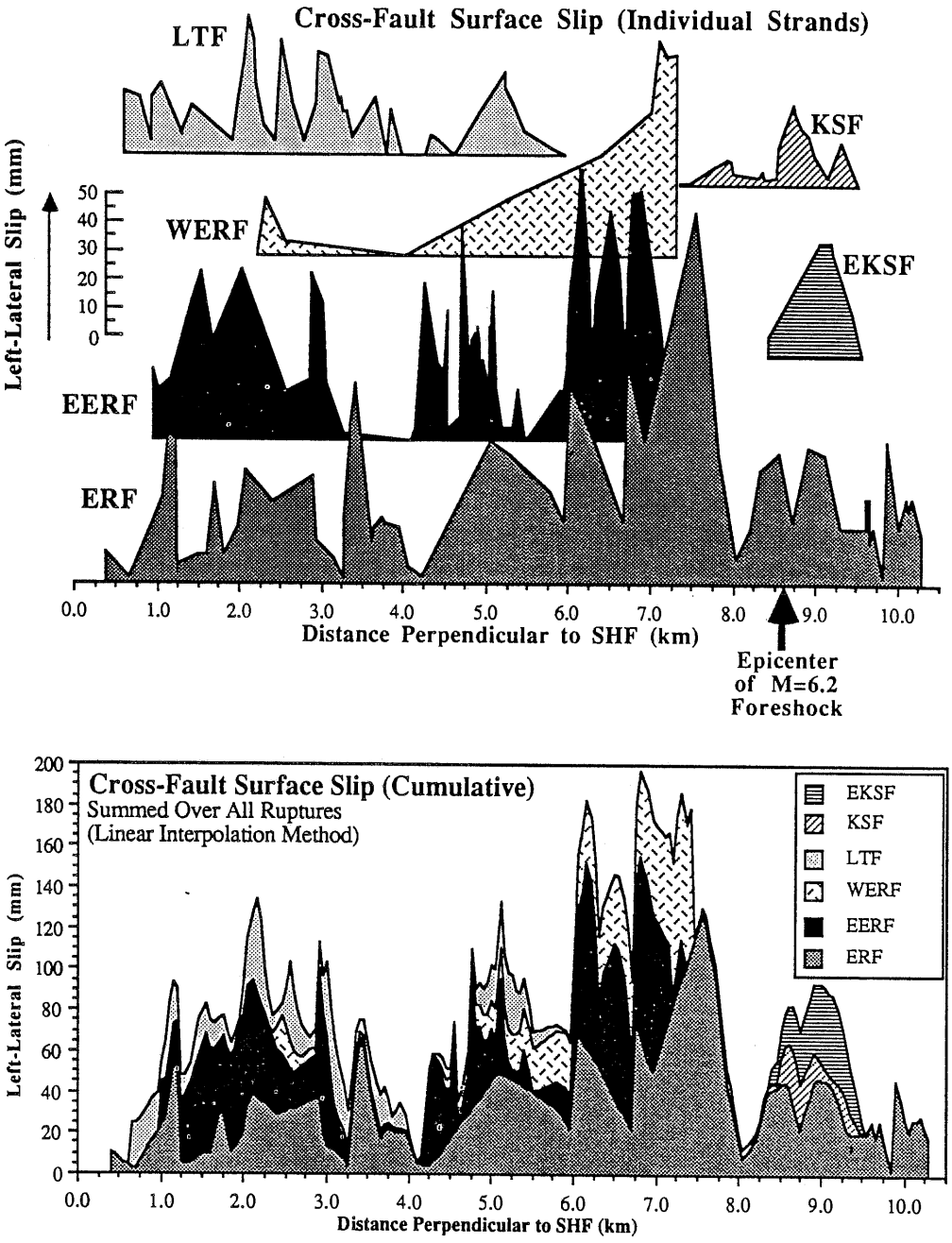

FIG. 3. a) Uninterpolated slip distribution curves (raw data) for each of the individual northeast-trending strands. b) Interpolated data (resampled at 50 m intervals), summed across all strands, i.e., total or cumulative slip distribution curves.

curves also appear jagged, as in the 1968 Borrego Mountain earthquake (Clark, 1972) and the 1979 Imperial Valley earthquake (Sharp *et al.*, 1982). We have calculated moment as directly as possible from the surface-slip data.

Raw surface rupture data (Fig. 3a) were first linearly interpolated, with a sampling interval of 0.01 km. Integration of the resulting series was computed using the

trapezoidal rule, to obtain the values in Table 1 (column $L \times x$) that were used in computing M_o for individual fault strands. The series were next decimated to a sampling interval of 0.05 km and then summed (Fig. 3b). Zero-phase low-pass filtering procedures were applied, but the smoothed curves (not shown) obscure details that we feel could be important, and were found to be less informative than Figure 3b. Complexity and splaying of the fault strands was not corrected for, so plots represent data from ruptures striking about N35 ± 10°E. Because of strike variations, some distortion (up to about 20 per cent of shown values) is present.

It is tempting to approach moment calculations based on surface slip by smoothing or averaging the surface-slip distribution curve, and claiming this more realistically represents slip at depth. Calculation of moment from distorted, smoothed, or simply averaged (over data sampled unevenly with distance) surface-rupture data does not accurately represent the field data and, depending on the methods used, may cause large errors. The method used here improves upon previous methods of calculating moment from surface-slip data on multiple parallel strands, but sparse data in places limits the accuracy of any technique one might use.

The total moment we calculated from the surface rupture data, 2.3×10^{24} dyne × cm (Table 1) is nearly an order of magnitude less than the moment obtained from teleseismic body waves for the largest foreshock ($M_s = 6.2$) of 1.8×10^{25} dyne × cm (Bent *et al.*, 1988). In our calculation, we assumed that μ (rigidity) = 3×10^{11} dynes/cm^2, and that rupture depth was 10 km, as constrained by the depth of most cross-fault seismicity (Magistrale *et al.*, 1989). Even if one were to assume 200 mm of left-lateral slip on a 10 km long break, this maximum estimate of moment from surface ruptures would be only 6 × 10 dyne × cm. There is also a discrepancy between rupture length determined by cross-fault seismicity of about 20 to 25 km, and that determined by surface rupture of about 10 km. These discrepancies may occur because rupture did not fully propagate to the surface.

Comparison to Other Earthquakes

These surface ruptures indicate differences in behavior between cross-faults and the main northwest-trending faults. Parallel faults spaced kilometers apart broke as a set in this sequence, with displacements on surface breaks distributed over a northeast-trending zone about 10 km wide and 10 km long. In contrast, ruptures on right-lateral faults such as the 1968 rupture of the Coyote Creek fault, the 1979 rupture of the Imperial fault, and the 24 November 1987 rupture of the SHF all occurred within narrower zones, usually of a kilometer or less wide, or even on a single strand.

In Table 1, we reduced the surface rupture data from each of the fault strands to the several quantities that have been commonly used to describe surface ruptures, as in Bonilla and Buchanan (1970), Slemmons (1977), and Scholz (1982). For the six discrete ruptures we studied, we compared fault length to both maximum slip (Fig. 4a) and mean slip (Fig. 4b).

Some consistency is seen in these comparisons; maximum and mean slip both increase with rupture length. Scholz (1982) points out that the physical basis for linear scaling between mean slip and fault length is that the proportionality constant, α, is proportional to stress drop, thus to friction on the fault surface. The value he obtained for large strike-slip events is $\approx 1.25 \times 10^{-5}$, whereas from our data alone we obtain $\alpha = 0.3 \times 10^{-5}$, but the line is poorly constrained and the values are not directly comparable. Without additional data from surface faulting or other

TABLE 1

SURFACE RUPTURE QUANTITIES AND MOMENT ESTIMATES

Fault	L (km)	Max. Slip (mm)	Mean Slip (mm)	$L \times x$ (m^2)	M_o (dyne×cm)
ERF	9.96	130	34.8	346.6	1.04×10^{24}
EERF	6.34	95	31.4	198.8	* 5.96×10^{23}
WERF	5.40	75	18.1	97.8	* 2.93×10^{23}
LTF	5.49	48	13.2	72.4	* 2.17×10^{23}
EKSF	1.44	40	20.0	28.8	* 8.64×10^{22}
KSF	2.16	28	8.3	17.9	* 5.37×10^{22}
Total				762.3	2.29×10^{24}

L = mapped surface rupture length.

$L \times x$ = Length times surface slip, obtained by integration using the trapezoidal rule on linearly interpolated data, sampled at 10 m intervals, using zero as the integration constant.

M_o = Moment, calculated from surface rupture data using the standard relation $M_o = \mu(L \times D)x$, where μ is rigidity (assumed to be 3.0×10^{11} dyne/cm^2), L is length of rupture plane, D is depth of rupture plane (assumed to be 10 km), and x is surface slip. Here, the quantity $L \times x$ is obtained by integration.

* Surface ruptures with $L/D \ll 1$, for which moment calculations are dominated by the assumed dimension D.

methods, one cannot yet reliably infer differences in friction between main faults and cross-faults.

CROSS-FAULT RUPTURE TIMING

The relation between major ruptures as defined by seismicity in the Superstition Hills sequence and by surface ruptures is complex in both space and time. It may be that not all of the cross-fault surface slip coincided with the Elmore Ranch event; some may have been associated with aftershocks in the ensuing ~11.4 hours, or caused by the main shock on the Superstition Hills fault. Lack of surface rupture observations immediately following the Elmore Ranch earthquake leave many questions regarding the temporal sequence of surface rupture unresolved. In one way, the temporal behavior of the northwest- and northeast-trending faults clearly differs; a significant portion of the total slip on the SHF has occurred as afterslip. In contrast, no afterslip has been detected on any of the northeast-trending surface ruptures since the evening of 24 November when some of the first afterslip markers were put out. Perhaps relevant to this lack of observed afterslip, seismicity on the cross-faults reportedly decreased substantially after the main rupture on the SHF occurred (H. Magistrale and K. Hutton, personal comm., 1988).

DISCUSSION

Some implications of the data warrant discussion as follows:

1. Cross-Fault Triggering. Northwest of the intersection between the cross-faults and SHF, no surface slip was observed on the SHF. The main event (M_S = 6.6) epicenter is located slightly southeast of the ERF intersection; the main shock rupture propagated towards the southeast from the intersection. We suggest that the main shock on the Superstition Hills fault was triggered primarily by the rapid decrease in normal stress across the Superstition Hills fault caused by the left-lateral displacement on the cross fault, which locally weakened the SHF (Fig. 5). The cross-fault rupture presumably also caused increased normal stress to the

northwest of the faults' intersection, thereby inhibiting bilateral rupture to the northwest. These concepts are developed further in Hudnut *et al.* (1989).

2. Potential Cross-Fault Triggering of the San Andreas Fault. Future slip on other known cross-faults would decrease normal stress across the southern San Andreas fault, potentially triggering an earthquake there by a mechanism similar to that observed in the Superstition Hills sequence. Other cross-faults are mapped northwest of the ERF; these form the Extra fault zone, labelled A-A′ in Fig. 1. Identification and mapping of these and other cross-faults that could trigger larger future earthquakes may help to evaluate whether hypocenters in a potential foreshock sequence are on a mapped cross-fault. Recognition of this mechanism should be helpful in developing a basis for prediction of earthquakes on the San Andreas fault.

Dibblee (1984) mapped a portion of the Extra fault in the eastern San Felipe

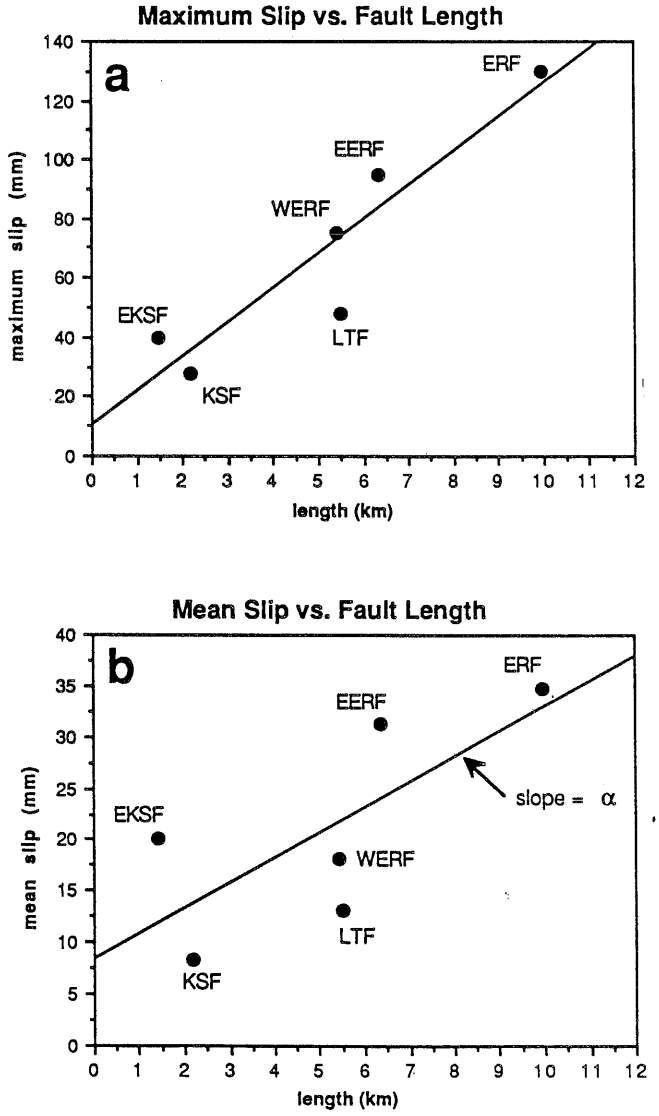

FIG. 4. Relations of quantities typically used to describe surface rupture. a) Maximum slip versus fault length. b) Mean slip versus fault length. Using Scholz (1982) equation; $\mu = \alpha L$, we determine $\alpha = 0.3 \times 10^{-5}$ from the poor linear fit to these data (see text).

Hills between highways 78 and 86, and further mapping has been done by Sharp (1981; personal comm., 1988), and recently by authors of this paper. The fault is associated at the surface with a northeast-trending linear concentration of roughly en-echelon anticlines, as is observed along the Kane Spring and Elmore Ranch faults. Along this fault, the belt of anticlines is mappable along strike for about 10 km through the eastern San Felipe Hills. Between anticlines, where the fault is best expressed, the fault trace offsets Pleistocene strata. Good exposures of the fault are seen in the deeper dry stream channels. Towards the southwest from this area, the fault is covered by sand dunes and alluvium, but a strong lineament is seen on airphotos and satellite images, extending the fault close to the Coyote Creek fault.

Toward the northeast, the fault is expressed by bathymetric contours in the Salton Sea, by a weak seismicity cluster along the Brawley seismic zone, and by several small earthquakes under the Salton Sea in April 1988 (CIT/USGS catalog). Straight extrapolation of the Extra fault zone intersects the San Andreas fault at its southern terminus, where its trace is deflected into the Brawley seismic zone.

Fuis *et al.* (1984) showed a northeast-trending graben structure in their basement map, based on refraction survey data. The northwest edge of this graben coincides with the surface expression of the Extra fault zone. There had been almost no seismicity on or near this structure in the past decade or more, before the minor activity in April 1988. The Elmore Ranch fault was also seismically quiet before its 1987 activity and rupture.

We observed cracking and possibly minor left-lateral slip along a few hundred meter section of the Extra fault, just south of highway 78, following the November 1987 earthquake sequence. In 1968, following the Borrego Mountain earthquake, Clark (1972) mapped rupture on a secondary fault which may be a branch of the Extra fault. Again in 1987, cracking was observed along this secondary fault (Hudnut and Clark, 1989).

Excavations on the southern San Andreas fault have demonstrated a lack of any large earthquakes along the southern section of the San Andreas fault for the last 300 yrs (Sieh, 1986; Williams and Sieh, 1987). Since it appears that the southern San Andreas fault is in a late stage of the earthquake cycle, a decrease in normal stress on the San Andreas fault may potentially trigger a great earthquake on the Coachella Valley segment. Future studies of the Extra fault zone may assist in the evaluation of this potential.

3. Modification and Attenuation of Slip. The slip data presented in Fig. 3a and 3b show variability along strike, and our calculation of moment based on these data is nearly 10 times less than the seismic moment. These and other surface rupture data (Clark, 1972; Sharp *et al.*, 1982) indicate that large variations in slip along surface ruptures may be common. Attempts to correlate surface slip to slip at depth are an effort to match geological data with seismological and geodetic results.

In our data, two conclusions are implied: first, slip at depth was greater than surface slip—a tenth the moment and a two-fold shorter rupture length were obtained from surface rupture than from seismological data. This implies that slip is attenuated as it propagates to the surface. Second, short-wavelength variations in surface slip correspond to geological structures that are probably shallow. Evidence for this is the termination of several surface breaks at small anticlines associated with fault trace steps of less than 1 km. These structures are presumably shallow and do not continue to the basement. Fault slip is apparently modified as it propagates into these structures and to the surface—perhaps being distributed into active folding as Klinger and Rockwell (1989) have shown.

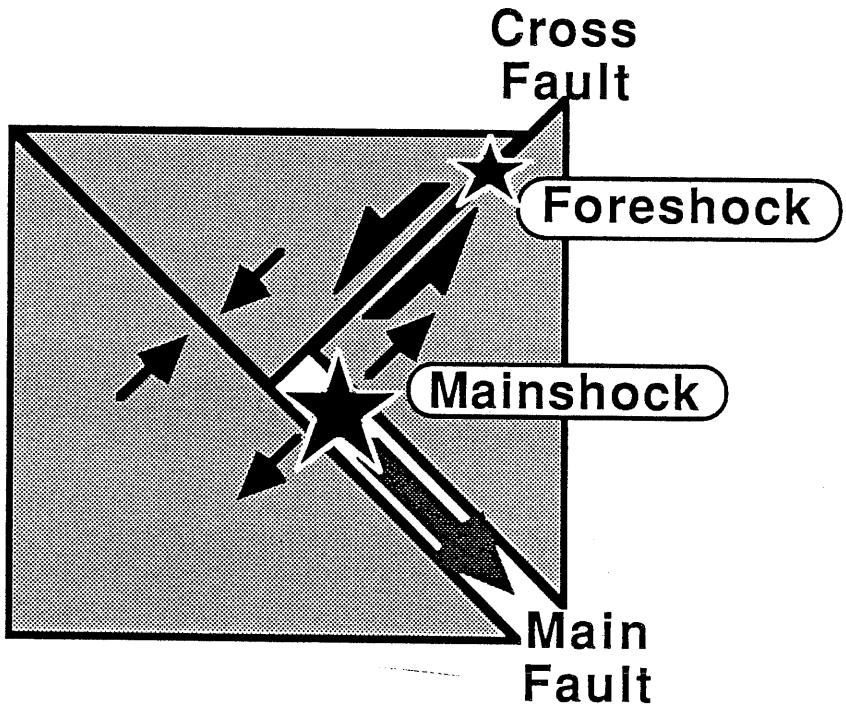

FIG. 5. Diagram of the proposed cross-fault triggering mechanism. Normal stresses on the main fault are altered by foreshock slip on cross-faults, triggering the main fault rupture near the faults' intersection. Main shock nucleates in the region of decreased normal stress and propagates southeastward, away from the region of increased normal stress. The diagram schematically represents stress changes as virtual displacements; it is not meant to be interpreted literally as actual displacements.

4. Lack of Afterslip on the Cross-Faults. If a reciprocal geometry to the foreshock/main shock triggering occurred, slip during the main shock on the Superstition Hills fault should have produced a rapid decrease in normal stress on the set of cross-faults. Suppose that slip on the cross-faults before the main shock occurred only in the basement, then a decrease in fault-normal stress on the cross-faults following the main shock allowed slip to propagate up through the sediments. This could have occurred and not been observed because of the timing of field observations. A sudden decrease in normal stress on the cross-faults accompanying the main shock might also account for the observed decrease in seismicity on these faults following the mainshock.

The greater slip at depth, shown by the seismic moment, apparently only partly propagated to the surface. Thus, some slip might still be propagating towards the surface. The above hypothesis predicts that the lack of afterslip seen through October 1988 might eventually be followed by afterslip that would be detected by future monitoring of the alinement arrays.

CONCLUSIONS

A set of parallel faults ruptured in association with the Elmore Ranch earthquake (M_S = 6.2). The ruptures occurred in a zone 10 km long and about 10 km wide along a roughly N35°E trend. Nearly 200 mm of left-lateral slip occurred across this zone, and only minor amounts of dip slip were observed. The moment obtained from surface rupture data is about an order of magnitude less than the seismic moment for this event. Seismicity indicates a 20- to 25-km-long rupture in this

event, whereas surface rupture was only half that length. No afterslip has yet been noticed on any of these surface breaks. Because these faults had left-lateral slip during the 1987 seismic events, a tectonic explanation is needed to also account for basement morphology (Fuis *et al.*, 1984), which indicates that dip slip on these faults has occurred in the past.

ACKNOWLEDGMENTS

We thank H. Kanamori and the staff at the CIT/USGS office in Pasadena, especially L. Jones and D. Given, for epicenter locations soon after the earthquakes. We also thank T. Hanks at the USGS for providing us with the new airphotos. We thank R. Sharp, M. Clark, M. Rymer, and J. Lienkaemper at the USGS, J. Kahle at CDMG, P. Williams at L-DGO/CIT, and others for their advice and comments in the field. L. Sykes pointed out the April 1988 seismicity on the Extra fault to us. Reviews by R. Wallace, C. Scholz, and D. Simpson greatly improved this paper. Research was supported by U. S. Geological Survey grant No. 14-08-00001-G1330. Lamont-Doherty Geological Observatory contribution No. 4429.

REFERENCES

Bent, A., P. Ho-Liu, and D. Helmberger (1988). The November 1987 Superstition Hills earthquake and comparisons with previous neighboring events (abstr.), *Seism. Res. Lett.* **59**, 49.

Bonilla, M. and J. Buchanan (1970). Interim report on worldwide historic surface faulting, *U.S. Geol. Surv. Open-File rept.* 32 pp.

Budding, K. E. and R. V. Sharp (1988). Surface faulting associated with the Elmore Desert Ranch and Superstition Hills, California, earthquakes of 24 November, 1987 (abstr.), *Seism. Res. Lett.* **59**, 49.

Clark, M. M. (1972). Surface rupture along the Coyote Creek fault, *U.S. Geol. Surv. Profess. Paper 787*, 55–86.

Clark, M. M. and K. Hudnut (1988). New slip along parts of the 1968 rupture of the Coyote Creek fault, California (abstr.), *Seism. Res. Lett.* **59**, 49.

Dibblee, T. W. (1984). Stratigraphy and tectonics of the San Felipe Hills, Borrego Badlands, Superstition Hills, and vicinity, in *The Imperial Basin—Tectonics Sedimentation, and Thermal Aspects: Pacific Section S.E.P.M.*, C. A. Rigsby, Editor, 31–44.

Fuis, G. S., W. D. Mooney, J. H. Healey, G. A. McMechan, and W. J. Lutter (1984). Crustal structure of the Imperial Valley region, California, in *The Imperial Basin—Tectonics, Sedimentation, and Thermal Aspects: Pacific Section S.E.P.M.*, C. A. Rigsby, Editor, 1–13.

Hudnut, K. and M. Clark (1989). New slip along parts of the 1968 Coyote Creek fault rupture, California, *Bull. Seism. Soc. Am.* **79**, 451–465.

Hudnut, K., L. Seeber, and J. Pacheco (1989). Cross-fault triggering in the November 1987 Superstition Hills earthquake sequence, southern California, *Geophys. Res. Lett.* **16**, 199–202.

Johnson, C. E. and L. K. Hutton (1982). Aftershocks and pre-earthquake seismicity, in *The Imperial Valley earthquake of October 15, 1979, U.S. Geol. Surv. Profess. Paper 1254*, 59–76.

Kahle, J. E., C. J. Wills, E. W. Hart, J. A. Treiman, R. B. Greenwood, and R. S. Kaumeyer (1988). Preliminary report: surface rupture—Superstition Hills earthquakes of November 23 and 24, 1987, *California Geology*, **41**, 4, 75–84.

Klinger, R. E. and Rockwell, T. K. (1989). Flexural-slip folding along the eastern Elmore Ranch fault in the Superstition Hills earthquake sequence of November 1987, *Bull. Seism. Soc. Am.* **79**, 297–303.

Lomnitz, C., F. Mooser, C. R. Allen, J. N. Brune, and W. Thatcher (1970). Seismicity and tectonics of the northern Gulf of California region, Mexico: preliminary results: *Geofísica Internacional* **10**, 37–48.

Magistrale, H., L. Jones, and H. Kanamori (1989). The Superstition Hills, California, earthquakes of 24 November 1987, *Bull. Seism. Soc. Am.* **79**, 239–251.

McGill, S. F., C. R. Allen, K. W. Hudnut, D. C. Johnson, W. F. Miller, and K. E. Sieh (1989). Slip on the Superstition Hills fault and on nearby faults associated with the 24 November 1987 Elmore Desert Ranch and Superstition Hills earthquakes, southern California, *Bull. Seism. Soc. Am.* **79**, 362–375.

Nicholson, C., L. Seeber, P. Williams, and L. Sykes (1986). Seismic evidence for conjugate slip and block rotation within the San Andreas fault system, southern California, *Tectonics* **5**, 4, 629–648.

Scholz, C. H. (1982). Scaling laws for large earthquakes: consequences for physical models, *Bull. Seism. Soc. Am.* **72**, 1–14.

Sharp, R. V. (1981). Variable rates of late Quaternary strike slip on the San Jacinto fault zone, southern

California, *J. Geophys. Res.* **86,** 1754–1762.

Sharp, R. V. (1989). Pre-earthquake displacement and triggered displacement on the Imperial fault associated with the Superstition Hills earthquake of 24 November 1987, *Bull. Seism. Soc. Am.* **79,** 466–479.

Sharp, R. V., K. E. Budding, J. Boatwright, M. J. Ader, M. G. Bonilla, M. M. Clark, T. E. Fumal, K. K. Harms, J. J. Lienkaemper, D. M. Morton, B. J. O'Neill, C. L. Ostergren, D. J. Ponti, M. J. Rymer, J. L. Saxton, and J. D. Sims. (1989). Surface faulting along the Superstition Hills fault zone and nearby faults associated with the earthquakes of 24 November 1987, *Bull. Seism. Soc. Am.* **79,** 252–281.

Sharp, R. V., J. Lienkaemper, M. Bonilla, D. Burke, B. Fox, D. Herd, D. Miller, D. Morton, D. Ponti, M. Rymer, J. Tinsley, J. Yount, J. Kahle, E. Hart, and K. Sieh (1982). Surface faulting in the central Imperial Valley, *U.S. Geol. Surv. Profess. Paper 1254,* 119–143.

Sieh, K. E. (1986). Slip rate across the San Andreas fault and pre-historic earthquakes at Indio, California, *EOS* **67,** 1200.

Slemmons, D. B. (1977). State of the art for assessing earthquake hazards in the U.S., faults and earthquake magnitudes, U.S. Army Eng. Waterway Exp. Sta., Vicksburg, Mississippi, 229.

Williams, P. L. and H. W. Magistrale (1989). Slip along the Superstition Hills fault associated with the 24 November 1987 Superstition Hills, California, earthquake, *Bull. Seism. Soc. Am.* **79,** 390–410.

Williams, P. and K. E. Sieh (1987). Decreasing activity of the southernmost San Andreas fault during the past millenium, *Geol. Soc. Am. Abstracts with Programs* **19,** 891.

LAMONT-DOHERTY GEOLOGICAL OBSERVATORY
PALISADES, NEW YORK 10964
(K.W.H., L.S.)

DEPARTMENT OF GEOLOGICAL SCIENCES
SAN DIEGO STATE UNIVERSITY
SAN DIEGO, CALIFORNIA 92182
(T.R., J.G., R.K., S.L., R.M.)

DEPARTMENT OF GEOLOGICAL SCIENCES
COLUMBIA UNIVERSITY
NEW YORK, NEW YORK 10027
(K.W.H.)

Manuscript received 28 July 1988

FRIENDS OF THE PLEISTOCENE FIELDTRIP 1990

ROADLOG

Day One - Laguna Salada Fault (optional)

This portion of the trip will begin at 7 A.M. from the Desert Kitchen restaurant in Ocotillo, just south of I-8 on Highway S2. Milage, at this point, is zero.

TOTAL MILAGE	INTERVAL MILAGE	COMMENTS
0	0	Desert Kitchen restaurant. Proceed south on Highway S2 to intersect Highway 98.
0.4	0.4	Highway 98. Turn left! Proceed east on Highway 98 through Yuha desert. We will be back here tomorrow.
4.4	4.0	We are crossing one of several NE-trending left-lateral faults of the Yuha desert area (see Thomas and Stinson, this volume). Note the hill to your right: the fault runs through the cleft and left-separates the hill front.
6.0	1.6	Scarps in late Quaternary alluvium are present along the Yuha Wells fault, along the hill front to your left. We'll be back tomorrow for this one.
6.8	0.8	The mountain ahead is Signal Hill (Cerro Centinela) with the Sierra de los Cucapas extending to the southeast. After a rather circuitous route across the border and through Mexicali, we will end up to the west of the Cucapas along the Laguna Salada fault.
10.4	3.6	You are crossing the northern extension of the Laguna Salada fault near it's northern terminus. Sunrise Butte is just to your left. Closed depressions, sags, scarps, and small right-lateral offsets characterize this section of the fault. The highway climbs over 10 m to cross the scarp. The Laguna Salada fault is truncated to the northwest by the NE-trending Yuha Wells fault zone.
~20	~10	We're crossing the Holocene (13 m) shore line of Lake Cahuilla.

28.4	8.0	Crossing the New River, no time to go swimming. The river flows north from the Colorado delta, through Mexicali, to drain into the Salton Sea. The section of lake sediments exposed along the river are Holocene and were deposited during one of the many Holocene highstands, the most recent being about 330 years B.P. (Sieh, 1986).
31.0	2.6	Highway 111, turn right (south)! Continue through Calexico to the border.
32.1	1.1	International border. Make sure you smile. As you cross, the road splits immediately; veer right and continue through the lights down LIC. A Lopez Mateos (with Railroad track in the middle divider). 40 km/hr max!
33.7	1.6	Mileage sign. Continue straight for now, we're going to "Tijuana, B.C." (Highway 2 west).
34.4	0.7	The Bull Ring should be on your right.
34.7	0.3	Turn right at Tijuana sign onto Cal. Z Anahuac. The Bull Ring is again on your right. Continue straight and then veer left after two blocks.
35.0	0.3	You're still on Calle Anahuac.
35.3	0.3	You should pass under a Tijuana sign.
35.7	0.4	Crossing the New River again. The river flows north from here to the border.
36.0	0.3	Turn right on the major highway (follow the Tijuana sign) and go west. You are now on Boulevard Cardenas.
36.6	0.6	Another branch of the New River.
37.5	0.9	Round about! Alto means STOP! Be in the left hand lane and continue around to go to the left (south) to follow the Tijuana sign. Do not go "straight".
38.5	1.0	Intersect Highway 2. Zero km mark on the highway post. Go west.

43.8	5.3	Signal Hill is now straight ahead again. We will be turning off of the highway soon to go through the low pass to your upper left that separates Signal Hill from the Sierra de los Cucapas.
47.6	3.8	Inspection Station. Get ready to turn.
47.65	0.05	Turn left (south) and go through the small gate onto a dirt road before the little white structure on the left. There should be two small, lone trees in the open field. The turnoff is directly across from a turquoise building and a blue building with a "Cervesa Pacifico" sign hanging in front. If you pass the cemetary on Highway 2, you've gone too far.
47.7	0.05	Once you're off the highway, the dirt road veers slightly left to go between the two trees. Continue on this dirt road and take the right fork beyond the trees. Stay on the main road.
48.3	0.6	Road forks again just before the powerline undercrossing. Take the left fork and go "straight".
48.5	0.2	Second powerline undercrossing. Continue past the piles of shredded nylon stuff.
48.8	0.3	Cross a small drainage. You may need 4-wheel drive at times from here on out.
51.7	2.9	Loose sand.
52.2	0.5	Laguna Salada (or what's left of it) can be seen to your right. The lake is now hypersaline and has dropped several meters in the past couple of years. There are fish kills along the playa margin that occur in bands that are all the same species - a function of their salt tolerance.
53.5	1.3	4-wheel drive required.
53.7	0.2	Go straight. Road to the right goes to the lake.

55.0	1.3	The hill or horst, as the case may be, separates the Laguna Salada fault on the west from the Borrego fault (strike-slip), which runs down the Borrego Valley on the left.
57.2	2.2	Road splits. Take the right fork, the left one follows the wash up into Borrego Valley.
58.0	0.8	We are now on a small fan extending out into the playa (or lake, when full). The scarp to your left in alluvium is wave cut. The scarp in bedrock is a wave-modified fault scarp. They'll get better. Notice the barnacles covering everything.
59.5	1.5	To your left, you will see bonified fault scarps in alluvium and bedrock. Note the wavecut shoreline below the fault, which may be wave-modified fault scarps in places.
62.2	2.7	Stop 1. We will examine both alluvial and bedrock fault scarps along the central portion of the Laguna Salada fault, and look at the evidence for oblique slip. We will also look at up to several soil pits on the early Holocene alluvial fans that have been vertically displaced by up to 20 m. Follow the leader. Stop 2. Continue south with the crowd to the intersection of the Canon Rojo and Laguna Salada faults. We will examine this corner of the pull-apart system, look at how slip was transfered around the corner, and enjoy bedrock scarps from the last rupture of up to 5 m.

End of day 1. Return to Mexican Highway 2 by following your exact route down here. Go east on Highway 2 until you intersect Highway 5 and go north towards Mexicali. At the roundabout (this is a different one), don't go straight but rather go 210 degrees around (ends up veering to the left) or slightly more than half way around. This puts you on the road that we came in on. You will again pass the Bullring (on your left this time). Follow the Calexico signs, they will feed you to the frontage road at the border. You will then turn left along the border to the border crossing. It may take awhile so relax. Once across the border, go north on Highway 111 to Highway 98 and go left (west) to Ocotillo.

To get to camp from Ocotillo, reset your odometer at the Desert Kitchen to zero and go north on Highway S-2 under the freeway. The road bends sharply at mile 1.1, continue around the bend. At mile 1.6, you will intersect Shell Canyon Rd. (4-way stop), turn right (northeast) towards the Coyote Mountains. Shell Canyon Road is straight for about 1.5 miles and then makes a couple of S-turns just before it crosses the fault. At 2.2 miles from the intersection of Highway S-2, the paved road turns left into a quarry but you will go straight onto a dirt road. Go about a quarter of a mile to where the road forks and take either fork (the left fork is easier) and then veer to the right up into the canyon. As you enter the canyon, the vertically foliated rock on your right is amphibolite that was cooked and squeezed during the Mesozoic. In another quarter of a mile, the road forks again. Go right, up into the range to our camp. We will pretty much cover most of the area from the road up to the base of the hills but our campfire will be in a bowl-like area near the base of the hills. See ya there.

DAY 2

Total Mileage	Interval Mileage	Comments
0	0	Stop 1. Get out of your sleeping bags and start walking. We will spend all morning within walking distance of camp (you can leave everything set up, we'll be back). We will meet on the road by the fault at 8 A.M. sharp to start todays part, and will walk the few hundred meters to the first outcrop. We will look at soils of many different ages that are developed in alluvial deposits that have been laterally displaced by the Elsinore fault. We will also look at the fault in some detail and examine the evidence for multiple slip events and their sizes.
0	0	From camp, go back down Shell Canyon Road to Highway S-2. Zero your mileage marker at the intersection.
0	0	Turn right and proceed northwest on Highway S-2.
2.4	2.4	Turn right on the paved road that leads up to the rangefront. Go to the base of the mountain.
4.3	1.9	Locked gate! Turn around and park off of the road on the north side. We will walk from here (< 1 km).

-	-	Stop 2. We will look at more evidence of slip per event and the like. We will look at more soils, varnish and other good stuff, and see more slip for the last couple of events than was present in Alverson and Fossil Canyons.
6.2	1.9	Return to Highway S-2. Go left.
8.7	2.5	4-way stop at Shell Canyon Rd. Go straight on S-2.
10.0	1.3	Go straight under the freeway.
10.7	0.7	Highway 98 intersection. Go left.
16.3	5.6	Highway curves left to the east, be prepared to stop and turn off the highway to the left.
16.65	0.35	Go left onto BLM road Y1928. There is an orange arrow painted on the Highway 98 pavement at the turn (I didn't do it).
17.1	0.45	Stop 3. Yuha Wells fault stop. We will look at a degraded scarp in late Quaternary alluvium along the Yuha Wells fault, a northeast-trending left-lateral fault that appears to truncate the northern end of the Laguna Salada fault.

End of Day 2. Return to camp for good times and the annual meeting! You should know the way by now.

DAY 3

Today, what we do depends on logistics that were not known at the time that the guidebook was sent to the printers. We will either proceed straight to Plaster City to look at soils developed on late Pleistocene lacustrine bars, or we will proceed to the Superstition Hills to look at evidence of repeat earthquakes there. Follow the leader. If we go to Plaster City, go back down to Highway S-2 and go left (south). Just befor the freeway, turn left onto S-80 (old Highway 80) which more or less serves as a frontage road to the freeway. Go 7.65 miles to the Plaster City lake bar turnoff. We will either go left or right depending on what's on the menu. If we go to Superstition Hills first, continue through Plaster City (it's actually a sheet rock processing plant). Go to Huff road (16.5 miles from S-2) and turn left (north). The road marker is hard to see until you're right at the road but it's just past a group of trees and buildings. Huff road goes north, bends around to the east in the Superstition Mountain badlands (where we cross the Superstition Mountain fault) and becomes Imler Road as it turns

east. We will either stop at the Superstition Hills fault where it breaks Imler Rd. or turn left into the NAS El Centro base to look at the better exposures (It all depends on permission for 150 people, which is not certain at this point).

Day 3 will end early (about 2 P.M.) so that everyone can enjoy their drive home or make it to the airport for their flights. Hope you enjoyed the trip.


B.C. By Johnny Hart
DIG
DIG
DIG
DIG
DIG
DID THEY HAVE PHONE BOOTHS DURING THE PLEISTOCENE EPOCH?
I DON'T KNOW... WHY?
ON THE WALL NEXT TO THIS DIXIE CUP, HERE ...IT SAYS, 'FOR A GOOD TIME, CALL! TOM'

J. Paul Dauphin and Bernd R. T. Simoneit, editors
American Association of Petroleum Geologists: Memoir Number 47

FIGURE 4. Neotectonic map of the Laguna Salada and Canon Rojo fault zones.

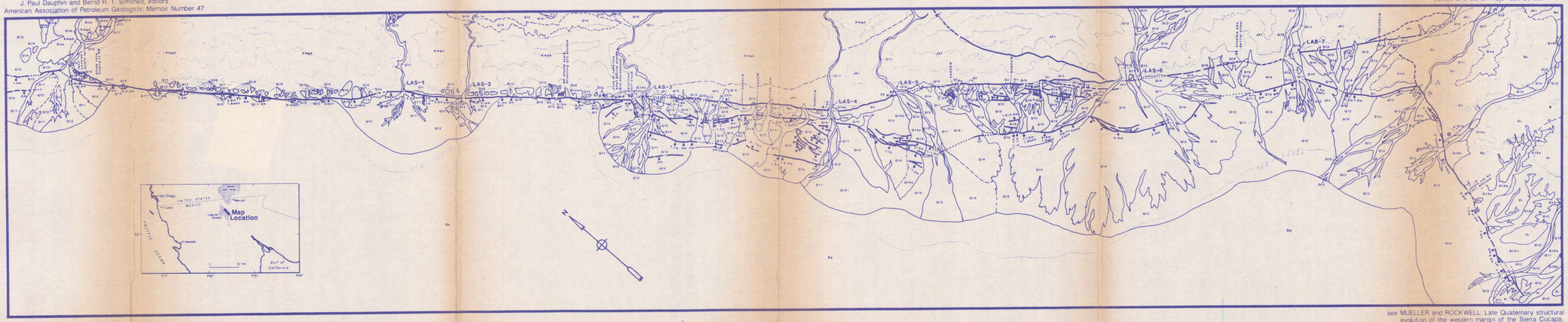

see MUELLER and ROCKWELL: Late Quaternary structural evolution of the western margin of the Sierra Cucapa, Baja California Norte (this volume).

Quaternary — Holocene

- Qp — Historic playa lake sediments
- Qf1 / Qt1 — Very poorly developed Typic Torrifluvents: historic, active alluvial fan (f) and stream terrace (t) deposits; no visible soil development or horizonation, although calcareous
- Qf2 / Qt2 — Moderately developed Typic Torrifluvents: latest-Holocene and historic (?) alluvial fan (f) and stream terrace (t) deposits; soils consist of thin , very poorly developed A-C profiles
- Qf3 / Qt3 — Poorly to moderately developed Typic Camborthids: late-Holocene alluvial fan (f) and stream terrace (t) deposits; soils have incipient, poorly developed Bca horizons separating Avca and Cca horizons
- Qf4 / Qt4 — Poorly developed Arenic Haplargids: early and mid-Holocene alluvial fan (f) and stream terrace (t) deposits; soils have partially engulfed Avca horizons and poorly to moderately developed Btca and Cca horizons; ($CaCO_3$, NaCl, $CaSO_4$) locally common and are contained in the upper 70cm of soil profiles; geomorphic surfaces have a poorly developed desert pavement in regions with accelerated salt weathering

Quaternary — Pleistocene

- Qf5 / Qt5 — Moderately to well developed Arenic Haplargids: latest-Pleistocene alluvial fan (f) and lake terrace (t) deposits; soils have thin Avca horizons which have been partially engulfed by underlying well developed Btca horizons; soil profiles also have transitional BCca and Cca horizons; salts ($CaCO_3$, NaCl, $CaSO_4$) common to several meters depth, although concentrations occur in uppermost meter; geomorphic surfaces have a poorly to moderately well developed desert pavement
- Qoa — Late-Pleistocene alluvial fan deposits (appear similar to younger alluvium except better lithified)
- Qc — Mid-Pleistocene alluvial fan deposits (have higher degree of intrastratal reddening and cementation in comparison to younger alluvial fan deposits)

Tertiary — Pliocene

- Pi — Imperial Formation (claystone and sandstone), uppermost portion of section south of Canyon Rojo fault zone may be in part Pleistocene Palm Spring Formation

Jur. Cret.

- Kmgd — Cucapas granodiorite
- JKt — La Puerta tonalite

Unknown

- Ms — Prebatholithic metasedimentary rocks

Note: Subscripts for Qt thiough Q5 deposits include + and - (ie Qt3-) signifying geomorphic surfaces respectively containing an especially well or poorly developed soil of a given type. Also a,b,c...(ie Qt4b) respectively denotes adjacent stream terraces containing a given soil type which increase in elevation and age.

Fault in/or bounding bedrock: dotted if covered, dashed if inferred; dip of exposed fault surface and trend and plunge of striations or mullions given where visible; bedrock (BFS) fault surface exposed during recent groundbreaking seismic event ; vertical displacement in meters (3m).

Fault scarp in alluvial deposits: dotted if covered, dashed if inferred; 1. total (8m) vertical displacement in meters; 2. free face (4mFF) created during most recent groundbreaking seismic event; vertical displacement in meters; 3. multiple scarps, individual offset in meters

Contact: solid where well located or exposed ; dashed where approximate or inferred, queried where uncertain

34 — Strike and dip of bedding

⊕ — Flat bedding

27 — Foliation of fault zone rocks

BS — Beheaded stream

LAS-3 — Large antecedent stream (referenced in text)

DOCW-3m — Dextrally offset stream channel wall, offset in meters

DS-25m — Deflected stream channel, offset in meters

Morphology of an Alluvial Fault Scarp

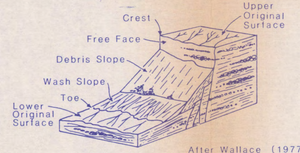

After Wallace (1977)

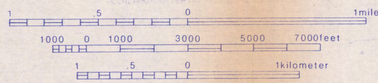

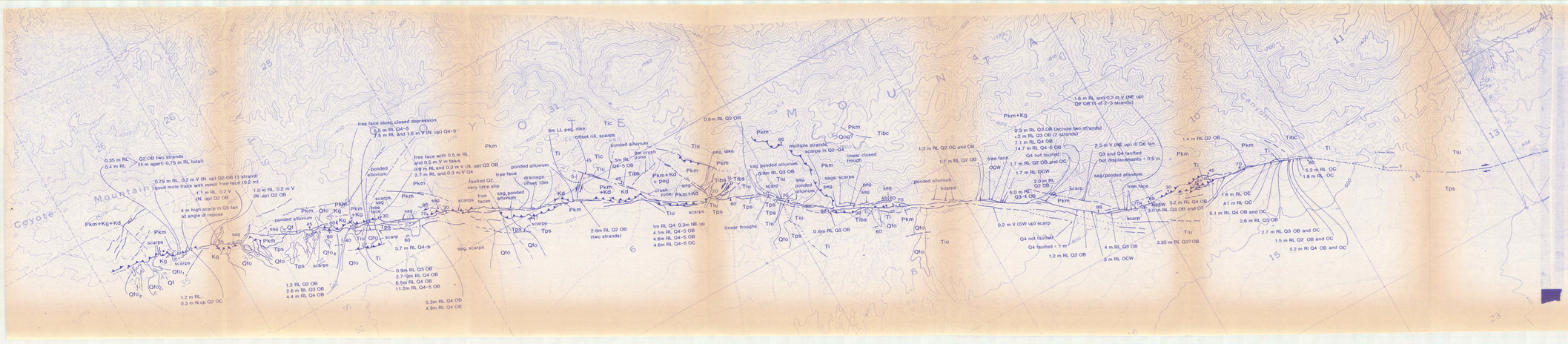

EXPLANATION

- Tiu — Upper Imperial Formation
- Ti — Imperial Formation (undif.)
- Tibs — Imperial Formation (basal sandstone unit)
- Tibg — Imperial Formation (basal conglomerate unit)
- Tps — Palm Spring Formation
- Qfo — Undif. Pleistocene Alluvial Fan
- Qal — Active Channel Alluvium
- Kg — Cretaceous Granitic Rocks (undif.)
- Pkm — Pre-Cretaceous Metamorphic Rocks
- peg — Pegmatite Dike
- Ta — Alverson Andesite

OB – Offset Alluvial Bar
OC – Offset Channel
OCW – Offset Channel Wall
OR – Offset Rill